

Modulating antibody-antigen binding by light

Thomas Declan Bridge

September 2019

A thesis submitted for the degree of Doctor of Philosophy at the School of Chemistry,
University of East Anglia.

This copy of the thesis has been supplied on condition that anyone who consults it is understood to recognise that its copyright rests with the author and that use of any information derived there from must be in accordance with current UK Copyright Law. In addition, any quotation or extract must include full attribution.

Abstract

Antibodies are an important class of biomolecules that have contributed immensely to several fields including, medicine, diagnostics, and as an important biomolecule required for a plethora of scientific procedures. However, methods to control antibody-antigen binding using exogenous stimuli such as light remain limited. The use of antibodies in a therapeutic setting has become a dominant biological platform in the pharmaceutical market and has been successfully employed for the treatment of numerous diseases including autoimmune disorders, cancers, infections, and cardiovascular diseases.

Cancer immunotherapeutics are often developed to target overexpressed antigens near tumour cells or on the surface of malignant cells. Often these disease targets are essential biological receptors that have developed mutations affecting expression levels or activity. Although highly expressed on targeted tumour cells, basal levels of targeted receptors can be present on healthy cells. Consequently, the reduced specificity of antigen targeting between healthy and diseased cells can cause severe side-effects of antibody therapeutics. By introducing methods to enable the spatiotemporal control of antibody-antigen binding affinities by light, an additional level of safety and improved targeting is achieved for these therapeutic molecules.

The research performed in this thesis aimed to explore strategies and available technologies for the site-specific incorporation of designer amino acids with unique chemistries that could facilitate the spatiotemporal control over antibody-antigen binding with the use of external stimuli. A simple and robust method was designed for the genetic incorporation of photocaged tyrosine (pcY) into the structure of an anti-EGFR antibody fragment, 7D12. Subsequent techniques developed to evaluate light-mediated binding of 7D12 mutants to its target on the surface of cancer cells demonstrated binding inhibition with the presence of pcY in two positions, Y32pcY and Y113pcY and upon irradiation with 365 nm light and de-caging of pcY, binding was restored.

Access Condition and Agreement

Each deposit in UEA Digital Repository is protected by copyright and other intellectual property rights, and duplication or sale of all or part of any of the Data Collections is not permitted, except that material may be duplicated by you for your research use or for educational purposes in electronic or print form. You must obtain permission from the copyright holder, usually the author, for any other use. Exceptions only apply where a deposit may be explicitly provided under a stated licence, such as a Creative Commons licence or Open Government licence.

Electronic or print copies may not be offered, whether for sale or otherwise to anyone, unless explicitly stated under a Creative Commons or Open Government license. Unauthorised reproduction, editing or reformatting for resale purposes is explicitly prohibited (except where approved by the copyright holder themselves) and UEA reserves the right to take immediate 'take down' action on behalf of the copyright and/or rights holder if this Access condition of the UEA Digital Repository is breached. Any material in this database has been supplied on the understanding that it is copyright material and that no quotation from the material may be published without proper acknowledgement.

Table of contents

Abstract.....	i
Table of contents	iii
Acknowledgements.....	vii
List of abbreviations.....	viii
List of figures.....	x
List of tables	xiv
CHAPTER 1 Introduction	1
1.1 The importance of expanding the genetic code	2
1.2 Generation of orthogonal translation machinery.....	4
1.3 How non-canonical amino acids (ncAAs) are incorporated.....	7
1.4 Application of non-canonical amino acids.....	13
1.4.1 Probing protein structure and function.	14
1.4.2 Photo-cross-linking ncAA to map protein-protein interactions.....	15
1.4.3 Fluorescent imaging.	16
1.4.4 Post-translational modifications.	18
1.4.5 Biorthogonal chemical handles.....	19
1.4.6 Stimuli control over bioactivity.	20
1.5 Introduction to antibodies and antibody fragments	22
1.6 Uses of ncAA in antibody therapeutics.....	26
1.7 Light mediated release of photo-active therapeutics.....	30
1.8 Focus of research described in this PhD thesis.....	33
CHAPTER 2 Methods.....	35
2.1 Methods.....	36
2.1.1 Cell Lines	36
2.1.2 Escherichia coli strains	36
2.1.3 Plasmids	37
2.1.4 Subculturing adherent cell line	39
2.1.5 Cell line storage.....	40
2.1.6 Competent cells	41
2.1.7 Transformation	41
2.1.8 Molecular cloning.....	42

2.1.8.1 DNA measurements	42
2.1.8.2 Restriction enzyme digestion.....	43
2.1.8.3 Agarose gel extraction	43
2.1.8.4 Plasmid DNA amplification and extraction	44
2.1.8.5 Polymerase chain reaction (PCR).....	44
2.1.8.6 Gibson assembly	45
2.1.8.7 T4 ligation.....	46
2.1.8.8 Sequencing.....	46
2.1.8.9 Site-directed mutagenesis	47
2.1.9 Periplasmic expression.....	47
2.1.10 Ni-NTA purification	48
2.1.11 Concentrating protein.....	48
2.1.12 SDS Polyacrylamide gel electrophoresis (PAGE)	48
2.1.13 Western blot	49
2.1.14 BCA protein assay	50
2.1.15 De-caging genetically incorporated pcY.....	50
2.1.16 On-cell assay	51
2.1.17 Labelling reaction.....	52
2.1.18 Stationary Microscopy	52
2.1.19 Dynamic Microscopy.....	53
2.1.20 Cell viability.....	53
CHAPTER 3 Periplasmic expression of antibody fragments.....	55
3.1 Introduction	56
3.1.1 Promoter	57
3.1.2 Plasmid copy number.....	59
3.1.3 Selection marker	60
3.1.4 Affinity tag.....	61
3.1.5 Leader sequence	62
3.2 Results & discussion.....	64
3.2.1 Construction of periplasmic expression vectors.....	64
3.2.2 Periplasmic expression of anti-EGFR VHH 7D12 in <i>E. coli</i>	70
3.2.3 Periplasmic expression of alternative VHH in <i>E. coli</i>	73
3.2.4 Expression of FAB fragments in <i>E. coli</i>	79
CHAPTER 4 Genetic incorporation of non-colonial amino acids in antibody fragments	86

4.1 Introduction	87
4.1.1 Expanding the genetic code for <i>in vivo</i> site-specific incorporation of non-canonical amino acids	87
4.1.2 Expression of orthogonal aaRS/tRNA pairs in cells.....	89
4.1.3 Suppressor plasmids containing <i>Methanococcus janaschii</i> derived <i>MjTyrRS/tRNA_{CUA}</i> pair	90
4.1.4 <i>Methanosarcina mazei</i> / <i>Methanosarcina barkeri</i> derived <i>PylRS/tRNA</i> pair.....	94
4.1.5 Orthogonal synthetase and corresponding suppressor tRNA for genetic encoding of photocaged amino acids.....	96
4.1.6 Non-canonical amino acids	97
4.2 Results & discussion.....	100
4.2.1 Construction of VHH amber mutants	100
4.2.2 Construction of suppressor plasmids.....	103
4.2.3 Comparison of suppressor plasmids.....	104
4.2.4 Expression of VHH 7D12 with photocaged ncAA.....	109
4.2.5 Expression and optimisation of VHH 2Rs15d with photocaged ncAA	114
CHAPTER 5 Assessment of antibody-antigen binding on the surface of live cancer cells ...	119
5.1 Introduction	120
5.1.1 Techniques to measure binding affinity and kinetics of antibody-antigen interactions	121
5.1.1.1 Enzyme-linked immunosorbent assay	121
5.1.1.2 Surface plasmon resonance (SPR).....	123
5.1.1.3 Isothermal titration calorimetry	126
5.1.2 Experimental drawbacks of current techniques to measure antibody-antigen interactions	128
5.2 Results & discussion.....	130
5.2.1 Development of on-cell assay to measure the interaction of an antibody to cell surface antigen.....	130
5.2.2 Optimisation of on-cell ELISA.....	132
5.2.2.1 Preliminary investigation of VHH 7D12 binding interactions with A431 carcinoma cell line	132
5.2.2.2 Adjusting on-cell assay to reduce background signal	134
5.2.2.3 Investigations into cell line serum starvation	135
5.2.4 Evaluation of the on-cell assay efficacy with control experiments	137
5.2.4.1 Negative EGFR cell line control	137
5.2.4.2 Negative VHH control	139

5.2.5 Restoring EGFR binding affinity to photocaged VHH 7D12	140
5.2.6 Determining binding affinity of VHH 7D12 to EGFR using on-cell assay.....	143
CHAPTER 6 Light dependant real-time delivery of fluorophores to the surface of live cells	147
6.1 Introduction	148
6.1.1 Receptor mediated internalisation	149
6.1.2 Live-cell microscopy design considerations	151
6.1.3 Fluorescent tools for live-cell imaging	153
6.2 Results & discussion.....	155
6.2.1 Optimisation of live-cell microscopy experimental procedures	155
6.2.2 Real-time live-cell imaging with pH-sensitive dyes.....	162
6.2.3 Dynamic real-time live-cell imaging.....	168
6.2.4 Assessing the binding influence caused by fluorophore on labelled VHH 7D12	177
6.2.5 Evaluating the effect of 365 nm light on cell viability.....	179
CHAPTER 7 Discussion and future work.....	182
7.1 Introduction	183
7.2 Discussion.....	184
7.2.1 Importance of immunotherapeutics to oncology.....	184
7.2.2 Spatial and temporal control over antibody-antigen binding with light	186
7.2.3 Light induced delivery of toxic payload to EGFR positive cancers.....	188
7.3 Future work.....	189
7.3.1 Applying photo-control strategies to alternative antibody fragments.....	189
7.3.2 Improving binding affinity using phage display	190
References	191
Appendix	217

Acknowledgements

First and foremost, I would like to thank my primary supervisor Dr Amit Sachdeva for providing me with his guidance, support, and extensive scientific knowledge throughout my PhD. From humble beginnings 4 years ago, with only two members of the Sachdeva group, I have had the pleasure of witnessing the growth and progress made by the new members Saher Shaikh, Kate Orman, and Udo Wegmann; and I wish the Sachdeva group many more year of success. Secondly, I would like to thank my secondary supervisor Dr Nick Le Brun for evaluating my progress through the duration of my PhD and providing guidance when needed. I would like to thank Dr Paul Thomas for his expertise in fluorescent microscopy and the support he provided during this research. Special thanks to Dr Joaquin Botta for the initial help and guidance he offered in teaching tissue culture procedures, Dr Jason Crack and Dr Justin Bradley for help with mass spectroscopy.

Over the duration of this PhD, I will never forget, and will forever be grateful to the friends I have made that have truly made this journey an enjoyable one. Dr Ross Goodyear, Dr Tom Storr, Dr Gerald Keil, Gareth Hughes, Dr Greg Hughes, Sarah Woodhouse, Lučka Bibič, Nikita Wright, Katja Kirmizakis, Nicholas Trull, and Robert Bellow, for supplying me with an unhealthy amount of coffee and beer, and for their constant support, even in the hardest times.

I'd also like to thank my family for showering me in love and support from day 1, and their ensuing enthusiastic grinning and "head-nodding" when I attempt to explain my research. To my grandfather Ron Bridge, who will sadly not see me graduate but has instilled some of his most important life lessons that have made me who I am today, I hope the work I have achieved here will be my first step in showing you my gratitude.

And last, but not least. I would like to give a massive thank you to my undergraduate friend Željka Kalinić for without her well-timed wise words and infectious passion for science I would likely be following a vastly different career pathway (presumably involving sticking people with needles).

List of abbreviations

aaRS - Aminoacyl-tRNA synthetase

ADC – Antibody drug conjugates

BocK – Boc lysine

bsAb – Bispecific antibody

CDR – Complementarity determining regions

CME - Clathrin-mediated endocytosis

DNA - Deoxyribonucleic acid

EF-Tu - Elongation factor thermo unstable

EGF - Epidermal growth factor

EGFR - Epidermal growth factor receptor

ELISA - Enzyme-linked immunosorbent assay

EMA - European Medicines Agency

ESI-MS - Electrospray ionization mass spectroscopy

Fab – Antigen binding fragment

FDA - Food and Drug Administration

FP – Fluorescent protein

GFP – Green fluorescence protein

GRO - Genomically recoded organism

HER2 - Human epidermal growth factor receptor 2

HRP - Horseradish peroxidase

IB – Inclusion bodies

IgG - Immunoglobulin G

IPTG - Isopropyl β -d-1-thiogalactopyranoside

ITC - Isothermal titration calorimetry

mAb - Monoclonal antibody
mRNA – Messenger RNA
ncAA - Non-canonical amino acid
NIR - Near infrared
oRBS – Orthogonal ribosomal binding site
ORI – Origin of replication
pcK – Photocaged lysine
PCR – Polymerase chain reaction
pcY – Photocage tyrosine
PPG - Photo-protective groups
PM – Plasma membrane
PTM – Post translational modifications
RBS – Ribosomal binding site
RF1 - Release factor 1
RNA - Ribonucleic acid
scFv - Single-chain variable fragment
sEGFR – Soluble epidermal growth factor receptor
SPR – Surface plasmon resonance
T7 RNAP – T7 RNA polymerase
TPA - Two-photon absorption
tRNA – Transfer RNA
VHH – Variable heavy fragment

List of figures

Figure 1.1: Diagram representation of photo control over antibody-antigen binding.....	3
Figure 1.2: Positive and negative selection methods for the directed evolution of aaRS/tRNA pairs.....	5
Figure 1.3: Codon table for E. coli.....	7
Figure 1.4: Nonsense codon incorporation of unnatural amino acid into a protein via cellular transcription.....	8
Figure 1.5: Genetic incorporation of multiple distinct ncAA with amber suppression and quadruplet codons.....	12
Figure 1.6: Examples of ncAAs used in the investigation of protein structure and functions.	14
Figure 1.7: Diagram representation of various naked antibody formats..	24
Figure 1.8: Layout of various bispecific antibodies formats, typically defined as two categories; immunoglobulin G (IgG)-like and non-(IgG)-like..	29
Figure 1.9: Diagram illustrating depth of tissue penetration by light relative to wavelength	32
Figure 3. 1 Graphic illustrating Gibson assembly insertion of expression construct.....	65
Figure 3. 2 Plasmid maps of pSANG10-7D12 and pRSF-D11-7D12 with inserted 7D12 expression construct.....	67
Figure 3.3 Expression and identification of VHH 7D12.....	71
Figure 3. 4 Comparison of two expression vectors pSANG10 and pRSF-D11 in the production of VHH 7D12 with and without IPTG induction.	72
Figure 3. 5 Plasmid map of pSANG10-VHH-R2 designed for the periplasmic expression of anti-RR6 VHH R2 with the induction of IPTG.	74
Figure 3. 6 Periplasmic expression of VHH R2	75
Figure 3. 7 Plasmid map of pSANG10-VHH-2Rs15d.....	76
Figure 3. 8 Periplasmic expression of 2Rs15d.....	78
Figure 3. 9 Plasmid map of pSANG10-FABC225.....	81
Figure 3. 10 Plasmid map of pAraH6HATT.....	83
Figure 4.1: Pictorial representation of plasmids, pSUP, pEvolv and pULTRA for incorporation of ncAA using MjRS/MjtRNA _{CUA}	93
Figure 4.2: pCDF_3xPylRS/PyltRNA suppressor plasmid design.	96

Figure 4.3: Crystal structure complex of 7D12-EGFR showing VHH 7D12 bound to domain III of sEGFR (sEGFRd3).....	101
Figure 4.4: Screening of amber suppression efficiency of pCDF_3xMbPylRS/MbPyltRNA _{CUA} , pSUP_MjCNFRS/6xMjtRNA _{CUA} , pEvolv_2xMjCNFRS/MjtRNA _{CUA} and pULTRA_MjCNFRS/MjtRNA _{CUA} plasmids.....	105
Figure 4.5: Screening of several versions of pULTRA suppressor plasmid with the genetic site-specific incorporation of various ncAA in VHH 7D12-Y32TAG.....	107
Figure 4.6: Suppressor plasmid efficiency comparison between PylRS/tRNA pair in pULTRA and pCDF vectors.	108
Figure 4. 7: Expression of 7D12 with genetic site-specific incorporation of two ncAA in response to five lysine amber mutants.	110
Figure 4.8: Genetic site-specific incorporation of pcY in VHH 7D12.....	111
Figure 4.9: Electrospray Ionization Mass Spectrometry (ESI-MS) measurements of expressed 7D12 and three amber mutants (Y32, Y109, and Y113).....	112
Figure 4.10: Electrospray Ionization Mass Spectrometry (ESI-MS) measurements of expressed 7D12 and three amber mutants (Y32, Y109, and Y113) before and after irradiation with light (365 nm, 4 minutes).....	113
Figure 4.11: Western blot detection of his-tagged proteins from the expression of pSANG10-7D12 (And Y32TAG mutant) compared to pSANG10-VHH-2Rs15d (And Y37TAG mutant).....	115
Figure 4.12: Screening of pSANG10-VHH-2Rs15d amber codon context at position Y37 with the incorporation of pcY.....	117
Figure 5. 1 Diagrammatic representation of common ELISA formats.	122
Figure 5. 2 Schematic representation of key features in surface plasmon resonance based affinity measurements.	125
Figure 5. 3 On-cell assay for measurement of binding between antibody fragment to cell surface antigen.	131
Figure 5. 4 Cell based assay experiments to assess the interaction of wt7D12 and three pcY mutants to EGFR on the surface of A431 cells.....	133
Figure 5. 5 Cell based assay assessing wt7D12 affinity to EGFR on A431 cells treated with and without serum starvation	136
Figure 5. 6 Experimental control of cell based assay determining specificity of wt7D12 to EGFR on positive cell line (A431) and negative cell line (MDA-MB-231).....	138

Figure 5. 7 Experimental control of cell based assay determining specificity of his-tagged heavy chain only antibody fragments to A431 cell surface.	140
Figure 5. 8 Cell based binding experiments to assess the interaction of EGFR with wt7D12 and amber mutants containing site-specifically incorporated pcY.	142
Figure 5. 9 On-cell assay analysis to determine binding kinetics of 7D12 (wt and pcY mutants) to EGFR in the presence and absence of 365 nm light.	144
Figure 6. 1 Diagram overview of activated EGFR clathrin-mediated endocytosis.....	151
Figure 6. 2 Microscopy images of BODIPY-FL labelled 7D12 and pcY mutants (Y32pcY, Y109pcY, and Y113pcY) binding interactions to A431 cell surface EGFR.....	157
Figure 6. 3 Microscopy images of BODIPY-FL labelled 7D12 binding interactions to A431 and MDA-MB-231 cell surface EGFR.....	159
Figure 6. 4 Microscopy investigation into reduction of exposure time.....	160
Figure 6. 5 Exploring the use of pH sensitive dyes.....	163
Figure 6. 6 Evaluating efficacy of Protonex Red 600 labelled 7D12 (wild type and Y32pcY) to A431 cells.	165
Figure 6. 7 Evaluating efficacy of Protonex Red 600 labelled 7D12 (wild type and Y32pcY) to A431 and MDA-MB-231 cells.	166
Figure 6. 8 Detected fluorescence signal from pHrodo Red, Protonex Red and pHrodo Green labelled 7D12 (wild type and Y32pcY) with additional purification steps	168
Figure 6. 9 Diagram of dynamic microscopy setup for time-lapse experiments of live-cells with constant flow.	170
Figure 6. 10 Dynamic microscopy experiment investigating de-caging of Y32pcY-BODIPY-FL with microscope DAPI channel and measuring subsequent binding to A431 cell surface..	172
Figure 6. 11 Dynamic microscopy experiment investigating pre-experimental de-caged Y32pcY-BODIPY-FL (de-caged <i>via</i> UV transilluminator) and measurements of binding to A431 cell surface.....	173
Figure 6. 12 Dynamic microscopy experiment investigating Y32pcY-BODIPY-TMR-X binding to A431 cells in the presence and absence of 365 nm irradiation (<i>via</i> DAPI exposure for 1 minute).....	176
Figure 6. 13 Comparison of binding of labelled and unlabelled wt7D12 to EGFR assessed using on-cell assay on the surface of A431 cells.....	177
Figure 6. 14 Cell viability assay of irradiated A431 cells demonstrated minor decreases in cell growth after 48 hour incubation	180

Figure 7. 1 The site-specific genetic incorporation of pcY and subsequent photo-control over antibody-antigen binding..... 187

Figure A. 1 On-cell assay evaluating optimum dilutions of primary and secondary antibody for detection of wt7D12 binding interactions to EGFR..... 229

Figure A. 2 On-cell assay to determine binding kinetics of 7D12 (wt and pcY mutants) to EGFR in the presence and absence of 365 nm light 230

List of tables

<i>Table 2.1: E. coli strains.....</i>	<i>36</i>
<i>Table 2.2: Plasmid list of cloned plasmids synthesised during this project. Details of cloning strategies are listed in results section, or alternatively, AddGene product code is provided in description</i>	<i>37</i>
<i>Table 2.3: PCR reagents list with concentrations used followed to manufacturer’s standards.....</i>	<i>44</i>
<i>Table 2.4: PCR cycle times and temperatures</i>	<i>45</i>
<i>Table 3.1: Promoters</i>	<i>58</i>
<i>Table 3.2: Leader sequences used throughout this study</i>	<i>64</i>
<i>Table 3.3: List of commonly used ORI’s.....</i>	<i>68</i>
<i>Table 4.1: Suppressor plasmids investigated in this study.....</i>	<i>89</i>
<i>Table 4.2: non-canonical amino acids utilized during this thesis.....</i>	<i>98</i>
<i>Table 4.3: Synonymous codon mutations made to downstream arginine codon (R38).</i>	<i>117</i>
<i>Table 5.1: OriginLab parameters obtained after fitting the data to sigmoidal nonlinear equation</i>	<i>144</i>
<i>Table 6.1: List of small molecule fluorophores used in this study.....</i>	<i>153</i>
<i>Table A.1 Antibiotic stock solutions</i>	<i>218</i>
<i>Table A.2: Primers used throughout this study.....</i>	<i>223</i>
<i>Table A.3: gBlocks used throughout this study</i>	<i>225</i>

CHAPTER 1

Introduction

1.1 The importance of expanding the genetic code

The past two decades have witnessed the rapid growth in diversity and scope of our knowledge in expanding the genetic code. Our understanding, together with a powerful set of tools for the manipulation of cellular machinery, has allowed scientists to accomplish diverse applications in probing, imaging and controlling protein function.

In nature, the precursors of proteins are amino acids encoded by nucleotide codons, and while DNA and RNA are two methods employed by organisms to store hereditary information, it is proteins that are responsible for the complex biological processes found within all living organisms. Often referred to as the building blocks of life, amino acids have a limited conserved set of 20 canonical groups decoded from 64 triplet codons, that are utilised by the translational machinery for the biosynthesis of proteins. Although the limited chemical properties contained within this set of building blocks has allowed for the development of proteins with highly complex structures and functions observed in living organisms, it has equally restricted the development of protein diversity. Further protein diversity can be achieved with expansion of the genetic code as this allows the site-specific incorporation of non-canonical amino acids (ncAA) that display a plethora of interesting chemical properties. Therefore, expanding the genetic code to include building blocks outside of the 20 canonical amino acids in the biosynthesis of proteins enables the development of novel and enhanced protein biological activities and is useful in the study of protein structure and function. Some examples of this include the incorporation of ncAAs containing post-translational modification (PTM), chemically reactive side chains, fluorophores, photo-cross-linkers, altered pK_a 's, and redox properties (Fahmi *et al.*, 2007; Chin *et al.*, 2002b; Murakami *et al.*, 2000; Lin *et al.*, 2014; Neumann *et al.*, 2008a).

Considerable interest has been shown in the field of expanding the genetic code for the incorporation of ncAAs into antibodies to generate novel and enhanced biotherapeutics. Typically, the antibodies are generated with site-specific

incorporation of an ncAA containing bioorthogonal functional groups. This allows for the site-specific coupling of drug molecules to the antibody for the generation of antibody-drug conjugates (ADCs) or for the linking together of different antibodies to engineer bispecific antibodies (bsAb) that have the ability to simultaneously recognise multiple types of epitopes (Zhou *et al.*, 2014; Kim *et al.*, 2012a). An alternative approach was taken in this thesis work, where ncAAs that influence the binding of antibodies were site-specifically incorporated for the development of a novel therapeutic. This project aimed to investigate if the site-specific incorporation of a photocaged ncAA into the antigen binding site of an antibody (in response to an amber codon, TAG) would make it inactive until exposed to light (Figure 1.1).

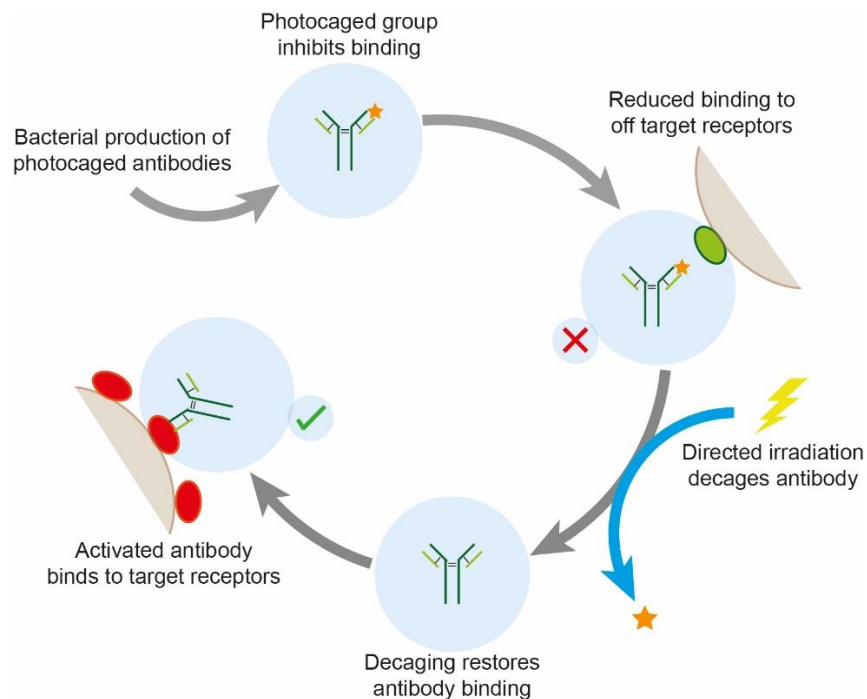


Figure 1.1: Graphic representation of photo control over antibody-antigen binding. The site-specific replacement of a canonical amino acid in an active site of the antibody fragment with a photocaged analogue (represented by the orange star) for temporary binding inhibition to the targeted antigen. Upon irradiation with light (365 nm) the photo-protective group is de-caged restoring functionality to the bioactive molecule with the conversion of the photocaged ncAA to the natural analogue.

When irradiated with light (365 nm) the irreversible photo-decaging process would occur, and natural functionality would be restored to the molecule as the photolabile group is removed. The application of light as an exogenous activation mechanism enables the spatiotemporal control over the treatment and could have many interesting applications. A common drawback of immunotherapy is the undesired side-effects of specific binding to targeted receptors on healthy cells. For example, the therapeutic antibody Cetuximab targets the cell surface epidermal growth factor receptor (EGFR) resulting in cell growth inhibition and induction of apoptosis (Baselga, 2001). It has been shown that the binding of this therapeutic antibody to healthy cells results in undesired side-effects (Nguyen *et al.*, 2009a). Controlled activation of antibodies with light at the site of tumours could potentially reduce these side effects.

1.2 Generation of orthogonal translation machinery

The incorporation of ncAA into recombinant proteins relies on the reassignment and suppression of canonical codons with mutually orthogonal aaRS/tRNA pairs. This is achieved by transferring an aaRS/tRNA pair from a different kingdom to the host organism, and evolving the amino acid binding pocket of aaRS to specifically aminoacylate its corresponding tRNA with ncAA. These evolution experiments involve using positive and negative selection methods (Figure 1.2) to identify orthogonal aaRS that bind to ncAA over endogenous amino acids in the cell (Chin, 2014). Usually, this process begins with crystal structure analysis of the aaRS to identify residues in the active site that can be rationally or randomly mutated to generate large aaRS libraries. For the positive selection, an amber codon is inserted into a gene conferring antibiotic resistance so that survival of the organism is reliant on mutated aaRSs that can aminoacylate its corresponding tRNA_{CUA} with the desired ncAA to incorporate into the gene. Survivors of the positive selection are then subjected to the negative selection in the absence of ncAA. An amber codon is inserted into a lethal gene in order to ensure mutated aaRS does not aminoacylate

tRNA_{CUA} with endogenous amino acids resulting in cell death. This process is repeated for several rounds to generate highly selective aaRS. Using this approach, highly efficient orthogonal aaRS have been engineered to incorporate hundreds of diverse ncAAs into recombinant proteins (Dumas *et al.*, 2015).

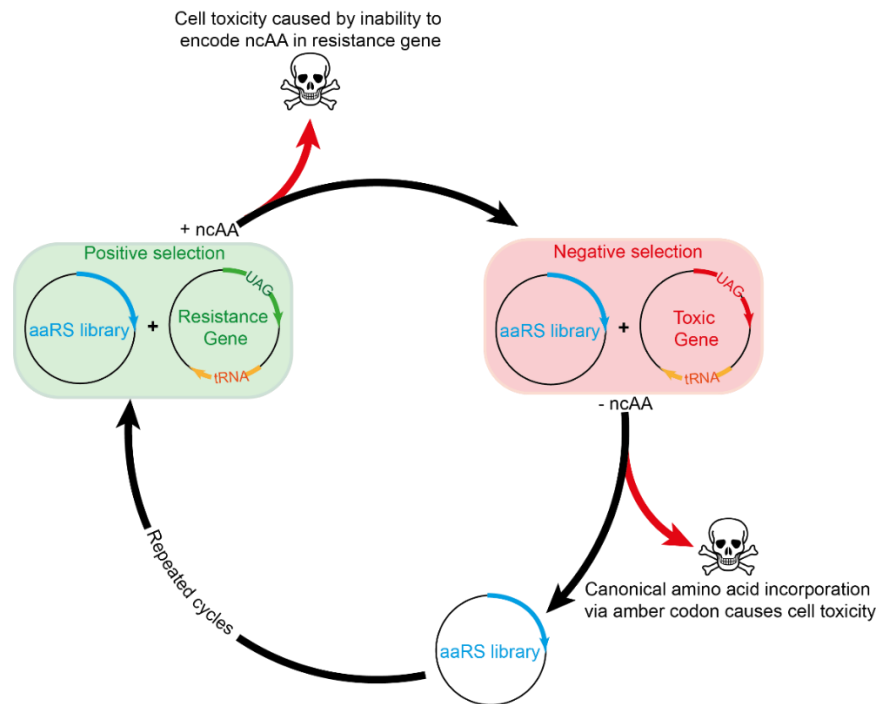


Figure 1.2: Directed evolution of aaRS/tRNA pairs for site-specific incorporation of ncAA. For positive selection, two plasmids are transformed into the host cell. The plasmid containing the aaRS library allows for the constitutive expression of potential orthogonal aaRS while the other plasmid contains an antibiotic gene required for host survival and tRNA_{CUA}. Successful aminoacylation of tRNA_{CUA} by a member from aaRS library allows for the genetic encoding of ncAA and successful expression of antibiotic gene. aaRS molecules in the library that do not aminoacylate tRNA_{CUA} with ncAA in response to amber codon will not avoid cell death in presence of antibiotic. Plasmids containing aaRS from surviving organisms are then used in negative selection to ensure that these do not aminoacylate tRNA_{CUA} with endogenous amino acids. Amber codon is substituted into a toxic gene and no ncAA is supplied to host. In the case of canonical amino acid incorporation in response to amber codon, toxic gene is expressed which leads to cell death. This process of positive/negative selection is repeated several times to generate highly selective aaRS.

The first reported *in vivo* site-specific incorporation of a ncAA in response to an amber codon was by Wang *et al.* in 2001. The recombinant protein was expressed in *Escherichia coli* (*E. coli*) using the evolved orthogonal aaRS/tRNA pair (TyrRS/tRNA_{CUA}) isolated from *Methanocaldococcus jannaschii* (*M. jannaschii* or *Mj*). The

incorporation of the ncAA *p*-Methoxyphenylalanine into the protein of interest was shown to be site-specifically expressed with high fidelity and efficiency which later led to widespread use of the *Mj*TyrRS system for the incorporation of an extensive range of aromatic ncAAs (Santoro *et al.*, 2002). The orthogonality originated as a result of the absence of a major anticodon binding region in the aaRS of *Mj*TyrRS and the significant difference between the tRNA acceptor loop of *M. jannaschii* and *E. coli* tRNAs (Steer *et al.*, 1999). Two publications in 2002 reported the discovery of pyrrolysine, the 22nd canonical amino acid used in the biosynthesis of proteins in some methanogenic archaea and bacteria (Srinivasan *et al.*, 2002, Hao *et al.*, 2002).

Interestingly, this amino acid was inserted during translation in response to an amber stop codon, this natural example of amber suppression prompted interest in the aaRS/tRNA pair, PylRS/tRNA_{CUA}, for its potential orthogonality to the translational machinery of *E. coli* and eukaryotes. It was later shown that the PylRS/tRNA_{CUA} system from *Methanosarcina barkeri* (*M. barkeri* or *Mb*) is orthogonal in *E. coli* and could incorporate many pyrrolysine analogues in response to an amber stop codon (Polycarpo *et al.*, 2006). Although wild-type PylRS was reported to have good incorporation efficiency of pyrrolysine analogues, the potential orthogonality of the PylRS/tRNA_{CUA} system in *E. coli* and eukaryotes prompted further evolutionary studies to increase the incorporation capabilities for additional ncAA with diverse chemistries. In these studies, random or targeted mutations to the active site residues of PylRS were designed using the crystal structures of *Methanosarcina mazei* (*M. mazei* or *Mm*) or *M. barkeri* as a guide, as the binding pocket of PylRS from both these organisms are well-conserved. (Neumann *et al.*, 2008b, Yanagisawa *et al.*, 2008). These evolutionary studies showed increased capabilities for the site-specific incorporation of ncAA containing functional groups at the *N*^ε nitrogen of lysine, such as *N*^ε-acetyl-lysine (Neumann *et al.*, 2008b), *N*^ε-(*tert*-butyloxycarbonyl)-L-lysine (BocLys) and *N*^ε-allyloxycarbonyl-L-lysine (AlocLys) (Yanagisawa *et al.*, 2008). The degree of specificity PylRS shows towards structurally related ncAA allows for a higher capability of incorporating ncAA derivatives which improved its desirability as an efficient aaRS.

In addition to *Mj*TyrRS/tRNA_{CUA} and *Mm/Mb*PylRS/tRNA_{CUA} pairs several other aaRS/tRNA pairs that have been less investigated for genetic code expansion, include *E. coli* TyrRS/tRNA pair and LeuRS/tRNA pair which are orthogonal in yeast (Edwards & Schimmel, 1990; Soma & Himeno, 1998) and AspRS/tRNA, SerRS/tRNA, LysRS/tRNA, GluRS/tRNA and ProRS/tRNA pairs which have been generated to have orthogonality in either prokaryotic and/or eukaryotic cells (Hughes *et al.*, 2010; Pastrnak *et al.*, 2000; Liu & Schultz, 1999; Chatterjee *et al.*, 2012).

1.3 How non-canonical amino acids (ncAAs) are incorporated

Numerous methods for incorporating ncAA into polypeptides or proteins have been developed (Dumas *et al.*, 2015). The most wide-spread method for *in vivo* incorporation of ncAA is by codon reassignment of the amber stop codon (TAG). Three of the 64 possible triplet codons are stop codons (Figure 1.3); named amber (TAG), ochre (TAA) and opal (TGA).

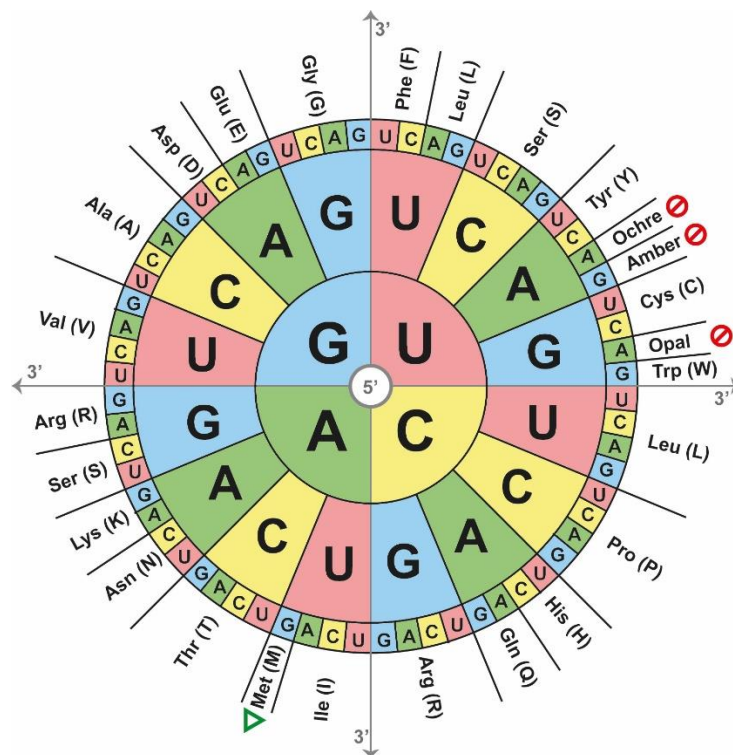


Figure 1.3: Codon table for *E. coli*. Reading for 5' (centre) to 3' (edge) enables decoding of 3 letter triplet codons to their corresponding amino acid. Stop codons are highlighted (Red stop symbol).

As these stop codons lack the corresponding tRNA charged with amino acids and instead terminate the translation process with the use of release factors, they make excellent candidates for codon reassignment. This is especially the case for the amber stop codon, which is the rarest of the three stop codons with an estimated use of 7% in *E. coli* (Nakamura *et al.*, 2000). Three key components (Figure 1.4) are required for the site-specific incorporation of ncAAs into proteins within a host organism *via* codon reassignment. First, a unique aminoacyl-tRNA synthetase (aaRS)/tRNA pair that is orthogonal to other aaRS/tRNA pairs in the host organism needs to be evolved so that it exclusively aminoacylates its corresponding orthogonal tRNA with a desired ncAA while remaining unreactive to endogenous tRNA and amino acids. The next requirement is an unassigned codon (usually the amber stop codon, TAG) that can be recognised by the orthogonal tRNA anticodon loop. Introducing this unassigned codon into a desired site in the gene of interest enables the site-specific encoding of a ncAA. The final requirement is the ncAA itself, which is commonly supplemented into the growth media or can be biosynthesised by the cell (Liu & Schultz, 2010).

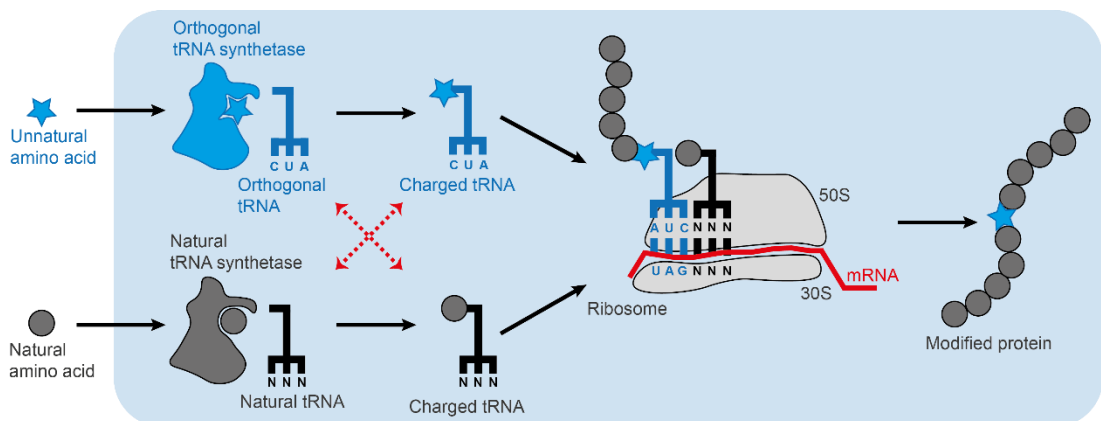


Figure 1.4: Incorporation of ncAA into a protein *via* a nonsense codon during translation. The orthogonal tRNA synthetase/tRNA recognise the amber stop codon (UAG) with the anticodon (CUA) while not interfering with endogenous translational processes (indicated by red lines). This allows for the site-specific encoding of ncAA into the structure of a recombinant protein *in vivo*.

While the amber stop codon has had the most prevalent use for codon reassignment, the developments of aaRS/tRNA for suppression of ochre and opal have also been reported (Wan *et al.*, 2010). Although these codons have a higher frequency of use in the *E. coli* genome which could lead to cell toxicity due to their suppression, they are potentially useful for the incorporation of multiple distinct ncAA (Chatterjee *et al.*, 2013).

Another active area of research in this field is to remove TAG specific release factors (RF1) within an organism allowing for higher efficiency of amber stop codon reassignment. Removal of RF1 is particularly useful when attempting to incorporate the same ncAA multiple times in different positions. Normally the efficiency of codon reassignment incorporation dramatically reduces after encoding the first ncAA; this was improved by removing competition with RF1. However, this method can affect fitness of cells as TAG codons in the host's endogenous genes are no longer read as stop codons, and the undesired extensions of polypeptide sequences causes complications in the cell (Johnson *et al.*, 2011). An effective method to avoid the negative effects of RF1 knockout is to replace the amber codons within the organism to alternative synonymous stop codons. The techniques multiplex automated genome engineering (MAGE) and hierarchical conjugative assembly genome engineering (CAGE) were used to change 321 instances of TAG amber codons to TAA ochre codons in *E. coli* strain C321.ΔA (Addgene #48998) to construct a genomically recoded organism (GRO) that has had RF1 removed and all amber codons reassigned (Lajoie *et al.*, 2013a). It was shown that the GRO had improved incorporation of ncAA in response to an amber codon without deleterious effects to host fitness. Interestingly, the GRO was reported to have increased resistance to T7 bacteriophage, likely caused by deleterious effects of the *prfA* knockout on the translation of viral proteins.

The genomic reassignment of the amber stop codon was a significant breakthrough in the emerging field of synthetic genomics. The genome editing techniques developed in this area of research have more recently been used to accomplish an engineered GRO with rare codon reassignment. Although the *E. coli* strain C321.ΔA had reassigned less frequently used stop codon for the incorporation of ncAA, it had

limited potential for the incorporation of multiple distinct ncAA. To increase the number of free codons for reassignment, Fredens *et al.* focused their attention on alternative codons (Fredens *et al.*, 2019). The genetic code has an inherent redundancy as 64 codons only encode for 20 canonical amino acids and three stop codons. This redundancy means multiple codons can synonymously encode for the same amino acid. However, it has been shown that synonymous codons can be non-equivalent, and many synonymous substitutions can have detrimental effects on regulating gene expression (Lajoie *et al.*, 2013b). Using this knowledge, Fredens and colleagues investigated reducing the redundancy of the genetic code by identifying rarely used codons and replacing all instances of the redundant codons found within the genome with synonymous codons. These techniques enabled the construction of a four-megabase synthetic *E. coli* genome that uses only 61 out of the 64 codons, by reassigning two serine codons (TCG→AGC and TCA→AGT) and the amber stop codon (TAG→TAA). This required the reassignment of 18,214 codons to remove all instances of TCG, TCA and TAG from the genome. Strain Syn61 was reported to have an increased generation time of 90 minutes when compared to MDS42, another GRO *E. coli* strain with a reported generation time of 57 minutes. However, successful incorporation of ncAA in response to the reassigned serine codon (TCG) was achieved using an orthogonal PyIRS/tRNA_{CGA} pair in Syn61 while being extremely toxic to MDS42 cells. While this is a recent breakthrough in this field, it is certainly not the last with reports of 57-codon synthetic *E. coli* genome currently in research (Ostrov *et al.*, 2016).

The number of distinct ncAA that can be incorporated into a protein is theoretically limited by the number of non-coding codons. The research mentioned above on genomically recoded organisms is a unique approach to increase the number of non-coding codons available within the organism. Another interesting concept is to incorporate nCAAs in response to quadruplet codons while simultaneously decoding standard triplet codons in the mRNA to avoid protein truncation and degradation. Quadruplet codons could offer a possible 256 additional codons to the cell (O'Donoghue *et al.*, 2012). The first report of simultaneous incorporation of distinct ncAA in response to a quadruplet codon and an amber stop codon was by Anderson

et al. in 2004. In this study L-homoglutamine (hGln) was incorporated into myoglobin *in vivo* within *E. coli* using *Pyrococcus horikoshii* orthogonal LysRS/tRNA_{AGGA} in combination with *M. jannaschii* TyrRS/tRNA_{CUA} for the incorporation of the ncAA O-methyl-L-tyrosine. Although decreased efficiency was observed with the incorporation of two distinct ncAA it was shown that the ribosome can recognise and decode quadruplet codons. Following this, investigations into the evolution of an orthogonal ribosome with higher amber suppression efficiency was reported (Wang *et al.*, 2007). To ensure minimal interaction with the endogenous translational machinery, an orthogonal translational pathway was developed based on an alternative Shine-Dalgarno sequence (Rackham & Chin, 2005). The natural Shine-Dalgarno sequence is a short recognition sequence (AGGAGG) typically found at position -7 to -4 upstream of the 5' translational start codon in mRNA (Shine & Dalgarno, 1974). Slight mutations in the sequence can increase or decrease the translation initiation efficiency in prokaryotes by altering the complementary interactions between the mRNA and ribosomal RNA and can be used as a method to control gene expression (Kozak, 1983). Instead of controlling the initiation of translation with slight mutations in the Shine-Dalgarno sequence, Rackham *et al.* developed pairs of mRNA and ribosome that do not bind to natural ribosome and endogenous mRNA in *E. coli* (Rackham & Chin, 2005), providing an orthogonal translational machinery in *E. coli*. Wang and colleagues later evolved this orthogonal ribosome (ribo-X) for efficient amber suppression (Wang *et al.*, 2007). At the time of the report, typical efficiency (defined as the ratio of full-length recombinant protein to terminated truncated protein) of ncAA incorporation into proteins in response to an amber codon was limited to 20-30%. The limited incorporation efficiency was caused by the competition between RF1 mediated peptide termination in response to an amber stop codon and orthogonal tRNA_{CUA} mediated peptide chain elongation with the addition of an ncAA. By designing an orthogonal translation pathway, the orthogonal ribosome could be evolved towards higher efficiency of amber suppression through ncAA incorporation without affecting the endogenous cellular processes. It was shown that the directed evolution of ribo-X had increased the *in vivo* incorporation efficiency of p-benzoyl-L-phenylalanine (Bpa) in response to an amber codon from 24% to 62% with the BpaRS/tRNA_{CUA} pair and ribo-X. The reported

high-fidelity and increased efficiency of the amber suppressor tRNA was in part attributed to the orthogonality of the mRNA as a result of the alternative Shine-Dalgarno sequence. The orthogonality of the mRNA allowed for separate translation systems to function independently within the living cell. A later study (Neumann *et al.*, 2010) describing an evolved ribosome (ribo-Q1) was established on the research described above. Ribo-Q1 was designed for the efficient decoding of quadruplet codons (Figure 1.5) and the highly efficient incorporation of two distinct ncAA was reported.

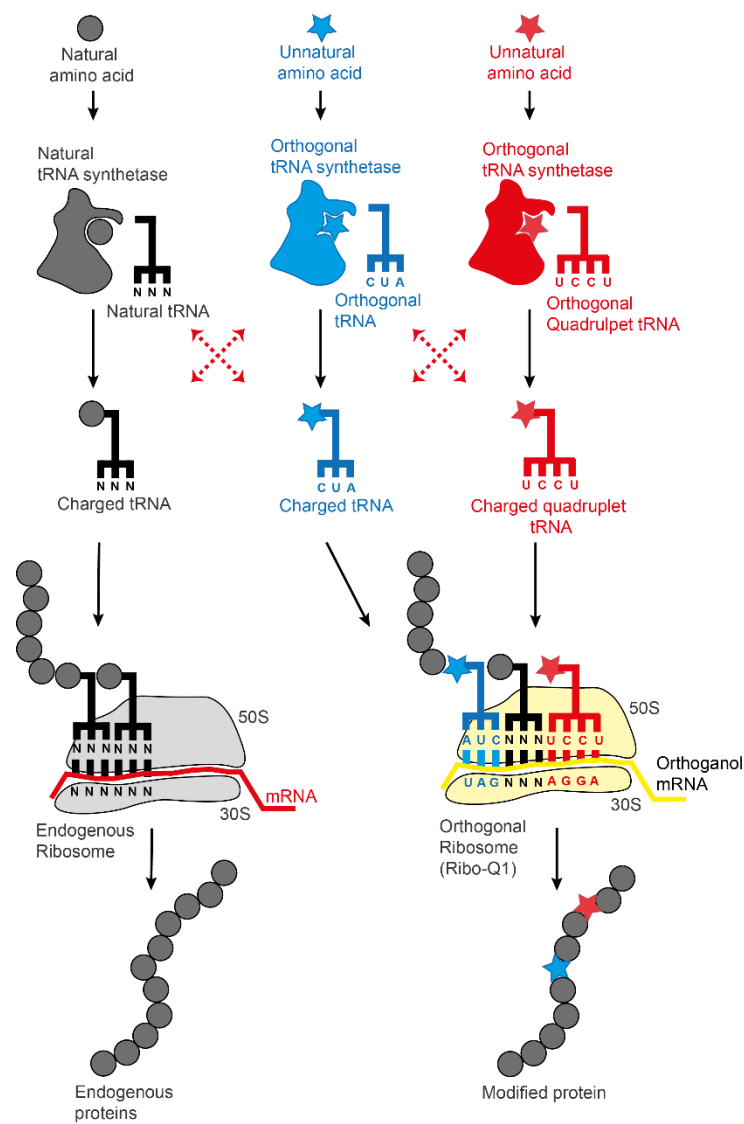


Figure 1. 5: Genetic incorporation of multiple distinct ncAA by decoding amber and quadruplet codons. In the same host organism, both the orthogonal translation pathway that uses orthogonal mRNA for the expression of modified proteins and the endogenous translation pathway that is responsible for endogenous proteins are simultaneously active. Evolved ribosome (Ribo-Q1)

exclusively recognises alternative Shine-Dalgarno sequence on orthogonal mRNA but is designed to use endogenous charged tRNA, orthogonal charged tRNA and orthogonal charged tRNA with quadruplet anticodon. This allows for the expression of modified protein with two distinct site-specifically incorporated ncAA.

This study achieved expression of glutathione S-transferase calmodulin (GST-CaM) fusion protein with the simultaneously incorporation of *N*6-[(2-propynyloxy)carbonyl]-L-lysine (CAK) with MbPylRS/ MbtRNA_{CUA} pair in response to an amber codon (TAG) and *p*-azido-L-phenylalanine (AzPhe) with AzPheRS/tRNA_{UCCU} pair in response to a quadruplet codon (AGGA). The orthogonal evolved ribosome with cognate orthogonal mRNA enabled high fidelity and efficient translation of quadruplet codons without affecting cell viability as interaction with the endogenous translational pathway was minimised reducing toxicity from frameshifts occurring *via* quadruplet decoding of the transcriptome.

1.4 Application of non-canonical amino acids

A considerable amount of literature has been published on investigating new techniques for the incorporation of ncAA *in vivo* and has demonstrated the efforts invested in designing separate cellular systems to work mutually with the natural endogenous processes within the cell. Although the foundation built through this research has been vital for the progression of this field, the applications of these techniques to alter or enhance protein function truly demonstrates the utility and flexibility of these technologies. This section will highlight research that has used ncAAs for the understanding of protein structure and function. A diverse range of genetically encoded ncAA have been used to investigate fundamental questions on protein structure and function both *in vitro* and *in vivo* (Figure 1.6). These include redox probes to investigate electron transfer in mechanistic studies (Minnihan *et al.*, 2011), isotopic labels for infrared spectroscopy and nuclear magnetic resonance (NMR) studies (Schultz *et al.*, 2006; Cellitti *et al.*, 2008), ncAA containing heavy atoms for X-ray crystallography (Pearson *et al.*, 2015), photo-crosslinkers for mapping

biological interactions *in vivo* (Chin *et al.*, 2002a) and fluorescence nAA for optical imaging (Wang *et al.*, 2006).

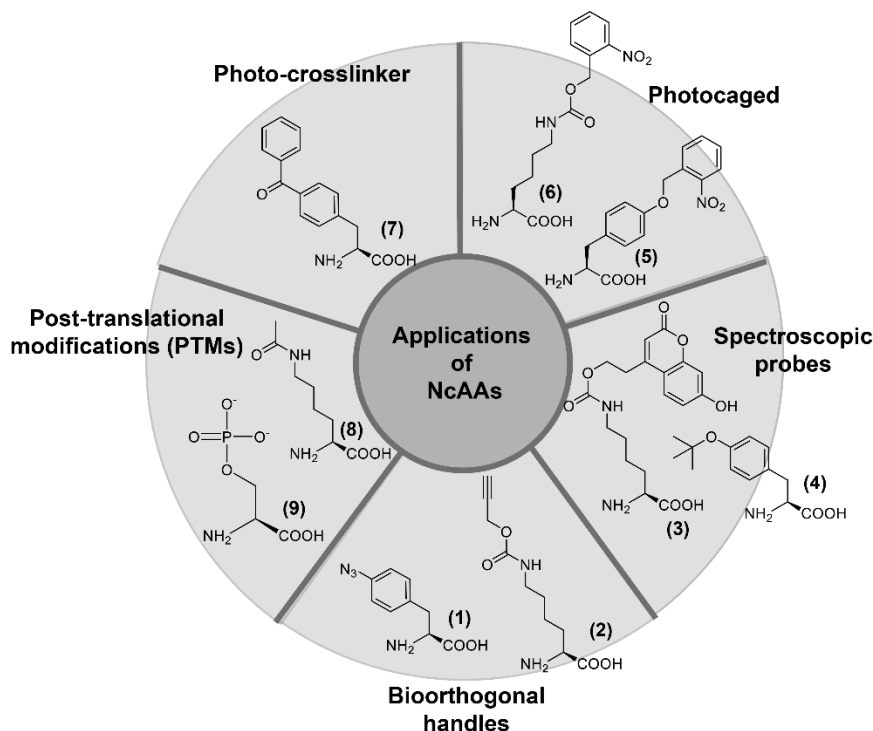


Figure 1. 6: Examples of nCAAs used in the investigation of protein structure and functions. (1) *p*-azido-phenylalanine, (2) Alkyne lysine, (3) Coumarin Lysine analogues, (4) tert-butyl tyrosine, (5) *o*-nitrobenzyl tyrosine, (6) *o*-nitrobenzyl lysine, (7) Benzoyl-phenylalanine, (8) Phosphoserine, (9) *N* ϵ -acetyl-lysine.

1.4.1 Probing protein structure and function.

Electron transfer (ET) through and between proteins is widely used in biological processes and is a fundamental driving force of the chemistry of life. The conversion of energy such as light, into forms that are usable for chemical transformations often occur as a cascade of many biological processes, such as photosynthesis. Our ability to probe electron transfer in proteins is often limited by the difficulties to site-specifically insert electron acceptors *in vivo*. The development of site-specific incorporation of nAA has facilitated the control over the acidity, basicity and redox

potential of key residues in a protein of interest. For example, the addition of fluorotyrosines (*N*-acetylfluorotyrosinamides) proved to be a useful EPR probe for studying the mechanism of radical formation in ribonucleotide reductase (Minnihan *et al.*, 2011). A more recent study (Lv *et al.*, 2015) described the insertion of 4-fluoro-3-nitrophenylalanine (FNO₂Phe) into green fluorescent protein (GFP). FNO₂Phe has been shown to have similar reductive potential to important biological reductants such as NAD(P)H. With the genetic incorporation of this ncAA it was possible to measure high-speed photoinduced electron transfer (PET) from the GFP chromophore to FNO₂Phe. These genetically incorporated probes have proved to be useful tools for the investigation of protein function. Infrared spectroscopy (IR or vibrational spectroscopy) is a powerful methodology that utilises the interaction of infrared radiation and matter to identify and characterise molecules. Introduction of functional groups with unique vibrational signature that can be identified over naturally-occurring functional groups in the protein can be achieved by genetic incorporation of ncAA infrared probes. In one example, the site-specific introduction of deuterium probes (Carbon-Deuterium C-D) *via* photocaged tyrosine analogues allowed for characterisation of specific microenvironments and dynamics of the enzyme dihydrofolate reductase (DHFR) and the ability to monitor conformation changes during its catalytic pathway (Groff *et al.*, 2009).

1.4.2 Photo-crosslinking ncAA to map protein-protein interactions.

Another method of probing and mapping protein function uses of ncAA containing photo-crosslinking side chains. Multiple photocrosslinkers have been genetically incorporated both *in vivo* and *in vitro*, including benzophenones (Chin *et al.*, 2002a), diazirine (Ai *et al.*, 2011), and aryl azides (Tippmann *et al.*, 2007) to define the structure and function of protein complexes. These photo-crosslinking side chains form covalent bonds to molecules in close proximity upon irradiation. The fast formation of covalent bonds provides positional and structural information and

allows for the investigation of weaker protein-protein interactions in their native environment that could be missed by other non-covalent methods.

For example, the use of ncAA containing benzophenone (*p*-benzoyl-L-phenylalanine or pBpa) was used to investigate lipopolysaccharides (LPS) assembly in the outer membrane of *E. coli* and allowed elucidation of intermolecular interactions within key protein complexes responsible for this task (Freinkman, *et al.*, 2011). Another use of pBpa was in the attempt to further characterise the protein-protein interactions that define transcriptional activation, and increase fundamental knowledge in functionality and binding modes of the transcription activation *in vivo* in their native context (Majmudar *et al.*, 2009). This study showed that the genetic incorporation of pBpa into the transcriptional factor (Gal4) enabled photo-cross linking *in vivo* and the identification and characterisation of a key masking protein (Gal80). Although this study was fundamentally important for the development of our understanding of transcriptional activation, several steps of isolation and purification, as well as technically challenging experiments, were required to isolate the protein of interest. A later study that aimed to reduce these experimental challenges used a bifunctional ncAA that contained benzophenone for photoactivatable cross-linking and alkynyl moiety for isolation after crosslinking (Joiner *et al.*, 2017). The bifunctional ncAA 4'-ethynyl-*p*-benzoyl-L-phenylalanine (BPKyne) was genetically incorporated with *E. coli* TyrRS/tRNA_{CUA} in yeast and photo-crosslinked with the Gal4–Gal80 transcriptional complex. The crosslinked complex was then isolated and purified by employing a subsequent reaction with the alkynyl handle.

1.4.3 Fluorescent imaging.

Another interesting application of encoding designer amino acids is the genetic incorporation of fluorescent ncAAs. The ability to modify proteins with fluorescent probes has greatly enhanced our capability to study protein dynamics *in vitro* and *in vivo*. Fluorescent proteins have been isolated from many organisms such as avGFP from the jellyfish *Aequorea victoria* (Ormö *et al.*, 1996) or DsRed derived from the

coral *Discosoma striata* (Gross *et al.*, 2000). However, due to the large size of the naturally-occurring fluorophores a common limitation of expressing fluorescent fusion proteins is the restriction of labelling the C- or N- terminus of the target protein as this can cause significant structural perturbation to the protein. Another labelling approach relies on the direct chemical labelling of reactive canonical amino acids (cysteine and lysine) with a variety of synthetic fluorophores. While methodologies for fluorescent labelling of amino acids are relatively simple, complications can arise if key residues are labelled, which can perturb protein functionality.

Furthermore, as target residues can be present at several sites within a protein with varying levels of accessibility, numerous fluorophores can be conjugated to the protein resulting in heterogeneous labelled product. Therefore, the ability to site-specifically encode fluorescent amino acid into recombinant proteins would be a powerful tool. In one example, the *MjTyrRS/MjtRNA_{CUA}* pair was evolved to incorporate L-(7-hydroxycoumarin-4-yl) ethylglycine in response to an amber codon (Wang *et al.*, 2006). This ncAA was chosen for investigation due to its high fluorescence quantum yield, small size and pH-sensitivity. Successful incorporation into whale myoglobin at Ser4TAG position was verified by electron spray ionisation mass spectrometry (ESI MS). Summerer and colleagues reported another example of a genetically incorporated fluorescent ncAA in 2006 (Summerer *et al.*, 2006), where the fluorescent amino acid dansylalanine was encoded into proteins in yeast in response to an amber codon. The majority of encoded fluorescent amino acids have excited at shorter wavelength which could present problems in live-cell microscopy. However, the methodology for genetic site-specific incorporation of these fluorescent probes provides a fast and convenient technique to label proteins with fluorophores compared to the conventional protein fusions or chemical labelling methods discussed above. The generation and encoding of longer wavelength fluorescent amino acids is an important future direction for this field.

1.4.4 Post-translational modifications.

Although over 140 different amino acids have been identified within naturally occurring proteins, the majority of these originate from post-translational modification (PTM) of the 20 canonical amino acids (Uy & Wold, 1977). PTMs are ubiquitous and highly conserved in biology and are responsible for critical roles in cellular processes such as signal transduction, which controls the underlying mechanisms of cell proliferation, gene regulation, cellular growth and metabolism (Krauss *et al.*, 2003). To further study these processes both *in vitro* and *in vivo*, it would be highly beneficial to have the ability to site-specifically incorporate amino acids with PTMs into targeted proteins. However, this is often a challenge as the enzymes responsible for the generation of PTM could be largely unknown or are not site-specific. With the powerful tools available for genetic encoding of ncAA, the ability to site-specifically incorporate amino acids with PTMs enables the direct localisation of selectively modified residues into proteins which are highly valuable for the discovery of the biological roles of these modifications. Some examples of PTMs that have been achieved with the incorporation of ncAA are phosphorylation, sulfurylation and nitration, which will be briefly discussed in this section. Numerous studies have reported the incorporation of phosphorylated amino acids such as phosphoserine (Park *et al.*, 2011), phosphothreonine (Zhang *et al.*, 2017) and phosphotyrosine (Luo *et al.*, 2017). Phosphorylation/dephosphorylation is the addition/removal of a phosphoryl group to a molecule and is critical in many biological processes, and can act as a molecular switch for protein function. For example, it has been estimated that almost half of the regulatory enzymes responsible for metabolism in yeast are subjected to phosphorylation, which offers a dynamic way to regulate protein activity and allows for higher regulation of protein-protein interactions compared to their non-phosphorylated counterparts (Vlastaridis *et al.*, 2017). In a recent study, the generation of an orthogonal aaRS/tRNA for the genetic incorporation of *O*-phosphotyrosine (pTyr) and its non-hydrolysable analogue 4-phosphomethyl-L-phenylalanine (Pmp) in *E. coli* was reported (Luo *et al.*, 2017). The encoding of pTyr and Pmp proved to be more

challenging than the incorporation of other ncAA as pTyr and Pmp required a propeptide strategy to increase the cellular uptake of these ncAA. Commonly, ncAAs are supplemented into the growth media, and cellular uptake occurs *via* transport pathways of other amino acids or small molecules. The controlled encoding of pTyr analogues at tyrosine sites facilitated the investigation of phosphotyrosine PTM in a variety of proteins sizes. *O*-Phosphoserine (Sep) is the most abundant phosphorylated amino acid within eukaryotes with 48 and 7.3 times higher abundance than phosphotyrosine and phosphothreonine, respectively (Olsen *et al.*, 2006). The evolution of an orthogonal aaRS/tRNA for the genetic incorporation of phosphoserine (Sep) was reported in model proteins within *E. coli* (Park *et al.*, 2011 & Rogerson *et al.*, 2015). This study achieved high yields of proteins containing site-specifically incorporated Sep in response to amber codon to produce biologically relevant phosphorylated proteins that were previously challenging to express.

1.4.5 Biorthogonal chemical handles.

The ability to perform chemical conjugations on biological systems is a growing area of interest in chemical biology, more specifically being able to modify biomolecules with synthetic moieties for use as diagnostic tools, therapeutic agents or for fundamental research. A general strategy for labelling proteins is the chemoselective targeting of deprotonated thiolate nucleophiles in cysteine residues or amine nucleophile in lysine residues for conjugation. However, these targets can be limiting as cysteines are often required for correct folding of proteins and lysines are often important for protein function. Furthermore, as there are often multiple targeted sites in a protein it is difficult to label a protein of interest homogeneously. A method designed to avoid these challenges is the genetic site-specific incorporation of bioorthogonal chemical handles into proteins using ncAA. Three examples of commonly used bioorthogonal groups in ncAAs are ketones (Wang *et al.*, 2003), acetylenes and azides (Deiters *et al.*, 2003). Keto groups are a versatile functional group but are absent in the 20 canonical amino acids, to overcome this natural

limitation, Wang and colleagues evolved an orthogonal aaRS/tRNA to site-specifically encode *p*-acetyl-L-phenylalanine in response to an amber codon. They demonstrated high-efficiency incorporation and showed useful protein modification by selective conjugation to a small molecule fluorophore. A similar approach was used for the incorporation of acetylenes and azides containing groups in ncAA by Deiters *et al.* Orthogonal aaRS/tRNA pairs were developed for the encoding of *p*-(propargyloxy)phenylalanine and *p*-azidophenylalanine in yeast. They then demonstrated small molecule conjugation to these unique chemical handles *via* an azide-alkyne cycloaddition reaction. More recently, a study demonstrated the attachment of two distinct bioorthogonal chemical handles in proteins to facilitate double labelling for a variety of applications (Sachdeva *et al.*, 2014). The simultaneous incorporations of two distinct ncAAs in the recombinant protein was achieved by using the *MjPrpRS*/tRNA_{CUA} pair to encode a terminal alkyne containing amino acid in response to an amber codon, and *PyIRS*/tRNA_{UACU} pair that encoded a cyclopropene containing amino acid in response to a quadruplet codon on orthogonal mRNA (using evolved ribosome, Ribo-Q1). The resulting full-length protein showed site-specific incorporation of two distinct ncAAs which were mutually orthogonal to each other. This allowed for a one-pot double labelling reaction at targeted chemical handles at physiological pH and temperature.

1.4.6 Stimuli control over bioactivity.

The ability to develop new strategies for the control over protein function *in vivo* is an interesting application of the genetic encoding of ncAAs. Versions of amino acids, for example tyrosine, lysine, serine and cysteine, containing blocking groups have been genetically encoded. Incorporating these ncAAs, in place of naturally occurring amino acid, in the active site of proteins would generate inactive versions that can be activated by certain stimuli, such as light, pH or addition of a small molecule, for detaching the blocking group. Photocaged amino acids are one such example that requires light to remove the blocking group. The photo-cleavable group allows for

the rapid control over spatial and temporal activation of the biomolecule back to its native function, which can facilitate investigations into biological processes. One strategy employed for the optical control over genome engineering was the insertion of photocaged lysine into potentially active sites within the CRISPR/Cas9 system (Hemphill *et al.*, 2015). The clustered regularly interspaced short palindromic repeats (CRISPR) targeted invasive nucleic acids with Cas proteins as an antiviral defence mechanism utilised by prokaryotes and archaea (Brouns *et al.*, 2008). Guide RNA (gRNA) is combined with Cas9 enzymes to recognise and cleave specific DNA strands dictated by the CRISPR sequence. The Cas9 enzyme has been optimised for gene editing, gene deletions and gene mutations (Hsu *et al.*, 2013) in human cells and animal models (Mali *et al.*, 2013; Gratz *et al.*, 2013). The authors showed that by replacing lysine in the Cas9 complex at position 866 with the encoding of photocaged lysine in response to an amber codon they enabled light-activated control over gene editing by CRISPR/Cas9 system. This accomplishment could allow for future spatial and temporal control of gene activation/deactivation within human cells. However, the photo-cleavage mechanism is activated upon 365 nm irradiation. Ultraviolet radiation has been shown to have poor tissue penetration which could represent additional challenges for deep tissue targets or animal models.

Furthermore, the radiations on live cells can alter the intracellular signalling networks and cause cytotoxic effects. The development of using non-invasive approaches to activate protein activity *in vivo* has gained widespread attention in recent years (Zorn & Wells, 2010). One strategy is to use small molecules to modulate protein functionality by triggering catalytic deprotection of ncAA containing blocking groups and converting these amino acids back to their native form. In one study, a palladium-mediated deprotection of a lysine derivative was designed for the activation of protein functionality *in vivo* (Li *et al.*, 2014). It was reported that the chemically caged lysine inhibited protein function until removal of caging group *via* a palladium-catalysed reaction.

1.5 Introduction to antibodies and antibody fragments

In 1975, Nobel prize winners Milstein and Köhler first described the hybridoma technology, which started the revolution of therapeutic antibody research (Köhler & Milstein, 1975). This technology allowed for large scale synthesis of antibodies and paved the way for advances in antibody engineering and development. The first generation of monoclonal antibodies (mAbs) were of murine origin and had limited clinical success, mainly due to the immune response they caused in humans, making the half-life of the molecules too short for them to act as a viable treatment (Van Kroonenburgh & Pauwels, 1988). Following this, chimeric mouse-human antibodies were designed by using the human constant (Fc) region to which a murine variable region was attached (Morrison *et al.*, 1984). These were further humanised by using whole human antibodies with the exception of the complementary determining regions (CDRs) isolated from mouse antibody (Jones *et al.*, 1985). Through the use of cloning technologies, isolation and expression of the genes encoding for full human mAbs became possible in the late 1980s (Chiang *et al.*, 1989). Although these full-length antibodies offered high-specificity, high-affinity targeting, along with increased retention time, they still suffered in their efficiency in *in vivo* applications as repeated administration resulted in human anti-mouse antibody response. Furthermore, due to the complexity of the molecule a high cost is often associated with it, along with long-term storage stability problems.

Monoclonal antibodies have become an essential research tool in experiments such as flow cytometry, immunohistochemistry, Western blots, enzyme-linked immunosorbent assay (ELISA) and many more. Additionally, they are a promising therapeutic agent owing to outstanding specificity to targeted molecules. The variable region of an antibody can be customised to bind almost any extracellular or cell surface protein, which can result in several outcomes, such as blocking downstream signalling or activating biochemical pathways (Hori *et al.*, 1991). Another advantage of non-immunogenic antibodies is their long circulation half life, which is due to their large molecular size and the binding of Fc-domain to the neonatal receptor reducing clearance from the body. Generally, full-length mAbs are

expressed in mammalian cell line cultures due to the complexities of the molecule (Birch & Racher, 2006). Full-length antibodies have been shown to express in *E. coli* as aggregates that after expression can be refolded using *in vitro* methods to generate bioactive mAbs. However, these methods are hindered by low expression yields and complex procedures (Boss *et al.*, 1984). A more recent study showed high expression yields and correct assembly of full-length mAbs in *E. coli* periplasm, which offers many advantages over mammalian expression such as shorter fermentation times and reduced costs (Simmons *et al.*, 2002). However, antibodies expressed in bacterial system lack post-translational modifications which can be important for biological application of monoclonal antibodies as glycosylation of the constant region of antibodies play an important role in humoral immune response.

Smaller antibody fragments have also gained importance due to advantages of easier expression, low cost and their ability to penetrate deeper into human tissues (Figure 1.6.A). With careful design scientists have reduced the size of mAbs without compromising on their ability to bind the target; the short chain variable fragment (scFv) is the smallest antibody fragment and only contains the variable (V_H/V_L) domains of the antibody, held together with a flexible polypeptide linker. Fragment antigen binding (Fab) fragments contain one constant and one variable domain of both the heavy and the light chain. When compared to full-size antibodies these smaller fragments promote better tissue penetration while keeping high specificity as the antigen-bind site is not modified. However, due to their monovalent nature, these antibody fragments often exhibit low retention time on the target (Adams *et al.*, 2001). This can be improved by engineering Fab and scFv fragments into dimeric, trimeric or tetrameric conjugates.

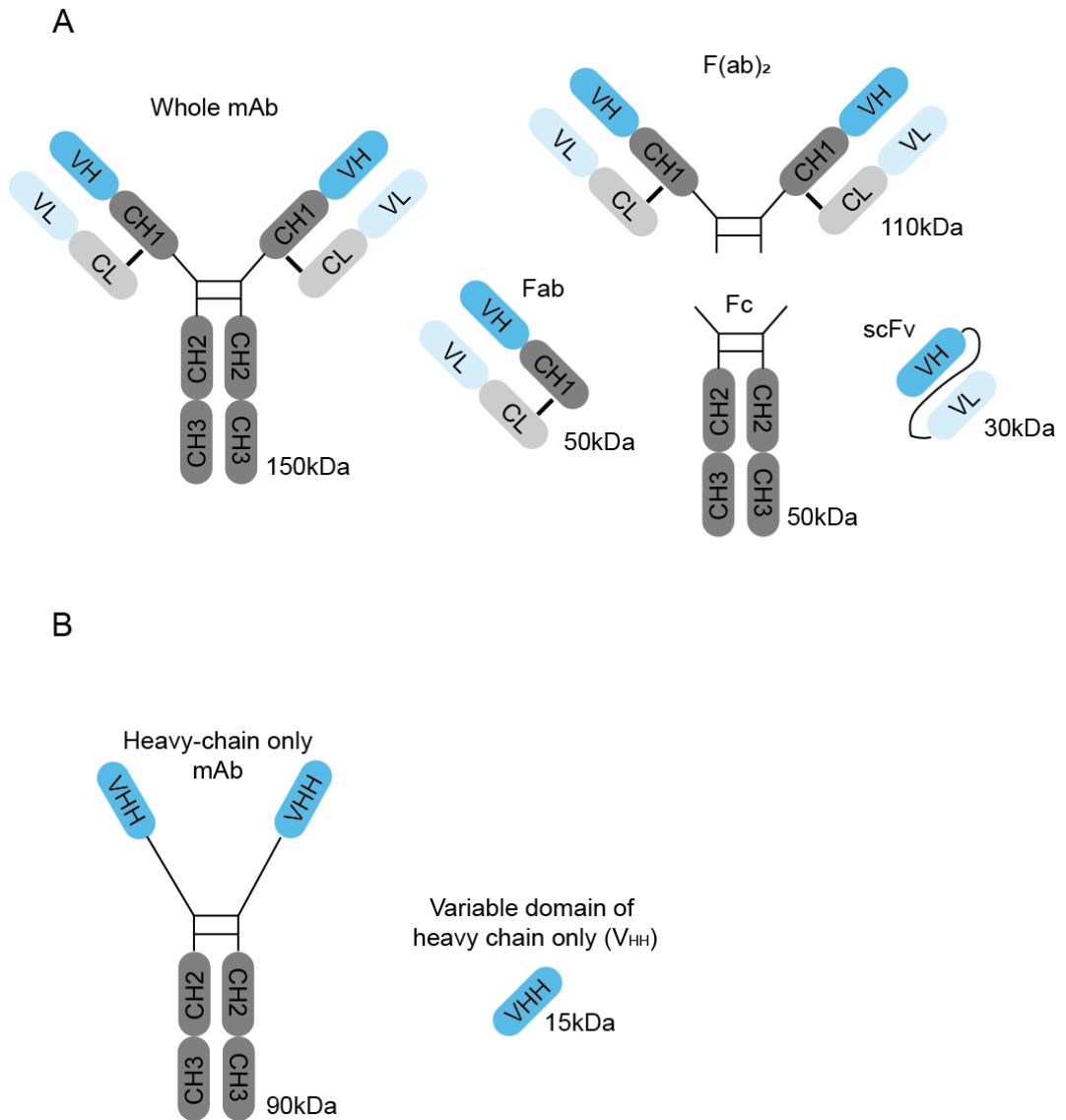


Figure 1.7: Diagram representation of various naked antibody formats. Blue ovals depict variable regions, and grey oval represent conserved regions (difference between light and heavy chains are shown by different colour intensity). A) Layout of full length mAb (150kDa) and commonly used antibody fragments (Fab, F(ab)₂, scFv, and Fc region). B) Heavy-chain only antibody (90kDa) and variable domain fragments (VHH or nanobody).

There are a number of ways to express antibodies and their corresponding fragments in *E. coli* i) the periplasm (space between the inner and outer membrane) of *E. coli* has an oxidative microenvironment making it suitable for the formation of intra-domain disulphide bonds in antibodies and antibody fragments (Charlton, 2004). To direct the polypeptide chain to the periplasmic space, the addition of an N-terminal

peptide secretion sequence upstream of the gene of interest is required, few examples of such sequences include PelB, OmpA, and PhoA. During transport to the periplasm the signalling peptide is cleaved leaving the protein of interest intact. Proteins from the periplasmic space can then be easily extracted and purified. (Rouet *et al.*, 2012). ii) Another technique for bacterial production of Ab fragments is to use *E. coli* strains engineered for the expression of recombinant proteins that contain disulphide bonds; these strains such as SHuffle (Lobstein *et al.*, 2012) contain genomic copies of proteins that can assist in the correct folding of proteins and have reductive pathway enzymes such as thioredoxin reductase (*trxB*) and glutathione reductase (*gor*) suppression and a cytoplasmic chaperone to aid in disulfide bond formation (DsbC).

In 1993, heavy chain only antibodies were discovered in camel blood when unexpected bands were observed on a Coomassie stained protein gel (Hamers-Casterman *et al.*, 1993); these results were inconsistent with the size of standard four chain (two light and two heavy) antibodies. It was later discovered that these heavy chain only antibodies are found in all camelid species and sharks. Interestingly it has also been claimed that the heavy chain antibodies in camelids evolved independently from those found in sharks (Nguyen *et al.*, 2002). These antibodies consist of two heavy chains that are each composed of two constant domains linked via a hinge to a variable domain called VHH or nanobody (Figure 1.6.B).

The variable domain (VHH or nanobody) of a heavy chain only antibody is the main part responsible for antigen binding. This has resulted in the expression of extremely small antigen binding molecules (around 15 kDa), half the size of the smallest antibody fragment (scFv 30kDa). This small molecular size offers many advantages and some potential disadvantages when compared to full-size mAb. Studies on nanobodies have revealed many interesting antigen binding characteristics that are not possible with full size or fragmented antibodies. It has been shown that due to the small size of nanobodies they are able to bind to difficult to access antigens and have higher binding affinity to cavities (De Genst *et al.*, 2006) and hidden epitopes. They can thus be used as enzyme inhibitors and antagonists for receptor function (Lauwereys *et al.*, 1998) with possible application in combating viral infection (Van

der Vaart *et al.*, 2006). Furthermore, nanobodies have the added benefits of improved solubility, ease of cloning, stability and simple production procedures, over full-length antibodies or antibody fragments.

The apparent disadvantage nanobodies have in terms of their therapeutical application is having a mass below the threshold of filtration for the renal glomeruli, thus after injection into the bloodstream they are rapidly excreted by the kidneys. It has been shown that when BALB/c mice were injected intravenously with nanobodies, their elimination half-life was estimated to be 90 minutes (Cortez-Retamozo *et al.*, 2002). This problem can be circumvented by coupling two or more nanobodies, which can also increase their pharmaceutical potential as such multimeric nanobodies can have multiple functions. Nanobodies have also been fused to albumin specific nanobody to increase their molecular size, which in turn reduces the clearance of the molecule (Dennis *et al.*, 2002). This modular nature of nanobodies means they can be linked to any molecule of interest for pharmaceutical (Conrath *et al.*, 2001), biotechnological (Szynol *et al.*, 2004) or for fundamental biological research (Hassaine *et al.*, 2014).

1.6 Uses of ncAA in antibody therapeutics

As of December 2018, the international ImMunoGeneTics information system (Lefranc *et al.*, 2008) database lists 65 whole mAb formats (including naked whole mAbs, ADCs, and bispecific mAbs) and 18 antibody fragments (including Fabs, Fc fusions, scFv fusions and bispecific scFv's) approved for clinical use. The significant industrial interest in the development and improvement of antibody treatment continues to dominate the biological therapeutic platform. Although naked whole mAbs make up the majority of the approved antibody-based therapies (60 approved out of the 65 whole mAb formats), as a single therapeutic agent, clinical efficacy remains limited. Conjugation of small molecule therapeutic agents to mAbs is one strategy to enhance clinical efficacy by increasing receptor specificity, binding affinities, structural stability and targeted toxicity (*via* drug molecules).

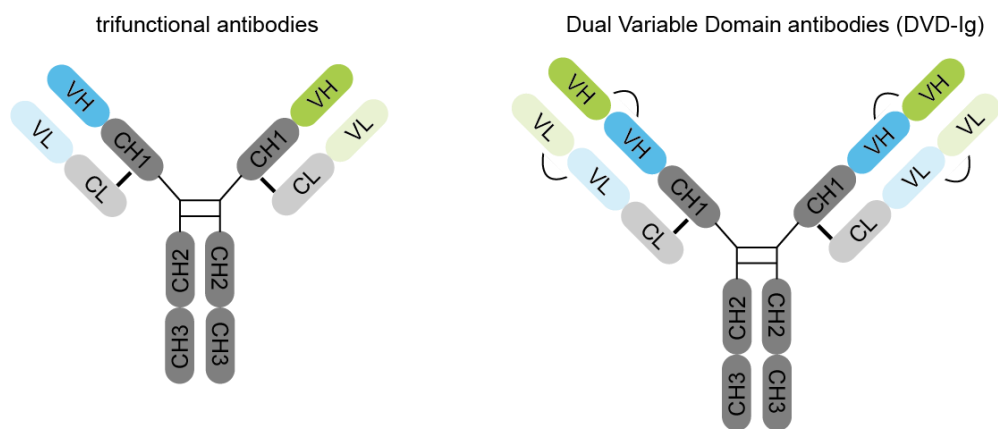
Antibody-drug conjugate (ADC) is a form of biopharmaceutical that combines the targeting specificity of mAbs with the delivery of a highly potent cytotoxic drug. Up to June 2019, five ADCs have been approved for the treatment of cancer by the European Medicines Agency (EMA) and the Food and Drug Administration (FDA). These include Gemtuzumab ozogamicin (Appelbaum *et al.*, 2017), Brentuximab vedotin (de Claro *et al.*, 2012), Trastuzumab emtansine (Amiri-Kordestani *et al.*, 2014), Inotuzumab ozogamicin (Lamb, 2017), and Polatuzumab vedotin (Deeks, 2019). Although these ADCs have shown promise in clinic, they have drawbacks through their methods of non-specific conjugation of cytotoxic drug to the antibody resulting in heterogeneous products, which can negatively affect stability, tolerability, half-life and potency of the treatment (Sievers & Senter, 2013). For example, Gemtuzumab ozogamicin (Mylotarg™) an anti-CD33 antibody conjugated to the DNA cleaving agent calicheamicin (Hamann *et al.*, 2002) was the first ADC approved for acute myeloid leukaemia and was withdrawn from the market in 2010 due to toxicity and lack of efficacy. The specificity of targeted mAb is often directed to highly expressed antigens near tumour cells or to the surface of malignant cells in an attempt to reduce cytotoxic payloads to healthy cells and improve the safety of ADCs. Often the disease target antigens are essential biological receptors that have acquired mutations affecting expression levels or activity. Although highly expressed on targeted tumour cells, basal levels of targeted receptors can be present on healthy cells. Consequently, the reduced specificity of antigen targeting between healthy and diseased cells can cause severe side-effects. For example, Cetuximab (Erbix™) is an FDA approved anti-EGFR mAb used for the treatment of head and neck cancer, metastatic colorectal cancer and metastatic lung cancer (Cunningham *et al.*, 2004). It has been reported that 70% to 80% of patients treated with Cetuximab have exhibited adverse effects, such as localised rash formation or drug-induced acneiform folliculitis (Nguyen *et al.*, 2009a). These observed side-effects of Cetuximab have been linked to the binding of mAb to healthy epidermis cells expressing basal level EGFR (Harding & Burtneis, 2005). One strategy for overcoming these detrimental drawbacks is the site-specific genetic incorporation of ncAA for bioorthogonal chemical labelling. The optimisation of the biological, structural and pharmacological properties of ADCs with the site-specific incorporation and chemical

conjugation to *p*-Acetylphenylalanine (pAcF) was reported for the anti-Her2 FAB fragment in *E. coli* and full-length mAb in mammalian cells (Axup *et al.*, 2012). The study showed site-specific linkage of a single microtubule toxin auristatin F (AF) to pAcF in the FAB fragment and dual conjugation of two microtubule toxin AF to two distinct sites within a mAb. In another study, auristatin was conjugated to *p*-acetylphenylalanine (pAzF) that was genetically encoded into anti-CXCR4 mAb *via* a stable oxime linkage (Kularatne *et al.*, 2014). Both studies reported homogeneously labelled ADC products with improved potency in mouse tumour xenograft models and increased serum half-life. Although no significant toxicity was observed with the treatment of anti-CXCR4-ADC, a modest decrease was reported in bone marrow CXCR4⁺ cell populations which could be attributed to the unwanted targeting of healthy cells. In a recent study, cyclopropene derivative of lysine (CypK) was site specifically incorporated into an anti-HER2 monoclonal antibody, Trastuzumab. The cyclopropene group in this antibody was covalently linked to tetrazine-modified MMAE (tetrazine-vcMMAE) *via* a stable dihydropyridazine linkage to give homogeneously labelled ADC (Oller-Salvia *et al.*, 2018). Site specific incorporation of bioorthogonal chemical handles into antibodies have allowed development of clinically useful homogeneous ADCs with enhanced efficacy.

A bispecific antibody (bsAb) is an artificially designed antibody that can simultaneously bind to two different epitopes. This dual specificity enables a wide range of applications such as blocking two signalling pathways simultaneously, binding and redirecting specific immune cells to tumour targets and delivering payloads to targeted cells (Dhimolea & Reichert, 2012). There are a number of bsAb formats (Figure 1.7) that roughly fall into two main categories; immunoglobulin G (IgG)-like and non-IgG-like. The IgG-like bsAb retain the traditional mAb structure with two Fab arms (heavy and light chains), each of which are specific for a different antigen or epitope, and an Fc region. Examples of IgG-like bsAb are dual variable domain antibodies (DVD-Ig) and trifunctional antibodies (Wu *et al.*, 2007; Jäger *et al.*, 2009). Due to the inclusion of the Fc region in these bsAb formats, improved solubility and stability along with increased serum half life have been reported for such antibodies. The non-IgG-like bsAb formats lack the Fc region and mainly consist of

various Fab and scFv regions. Examples of non-IgG-like bsAb formats are bispecific T-cell engagers (BiTEs), Dual Affinity Re-Targeting (DARTs), diabodies and tandem diabodies (Baeuerle & Reinhardt 2009; Moore *et al.*, 2011; Holliger *et al.*, 1993; Cochlovius *et al.*, 2000). As the non-IgG-like bsAb are smaller in size they have improved tissue penetration.

IgG-like bsAb



Non IgG-like bsAb



Figure 1.8: Layout of various bispecific antibodies formats, typically defined as two categories; immunoglobulin G (IgG)-like and non-(IgG)-like. Different targeting variable regions identified as either blue or green ovals, and conserved regions depicted as grey ovals.

Clinical success of bsAbs was shown with the approval of Catumaxomab (Removab™) in 2009 for the treatment of malignant ascites (Holmes, 2011) and the FDA-approved

blinatumomab (Blincyto™) in 2014 for the treatment of Philadelphia chromosome-negative relapsed or refractory acute lymphoblastic leukaemia (Przepiorka *et al.*, 2015). Although bsAbs have many possible advantages over traditional antibodies, their development has been hindered due to low expression yields and structural instability (Spiess *et al.*, 2015). This is mainly caused by incorrect assembly of antibody chains through quadroma methodology, which relies on the random formation of usable bsAb and can be highly inefficient. Another method for bsAb assembly is by chemical conjugation, commonly by targeting lysine or cysteine residues. However, as previously discussed with methods for developing ADCs, this method often yields heterogeneous products which are often suboptimal as therapeutics. Strategies that take advantage of genetically encoded ncAAs have emerged as a promising alternative for the generation of bispecific antibodies. In one such study, *p*-acetylphenylalanine (pAcF) was site-specifically incorporated into two Fab fragments using amber suppression. The expression of pAcF in anti-HER2 and anti-CD3 Fab fragments enabled coupling *via* a bifunctional ethylene glycol linker to generate anti-HER2/anti-CD3 bsAb (Kim *et al.*, 2012a). This study showed a simple method to generate high yielding homogeneously conjugated bispecific antibodies with excellent *in vitro* activity.

1.7 Light mediated release of photo-active therapeutics

A great deal of interest has been shown in the development of “smart drugs” that are designed to improve therapeutic efficiency and performance while minimizing negative side-effects. One therapeutic approach is the use of stimuli to activate the therapeutic molecule or to regulate the delivery and release of a therapeutic payload. The two main categories of stimuli that have been explored are, i) endogenous stimuli which include, enzyme-based activation, redox potential, pH sensitivity and chemical activation, and ii) exogenous stimuli which include light, temperature, magnetic field, ionizing radiations and ultrasound (Karimi *et al.*, 2016). The use of light as a stimulus has gained considerable attention due to localised non-

invasive activation of light-activated molecules with precise spatial and temporal control. Some examples of light-activated therapeutics include precise drug delivery *via* the photo-triggered release of an encapsulated therapeutic agent (Agasti *et al.*, 2009) or therapeutic agent covalently linked to photocaged group that can be removed upon irradiation with light (Fleige *et al.*, 2012).

The use of light as an activation mechanism has shown promising outcomes in the engineering of light responsive therapeutics. Several articles were published in the 1960s on the synthesis of photo-protective groups (PPGs) (Barton *et al.*, 1962; Barltrop & Schofield, 1962; Sheehan & Wilson, 1964). These discoveries quickly led to interests in using these PPGs for biological applications. In 1977, Engels & Schlaeger demonstrated photo-regulation of cyclic adenosine monophosphate (cAMP), and in 1978, Kaplan *et al.* successfully caged an adenosine triphosphate (ATP) derivative. The development of these light responsive biologically active molecules offered scientists experimental opportunities to gain further understanding of otherwise difficult to study biochemical processes. Over the years, PPGs have been utilised in a plethora of biologically relevant molecules for the investigation of fundamental processes and in several biomedical applications. The technique of inhibiting bioactivity *via* photocaging has been applied to a variety of biomolecules such as proteins (Sinha *et al.*, 2010), enzymes (Mentel *et al.*, 2011), receptors (Zhao *et al.*, 2006), RNA (Chaulk & MacMillan, 2007), DNA (Wang *et al.*, 2015) and amino acids (Philipson *et al.*, 2001).

An ideal light-activated drug delivery system should allow for spatial and temporal control over release of the drug in diseased tissue, while reducing drug dosage and off target toxicity to healthy cells. However, prolonged exposure to light (especially in the case of shorter wavelengths) can cause adverse side effects on healthy cells, including DNA degradation and the damaging of endogenous cellular molecules. While shorter wavelengths such as UV (200-400 nm) has sufficient energy to break covalent bonds it also has low tissue penetration depth caused by strong scattering, absorption by water and tissue and potential phototoxicity to targeted areas containing healthy tissue (Ai *et al.*, 2016). In contrast, longer wavelength light such as near-infrared (NIR, 650-900 nm) can penetrate much deeper into the tissue (Figure

1.8) and have less toxicity. However, functional groups that can be decaged by NIR are usually more complex, require complicated synthesis and have low water solubility.

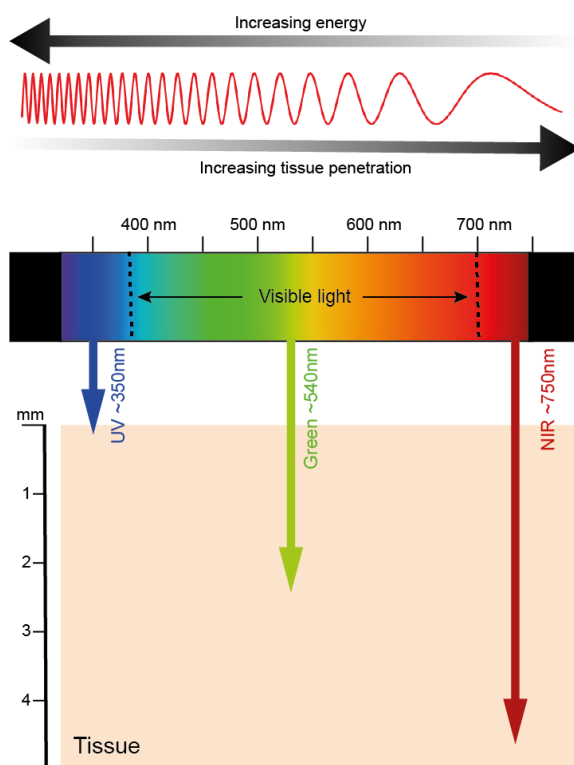


Figure 1.9: Diagram illustrating the depth of tissue penetration by light of different wavelengths. Although longer wavelength such as NIR can penetrate deeper in tissues, it often requires large complicated photocaging groups. Shorter wavelength such as UV can achieve de-caging but suffers from reduced tissue penetration.

Ideally, an upconverting strategy should be implemented to combine the advantages of short and long wavelengths. One upconverting method is the use of upconverting nanoparticles (UCNPs) which can exhibit photon upconversion. This works through the absorption of two or more incident low energy photons which are converted and emitted as a higher energy photon, this allows for the absorption of long NIR wavelengths with a resulting emission of short UV radiations (Michael Dcona *et al.*, 2015). Another method for upconversion is by using two-photon absorption (TPA). To photocleave a PPG a specific single-photon excitation is often required.

Alternatively, the application of light with approximately twice the wavelength can be used in TPA to photocleave at a higher energy state. However, this method is a third-order process and is a consequence of true nonlinear optical effect that is typically several orders of magnitude weaker than linear absorption (Warther *et al.*, 2010). The requirement of higher light intensities and specialised laser sources to adjust irradiation conditions so that the light beam focuses directly on the targeted site involves careful optimisation. However, this technique has the advantage that molecules can be activated very precisely in deep tissues (Brieke *et al.*, 2012).

As previously discussed in section 1.4.6, photocaged amino acids have been genetically encoded into proteins to achieve light mediated control over their activity. Such ncAAs has been employed for *in vitro* studies on photoregulation of ligand protein binding (Bose *et al.*, 2006), site-specific photocleavable polypeptide backbone of proteins (Peters *et al.*, 2009) and as probes for protein-DNA interactions (Lee *et al.*, 2009).

1.8 Focus of research described in this PhD thesis

The aim of this research was to develop and explore spatialtemporal control over antigen-antibody binding by light with the site-specific incorporation of photocaged ncAA into the binding site of antibody fragments. The control over antibody binding with exogenous stimuli could allow for interesting applications in improving immunotherapies. This thesis contains seven chapters. Below is a brief summary of each of these chapters:

Chapter 2: Methods and materials used during the period of this research.

Chapter 3: Investigations and development of efficient plasmid constructs for periplasmic expression of antibody fragments in *E. coli*.

Chapter 4: Exploring efficient suppressor plasmids for the genetic site-specific incorporation of several ncAAs into antibody fragments in response to an amber codon.

Chapter 5: The development and validation of an on-cell assay to assess antibody-antigen binding by light on the surface of live cancer cells.

Chapter 6: Microscopy investigation into the real-time antigen binding of photocaged antibody fragments on the surface of live cancer cells.

Chapter 7: Final discussion and future work.

CHAPTER 2

Methods

2.1 Methods

2.1.1 Cell Lines

For mammalian cell line tissue cultures; Epithelial squamous carcinoma cell line, A431, and human breast adenocarcinoma cell line, MDA-MB-231, were purchased from Sigma-Aldrich. All mammalian cell lines were cultured in DMEM (Gibco, Invitrogen) containing L-glutamine, 4.5 g/L D-Glucose, 110 mg/L Sodium pyruvate, 10% (v/v) foetal bovine serum (FBS), and a cocktail of penicillin and streptomycin (PEN/STREP). This medium will be referred to as complete medium (Appendix A.1).

2.1.2 Escherichia coli strains

Many different commercially available *E. coli* strains are commonly used for a specific purpose: fast growth, routine cloning, long-term storage, expression of recombinant proteins and many more. *Table 1* outlines the strains used during this thesis, along with their primary uses and their genotypes.

Table 2.1: E. coli strains

Strain	Natural resistance	Primary use	Genotype
DH10B	Streptomycin	General cloning and long-term glycerol stock storage	F ⁻ endA1 recA1 galE15 galK16 nupG rpsL ΔlacX74 Φ80lacZΔM15 araD139 Δ(ara,leu)7697 mcrA Δ(mrr-hsdRMS-mcrBC) λ ⁻
BL21(DE3)		High level expression of recombinant proteins under T7 control	<i>E. coli</i> B F ⁻ dcm ompT hsdS(r _B ⁻ m _B ⁻) gal λ(DE3)

BL21(DE3) pLysS	Chloramphenicol	Slightly reduced expression of recombinant proteins with tighter control over T7 basal expression	<i>E. coli</i> B F ⁻ <i>dcm ompT hsdS</i> (r _B ⁻ m _B ⁻) <i>gal</i> λ(DE3) [pLysS Cam ^r]
XL10 Gold	Tetracycline and Chloramphenicol	High competency cloning for PCR mutagenesis	<i>endA1 glnV44 recA1 thi-1 gyrA96 relA1 lac Hte</i> Δ(<i>mcrA</i>)183 Δ(<i>mcrCB-hsdSMR-mrr</i>)173 <i>tet^R F'</i> [<i>proAB lacI^qZΔM15 Tn10(Tet^R Amy Cm^R)</i>]
SHuffle T7	Low levels of streptomycin	T7 Protein expression with enhanced capacity to correctly form disulphide bonds in the cytoplasm	<i>F' lac, pro, lacI^q / Δ(ara-leu)7697 araD139 fhuA2 lacZ::T7 gene1 Δ(phoA)Pvull phoR ahpC* galE (or U) galK λatt::pNEB3-r1-cDsbC(Spec^R, lacI^q) ΔtrxB rpsL150(Str^R) Δgor Δ(malF)3</i>

2.1.3 Plasmids

Table 2.2: Plasmid list of cloned plasmids synthesised during this project. Details of cloning strategies are listed in the results section, or alternatively, AddGene product code is provided in description.

Plasmid name	Antibiotic resistance	Description
pSANG10-3F	Kanamycin	(AddGene 39264) Periplasmic expression vector
pSANG10-3F-BG4	Kanamycin	(AddGene 55756) Periplasmic expression vector for ScFv BG4
pSANG10-7D12	Kanamycin	Periplasmic expression vector for VHH 7D12 (Anti-EGFR)

pSANG10-7D12(K3TAG)	Kanamycin	Periplasmic expression vector for VHH 7D12 with amber stop codon in position 3 (Lysine)
pSANG10-7D12(K43TAG)	Kanamycin	Periplasmic expression vector for VHH 7D12 with amber stop codon in position 43 (Lysine)
pSANG10-7D12(K65TAG)	Kanamycin	Periplasmic expression vector for VHH 7D12 with amber stop codon in position 65 (Lysine)
pSANG10-7D12(K76TAG)	Kanamycin	Periplasmic expression vector for VHH 7D12 with amber stop codon in position 76 (Lysine)
pSANG10-7D12(K87TAG)	Kanamycin	Periplasmic expression vector for VHH 7D12 with amber stop codon in position 87 (Lysine)
pSANG10-7D12(Y32TAG)	Kanamycin	Periplasmic expression vector for VHH 7D12 with amber stop codon in position 32 (Tyrosine)
pSANG10-7D12(Y109TAG)	Kanamycin	Periplasmic expression vector for VHH 7D12 with amber stop codon in position 109 (Tyrosine)
pSANG10-7D12(Y113TAG)	Kanamycin	Periplasmic expression vector for VHH 7D12 with amber stop codon in position 113 (Tyrosine)
pULTRA_CNF	Spectinomycin	(AddGene 48215) Suppressor plasmid containing <i>MjCNFRS/MjtRNA_{CUA}</i>
pULTRA_PCY	Spectinomycin	Suppressor plasmid containing <i>MjPCYRS/MjtRNA_{CUA}</i>
pULTRA_(wt)PylRS_PylRNA	Spectinomycin	Suppressor plasmid containing <i>PylRS/PyltRNA_{CUA}</i>
pAS61_PCK	Spectinomycin	Suppressor plasmid containing <i>PylPCKRS/PyltRNA_{CUA}</i>
pSANG10-FAB225	Kanamycin	Periplasmic expression vector for FAB C225 (Anti-EGFR)

pAraH6HATT	Chloramphenicol	Periplasmic expression vector for human FAB against tetanus toxoid
pSANG10-VHH-R2	Kanamycin	Periplasmic expression vector for VHH R2 (Anti-R6)
pSANG10-VHH-2Rs15d	Kanamycin	Periplasmic expression vector for VHH 2Rs15d (Anti-HER2)
pSANG10-VHH-2Rs15d (Y37TAG)	Kanamycin	Periplasmic expression vector for VHH 2Rs15d with amber stop codon in position 37 (Tyrosine)
pSANG10-VHH-2Rs15d (R38AGA)	Kanamycin	Periplasmic expression vector for VHH 2Rs15d with amber stop codon in position 37 and upstream synonymous codon mutation
pSANG10-VHH-2Rs15d (R38CGA)	Kanamycin	Periplasmic expression vector for VHH 2Rs15d with amber stop codon in position 37 and upstream synonymous codon mutation
pSANG10-VHH-2Rs15d (R38CGG)	Kanamycin	Periplasmic expression vector for VHH 2Rs15d with amber stop codon in position 37 and upstream synonymous codon mutation
pSANG10-VHH-2Rs15d (R38AGG)	Kanamycin	Periplasmic expression vector for VHH 2Rs15d with amber stop codon in position 37 and upstream synonymous codon mutation
pSANG10-VHH-2Rs15d (R38CGT)	Kanamycin	Periplasmic expression vector for VHH 2Rs15d with amber stop codon in position 37 and upstream synonymous codon mutation

2.1.4 Subculturing adherent cell line

Cell line passaging was typically performed at 80-90% confluence. Growth medium was removed from T-75 flask, and adhered cells were washed once with 10 mL of DPBS. To detach cells, 3 mL of pre-warmed trypsin-EDTA (Sigma-Aldrich) was added

to T-75 flask and incubated at 37°C for 2 minutes. After 2 minutes, detachment was checked using a microscope, if cells were not completely detached they were further incubated at 37°C for 1 minute increments until complete dissociation occurred. Once cells were detached, 7 mL of complete medium was added, and 10 mL total volume was transferred to a sterile 15 mL falcon tube. Cells were pelleted at 300 g for 5 minutes. Supernatant was removed, and pellet was resuspended in 10 mL complete medium. 1 mL of suspended cells were added to 9 mL fresh complete medium and transferred to a sterile T-75 flask and incubated at 37°C, 5% CO₂. Every 2-3 days medium was replaced with complete medium until 80-90% confluence was observed, when re-passaging was performed.

2.1.5 Cell line storage

To thaw cell lines stored in liquid nitrogen, cryovials containing cells were placed in 37°C water bath with constant shaking until about 80% were thawed. 1 mL of thawed cells were quickly pipetted into 3 mL pre-warmed complete medium. Cells were pelleted at 300 g for 5 minutes, supernatant was removed, and pellet was resuspended in 4 mL complete medium. Resuspended cells were transferred to sterile T-25 flask and incubated at 37°C, 5% CO₂. After 24 hours, cells were checked for attachment, and medium was replaced.

To make cell line stocks for long-term storage, cells were passaged at least twice before being grown to 80-90% confluence. The protocol for subculturing adherent cell line (2.1.4) was followed to detach cells and centrifuge. 10 mL of freezing medium (90% FBS, 10% DMSO) was added to resuspend cell pellet, and then 1 mL of resuspended cells were aliquoted into cryovials. Cryovials were placed in an isopropanol chamber Mr Frosty Freezing Container (Thermo Scientific) and stored at -80°C overnight. The next day, cryovials were transferred to liquid nitrogen for long-term storage.

2.1.6 Competent cells

To produce a large stock of *E. coli* that can be used to efficiently transform bacterial cells, two methods are primarily used to induce competence. The first being chemical induced competent cells, and secondly, electroshock (electroporation) induced competent cells. To start, 5 mL of LB broth (Appendix A.1) was inoculated with an *E. coli* strain and incubated overnight at 37°C in a shaking incubator (220 rpm). The following day, 50 mL LB broth was subcultured with overnight culture to an OD₆₀₀-0.1 and grown at 37°C, 200 rpm until OD₆₀₀-0.4-0.5. After this stage the two methods for inducing competence differ.

For electrocompetent cells, the culture was centrifuged at 4000 rpm (20 minutes, 4°C). Supernatant was decanted, and pellet was resuspended in 25 mL ice-cold sterile Mili-Q H₂O. Cells were centrifuged again at 4000 rpm (20 minutes, 4°C), decanted and resuspended in 25 mL ice-cold 15% glycerol. A final centrifuge at 4000 rpm (20 minutes, 4°C) was performed. The supernatant was decanted, and cells were resuspended in remaining liquid. These electrocompetent cells were then aliquoted and stored at -80°C.

For chemically competent cells, the culture was transferred to a sterile falcon tube and centrifuged at 8000 rpm for 8 minutes at 4°C. The pellet was drained and resuspended in 8 mL of transformation buffer 1 (Appendix A.1) and incubated on ice for 15 minutes. Cells were then centrifuged again at 8000 rpm, 8 minutes at 4°C. The supernatant was thoroughly drained, and the pellet was resuspended in 4 mL transformation buffer 2 (Appendix A.1). The chemically competent cells were then aliquoted and stored at -80°C.

2.1.7 Transformation

Transformation and selection of bacteria is a crucial procedure in molecular biology. This is the process by which foreign DNA (plasmids) are inserted into a bacterial cell.

This is important not only for bacterial expression of recombinant genes but also because the cells can be used as a means of storage and replication of plasmid DNA.

To transform chemically competent cells, the cells were first removed from -80°C and left on ice for 5-10 minutes to thaw. 50 µL of competent cells were aliquoted into a fresh sterile Eppendorf tube, and 1 µL of plasmid DNA was added. After gentle mixing, the cells were incubated on ice for 15-20 minutes. Heat shock at 42°C for 45 seconds allows for cellular uptake of plasmid DNA. Cells were then immediately transferred onto ice for 5 minutes. 1 mL of pre-warmed SOB (Appendix A.1) was added to cells and incubated on a heatblock for 1 hour at 37°C (600 rpm). Cells were then centrifuged at 8000 rpm for 5 minutes, 800 µL of supernatant was removed, and the pellet was resuspended in remaining liquid. 50 µL of resuspended cells were transferred onto an LB agar (Appendix A.1) plate containing relevant selection antibiotics and grown overnight at 37°C.

2.1.8 Molecular cloning

Molecular cloning is a set of essential experimental methods in the life sciences that are used to assemble recombinant DNA molecules for propagation within a host organism (Lessard, 2013). For the work done in this thesis, these methods refer to the isolation of a DNA sequence (typically a gene), its insertion into a vector, the transformation of competent *E. coli* and identification of positive clones *via* an antibiotic selection marker.

2.1.8.1 DNA measurements

Concentrations of DNA were measured on NanoPhotometer (IMPLEN) that uses UV-Visible spectroscopy to detect DNA in the sample at a wavelength of 260 nm. To confirm the purity of DNA, 260/280 ratio was used, typically a ratio of around 1.8 is

accepted as pure DNA and a value of around 2 is accepted as pure RNA. 260/230 ratio was used to check for contaminants in the sample, with the expected value for a pure sample at 2-2.2.

2.1.8.2 Restriction enzyme digestion

A restriction enzyme is an enzyme that recognises specific sequences within DNA called restriction sites. These enzymes can cleave DNA at the restriction site resulting in DNA fragments. During the period of this study, several different restriction enzymes from NEB (New England BioLabs) were used. The reactions were set up to the manufacturer's specifications, typically with variations in temperature, incubation time and reaction buffer. For example, in a 25 μL reaction, 0.5 μg of DNA was mixed with 2.5 μL of 10X NEBuffer and 5 units of each restriction enzyme (generally 0.5 μL). Sterile Mili-Q water was added to make the final volume to 25 μL and the mixture was incubated at 37°C for 1 hour (temperature and time are dependent on enzymes). DNA fragments were then resolved on a 1% agarose-TAE gel, run for 40 minutes at 120V.

2.1.8.3 Agarose gel extraction

QIAquick Gel Extraction Kit (Qiagen) was used to purify DNA fragments from 1% agarose-TAE gel. Standard manufacturers protocol was followed, and DNA extracted was eluted in 40 μL of pre-warmed (50°C) sterile Mili-Q water.

2.1.8.4 Plasmid DNA amplification and extraction

QIAprep Spin Miniprep Kit (Qiagen) was used to isolate plasmid DNA from bacterial inoculations. To start, the plasmid was transformed into DH10B *E. coli* cells and grown overnight (37°C) on LB agar plates containing appropriate antibiotics (Appendix Table A.1). Then a single colony was inoculated into 5 mL LB broth with antibiotics and grown overnight in a shaking incubator (37°C, 200 rpm). Standard QIAprep Spin Miniprep protocol was followed to isolate plasmid DNA from overnight culture.

2.1.8.5 Polymerase chain reaction (PCR)

The polymerase chain reaction (PCR) is a widely used microbiology technique for exponential amplification of a particular region in DNA *in vitro*. This technique relies on the rapid heating and cooling to drive temperature-dependent reactions. Specifically, denaturation of DNA (98°C), annealing of primers (50-72°C) and extension of new DNA (72°C). During this period of study, Q5 High-Fidelity DNA Polymerase (NEB), reaction buffer (NEB) and dNTP's (NEB) was used and set up to manufacturers standards. Table 2.3 lists reagents used and final concentrations, and table 2.4 describes PCR reaction conditions.

Table 2.3: PCR reagents list with concentrations used followed to manufacturer's standards.

Reagent	50 µL reaction	Final concentration
Q5 Reaction Buffer (5X)	5 µL	1X
Forward Primer (10 µM)	2.5 µL	0.5 µM
Reverse Primer (10 µM)	2.5 µL	0.5 µM

dNTPs (10 mM)	1 μ L	200 μ M
Template DNA	\sim 0.2 μ L	< 1000 ng
Q5 High-Fidelity DNA Polymerase*	0.5 μ L	0.02 U/ μ l
Sterile mili-Q water	Adjust to 50 μ L	

*Reagent is added last before mixing.

Table 2.4: PCR cycle times and temperatures.

Step	Temperature	Time
Initial denaturation	98°C	30 Seconds
30 Cycles	98°C	5–10 seconds
Denaturation, annealing, extension	*50-72°C	10–30 seconds
	72°C	30 seconds/kb
Final extention	72°C	2 minutes
Hold	4°C	Indefinitely

*Calculated from NEB primer annealing tool.

2.1.8.6 Gibson assembly

Gibson assembly (NEB) is a cloning technique designed to ligate a DNA insert into a digested vector. The reaction is carried out by 5' exonuclease that creates a 25-40 bp single strand overhang on the DNA fragment. These overhangs which are designed to be complementary allow for the 2 or more fragments to anneal before being repaired by a polymerase and a DNA ligase (Gibson *et al.*, 2009). The reactions were set up to the manufacturer's specifications. For a 5 μ L reaction, 2.5 μ L of Gibson Assembly Master Mix (2X) was mixed with 0.02–0.5 pmols of vector and insert. For optimised cloning efficiency, the amount of insert used was 2-3 fold in excess of to

the amount of vector. Samples were then incubated at 50°C for 1 hour then transferred to ice or -20°C. 2 µL of assembly reaction was then directly transformed into DH10B.

2.1.8.7 T4 ligation

Another ligation technique used during this study was T4 ligation (NEB). T4 DNA ligase is an enzyme that catalyses the formation of covalent phosphodiester bonds between the 5' phosphate and 3' hydroxyl termini of digested DNA fragments. Before setting up this reaction, the vector and insert were digested with the same restriction enzymes. Following the manufacturers' specification, in a 20 µL reaction, 2 µL T4 DNA Ligase Buffer (10X) was mixed with vector DNA (0.020 pmol), insert DNA (0.060 pmol) and 1 µL T4 DNA Ligase. The reaction volume was adjusted to 20 µL with sterile Milli-Q water, and the reaction was incubated at room temperature for 1 hour. Heat inactivation of T4 DNA ligase can be done at 65°C for 10 minutes if ligation reaction needed to be stored at -20°C. Otherwise, DH10B cells were directly transformed with 2 µL of ligation reaction.

2.1.8.8 Sequencing

New clones assembled by Gibson or T4 ligation were sent for Sanger sequence verification. For each sanger sequence reaction, 5 µL of plasmid DNA (100 ng/µL) and 5 µL of appropriate sequencing primer (3.2 pmol/µL) were sent to Source Bioscience. Sequence analysis was carried out on CLC Main Workbench (Qiagen).

2.1.8.9 Site-directed mutagenesis

To carry out vector modification, QuikChange XL Site-Directed Mutagenesis Kit (Agilent Technologies) was used to the manufacturers specifications. Mutagenic primers (IDT) were used in combination with PCR (Table 2.3 and 2.4) to amplify parental DNA with mutated target site, generating nicked circular strands. To remove parental DNA, DpnI digestion (10 U/ μ L, 37°C, 1 hour) was used to digest methylated DNA and remaining nicked dsDNA was transformed (2.1.7) into XL10-gold ultracompetent cells and grown on LB agar plates with corresponding antibiotics.

2.1.9 Periplasmic expression (Rouet *et al*, 2012)

After expression plasmids were verified by Sanger sequencing, they were transformed into an expression cell line (Table 2.1) and grown overnight (37°C, 16 hours) on LB agar plates with appropriate antibiotics. A single colony from the agar plate was used to inoculate 10 mL 2XTY-G (2XTY media, 4% glucose and appropriate antibiotics; Appendix A.1) and grown in a shaking incubator overnight (37°C, 200 rpm, 16 hours). Once grown, the overnight culture OD₆₀₀ was recorded and used to subculture 500 mL fresh 2XTY-G to an OD₆₀₀ of 0.1. This was then incubated until OD₆₀₀ reached 0.4-0.6 (37°C, 220rpm, 2-3 h) and induced with IPTG (1 mM final concentration). After induction, cells were incubated overnight (30°C, 180 rpm, 16 hours). To extract periplasmic proteins, cells were pelleted at 3200 g, 4°C for 10 minutes. The supernatant was discarded, and pellet was resuspended with 25 mL periplasmic buffer 1 (Appendix A.1). The resuspended cells were incubated on ice for 30 minutes then centrifuged at 10,000 g, 4°C for 10 minutes. The supernatant was transferred to a sterile falcon tube and stored on ice (periplasmic fraction). The pellet was resuspended with periplasmic buffer 2 (Appendix A.1) and incubated on ice for 20 minutes. After incubation, cells were centrifuged again at 10,000 g, 4°C for 10 minutes. The resulting supernatant was collected (osmotic fraction) and pooled

together with the periplasmic fraction. To remove any bacterial cells that may have been collected in the extraction process, the fractions were filtered through a 0.22 μm vacuum filter unit. Overnight dialysis with 1X PBS (Appendix A.1) was carried out on the sample to remove unwanted macromolecules from solution.

2.1.10 Ni-NTA purification

To purify the protein of interest from periplasmic extraction, Ni-NTA gravity-flow columns were used. After overnight dialysis 1 mL of Ni-NTA resin was added to fractions and incubated at 4°C for 1 hour with gentle rocking. This was then transferred to gravity-flow column and washed twice with 10 mL PBS and once with 8 mL of Ni-NTA wash buffer (Appendix A.1), to remove non-specific binding to resin. To elute, 500 μL of Ni-NTA elution buffer (Appendix A.1) was added to resin bed and incubated at room temperature for 15 minutes before collection. This was repeated 8-10 times resulting in 4-5 mL total elution. To remove imidazole, overnight dialysis was performed against 1X PBS.

2.1.11 Concentrating protein

To concentrate protein samples, Vivaspin 500 MWCO 3 kDa spin concentrator (Sigma) were used. 500 μL of sample was added to the concentration column and centrifuged at 15,000 x g for 30 minutes until the desired volume was reached.

2.1.12 SDS Polyacrylamide gel electrophoresis (PAGE)

For further analysis of expressed proteins, SDS-PAGE was used as a method for separating protein by mass. Precast NuPAGE 4-12% Bis-Tris Protein Gels (Invitrogen)

were used in either 10-well or 20-well format with MES running buffer. 5 μ L of Precision Plus Protein Unstained Standards (Bio-Rad) was used as the protein ladder. For sample preparation, 15 μ L of protein (typically, 20 μ M results in a well-defined band) was mixed with 5 μ L of NuPAGE LDS sample buffer (4X) and heated to 95°C for 5 minutes. Before loading the sample onto the gel, it was centrifuged at 13k rpm, 4°C for 15 minutes. Optimal run time with MES running buffer is 200V for 35 minutes or until the dye front had reached the bottom of the gel. Gels were stained with InstantBlue (Sigma-Aldrich) at room temperature with gentle rocking for 2-16 hours, and destained with Mili-Q water. Images were acquired with a Gel Doc XR+ system (Bio-Rad) and processed on ImageLab software (Bio-Rad).

2.1.13 Western blot

A widely used analytical technique western blot was frequently used throughout the period of study. This is a general method of detecting a specific protein within a complex mixture of proteins, particularly, by detection of the C-terminus polyhistidine-tag (6xHis-Tag). For the qualitative detection of protein with 6xHis-tag, the protein was separated by mass on a polyacrylamide gel (as described in 2.1.12) and transferred onto a nitrocellulose membrane (iBLOT 2 Transfer Stack, Invitrogen). To achieve this, an iBLOT 2 Dry Blotting System (Invitrogen) was used, set to manufacturers specifications. After transfer, the membrane was incubated in western blot blocking buffer (10% milk in PBST) for 1 hour, room temperature and gentle rocking. After removing blocking buffer, the membrane was incubated in primary antibody (Mouse-anti-6X-HIS tag, Invitrogen) for 1 hour, with gentle rocking at room temperature. After primary antibody incubation, the membrane was washed three times with PBST (5-10 minutes, gentle rocking), and incubated in secondary antibody (Anti-mouse, IgG, HPR-linked, Invitrogen) for 1 hour at room temperature with gentle rocking. The two antibody incubation steps for 1 hour at room temperature can alternatively be done overnight at 4°C. Three final washes in PBST (5-10 minutes, gentle rocking) are done after secondary antibody incubation.

Membrane was then developed using SuperSignal Chemiluminescent Substrate (Thermo Scientific) and imaged using GelDoc XR+ system (Bio-rad).

2.1.14 BCA protein assay

To measure the total protein concentration of a sample, the Pierce BCA Protein Assay Kit (Thermo Scientific) was used. This Colorimetric assay measured total protein concentration at 562 nm using a standard spectrophotometer or plate reader (A562nm). Setting up the Microplate procedure for measurement on a plate reader, nine standards of known BSA concentrations are used for plotting a standard curve.

To make the BCA working reagent, 50 parts Reagent A was mixed with 1 part Reagent B (50:1, reagent A:B). 10 μ L of protein of interest and standards were pipetted into separate wells of a 96-well plate, and 200 μ L of WR was added. Plate as then incubated at 37°C for 30 minutes, then absorbance measured at 562 nm on a plate reader.

2.1.15 De-caging genetically incorporated pcY

Irradiated samples used in on-cell assay were acquired by irradiating wt7D12, 7D12pcY32, 7D12pcY109 and 7D12pcY113 with 365 nm light from a UV transilluminator (GelDocMega; BioSystematica). Measured 365 nm UV intensity of the transilluminator by laser power meter (FieldMate; Coherent) resulted in 14 mW intensity and a calculated photon flux of 32.8 mW/cm² (Surface area of coverslip 2.54cm²). Samples were loaded onto an 18 mm glass coverslip irradiated for 4 minutes with 365 nm light for de-caging and de-caged samples were transferred to 1.5 ml Eppendorf tube for protein concentration measurements and direct use in on-cell assay. For de-caging pcY with the microscope, DAPI channel was used for 1 minute during microscopy experiment. Measured 365 nm UV intensity of the DAPI

channel by laser power meter (FieldMate; Coherent) resulted in 8 mW intensity and a calculated photon flux of 0.25 mW/cm² (40x 1.3 NA Plan-Neofluar objective area of 3.06mm²).

2.1.16 On-cell assay

Cell lines A431 (Sigma-Aldrich, Cat. No. 85090402) and MDA-MB-231 (Sigma-Aldrich, Cat. No. 92020424) were used in these experiments. Cell lines were grown in complete medium using standard tissue culture procedures in T-75 flasks until 80-90% confluence. After washing with 1X PBS and trypsinising cells, cells were pelleted (300 g, 5 min) and resuspended in 10 mL complete medium. The cells were then counted on a hemocytometer and diluted to 200,000 cells/mL. 200 µL of this solution was dispensed into each well (40,000 cells/well) of white 96-well plate (Corning, 3903) and grown overnight until 80-90% confluence. Once the desired confluence was reached the medium was replaced with 200 µL of fresh complete medium. Dilutions of antibody fragments were prepared on a clear 96-well plate in complete medium and transferred to white 96-well plate containing cells *via* multichannel pipette. The plate was incubated for 10 minutes (37°C, 5% CO₂). After removing medium, the cells were washed with complete medium then fixed using 150 µL of 3.7% formaldehyde in each well and incubated at room temperature for 20 minutes. Formaldehyde solution was removed, and cells were washed 3 times (200 µL, 5 minutes, gentle rocking) with PBST (1X PBS, 0.1% Tween 20). After removing wash buffer, 100 µL of blocking buffer (10% milk in PBST) was added to each well and incubated at room temperature for 1 h with gentle rocking. The blocking buffer was removed. 50 µL of solution containing primary anti-6x-His tag antibody was added to each well, and the plate was incubated (room temperature, 1 hour, gentle rocking). The primary antibody solution contained mouse anti-6x-His tag antibody (Thermo Fisher Scientific) at 1:500 dilution and 1% milk in PBST. After primary antibody incubation cells in each well were washed three times with PBST (200 µL, 5 minutes, gentle rocking). 50 µL of secondary antibody solution was added to each well and

incubated (room temperature, 1 hour, gentle rocking). This solution contained an HRP-linked antibody (Anti-mouse, IgG, HRP-linked) at a dilution of 1:1000 in 1% milk and PBST. Secondary antibody was removed, and cells in each well were washed five times with PBST (200 μ L, 5 minutes, gentle rocking). Finally, 200 μ L of SuperSignal Chemiluminescent Substrate (Thermo Scientific) was added, and the plate was imaged using BIORAD GelDoc XR+. The plate was further quantified by measuring chemiluminescence signal using a CLARIOstar plate reader (BMG labtech).

2.1.17 Labelling reaction

To a 37.5 μ L solution of antibody fragments (100 μ M), 51 μ L of water, 1.5 μ L of 10 mM dye in DMF (Thermo Fisher Scientific) and 10 μ L of 1 M NaHCO₃ (pH 8) was added. The reaction mixture was incubated at 25°C for 1 h with shaking (600rpm). To remove excess fluorophore, the labelled samples were applied to Zeba desalting columns (MWCO 7000 Da, Thermo Fisher Scientific). To ensure that all the unbound fluorophore was removed, each sample was passed through the columns three times. The concentration was determined using a calorimetric Pierce BCA protein assay (Thermo Fisher Scientific) measured at 562 nm.

2.1.18 Stationary Microscopy

A431 cell line was seeded at 80,000 cells/well in a 24-well plate (Corning, 3526) and grown until 80% confluence was reached (16-18 hours, 37°C, 5% CO₂). For all live-cell imaging experiments, a physiological imaging medium was used to provide better clarity and reduced background Imaging medium (Appendix A.1) contained 120 mM NaCl, 5 mM KCl, 2 mM CaCl₂.2H₂O, 1 mM MgCl₂.6H₂O, 1 mM NaH₂PO₄, 1 mM NaHCO₃, 25 mM HEPES and adjusted to 7.2 pH. Once adjusted, medium was supplemented with 11 mM Glucose, 2.5 mM myo-Inositol, 2 mM Glutamine and 50X BME amino acids (Sigma-Aldrich). Once desired confluence was reached, cells were

washed three times with imaging medium and 297 μL of fresh imaging medium added to each well. 3 μL stocks of 100x labelled nanobody were added to each well making the total volume 300 μL . Then the 24-well plate was incubated for 10 minutes (37°C, 5% CO_2) before washing with fresh imaging medium and acquiring data. Filter sets used during these experiments were; blue filter set (Zeiss cube #49, Ex = 365 nm, Em = 445/450 nm), red filter set (TexRed, Zeiss cube #43HE, Ex = 572 \pm 14 nm, Dichroic = 593 nm (Semrock), Em = 629 \pm 28 nm (Semrock)), GFP filter set (Zeiss cube #13 dichroic, Ex = 472 \pm 15 nm, Dichroic = 495 nm (Zeiss), Em = 520 \pm 17.5 nm).

2.1.19 Dynamic Microscopy

A431 cell line was seeded at 400,000 cells/mL in an ultra-low attachment 6-well plate (Corning, 3471) containing 18 mm cover glass (2 mL per well). Once 80-90% confluence was observed, the coverslip was washed three times with imaging medium and mounted into a Ludin chamber (Life imaging services). A peristaltic pump was connected to the microscope chamber and allowed for a constant flow of imaging media over live cells at a rate of 1 mL/min. Time-lapse was set up to take brightfield and fluorescence images every 30 seconds. Cells were imaged on a Zeiss Axiovert 200M microscope at 37°C using Zeiss AxioVision software. Brightfield and fluorescence images were captured using a 40x (1.3 NA) Plan-Neofluar, oil-immersion objective lens and a Zeiss AxioCam MRm CCD camera. BODIPY-TMR-X fluorescence was excited at 572 \pm 14 nm and emission collected at 629 \pm 28 nm. BODIPY-FL fluorescence was excited at 472 \pm 15 nm and emission collected at 520 \pm 17.5 nm. Microscopy images were processed by Fiji (ImageJ).

2.1.20 Cell viability

A431 cells were seeded (2 mL, 400,000 cell/well) into ultra-low attachment 6-well plate (Corning, 3471) containing 18 mm cover glass and incubated overnight (37°C, 5% CO₂). For irradiation with 365 nm light, glass coverslip was transferred to either a microscopy chamber for UV exposure via Zeiss Axiovert 200M microscope or placed on a UV transilluminator (GelDocMega; BioSystematica). Irradiation treatment of A431 cells occurred for 1 minute and 4 minutes with control at 0 minutes before coverslip was transferred to complete medium. Cells were allowed to proliferate for 24-48 hours before cells were detached from the coverslips with trypsin, centrifuged (300 *g*, 5 minutes), resuspended in complete medium and added at 200 µL/well in a 96-well plate. Resaruzin (0.1 mg/mL in PBS; Sigma-Aldrich) was added to the cells in a 1:10 dilution for 2 h at 37 °C. Resaruzin exhibits a blue colour and low fluorescence in metabolically inactive cells but is converted to a highly fluorescent product (resorufin) upon metabolism by viable cells. Fluorescence was then measured on a Flexstation 3 plate reader (Molecular Devices; laser excitation, 570 nm; emission detection, 600 nm).

CHAPTER 3

Periplasmic expression of antibody fragments

3.1 Introduction

The first chapter of this thesis provided extensive examples of protein modification with the site-specific encoding of ncAAs and illustrated the utility and flexibility of expanding the genetic code to alter or enhance protein function and/or structure. This chapter will build the groundwork for the design and optimisation of expression systems to achieve high fidelity production of therapeutically relevant antibodies and antibody fragments for later modification with ncAAs. Before the genetic incorporation of ncAA into proteins, a highly efficient expression platform is required that allows for high expression yields of correctly folded antibody/antibody fragments. One of the most popular host organisms for the expression of recombinant proteins is *E. coli*. This well-established host organism offers short culturing times, simple and effective genetic manipulations while retaining low culturing and maintenance costs.

Prior to implementing this host organism for the high-level production of recombinant proteins, numerous design considerations require careful attention for the generation of highly efficient expression platforms. Often expressed recombinant proteins can cause toxicity to the host organism affecting cell growth and production yields. The challenging endeavour of balancing minimal cell toxicity to maximum recombinant protein yields has led researchers to develop a repertoire of genetic tools. A standard method to reduce toxicity is to tightly control the expression of the recombinant protein with the addition of inducible promoters, transcription terminators, and leader sequences or by regulating the origin of replication (Ori) which confers control over the number of plasmids present in the cell. The next section will briefly introduce the various genetic techniques developed by researchers over the years while highlighting specific systems used in this chapter.

3.1.1 Promoter

A straightforward method of controlling the regulation of expressed recombinant proteins is with the addition of an upstream promoter region. A promoter is a region of DNA that initiates transcription of a particular gene and is typically either constitutive (always active) or inducible (active in response to a stimuli). A natural example of tight inducible regulation of gene expression is the *lac* operon found in *E. coli*. The *lac* promoter controls expression of the *lac* operon and is inhibited by the *lac* repressor (LacI) in the absence of lactose. When glucose is not available to the cell, and an abundance of lactose is present, the tightly regulated *lac* promoter is activated when allolactose binds and inactivates the *lac* repressor which allows for the transcription of three structural genes (LacZ, LacY, and LacA) required for the metabolism of lactose (Oehler *et al.*, 1990). Researchers have used this knowledge in the development of inducible systems with a derivative of the *lac* promoter (*lacUV5* promoter) that is insensitive to catabolite repression (enabling expression in the presence of glucose) and is only switched on in the presence of allolactose (Wanner *et al.*, 1978). As allolactose is degraded by the cell (catalysed by β -galactosidase), a synthetic non-hydrolyzable analogue isopropyl β -D-1-thiogalactopyranoside (IPTG) can be used as a stable activation substrate for transcription under *lac* and *lacUV5* promoters as concentrations remain constant during the experiment. Although this control mechanism has been described as a tightly regulated expression system, in actuality, the *lac* operon is active at low levels which lead to low level expression without addition of the inducer (Pothoulakis & Ellis, 2015). Furthermore, the *lac* promoter and its derivative *lacUV5* are relatively weak and are rarely used for the high-level expression of recombinant proteins (Baneyx, 1999). Rather synthetic hybrids such as *tac* and *trc* promoters are commonly used which consist of the -35 region of the *trp* (tryptophan) promoter and the -10 region of the *lac* promoter (*tac* and *trc* promoters differ by 1 bp) resulting in two relatively strong promoters (De Boer *et al.*, 1983; Brosius *et al.*, 1985).

Since its development, the T7 promoter system has become an extremely popular tool for recombinant protein expression in molecular biology. Almost three decades ago, three independent studies were published on the T7-*lac* promoter-operator system (Deuschle *et al.*, 1989; Giordano *et al.*, 1989; Dubendorf & Studier, 1991) based on earlier work that introduced the bacteriophage T7 RNA polymerase (T7 RNAP) into *E. coli* for high level expression of a specific target gene (Tabor & Richardson, 1985). It was shown that the highly active T7 RNAP could transcribe mRNA at rates several times higher than endogenous *E. coli* RNA polymerase and was highly selective for its own promoter sequence. However, such transcriptional activity when uncontrolled could cause cellular toxicity due to high basal level expression of recombinant proteins. In the T7 system the transcription of the gene of interest is controlled by the T7 promoter which is recognised by T7 RNAP. The highly active T7 RNAP is encoded into the genome of certain strains of *E. coli* (Such as BL21(DE3)) and is under the control of the *lacUV5* promoter so that production of T7 RNAP is dependent on addition of IPTG which then enables T7 RNAP to transcribe the gene of interest. The leaky expression of the *lac* promoter can lead to production of low levels of T7 RNAP but can be controlled with the basal expression of T7 lysozyme provided to the cell *via* a plasmid, pLysS (Studier, 1991).

Transcription from the promoters discussed so far has focused on the initiation by IPTG induction. However, several systems have been developed to respond to alternative chemical or physical signals such as arabinose induction (*ara* promoters) and temperature induction (*cspA* promoter). The constitutive and inducible promoters used or discussed in this thesis have been listed in Table 3.1.

Table 3.1: Promoters

Promoter	Induction	Level of expression	Additional information
<i>lac</i>	IPTG	Weak	
<i>lacUV5</i>	IPTG	Weak	Derivative of the <i>lac</i> promoter not subject to cAMP dependent regulation

<i>tac</i>	IPTG	Strong	Accumulation of recombinant protein 15-30% of total cell protein
<i>trc</i>	IPTG	Strong	Accumulation of recombinant protein 15-30% of total cell protein
T7-<i>lac</i> operator	IPTG	Very strong	Accumulation of recombinant protein 40-50% of total cell protein
<i>araBAD</i>	Arabinose	Moderately Strong	Weaker than the <i>tac</i> and <i>trc</i> promoters
<i>proK</i>	Constitutive	Weak	
<i>glnS'</i>	Constitutive	Weak	modified variant of the <i>glnS</i> promoter

E. coli mRNA promoter information compiled from databases and literature (Hershberg *et al.*, 2000; Lisser & Margalit, 1993).

3.1.2 Plasmid copy number

A plasmid origin of replication is a stretch of sequence within a plasmid at which replication is initiated (Del Solar & Espinosa, 2000). The nature of the origin of replication determines the copy number of the nucleic acid molecule and variations in this sequence can result in varying levels of plasmid populations. A simple misunderstanding would be to assume that a higher plasmid copy number directly equates to an increase in recombinant protein yield. However, this can often place a metabolic burden on the host and cause plasmid instability leading to detrimental effects to cell viability and reduced expression levels (Bentley *et al.*, 1990). The regulatory mechanisms of high copy plasmids often differ considerably compared to low copy number plasmids. Typically, the control of replication of an ORI is referred to as relaxed or stringent depending on the method of replication initiation by countertranscribed RNA (ctRNA), or protein, or both (Snyder & Champness, 2013). ORI incompatibility is the inability of two plasmids to coexist stably within a cell and can result in plasmid “curing” (loss of plasmid during cell division). If two plasmids cannot coexist stably within a cell they belong in the same incompatibility group, similarly, if plasmid stability is observed between two plasmids they are members of

different incompatibility groups. Two factors determining the incompatibility grouping of plasmids is if they share the same replication control or if they share the same partitioning system.

If similar replication controls are used between different plasmids it can cause underrepresentation of one of the plasmids as the replication control system does not recognise the two plasmids as different. As the cell divides, the plasmid with less copies are not equally distributed to the daughter cell, and through subsequent cell divisions, the daughter cells are more likely to be cured of one of the plasmids. The partitioning system is important for its role in segregating plasmids into daughter cells during cell division, if two plasmids share the same partitioning system, unequal distribution of plasmids to the daughter cells can occur resulting in the curing of one the plasmids. Incompatibility grouping becomes an important factor in the genetic encoding of ncAAs as two or more plasmids are often required for the production of the recombinant protein (*via* expression plasmid) with the basal expression of orthogonal translational machinery (*via* suppressor plasmid).

3.1.3 Selection marker

During this thesis, many different antibiotic resistance genes were used as positive selection markers for plasmid maintenance. This positive selection method confers antibiotic resistance to host cells that carry the plasmid of interest while inhibiting the growth of plasmid free cells. Usually, the resistance gene inserted into the plasmid backbone contains the information required for the production of an enzyme that inactivates certain antibiotics. Antibiotics such as ampicillin (*bla* gene; Sutcliffe, 1978), chloramphenicol (*cat* gene; Shaw, 1983) and kanamycin (*Neo* gene; Umezawa, 1979) are degraded by the enzymatic counterpart facilitating antibiotic resistance to the host. However, the continuous production of these enzymes leads to sustained degradation and depletion of the antibiotic allowing the growth of plasmid free organisms over time (Korpimäki *et al.*, 2003). Alternatively, the use of

the antibiotic tetracycline could overcome this problem. Tetracycline facilitates cell toxicity by blocking the A site of the ribosome and inhibiting protein synthesis (Roberts, 1996). Resistance to this molecule is primarily achieved due to genes encoding an energy-dependent efflux pump that actively eject tetracycline from the cell or with the production of ribosomal protection protein (Roberts, 2005). As the antibiotic is not degraded it has been shown that host resistance and tetracycline activity remain highly stable during cultivation. Typically, the plasmid used during this thesis had already been optimised for expression, and the genetic manipulation only required removal and insertion of expression genes, and no editing of the antibiotic marker was necessary. However, similar to the ORI considerations discussed above, careful planning was required when transforming two or more plasmids as inserting multiple selection markers of the same type would not allow the host to differentiate between plasmids and cell survival would not depend on the uptake of multiple plasmids.

3.1.4 Affinity tag

Although the incorporation of affinity tags to recombinant proteins do not directly control or maintain optimum expression, they can be used as a method for the purification of expressed proteins from the *E. coli* cellular milieu and as a method of protein detection during expression and purification steps (Nilsson *et al.*, 1997). Two types of affinity tags are often fused to proteins to achieve the above benefits; the first is a small stretch of amino acids which forms a peptide tag, and the second being a larger polypeptide called a fusion tag. Furthermore, the larger fusion tags can be used as solubility enhancers for difficult to express proteins. Commonly used fusion tags such as glutathione S-transferase (GST; Smith & Johnson, 1988) and ubiquitin (Baker, 1996) have been shown to enhance solubility of fused proteins (Raran-Kurussi & Waugh, 2012) but also require extra steps in the removal of the polypeptide tag which can result in unknown solubility of cleaved recombinant protein. Peptide tags have less interference with protein structure due to their smaller size and normally

do not inhibit the biological activity of the recombinant protein. However, certain cases have been reported in which the structure and activity of the protein was negatively influenced by peptide tags (Buchert *et al.*, 2002). Common examples of peptide tags are FLAG-tag, His-tag and c-Myc-tag which can be attached to the N-terminal or C-terminal ends of the recombinant protein. In this study, the use of His-tagged proteins allowed for the efficient downstream purification of the protein of interest from complex mixtures of extracted periplasmic proteins. Furthermore, the His-tag was used in analytical detection techniques such as Western blot to check for successful expression of full-length recombinant proteins and played a vital role in the development of an on-cell assay. The polyhistidine-tag (His-tag or 6xHis-tag) is a six histidine amino acid motif that is commonly added to the C- or N-terminal ends of a recombinant protein for later use in purification (Hochuli *et al.*, 1988). As histidine residues are strongly involved with binding to metal ions, the addition of a chain of histidine residues at the end of a protein directly increases the proteins affinity to binding to metal ions. This knowledge was used in the development of purification techniques for His-tagged proteins by immobilising Ni²⁺ or Co²⁺ to carriers to which the histidine residues are chelated or removed as a method of isolating His-tagged protein with high purity.

3.1.5 Leader sequence

Protein toxicity may arise if the recombinant protein expressed within the host cell has unnecessary and/or detrimental interactions with endogenous processes. A possible solution to this problem is the exporting of the protein to the periplasmic space or extracellular environment (Mergulhao *et al.*, 2005). This can be achieved by attaching a leader sequence region upstream of the initiation codon (N-terminus) that directs recombinant proteins outside of the cell or to the bacterial periplasm. Another interesting application of directing recombinant proteins to the periplasm is the ability to facilitate disulfide bond formation and the correct folding of certain proteins *via* the oxidising environment of the periplasm (Charlton, 2004). This is

especially relevant to this project as the troubled expression of correctly folded antibody and antibody fragments in *E. coli* (due to the reducing environment of the cytosol) is a well reported obstacle to overcome in a bacterial expression system designed for the production of therapeutically active antibodies.

3.2 Results & discussion

3.2.1 Construction of periplasmic expression vectors

As discussed previously, one of the major challenges in antibody fragment expression in bacterial systems is the reducing environment of the cytoplasm, which inhibits the formation of disulphide bridges. To overcome this challenge, researchers have designed a method to translocate expressed polypeptide chains to the periplasm as the oxidising conditions of the periplasm in Gram-negative bacteria, allow for the correct formation of intradomain disulphide bonds (Georgiou & Segatori, 2005). During this study, the pectate lyase B (PelB) signal peptide sequence identified in *Erwinia carotovora* (Lei *et al.*, 1987) was used extensively in expression vectors to direct antibody fragments to the periplasm. In Gram-negative *E. coli* cells this 22 amino acid sequence (Table 3.2) at the N-terminus is recognised and targeted by SRP (signal recognition particle, a protein-RNA complex) that directs specific proteins to the translocation machinery of the general secretory pathway so that they are secreted to the periplasmic space. For large scale production of heavy chain only variable fragments (VHH) an expression vector was designed for optimised periplasmic expression of recombinant protein.

Table 3.2: Leader sequences used throughout this study.

Leader sequence	Amino acid sequence*	Reference
Pectate lyase B (PelB)	MKYLLPTAAAGLLLLLAAQPAMA	Lei <i>et al.</i> , 1987
Outer membrane protein A (OmpA)	MKKTAIAlAVALAGFATVAQA	Ghrayeb <i>et al.</i> , 1984
Alkaline phosphatase (PhoA)	MKQSTIALALLPLLFTPVTKA	Oka <i>et al.</i> , 1985

* Sequences identified through signal peptide database (Kapp, 2010)

This expression system (Figure 3.1) included an inducible T7 promoter, N-terminal signal peptide (PelB) and a C-terminal 6xHis-tag for purification and analysis. These constructs were explicitly designed for direct cloning into selected plasmid backbones using Gibson assembly (New England Biolabs), this required 25-40 base pair (bp) overlapping regions at the 5` and 3` ends and codon optimisation for expression in *E. coli*. After designing these gene fragments, they were sourced as gBlocks from Integrated DNA Technologies (IDT) and cloned into the respective expression vectors.

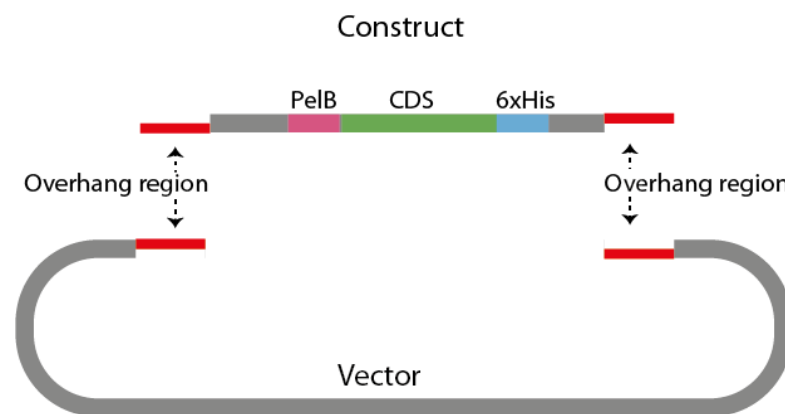


Figure 3.1: Graphic illustrating Gibson assembly insertion of expression construct. Red overhang regions designed as 25-40 bp complementary sequences.

Before ordering and synthesising the gBlocks, the IDT codon optimisation tool was used to optimise the codon usage of the expression construct for *E. coli*. As codon usage depends on the host organism, heterologous genes will often suffer from reduced expression due to the presence of rare codons. When rare codons are included in the CDS, the corresponding rare tRNAs are depleted at a faster rate than the abundant tRNAs which can lead to amino acid incorporation errors and protein truncation (Gustafsson *et al.*, 2004). By altering rare codons in a reading frame to a synonymous, frequently used codons expression yields of heterologous recombinant proteins are improved (Plotkin & Kudla, 2011).

Initially, two vectors were selected for the insertion of the periplasmic expression construct. First pRSF-D11-G9-GST was chosen due to its optimisation for incorporation of two distinct ncAAs. This large 11kb plasmid contains the sequences for a quadruplet decoding orthogonal ribosome along with an orthogonal ribosomal binding site (oRBS). The second plasmid was pSANG10-3F-BG4 (Addgene; 55756) which was selected for its optimised expression and characterisation of scFv antibody fragment BG4 (Biffi *et al.*, 2013). The recombinant protein selected for periplasmic expression was VHH 7D12 (PDB; 4KRL). The 7D12 sequence was obtained from in-depth literature search on crystal structures of EGFR specific antibody fragments. EGFR has been shown to be implicated in many human cancers including colorectal, brain, lung, head and neck (Baselga & Arteaga, 2005) and has become a popular cancer therapeutic target for antibody-based drugs. In a study characterising 7D12 together with other anti-EGFR VHH (Schmitz *et al.*, 2013) it was reported that 7D12 had relatively high K_D ($219 \text{ nM} \pm 20$) compared to other antibody fragments that target the same receptor (FABC225; $K_D - 2.3 \text{ nM} \pm 0.5$; Li *et al.*, 2005). However, these K_D results from SPR experiments measured binding of VHH 7D12 to sEGFR rather than cell-surface EGFR which had been previously reported in the low nanomolar range (Oliveira *et al.*, 2012). Additionally, Schmitz *et al.* showed that VHH 7D12 had similar binding mechanisms to the full-length mAb cetuximab, 7D12 was shown to bind strongly to domain III of sEGFR ($K_D - 47 \text{ nM} \pm 3.6$).

For the cloning of VHH 7D12 gene construct into the pRSF vector, plasmid pRSF-D11-G9-GST was digested with BamHI-HF and SpeI (37°C , 1 hour with Cutsmart buffer). The vector backbone was separated on a 1% agarose gel and purified with QIAquick Gel Extraction Kit (QIAGEN). A synthetic gBlock was designed (Appendix Table A.3; GB003) to contain 25 bp overlapping regions complementary to the insert area of the cut pRSF vector. This gBlock contained an oRBS required for multiple incorporation of unnatural amino acids. Gibson assembly was used to ligate the gBlock into digested pRSF-D11-G9-GST (50°C , 1 hour) and the ligation mixture was subsequently transformed into DH10B cells. Cells were plated onto LB agar (Kan), single colonies were isolated, and the plasmid DNA sequence was verified by Sanger sequencing (SourceBioscience). A similar cloning strategy was implemented to insert 7D12

periplasmic expression construct into pSANG10-3F vector. pSANG10-3F-BG4 was digested with HindIII-HF and XbaI (37°C, 1 hour with Cutsmart buffer), gBlock was designed (Appendix Table A.3; GB002) containing 25 bp overlapping regions and cloned into pSANG10-3F with Gibson assembly. After transformation with the ligation mixture, cells were plated on LB agar (Kan), and single colonies were isolated and the plasmid DNA sequence was verified by Sanger sequencing. This resulted in two new plasmids, pSANG10-7D12 and pRSF-7D12 (Figure 3.2).

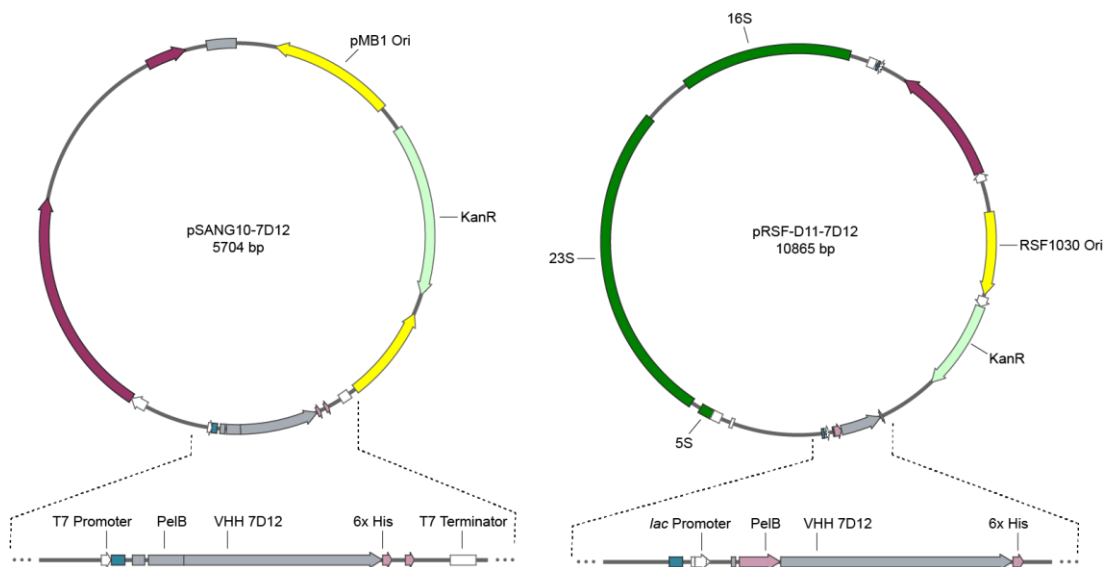


Figure 3.2: Plasmid maps of pSANG10-7D12 and pRSF-D11-7D12 with inserted 7D12 expression construct.

Several similarities between the two expression vectors are observed, such as kanamycin resistance marker, His-tag for purification and PelB leader sequence for periplasmic expression of recombinant proteins. An observable difference between the two plasmids is in the origin of replication. In the pSANG10 vector a mutated version of the pMB1 origin (ColE1-derivative; Minton, 1984) is used which facilitates a high plasmid copy number of 500–700 copies per cell. In contrast, the pRSF vector contains the RSF1030 origin, which is another high copy number origin (>100 copies per cell) that is compatible with ColE1 derived origins (Som & Tomizawa, 1982). The

high copy number ORIs contained in pSANG10-7D12 and pRSF-D11-7D12 relate to expected number of plasmid copies per host cell, which in some instances could result in the expression of high protein production yields in *E. coli* or alternatively could lead to protein aggregation and deleterious effects on the host cell (in the case of a toxic product). The resulting expression is often dependent on the gene of interest that is being expressed, and facilitating the production of correctly folded soluble protein is often of higher importance than the total expression yield of the protein.

As mentioned earlier, the pMB1 derivative origin and RSF1030 origin are not in the same incompatibility group. This means that if both plasmids are co-transformed into the same bacterial cell, it results in stable plasmid coexistence. The benefit of compatible expression vectors is not only due to the ability to co-transform them into the same bacterial cell (as typically the bacterial cell required only one expression vector), but with the additional flexibility in experimental design. Although the benefits of flexible plasmid strategies may seem unclear at this point, the later chapters that describe the co-transformation of plasmids (expression and suppression plasmids) for genetic incorporation of ncAA, highlight the importance of plasmid incompatibility groups and having multiple plasmid pairing options. Table 3.3 lists commonly used origins of replication and those used explicitly in this study. The incompatibility grouping of origins in this table is an arbitrary grouping system but will be necessary for explaining co-transformation choices later in this study.

Table 3.3: List of commonly used ORI's.

Origin of replication	Copy number	Control	Inc group*	Reference
ColE1	15-20	Relaxed	1	Lin-Chao & Bremer, 1986
pMB1	20-60	Relaxed	1	Bolivar <i>et al.</i> , 1977
pMB1 (Mutant)	500-700	Relaxed	1	Minton, 1984

p15A	10-12	Relaxed	2	Chang & Cohen, 1978
RSF1030	>100	Relaxed	3	Som & Tomizawa, 1982

* Arbitrary group numbering of incompatibility groups.

Another noticeable difference between the two expression vectors is the significant disparity between plasmid sizes. The pSANG10 expression vector carrying the VHH 7D12 construct has a plasmid size of 5.7 kb, while pRSF with a similar expression construct is almost double that in size at 10.8 kb. This significant difference is due to the ribosomal RNA genes encoding the 5S, 16S, and 23S rRNA contained on the pRSF vector which enables cellular production of an orthogonal ribosome (Ribo-X) that uniquely recognises an orthogonal ribosomal binding site (oRBS) on the protein of interest mRNA (Wang *et al.*, 2007). The generation of ribo-X orthogonality to the endogenous translational machinery was achieved with ribosomal mutations to the 16S rRNA (U531G and U534A), while the additional copies of the endogenous 5S and 23S rRNA are located on the pRSF vector to facilitate the correct formation of the orthogonal ribosome. Due to this expression setup, the gene encoding 7D12 is not under T7 control and is expressed *via* the *lacUV5* promoter, while the genes responsible for the orthogonal ribosome are controlled by the *trc* promoter (*trp/lac* hybrid). The *trc* promoter is a hybrid of the *trp* and *lac* promoters and facilitates stronger promoter mediated expression in comparison to the *lac* promoter but still includes the *lac* operator region (*lacO*) which is inducible with the addition of IPTG. When IPTG is added to the growth medium, strong expression of orthogonal ribosomes is enabled under the control of the *trc* promoter, with the simultaneous expression of recombinant protein controlled by the weaker *lacUV5* promoter. In contrast, 7D12 expression from pSANG10 vector is tightly regulated by the strong T7 promoter. To facilitate the initiation of 7D12 transcription, the T7 promoter requires the highly active T7 RNAP, which in BL21(DE3) *E. coli* cells is under the control of the *lacUV5* promoter. Thus, to induce expression of 7D12, IPTG is required to induce T7 RNAP expression, which in turn activates transcription of 7D12 *via* the T7 promoter.

3.2.2 Periplasmic expression of anti-EGFR VHH 7D12 in *E. coli*

For periplasmic expression of anti-EGFR wild-type 7D12, expression plasmid pSANG10-7D12 was transformed into BL21(DE3) and grown on LB agar (Kan) plates. A single colony from these plates was used to inoculate 10 mL 2xTY-GK (4% glucose, 50 $\mu\text{g ml}^{-1}$ kanamycin) and grown overnight (37°C, 200 rpm). This overnight culture was used to subculture 500 mL fresh 2xTY-GK to an OD₆₀₀ of 0.1 and the resulting culture was grown until OD₆₀₀ of 0.4-0.6. Once the desired OD₆₀₀ was reached, IPTG (final concentration 1 mM) was added to induce expression of 7D12 and grown overnight (30°C, 160 rpm). After harvesting the cells as described in 2.1.9, the periplasmic fraction was filtered through a 0.2- μm filter unit and dialysed overnight (Slide-A-Lyzer dialysis cassette, 12-30 mL, 3500 MWCO) against 1X PBS. VHH 7D12 was purified from the complex mixture of periplasmic proteins using Ni-NTA gravity-flow columns as described in 2.1.10 and analysed using SDS-PAGE (Figure 3.3.A) as described in 2.1.12. The saturated band in figure 3.3.A represents expressed 7D12 in the presence and absences of IPTG induction. The protein concentration was measured using the BCA colourimetric protein assay and the total amount of purified 7D12 was found to be 10.1 mg/L. The identity of the protein was further verified using electrospray ionization mass spectrometry coupled with liquid chromatography, ESI-MS (Figure 3.3.B). The ExPASy ProtParam online tool was used to calculate the predicted molecular mass of 7D12 as 14241 Da. LC-MS results were in agreement with calculated molecular mass.

While the results demonstrate a high yield of VHH 7D12 with the use of pSANG10 vector in the presence of IPTG, a weak band likely corresponding to VHH 7D12 was observed at 15 kDa in the absence of IPTG. As discussed, the *lacUV5* promoter (which regulates T7 RNAP) has been reported to have a low basal expression level in the absence of IPTG which would result in low level production of T7 RNAP and subsequent initiation of T7 promoter and expression of VHH 7D12. One method to reduce this basal level of expression is by using an *E. coli* strain that contains a plasmid for the production of T7 lysozyme (such as BL21(DE3)pLysS). The pLysS

plasmid expresses low levels of T7 lysozyme, a natural inhibitor of T7 RNAP that inhibits basal levels of T7 RNAP activity but is titered out with increasing levels of T7 RNAP in the event of IPTG induction (Studier, 1991).

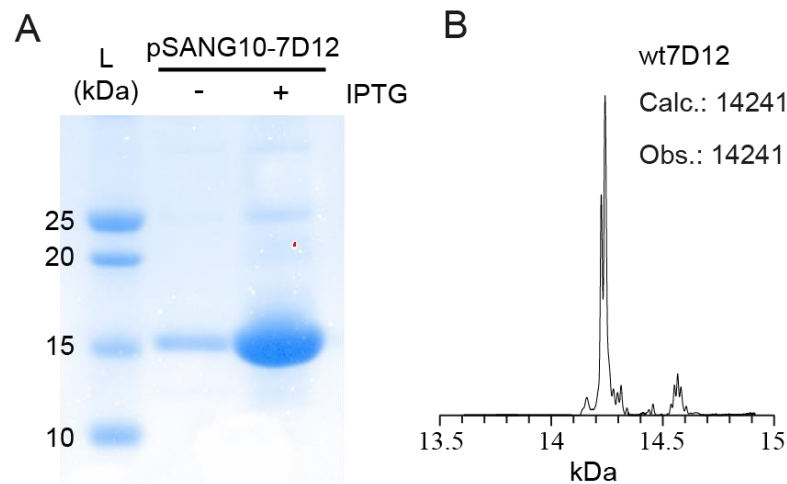


Figure 3.3: Expression and identification of VHH 7D12. A) Purified periplasmic protein extract separated by size on SDS-PAGE and stained with Coomassie Brilliant Blue. B) ESI-MS of purified VHH 7D12, mass peak observed at 14241.

For expression of wild-type 7D12 in the pRSF vector, a similar methodology as above was applied, with alterations to expression strain (BL21(DE3)pLysS) and a reduction in expression scale (100 mL 2xTY-GK). To compare the difference in expression between pSANG10 and pRSF vectors, plasmids pSANG10-7D12 and pRSF-7D12 were induced in the presence and absence of IPTG. Extracted periplasmic milieu was purified as described in methods (2.1.9) and His-tagged protein samples were resolved on SDS-PAGE (Figure 3.4).

Similarly to the above expression (Figure 3.3.A) a high level of VHH 7D12 expression was achieved with the use of the pSANG10 vector in the presence of IPTG. As expected, basal levels of VHH 7D12 in the absence of IPTG were reduced with the use of BL21(DE3)pLysS cells. Although a clear band corresponding to 7D12 was observed at around 15 kDa in the lane representing pSANG10-7D12 (+IPTG), high levels of background signal were also present. It was speculated that this

background signal was caused by periplasmic proteins that were still present in the sample due to insufficient purification of the His-tagged protein from the extracted periplasmic protein fraction.

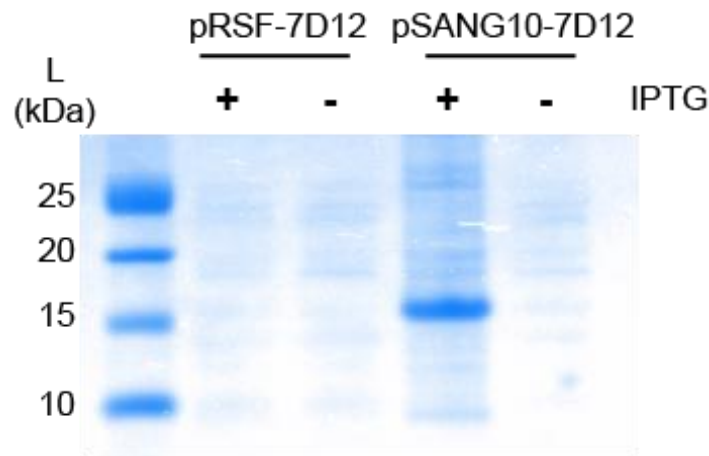


Figure 3.4: Comparison of two expression vectors pSANG10 and pRSF-D11 in the production of VHH 7D12 with and without IPTG induction. Samples were resolved on SDS-PAGE.

In contrast, although the same methodology was used for the growth, expression and purification of VHH 7D12 from pSANG10 and pRSF vector, no observable band at 15 kDa was present to indicate successful expression of VHH 7D12 from pRSF vector in the presence of IPTG. Several factors could have contributed to the unsuccessful expression of VHH 7D12 with pRSF vectors, such as a suboptimal expression cassette or toxicity of the expressed recombinant protein. As pSANG10-7D12 demonstrated high yields of VHH 7D12 with a high copy number ORI (pMB1 derivative) and strong promoter (T7 promoter) it is unlikely that VHH 7D12 would cause toxicity to the host cell. Furthermore, cell growth of both recombinant strains was monitored before induction by measuring the optical density, and similar growth was observed (data not shown) which indicates non-toxicity of the assimilated genes and basal expression of the mRNA/protein. Measurements of cell growth after induction of IPTG (following overnight incubation) demonstrated similar growth between the all samples (pSANG10 +/- IPTG, pRSF +/- IPTG) which provides further support to the notion that VHH 7D12 is non-toxic and tolerable to the bacterial host. Therefore, a

feasible explanation of the differences in expression between pSANG10 and pRSF is due to variations in the components used in the expression vector. The pRSF vector contained a lower copy number ORI (RSF1030; >100 copies), and VHH 7D12 expression was regulated by a weaker promoter (*lacUV5*). Both of these vector components could contribute to reduced expression of VHH 7D12 in comparison to pSANG10 vector. Furthermore, as pRSF vector functions with higher expression complexity (orthogonal ribosome expression required to recognise oRBS on mRNA), further analysis is required to ensure optimisation of these key components of the expression platform.

3.2.3 Periplasmic expression of alternative VHH in *E. coli*

To explore 7D12 binding affinities to an EGFR positive cell line, a negative heavy-chain only antibody fragment was required as a contrast between targeted binding to cell surface EGFR and non-specific binding to cell surface. After an extensive literature research, the negative control selected was the anti-RR6, VHH-R2 (PDB: 1QD0) as this has been commonly used as a negative control (Van Der Meel *et al.*, 2012). This VHH was generated against the hapten azo-dye Reactive Red (RR6) and was shown to be an efficient novel small molecule targeting agent compared to protein recognition which is the typical targeting method (Spinelli *et al.*, 2000). The gene encoding for periplasmic expression of VHH R2 was designed as a synthetic gBlock (Appendix Table A.3; GB032) and inserted into the pSANG10 backbone, resulting in a new plasmid called pSANG10-VHH-R2 (Figure 3.5). The pSANG10 vector was chosen as previous results demonstrated high yields of an alternative VHH (7D12), and it was assumed that by replacing the CDS coding of VHH 7D12 with VHH R2 similar high yields would be achieved. Briefly, pSANG10-3F-BG4 was digested with HindIII-HF and NdeI (37°C, 1 hour with Cutsmart buffer), gBlock was designed to contain 25 bp overlapping regions and cloned into pSANG10-3F with Gibson assembly and directly transformation into DH10B *E. coli* cells. Recovered cells were plated on LB agar (Kan) and the DNA sequence of respective clones was verified *via* Sanger sequencing.

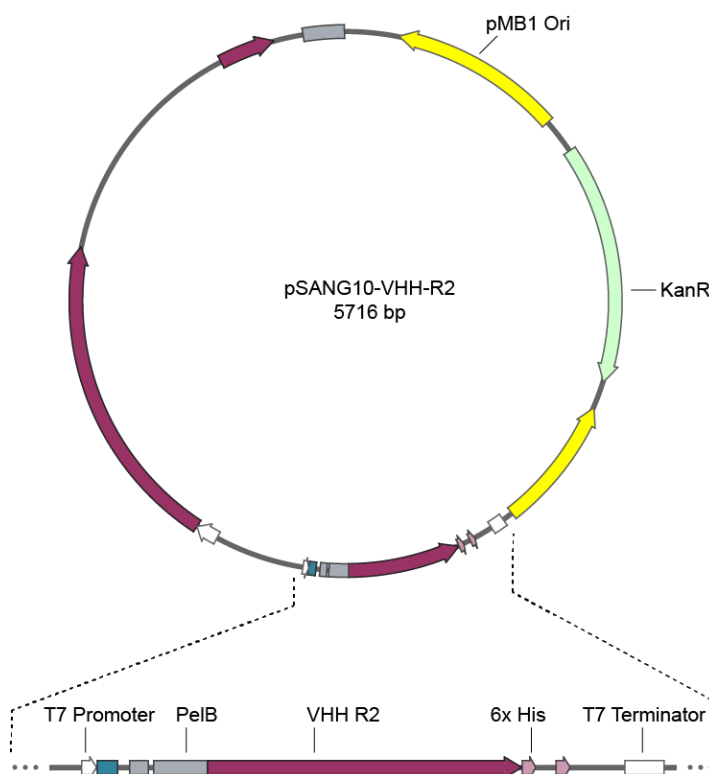


Figure 3.5: Plasmid map of pSANG10-VHH-R2 designed for the periplasmic expression of anti-RR6 VHH R2 with the induction of IPTG.

For periplasmic expression of anti-RR6 VHH R2, expression plasmid pSANG10-VHH-R2 was transformed into BL21(DE3)pLysS and grown on LB agar (Kan) plates. Similar methodology was followed as described in 3.2.2 wherein 100 mL of fresh 2xTY-GK was inoculated and induced with IPTG for the production of VHH R2. Periplasmic proteins were extracted as described in 2.1.9 and purified from the complex mixture of periplasmic proteins using Ni-NTA gravity-flow columns as described in 2.1.10. Purified his-tagged proteins were resolved using SDS-PAGE (Figure 3.6) as described in 2.1.12.

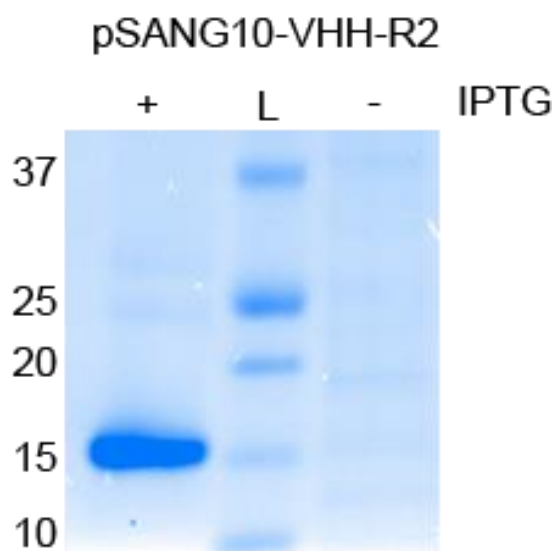


Figure 3.6: Periplasmic expression of VHH R2. Purified periplasmic protein VHH R2 extract separated on SDS-PAGE and stained with Coomassie Brilliant Blue. ExPASy ProtParam estimated size; 14733 Da.

The lane corresponding to pSANG10-VHH-R2 induced with IPTG contains a His-tagged protein that resolved as a well-defined band at 15 kDa. Using the ExPASy ProtParam online tool, the calculated molecular mass of VHH R2 was 14733 Da which is in agreement with SDS-PAGE results. In the absence of IPTG, no His-tagged protein was observed.

With the development and optimisation of the pSANG10 expression vector, the successful expressions of two separate VHH have been demonstrated. The anti-EGFR VHH 7D12 has clear therapeutic values illustrated in several studies, while the VHH R2 is an important negative control that can be used to highlight the specificity of 7D12 targeting to EGFR. One of the main aims of this study is the modification of the therapeutically relevant antibody or antibody fragments with the site-specific incorporation of ncAAs. To demonstrate the efficacy of the techniques developed for photo-control over antibody-antigen binding, it was important to show this control with a diverse range antibody fragments that target a plethora of antigens. HER2 (Human Epidermal Growth Factor Receptor type 2) is a member of EGFR family and overexpression of this receptor has been shown to play an important role in the development of certain types of cancers. Similarly, to the mAb developed anti-EGFR cetuximab, full-length antibodies have been developed for specific targeting of HER2.

Trastuzumab (Herceptin™) is a monoclonal antibody that was approved for the medical treatment of HER2 positive breast cancer in America in 1998 (Vogel *et al.*, 2002). A highly optimised VHH (2Rs15d) for high affinity tumour targeting of HER2 positive cell lines was recently generated (D'Huyvetter *et al.*, 2017). In this study it was shown that the binding mechanics of VHH 2Rs15d was slightly different to its full-length counterpart Trastuzumab in which VHH 2Rs15d binds to the HER2 domain I while Trastuzumab interacts with domain II and IV. For the expression of anti-HER2 antibody fragments, a cloning strategy was designed for insertion of the VHH 2Rs15d gene (PDB: 5MY6) into pSANG10 expression vector. The gene encoding for periplasmic expression of VHH 2Rs15d was designed as a synthetic gBlock (Appendix Table A.3; GB033) and inserted into the pSANG10 backbone, resulting in a new plasmid called pSANG10-2Rs15d (Figure 3.7). Briefly, pSANG10-3F-BG4 was digested with HindIII-HF and NdeI (37°C, 1 hour with Cutsmart buffer), gBlock was designed to contain 25 bp overlapping regions and cloned into pSANG10-3F with Gibson assembly. *E. coli* DH10B cells were transformed with the Gibson reaction mix, recovered and plated on LB agar (Kan) and the DNA sequence of respective clones was verified by Sanger sequencing.

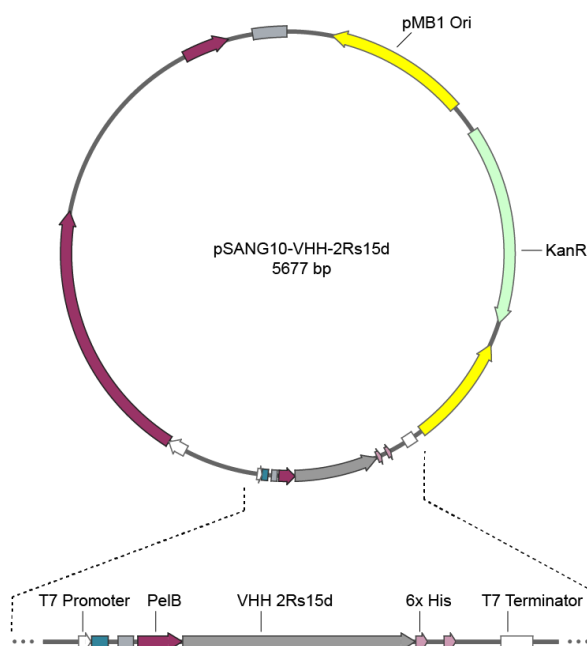


Figure 3.7: Plasmid map of pSANG10-VHH-2Rs15d designed for the periplasmic expression of anti-HER2 VHH 2Rs15d when grown in the presence of IPTG.

As initial test expressions of 2Rs15d showed low levels of expressed recombinant protein, Western blot was used as an analytical technique to detect the presence of His-tagged proteins. For periplasmic expression of anti-HER2 VHH 2Rs15d, expression plasmid pSANG10-2Rs15d was transformed into BL21(DE3)pLysS cells and grown on LB agar (Kan) plates. Similar methodology was followed as described in 3.2.2 wherein 100 mL of fresh 2xTY-GK was inoculated and induced with IPTG for the production of VHH 2Rs15d. Periplasmic proteins were extracted as described in 2.1.9. The use of Western blot as a detection method removed the need for purification of his-tagged protein from the complex mixture of periplasmic milieu as the technique directly identifies recombinant proteins with a C-terminal his-tag. The complete Western blot methodology is listed in methods (2.1.13), but briefly, after separation on SDS-PAGE, samples were transferred onto a nitrocellulose membrane *via* iBLOT2 transfer system. Non-specific protein interactions were blocked using 10% milk in 1x PBS for 1 hour at room temperature, which was followed by detection of his-tag with primary antibody (Mouse-anti-6X-HIS tag, Invitrogen) for 1 hour at room temperature. After washing off non-specifically bound primary antibody with PBST, secondary antibody (Anti-mouse, IgG, HPR-linked, Invitrogen) incubation was performed for 1 hour at room temperature. The Membrane was then developed using SuperSignal Chemiluminescent Substrate (Thermo Scientific) and imaged using a GelDoc XR+ system (Bio-rad). Figure 3.8 shows the chemiluminescence signal acquired from detection of his-tagged proteins expressed by pSANG10-2Rs15d plasmid in the presence and absence of IPTG.

Using the ExPASy ProtParam online tool, the calculated molecular mass of VHH 2Rs15d is 13452 Da. An intense band can be observed at 13 kDa with the addition of IPTG which likely corresponds to the VHH 2Rs15d, however an additional intense band at 25 kDa is also noted. This is likely caused by a dimeric molecular species of 2Rs15d wherein homodimer formation between two 2Rs15d molecules occur resulting in a His-tagged protein of double the molecular weight. The presence of dimeric molecular species suggests unfavourable protein interactions which could result in increased instability and aggregation of expressed recombinant proteins.

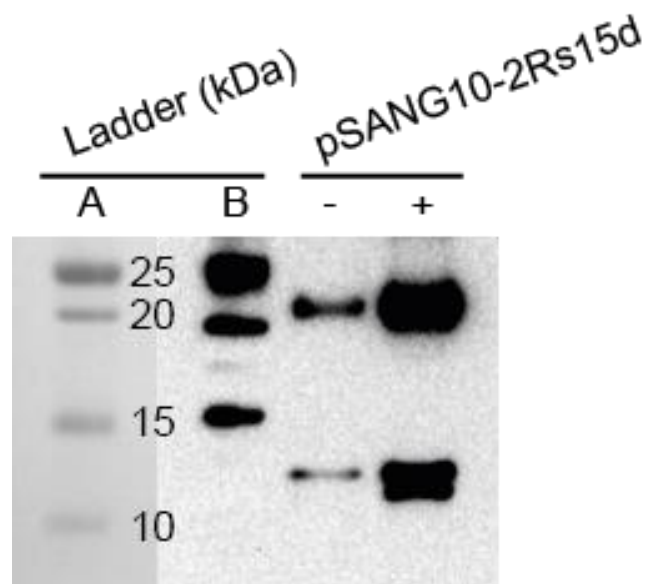


Figure 3.8: Periplasmic expression of 2Rs15d. Ladder (A) White light image of protein ladder (B) Ladder and pSANG10-2Rs15d Chemiluminescence signal of protein ladder and extracted periplasmic proteins detected by GelDoc XR+ system.

The build-up of protein aggregates can lead to the formation of insoluble inclusion bodies (IB) which reduces expression yields and can lead to cell toxicity (Carrio & Villaverde, 2002). To reduce IB formation, tighter control over bacterial expression is required to favour the biosynthesis of correctly folded recombinant proteins. Simple changes to the methodology such as shortened induction time, reduced induction temperature and regulating the concentration of the inducer can allow for improved control over the production of biologically functional proteins. Although the cell line BL21(DE3)pLysS was used to reduce basal expression in absence in IPTG, the presence of a His-tagged protein was observed at 13 kDa without IPTG induction. This is likely due to the highly sensitive detection of his-tagged protein when using Western blot as an analytical technique.

3.2.4 Expression of FAB fragments in *E. coli*

This chapter has demonstrated the expression of various variable domains from heavy chained only antibodies with diverse targets from the optimised expression vector pSANG10. The next section will explore the expression of monoclonal antibody fragments in a bacterial expression system. Fragment antigen-binding (FAB) consists of one constant and one variable region of both the heavy and light chain. The bacterial expression of FAB differs to VHH expression as the expression construct contains the variable and constant heavy chain (VH-CH) and the variable and constant light chain (VL-CL) with individual leader sequences for periplasmic expression. The Fab fragment from the monoclonal antibody cetuximab (FABC225; PDB: 1YY8) was designed as an expression construct and was inserted into pSANG10 vector for periplasmic expression. The crystallography study that characterised the structure of FABC225 (PDB; 1YY8) complex to sEGFR generated the fragments *via* papain digestion of full-length mAb (Cetuximab) and undigested mAb were removed by passing the mixture over protein-A column to isolate FABC225 in the flow through (Li *et al.*, 2005). Since then, expression of FABC225 has been reported in mammalian cell culture (Donaldson *et al.*, 2009) whereby, assembled FABC225 was secreted to the extracellular medium and purified *via* affinity tags (FLAG-tag and/or His-tag). A number of studies have shown bacterial expression of FAB fragments; however, these studies often express the light and heavy chain separately, and carry out refolding post purification by reducing a mixture of equal parts heavy and light chains (Hakim & Benhar, 2009). This resulted in correctly folded pure FAB fragments but at the cost of a reduced yield (90% loss of yield from refolding). An in-depth review of vector design for the characterisation and optimisation of bacterial expression of FAB fragments explored various factors relating to high purity yields of correctly assembled FAB fragments (Corisdeo & Wang, 2004). Through the expression of a human FAB against tetanus toxoid (tt) the study investigated three different expression vectors with different orientations of heavy and light chains and the use of a dicistronic expression construct compared to expression of the two chains with separate promoters. Once optimised expression vector was designed, further

experiments were conducted to find optimal culturing conditions. The resulting plasmid (Orientation; VL-CL before VH-CH, dicistronic expression with one *lac* promoter) showed a 10-fold increase of expressed FAB fragments when cultured in JM105 *E. coli* strain (similar expression to BL21(DE3)), induced at 37°C with 0.1mM IPTG.

The FABC225 expression cassette was designed for insertion into the pSANG10 vector. Alternative signal peptide encoding sequences, namely OmpA and PhoA were placed at the N-terminus of the heavy and light chain genes, respectively. A 6xHis-tag was encoded at the C-terminal part of the heavy chain for detection and purification. The orientation of the chains was designated as VH-CH before VL-CL, contrary to the optimisation study previously discussed, and in hindsight, this may have contributed to the low expression level observed later. A multiple fragment Gibson assembly was carried out for the insertion of two gBlocks into pSANG10 vector. First, pSANG10-3F-BG4 was digested with HindIII-HF and XbaI (37°C, 1 hour with Cutsmart buffer), gBlocks were designed (Appendix Table A.3; GB015 and GB016) to contain 25 bp overlapping regions and cloned into pSANG10-3F with Gibson assembly and directly transformed into DH10B cells. Recovered cells were plated on LB agar (Kan) and verified by Sanger sequencing. This resulted in a new plasmid for periplasmic expression of FABC225, pSANG10-FABC225 (Figure 3.9).

Sequencing confirmed the correct orientation of the ligated products; however, 100 mL small scale expressions experiment did not yield any FABC225 protein (results not shown). For small scale expression plasmid pSANG10-FABC225 was transformed into BL21(DE3)pLysS and grown on LB agar (Kan) plates. Similar methodology was followed as described in 3.2.2 wherein 100 mL of fresh 2xTY-GK was inoculated and induced with IPTG for the production of FABC225. Periplasmic proteins were extracted as described in 2.1.9 and purified from the complex mixture of periplasmic proteins using Ni-NTA gravity-flow columns as described in 2.1.10. Purified his-tagged proteins were analysed using SDS-PAGE as described in 2.1.12.

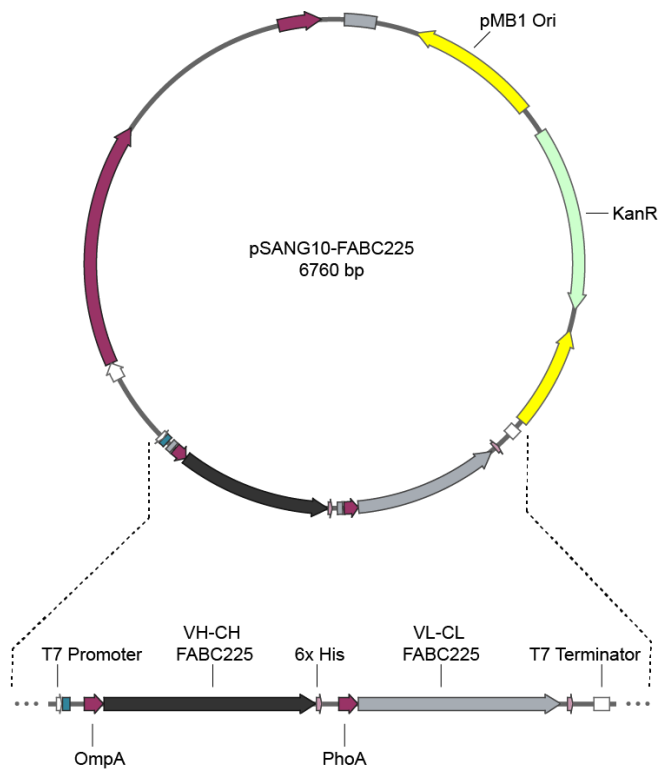


Figure 3.9: Plasmid map of pSANG10-FABC225 designed for the periplasmic expression of anti-EGFR FAB fragment (FABC225) when grown in the presence of IPTG. Orientations of FAB chains are heavy chain (VH-CH) before light chain (VL-CL) with preceding N-terminus leader sequences, OmpA and PhoA respectively.

Expected observation of successful expression should yield small amounts of FABC225 heavy chain with his-tag (25 kDa), while correctly assembled FAB heavy and light chain should form a well-defined protein band at 48.3 kDa under oxidising conditions. In the case of reduced samples similar amounts of heavy (25 kDa) and light (23.4 kDa) chains should be present on the gel. The SDS-PAGE results indicated that the expression attempt was unsuccessful, and expected bands were not present (data not shown). To investigate whether chemical cell lysis had adversely affected extracted cellular contents, methods based on physical cell lysis (sonication and French press) were used to extract recombinant proteins. The analysis of alternative extraction methods resulted in no apparent improvement of extracted FABC225 (results not shown).

Numerous factors could have contributed to the unsuccessful expression of FABC225 from the pSANG10 expression vector. Initially it was speculated that the observed decrease in production was due to the pSANG10 vector being optimised for expression of scFv and VHH and not alternative antibody fragment formats. The high copy number ORI in combination with the strong T7 promoter demonstrated efficient production of VHH fragments with high yields. However, by transitioning the pSANG10 expression platform for the production of FAB fragments, a significant loss of purified recombinant protein is observed, which could be due to overexpression and subsequent toxicity of the recombinant proteins. Monitoring cell growth of the recombinant strains before and after induction showed standard growth patterns observed in previous successful expression studies and provided evidence that the expressed recombinant proteins were non-toxic to the host. Another explanation for the reduced expression of FABC225 are the factors relating to recombinant protein instability and aggregation, which can cause a build-up of protein aggregates, known as inclusion bodies (IBs). By introducing foreign genes into *E. coli* for the expression in the hosts microenvironment, different environmental parameters (such as pH, osmolarity, cofactors, and folding mechanisms) may exist compared to the original source. The overexpression of recombinant proteins in such unfavourable conditions can lead to protein aggregation, a reduction in solubility and subsequently, formation of IBs. Several methods are available to reduce IB formation such as chaperone co-expression (De Marco *et al.*, 2005), the addition of solubility enhancer as a fusion partner or simply reducing expression rates (with reductions in temperature, induction time, and inducer concentration; Vera *et al.*, 2007).

Before investigating the parameters of reduced expression rates of FABC225 in an effort to increase production yield of correctly folded recombinant proteins, we first decided to test alternative expression vectors that had been designed for FAB expression. An extensive search of the literature revealed a plasmid designed explicitly for the expression of FAB fragments (AddGene; Plasmid #63901). The plasmid pAraH6HATT (Figure 3.10) is based on the expression vector pComb3H system (Cary *et al.*, 2000) had been optimised for periplasmic expression of tetanus toxoid FAB (FABtt).

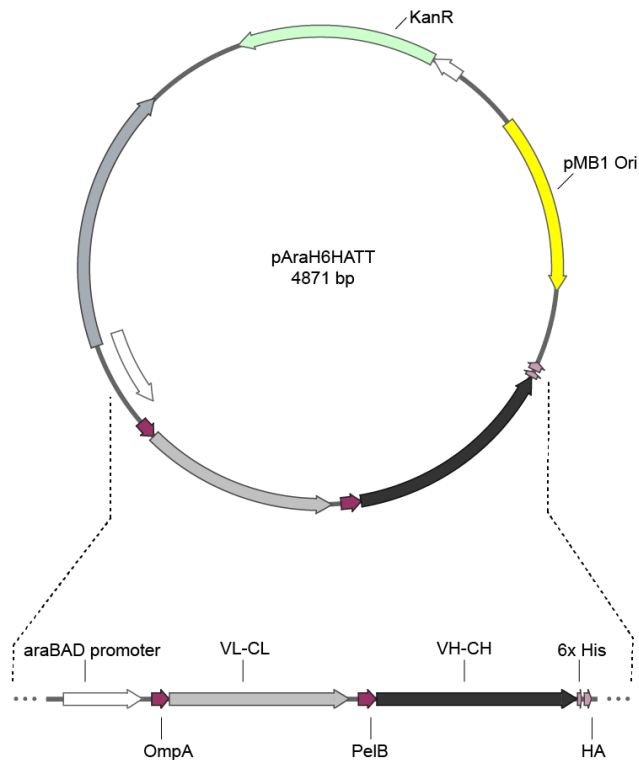


Figure 3.10: Plasmid map of pAraH6HATT designed for the periplasmic expression of FAB fragment against tetanus toxoid in the presence of arabinose. Orientations of FAB chains are light chain (VL-CL) before heavy chain (VH-CH) with preceding N-terminus leader sequences, OmpA and PelB respectively.

A noticeable difference between pSANG10 and pAraH6HA systems was the use of a different inducible promoter region for expression of recombinant proteins. The pSANG10 system is tightly regulated with the T7 promoter while pAraH6HA system uses araBAD inducible promoter. The araBAD promoter is induced with l-arabinose in the growth media and has been shown to have reduced background expression compared to the *lac* promoter (Siegele & Hu, 1997). However, the strength of the promoter has been reported to be somewhat weaker than the T7 and *tac* systems (Balzer *et al.*, 2014). As overexpression of recombinant proteins can cause IB formation, thus reducing the yield of correctly folded FAB fragments, a promoter that is weaker and under tighter control could facilitate improved expression yields. Another difference between pSANG10 and pAraH6 systems was the orientation of the heavy/light chain. Previously, the orientation of FABC225 chains in pSANG10

were designed as VH-CH before VL-CL; however, in pAraH6HATT, the orientation is VL-CL before VH-CH which were preceded with OmpA and PelB leader sequences, respectively. As previously demonstrated in the study of optimised FAB expression vectors, the orientation is important for the correct assembly of FAB fragments and the orientation of VL-CL before VH-CH has shown to result in higher yields (Corisdeo & Wang, 2004). A two-step assembly method was designed to insert FABC225 into pAraH6 vector.

First, primers were designed (Appendix Table A.2; D143, D144) to amplify the heavy chain region of FABC225 from pSANG10-FABC225. The primers contained 20 bp overhangs complementary to the pAraH6HATT vector with removed FABtt heavy chain. The PCR product was separated on a 1% agarose gel and purified with QIAquick Gel Extraction Kit (QIAGEN). The pAraH6HATT vector was digested with XhoI and SpeI (37°C, 1 hour with Cutsmart buffer) and the backbone was isolated and purified from an agarose gel. To insert the PCR product into digested pAraH6 backbone, Gibson assembly was used (50°C, 1 hour) and the resulting ligation mixture was transformed into DH10B cells. Recovered cells were plated on LB agar (Chloramphenicol) and grown overnight (37°C, 12-16 hours). A single colony was isolated and plasmid DNA extracted for Sanger sequencing. After verification of correctly inserted FABC225 heavy chain coding sequence, the next step was to insert the FABC225 light chain encoding sequence. Similar design methods were used in the generation of PCR primers (Appendix Table A.2; D145, D146) for the amplification of FABC225 light chain region from pSANG10-FABC225. The plasmid encoding the FABC225 heavy chain in pAraH6 vector was digested to remove FABtt light chain. Briefly, pAraH6-FABC225-HC was digested with XbaI and SacI (37°C, 1 hour with Cutsmart buffer) to remove the light chain, the digested sample was resolved by size on 1% agarose gel and pAraH6-FABC225-HC backbone was extracted. For ligation, PCR product (FABC225 light chain) was mixed with pAraH6-FABC225-HC backbone in a Gibson assembly reaction (50°C, 1 hour) and transformed into DH10B.

Sequence verification of pAraH6-FABC225-HC confirmed the correctly assembled plasmid sequence. However, problems occurred when attempting to insert the FABC225 light chain carrying sequence. DH10B cells transformed with Gibson

assembled pAra-FABC225 showed either no growth with Chloramphenicol or similar growth in comparison to the negative control plate indicating unsuccessful ligation of FABC225 light chain. After additional experiments to confirm the correct size of digested pAraH6-FABC225-HC vector and PCR product of FABC225-LC, an alternative ligation method was used in an attempt to resolve this problem. The T4 DNA ligase is an enzyme isolated from the bacteriophage T4 and is commonly used by researchers as a ligation method that catalyses the formation of covalent phosphodiester bonds between the 5' phosphate and 3' hydroxyl termini of two digested DNA fragments. T4 ligation details are listed in methods (2.1.8.9). Briefly, digested vector pAraH6-FABC225-HC (XbaI and SacI) was ligated with T4 DNA ligase (20°C, 2 hours) to digested insert PCR product FABC225-LC (XbaI and SacI) at a ratio of 1:3, vector to insert. Ligated mixture was transformed into DH10B and plated on Chloramphenicol agar plates. The use of T4 DNA ligase resulted in similar conclusions to the Gibson assembly with the unsuccessful ligation of FABC225 light chain to pAraH6-FABC225-HC vector. This led to speculation that an incorrect plasmid map was provided by AddGene and to resolve this would require full plasmid sequencing to determine the correct sequence. A further 8 primers (Appendix Table A.2; D177-86) were sequentially designed for full plasmid sequencing, and resulting sequence reads were assembled to form a circularised DNA map. The newly sequenced plasmid map was aligned with the previous plasmid map using the online tool Nucleotide BLAST (NCBI; Zheng *et al.*, 2000) resulting in a 95% consensus between the two plasmid maps. A total of 260 nucleotides (56 of which were gaps) were misaligned with consensus sequence with a high percentage of misaligned nucleotides occurred within the araBAD promoter region upstream of the light chain initiation codon. These misaligned nucleotides could have a negative influence on the design of Gibson overhangs. However, no additional restriction sites that were used in T4 ligation were introduced, and consequently the reason for unsuccessful ligation with T4 DNA ligase is still unknown.

CHAPTER 4

Genetic incorporation of non-colonial amino acids in antibody fragments

4.1 Introduction

In the previous chapter, the in-depth characterisation and optimisation of the expression vector pSANG10 resulted in a highly efficient platform for periplasmic expression of antibody fragments. The development of this expression platform was required before commencing investigations into the genetic encoding of non-canonical amino acids (ncAA) into recombinant proteins. In this chapter, I will discuss experiments performed for optimisation of site-specific incorporation of ncAAs into antibody fragments. Information gained from these experiments was used to develop an optimised plasmid for site-specific encoding of photocaged amino acid into heavy chain only antibody fragments (variable domain; VHH). ncAAs were site-specifically incorporated into VHH 7D12 and VHH 2Rs15d that bind EGFR and HER2, respectively, receptors that are important targets for cancer therapy.

4.1.1 Expanding the genetic code for *in vivo* site-specific incorporation of non-canonical amino acids

As discussed in the first chapter, *in vivo* site-specific installation of ncAA into proteins is achieved by directing the ncAA incorporation in response to an amber or quadruplet codon at a desired site in a gene of interest.

To comprehensively discuss the process of *in vivo* genetic incorporation of ncAA into proteins, certain aspects of protein translation will need to be highlighted. In its most basic form, the framework underpinning the central dogma of molecular biology describes the flow of genetic information within a biological system as a two-step process (transcription, followed by translation). In protein translation, endogenous transfer RNAs (tRNAs) are aminoacylated with their cognate amino acids using specific aminoacyl tRNA synthetase enzymes (aaRS) within the host organism. During translation, the aminoacylated tRNA reads triplet codons on the messenger RNA (mRNA) *via* Watson-Crick base-pairing interactions between the mRNA codon and

tRNA anticodon. This decoding of the mRNA codons is facilitated by the ribosome and as matching tRNA bearing the appropriate amino acid residues are used by the ribosome-mRNA complex, amino acids are linked to the growing polypeptide chain. This basic principle was used in the exploitation and development of reassigning non-sense codons for the site-specific genetic encoding of ncAAs. By evolving selective aminoacyl tRNA synthetase/tRNA (aaRS/tRNA) pairs that specifically recognises a desired ncAA of choice and a reassigned codon, the endogenous translation machinery can be used as a method of site-specific incorporation of a desired ncAA in response to an appropriate codon. Before the evolved aaRS/tRNA pair is used for the incorporation of ncAA, the orthogonality of the pair must be ensured so that there is no interaction with the existing host organism's synthetases, tRNAs and translational machinery. This orthogonality and compatibility in which the aaRS does not recognize endogenous tRNAs or amino acids and the tRNA does not act as a substrate for any endogenous aaRSs, while simultaneously the orthogonal tRNA pair can be recognised by the host ribosome, is a vital requirement before genetic decoding of a ncAA.

The most successfully reported codon used for the encoding of one ncAA is the amber nonsense codon (stop codon; TAG) which has been selected due to its less frequent use compared to other codons. Other systems that are based on the reassignment of ochre stop codon, opal stop codon, rare codons, and quadruplet codons have also been reported for site-specific incorporation of single ncAAs along with multiple distinct ncAAs. However, as the amber suppression technique is considered to be the most established and robust methodology for *in vivo* incorporation of ncAA, it was chosen as the primary method of genetic encoding of ncAA into *E. coli* during this thesis.

4.1.2 Expression of orthogonal aaRS/tRNA pairs in cells

To incorporate a ncAA in response to an amber codon, an orthogonal aaRS that recognises the desired ncAA and can specifically charge the orthogonal tRNA_{CUA} (CUA denotes the anticodon that recognises the amber nonsense codon) with the ncAA is required within the host cell. To supply the cell with orthogonal aaRS/tRNA_{CUA} pairs, the corresponding genes encoding the aaRS and tRNA_{CUA} are expressed using a plasmid (commonly referred to as suppressor plasmids). For the construction of efficient suppressor plasmids, careful optimisation of expressed aaRS/tRNA_{CUA} pairs is required, so that appropriate levels are present in the cell. A careful balance between expressing high amounts of tRNA_{CUA} to outcompete endogenous release factor (RF1; peptide termination factor that binds to amber stop codon in the ribosome) while not causing toxicity to the host *via* the incorporation of ncAA into endogenous proteins which can lead to detrimental effects on cellular processes. Over the last decade several suppressor plasmids have been developed that vary in their origin of replication, the promoter types and strengths that drive expression of aaRS and tRNA, and the number of copies of aaRS and tRNA genes contained within the suppressor plasmid. Table 4.1 lists suppressor plasmids that were evaluated for their efficiency to incorporate ncAA. A more detailed discussion on these plasmids is presented in the next few sections of this chapter.

Table 4.1: Suppressor plasmids investigated in this study.

Plasmid	aaRS/tRNA pair isolated from	ORI *	Number of aaRS copies	Promoter for aaRS	Number of tRNA copies	Promoter for tRNA
pSUP_ <i>Mj</i> CNFRS/ <i>Mj</i> tRNA	<i>M. jannaschii</i>	p15A (2)	1	modified <i>glnS'</i>	6	<i>proK</i>
pEVOL_ <i>Mj</i> CNFRS/ <i>Mj</i> tRNA	<i>M. jannaschii</i>	p15A (2)	2	1 by <i>glnS'</i> 1 by <i>araBAD</i>	1	<i>proK</i>

pULTRA MjCNFRS/MjtRNA	<i>M. jannaschii</i>	<i>CloDF13</i> (4)	1	tacl	1	<i>proK</i>
pCDF_ PyIRS/PyItRNA	<i>M. barkeri</i>	<i>CloDF13</i> (4)	3	modified <i>glnS'</i>	1	<i>lpp</i>

*See Table 3.3 for incompatibility groups.

4.1.3 Suppressor plasmids containing *Methanocaldococcus jannaschii* derived MjTyrRS/tRNA_{CUA} pair

As discussed above there are a number of suppressor plasmids that have been developed for the expression of aaRS/tRNA_{CUA} pairs in host organisms to facilitate the incorporation of ncAAs in response to an amber codon. A classic strategy for the generation of orthogonality in aaRS/tRNA_{CUA} pairs is by transferring them from another kingdom into the organism of interest. Often the orthogonality of the aaRS/tRNA_{CUA} pair is defined with respect to each host as endogenous translation machinery has differences between species. In the first chapter, an extensive review into examples of orthogonality between aaRS/tRNA pairs and host organisms demonstrated several orthogonal systems that can be used in prokaryotic and/or eukaryotic hosts.

This section will review the development of suppressor plasmids containing TyrRS/tRNA pair isolated from the archaeobacteria *Methanocaldococcus jannaschii* (MjTyrRS/tRNA_{CUA}) for the genetic encoding of ncAA into recombinant proteins expressed in *E. coli*. The first example of the directed evolution of an orthogonal aaRS/tRNA pair for *in vivo* site-specific incorporation of a ncAA in response to an amber codon was the tyrosyl aaRS/tRNA pair from *M. jannaschii* (MjTyrRS/tRNA_{CUA}) and has been primarily used for the incorporation of aromatic ncAA related to phenylalanine (Wang *et al.*, 2001). This orthogonal pair was an ideal candidate for *in vivo* studies due to its minimalistic anticodon loop binding domain and that it does not aminoacylate *E. coli* tRNA (Steer & Schimmel, 1999). Furthermore, it was shown that the TyrRS could efficiently aminoacylates a cognate tRNA^{Tyr} derivative (mutated

to recognise a reassigned amber codon) while remaining effective in orthogonal protein translation in *E. coli* (Wang *et al.*, 2000). However, compared to wild type *MjTyrRS/tRNA* incorporation, a considerable decrease in protein yield was shown when encoded ncAAs in response to an amber codon in *E. coli* systems *in vivo* (Smolskaya & Andreev, 2019). This was likely due to inadequate optimisation of orthogonal synthetase and its suppressor tRNA ratios in the host organism for efficient translational function which, as a consequence reduced ncAA incorporation capability.

The past decade has witnessed several versions of suppressor plasmids containing *MjTyrRS/tRNA_{CUA}* pair for incorporation of a diverse range of ncAAs in response to an amber codon. The first significant advance in improving the yield of recombinant protein with site-specific encoding on ncAA was the development of a single plasmid system containing both genes for synthetase and suppressor tRNA which replaced the two plasmid system (aaRS and tRNA genes located on two separate plasmids).

One of the first single plasmid systems; pSUP_ *MjCNFRS/6xMjtRNA* (Figure 4.1.A; Ryu & Schultz, 2006) contained six copies of *MjtRNA* in two polycistronic expression cassettes which was controlled by an *E. coli* prolyl-tRNA promoter and terminator (*proK*) to regulate levels of orthogonal *MjtRNA* expressed within the host. The expression of one copy of a mutant *MjTyrRS* (D286R) was controlled by *E. coli* glutaminyl-tRNA synthetase constitutively active promoter (modified variant *glnS'* promoter; Plumbridge & Söll, 1987). The plasmid contained the low/mid-level copy number p15A ORI which made it compatible with the most commonly used expression vectors (including pSANG10) and reduced the overexpression of *MjTyrRS/tRNA_{CUA}*. Although higher levels of expression could be achieved with stronger promoters and higher plasmid copy numbers, it was found that overexpression of foreign synthetase and suppressor tRNA in *E. coli* can cause toxicity to the host due to the interference with translation machinery (such as elongation factor Tu (EF-Tu) and ribosomal components) and unintentional modification of native genes containing naturally occurring amber codons. A significant factor that influences the suppression efficiency of aaRS/tRNA pairs is the compatibility between orthogonal tRNA and the translation apparatus of the host cell. The prokaryotic

elongation factor EF-Tu that is responsible for catalysing the binding of an aminoacyl-tRNA (aa-tRNA) to the A-site of the ribosome had been shown to have low affinity (specifically in *E. coli*) to charged *MjtRNA*_{CUA} which reduce its ability to recognise and deliver orthogonal aa-tRNA to the ribosome (LaRiviere *et al.*, 2001).

To overcome this challenge a novel series of vectors were developed by Schultz and colleagues in 2010 (Young *et al.*, 2010). The pEVOL_2x*MjCNFRS/MjtRNA* vector (Figure 4.1.B) contained two copies of *MjTyrRS*, with the expression of one copy being controlled by the constitutive *glnS'* promoter for basal levels of aaRS, while the second copy was controlled by the inducible *araBAD* promoter increasing the availability of aaRS to the cell when induced with arabinose. Furthermore, previously directed evolution work that identified modification of the GC-rich T-stem region of *MjtRNA* allowed for the optimisation of a suppressor tRNA_{CUA}^{opt} that demonstrated enhanced affinity to EF-Tu of *E. coli* (Guo *et al.*, 2009). This work was incorporated into the pEVOL series of aaRS/tRNA vectors which further enhanced site-specific incorporation efficiencies of ncAAs *in vivo* and allowed for expression levels approaching that of wild-type *MjTyrRS* system.

Although a substantial improvement was reported in the efficiency of ncAA incorporation *via* the pEVOL system, further enhancement was shown with the development of the pULTRA plasmid. The new suppressor plasmids (pULTRA series) was developed by Schultz and colleagues for improved efficiency at amber suppression and for the incorporation of multiple distinct ncAAs in response to amber and ochre codons by utilising the efficient incorporation qualities of both the *MjTyrRS*/tRNA and *MbPylRS*/tRNA pairs, respectively (Chatterjee *et al.*, 2013). The suppressor plasmid pULTRA_2x*MjCNFRS/MjtRNA* (Figure 4.1.C) was designed to contain one copy of both *MjTyrRS* and suppressor tRNA_{CUA}^{opt} on the pCDF-1b vector backbone which conferred spectinomycin resistance, *Clodf13* replicon and the *lacI* regulatory elements. The increased plasmid copy number (20–40 copies per cell) designated by the *Clodf13* replicon enhanced the expression level and suppressor efficiency of aaRS/tRNA pair.

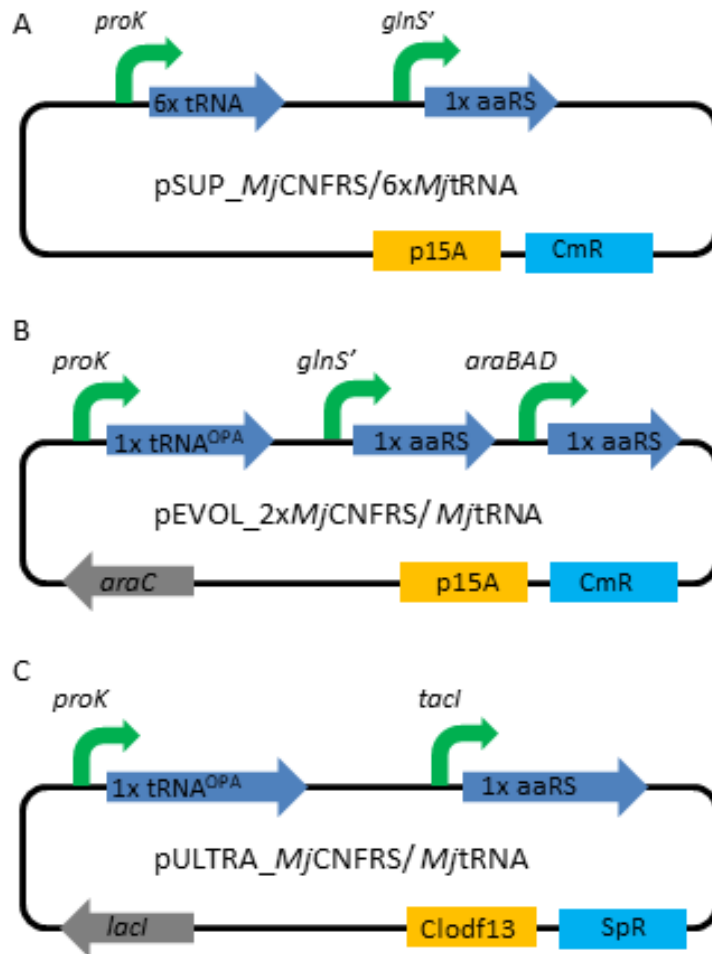


Figure 4.1: Pictorial representation of plasmids, pSUP, pEVOL and pULTRA for incorporation of ncAA using MjRS/MjtRNA_{CUA}. A) pSUP_MjCNFRS/6xMjtRNA suppressor plasmid designed with 6 copies of MjtRNA under *proK* promoter and one copy of MjTyrRS under *glnS'* promoter. pSUP vector contains p15A ORI and chloramphenicol resistance gene. B) pEVOL_2xMjCNFRS/MjtRNA suppressor plasmid designed with 1 copy of optimized MjtRNA under *proK* promoter and 2 copies of MjTyrRS under *glnS'* promoter and *araBAD* promoter. pEVOL vector contains p15A ORI and chloramphenicol resistance gene. C) pULTRA_MjCNFRS/ MjtRNA suppressor plasmid designed with 1 copy of optimized MjtRNA under *proK* promoter and 1 copy of MjTyrRS under *tacl* promoter. pULTRA vector contains Clodf13 ORI and Spectinomycin resistance gene.

Compared to the suppressor plasmid pEVOL the MjTyrRS expression on pULTRA is controlled by the *tacl* inducible promoter (hybrid of the *trp* and *lacUV5* promoters) which allows for relatively strong expression under IPTG induction. This promoter/terminator replaced the T7 elements of pCDF-1b vector as the *tacl*

promoter allows for IPTG concentration dependent expression of *MjTyrRS* (De Boer *et al.*, 1983). Furthermore, the notoriously leaky expression of *tacI* promoter actually benefited the system and allowed for the single copy *MjTyrRS* expression to mimic the two copy *MjTyrRS* system of pEVOL in which basal levels of *MjTyrRS* are constitutively achieved with the weak *glnS'* promoter, and high levels of *MjTyrRS* can be induced by the strong *araBAD* promoter. Similar to pEVOL the one copy of suppressor tRNA_{CUA}^{opt} was controlled by the *proK* promoter and terminator, this resulted in a highly efficient suppression system that contained one expression construct of *MjTyrRS* and suppressor tRNA_{CUA}. Additionally, this study reported the construction of pULTRA-II plasmid that contained single copies of aaRS/tRNA pairs of both the *MjTyrRS*/tRNA_{CUA} and *MbPylRS*/tRNA_{UUA} that encoded two distinct ncAAs in response to amber and ochre codons.

4.1.4 Methanosarcina mazei / Methanosarcina barkeri derived PylRS/tRNA pair

Alternative orthogonal aaRS/tRNA pairs derived from methanogens, most notably the *Methanosarcina mazei* (*Mm*) pyrrolysyl-tRNA synthetase pair (*MmPylRS*/*MmtRNA*_{CUA}) or the homologous *Methanosarcina barkeri* (*Mb*) pair (*MbPylRS*/*MbtRNA*_{CUA}) have been extensively developed for incorporation of many types of ncAA. In 2002, the discovery that certain methanogenic bacteria naturally incorporate pyrrolysine in several methyltransferase genes in response to an in-frame amber stop codon (Srinivasan *et al.*, 2002, Hao *et al.*, 2002) stimulated further research on PylRS and its cognate amber suppresser tRNA^{Pyl}. Not long after this discovery, it was demonstrated that by supplying pyrrolysine to *E. coli* and with the incorporation of genes responsible for expression of *MbPylRS* and the suppressor *MbtRNA*_{CUA} (*pylT* and *pylS*), the natural *in vivo* translation of amber codon occurs with the encoding of pyrrolysine (Blight *et al.*, 2004). While it was shown that wild-type PylRS had good incorporation efficiency of pyrrolysine analogues and that endogenous *E. coli* and eukaryotic aaRS did not interact with *MbtRNA*_{CUA}, conferring the additional advantage of being orthogonal in *E. coli* and eukaryotes (Polycarpo *et*

al., 2006), limitations in its incorporation capabilities for additional ncAA with diverse chemistries prompted further evolutionary studies. Since then many studies have explored directed evolution of PylRS/tRNA pairs to significantly broaden the aaRS/tRNA available substrate scope. Published crystal structures of *Mm/MbPylRS* complexes with pyrrolysine (Such as PDB; 2Q7H) are often used in the rational design of novel mutants that can bind to a diverse range of ncAAs, alternatively similar results can be achieved with the random mutations of active residues. The first example of a PylRS mutant was for the incorporation of a post-translational modified lysine (N^ϵ -acetyllysine) in recombinant proteins produced in *E. coli* (Neumann *et al.*, 2008b). The randomisation of six targeted residues (Leu266, Leu270, Tyr271, Leu274, Cys313 and Trp383) located in a hydrophobic cavity in close proximity to (and likely involved in binding to the pyrroline ring) pyrrolysine allowed for the rearrangement of *MbPylRS* so that it binds to the acetyl group. In another study it was shown that a single mutation to *MmPylRS*(Y384F), identified through random screening enabled higher aminoacylation and amber suppression incorporation of N^ϵ -(*tert*-butyloxycarbonyl)-L-lysine (Bock), N^ϵ -allyloxycarbonyl-L-lysine (AlloLys) and pyrrolysine compared to wtPylRS (Yanagisawa *et al.*, 2008), and when combined with another point mutation in *MmPylRS*(Y306A) it enabled large scale production of recombinant protein containing site-specific N^ϵ -(*o*-azidobenzoyloxycarbonyl)-L-lysine (AzZLys). In this thesis, the plasmid pCDF_3xPylRS/PyltRNA (Figure 4.2) is extensively used for the incorporation of Bock and N^ϵ -[(2-propynyloxy)carbonyl]-L-lysine (CAK). This plasmid was constructed by Chin and colleagues and has been used for efficient site-specific incorporation of Bock and CAK in *E. coli* (Sachdeva *et al.*, 2014; Wang *et al.*, 2014). This plasmid was generated with the introduction of two additional copies of *MbPylRS* gene into the pCDF plasmid that contained single copies of *MbPylRS*/tRNA pair. Similar design considerations as the *MjTyrRS* series of expression vectors were implemented in the construction of pCDF_3xPylRS/PyltRNA. The regulation of the three copies of expressed *MbPylRS* was under control of the weak *glnS'* constitutive promoter while the single copy of PyltRNA was under IPTG inducible expression of the relatively strong *lpp* promoter (Nakamura & Inouye, 1979). This achieved a highly regulated and optimized suppressor plasmid for the

expression of *Mb*PyIRS/tRNA pair for the site-specific incorporation of numerous ncAAs.

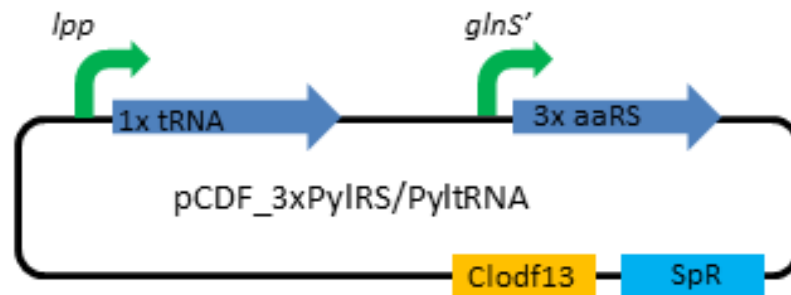


Figure 4.2: pCDF_3xPyIRS/PyItRNA suppressor plasmid designed with 1 copy of *Mb*PyItRNA under the *lpp* promoter and three copies of *Mb*PyIRS under the *glnS'* promoter. pCDF vector contains the Clodf13 ORI and the Spectinomycin resistance gene.

4.1.5 Orthogonal synthetase and corresponding suppressor tRNA for genetic encoding of photocaged amino acids

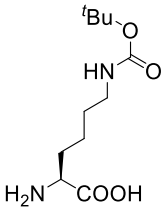
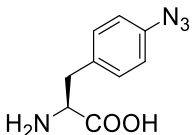
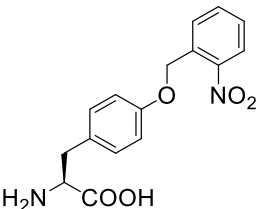
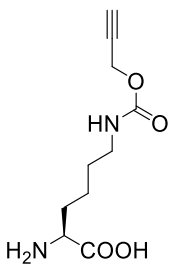
The ability to control protein activation by an external stimulus such as light is a useful tool for investigation into biological processes. The strategy used in this thesis involved the blocking of essential amino acids with a removable photo-protective moiety, which when removed, reverts the amino acid back to native form. Several analogues of natural amino acids have been synthesised with additional photo-protective groups, such as lysine, cysteine, and tyrosine, and have been genetically encoded *in vivo* in prokaryotic and eukaryotic host organisms. The incorporation of these ncAA in eukaryotic expression systems is not in the scope of this thesis. Therefore, the focus of this section will be aimed at examples of incorporation of photocaged ncAA in prokaryotes. In 2006, the genetic encoding of *o*-nitrobenzyl-*O*-tyrosine (photo-protected tyrosine derivative or ONBY/PcY) was reported in *E. coli* in response to an amber codon (Deiters *et al.*, 2006). To incorporate photocaged tyrosine into recombinant proteins, the *Mj*TyrRS/tRNA_{CUA} pair was evolved to

selectively recognise and aminoacylate photocaged tyrosine. The evolutionary study identified five residues in the tyrosine binding pocket of *Mj*TyrRS that when mutated (Y32G, L65G, F108E, D158S, and L162E) could accommodate the bulky *o*-nitrobenzyl moiety and allowed for *in vivo* incorporation with high fidelity and good efficiency using amber suppression in *E. coli*. Following the evolution of a mutant *Mj*TyrRS selected for encoding of photocaged tyrosine, a study on the directed evolution of a mutant *Mm*PylRS/tRNA_{CUA} was implemented to establish a system for encoding of *o*-nitrobenzyloxycarbonyl-N^ε-L-lysine (photo-protected lysine derivative or ONBK) in bacterial and mammalian cells (Chen *et al.*, 2009), resulting in four mutations (Y306M, L309A, C348A, Y384F) to *Mm*PylRS/tRNA_{CUA} which facilitated efficient site-specific incorporation of ONBK. *Mb*PylRS/tRNA_{CUA} has also been evolved for incorporation of *o*-nitrobenzyl-*O*-tyrosine (photocaged tyrosine), and contained four mutations to the synthetase (L270F, L274M, N311G, and C313G) expanding the pyrrolysine recognition pocket (Arbely *et al.*, 2012). For the incorporation of a photo-protected cysteine derivative (*S*-[(*R,S*)-1-{4',5'-(methylenedioxy)-2'-nitrophenyl}ethyl]-L-cysteine) Chin and colleagues once again evolved a *Mb*PylRS/tRNA_{CUA} pair, which has following mutations when compared to its wildtype precursor aaRS: N311Q, C313A and V366M in the active site (Nguyen *et al.*, 2014).

4.1.6 Non-canonical amino acids

The ncAA used in this chapter were either purchased from commercial suppliers or synthesised by colleagues. Table 4.2 lists the ncAA used in this study with additional information about their function, details about synthetic route or suppliers, and information about aaRS/tRNA pairs required for *in vivo* incorporation in proteins.

Table 4.2: Non-canonical amino acids utilized during this thesis.

Name/Structure	aaRS/tRNA pair	Function	Synthesis/Supplier Reference
<p>N6-(tert-butoxycarbonyl)-L-lysine</p> <p>Boc lysine (BocK)</p> 	<i>Mb</i> Pyl	PTM	Sigma-Aldrich (Product # 359661)
<p>4-Azido-L-phenylalanine</p> <p>(AzF)</p> 	<i>Mj</i> Tyr	Bioorthogonal functional group for site-specific conjugation	Thermo-fisher (Product # 50259191)
<p><i>o</i>-nitrobenzyl-<i>O</i>-tyrosine</p> <p>Photocaged Tyrosine (pcY)</p> 	<i>Mj</i> Tyr	Photocaged	Deiters <i>et al.</i> , 2006
<p>N6-[(2-propynyloxy)carbonyl]-L-lysine</p> <p>(CAK)</p> 	<i>Mb</i> Pyl	Bioorthogonal functional group for site-specific conjugation	Nguyen <i>et al.</i> , 2009b

The ncAAs N⁶-(tert-butoxycarbonyl)-L-lysine (Bock) and N⁶-[(2-propynyloxy)carbonyl]-L-lysine (CAK) are excellent substrates for *MbPylRS* and have been incorporated into proteins in response to an amber codon using *MbPylRS*/*PyltRNA_{CUA}* pair (Fekner *et al.*, 2009; Nguyen *et al.*, 2009b). While the ncAA 4-Azido-L-phenylalanine (AzF) has been incorporated into proteins using an evolved mutant of *MjTyrRS/tRNA_{CUA}* pair. (Chin *et al.*, 2002). As discussed earlier, the evolutionary studies on *MjTyrRS/tRNA* identified five mutations to the *MjTyrRS* for successful incorporation of *o*-nitrobenzyl-*O*-tyrosine (pcY) in response to an amber codon (Deiters *et al.*, 2006).

4.2 Results & discussion

4.2.1 Construction of VHH amber mutants

Two methods were used in this thesis to insert in frame amber codons into the coding sequence of the gene of interest. A commonly used method to create specific, targeted changes (including insertions, deletions and substitutions) in plasmid DNA is site-directed mutagenesis. Initially, a method that was pioneered in 1985 (Kunkel, 1985), this powerful technique is commonly used as a method to make changes in protein activity as a result of DNA manipulation. This *in vitro* method is based on the design of mutagenic DNA primers which are used with PCR to insert desired mutations in parent DNA. Further information on the specific protocol can be found in the methods chapter (2.1.8.9). The alternative method is by using a synthetic double-stranded DNA, which is ordered as geneblock from a commercial supplier. Although site-directed mutagenesis is a cost effective method compared to the use of synthetic DNA, it can often be a time consuming experiment with various troubleshooting steps. A combination of these two techniques was used in the construction of amber codon containing expression vectors, and specific details will be discussed in the results.

To site-specifically insert a photo-protected amino acid derivative into VHH 7D12, two approaches were taken. In the first approach, lysine was identified as the key residue to block with a photo-protective group. As lysine's side chain contains a positively charged amino group and is frequently located at proteins active or binding sites (Betts & Russell, 2003) it makes an excellent candidate for the substitution with photocaged lysine as a method of enabling photocontrol over antigen binding. Five lysine residues were identified in the structure of VHH 7D12 and Gibson cloning strategies was used to mutate each residue to an amber codon. The lysine residues within the structure of VHH 7D12 (K3, K43, K65, K76, K87) were targeted for insertion of ncAA using amber suppression. The cloning strategy for inserting amber mutations at these positions in 7D12 involved use of synthetic gBlocks and Gibson assembly. Synthetic gBlocks were ordered with corresponding TAG mutations and Gibson

overhangs (Appendix Table A.3; GB004-8). K3TAG, K43TAG, K65TAG, K76TAG were inserted by digesting pSANG10-7D12 with XbaI and Sall restriction enzymes, while K87TAG was inserted using Sall and HindIII restriction enzymes. After cloning, sequences were verified using Sanger sequencing which resulted in five new plasmids (pSANG10-7D12-K3TAG/ 43TAG/ K65TAG/ K76TAG/ K87TAG) with five possible locations to test photocaged lysine mediated inhibition of antigen binding.

The second approach taken to create a photo-active antibody fragment was with the genetic encoding of photocaged tyrosine. Seven tyrosine residues are present in VHH 7D12; using the crystal structure of VHH 7D12 in complex with domain III of the extracellular region of EGFR (PDB; 4KRL) as a guide, three tyrosine residues, Y32, Y109 and Y113, were selected (Figure 4.3). The three tyrosine residues are highlighted in magenta, and although all three seem to be in close proximity to the binding interface between 7D12 and EGFR, position Y109 seems to have a preferential parallel orientation to the EGFR surface while Y32 and Y113 protrude into the binding pocket of EGFR.

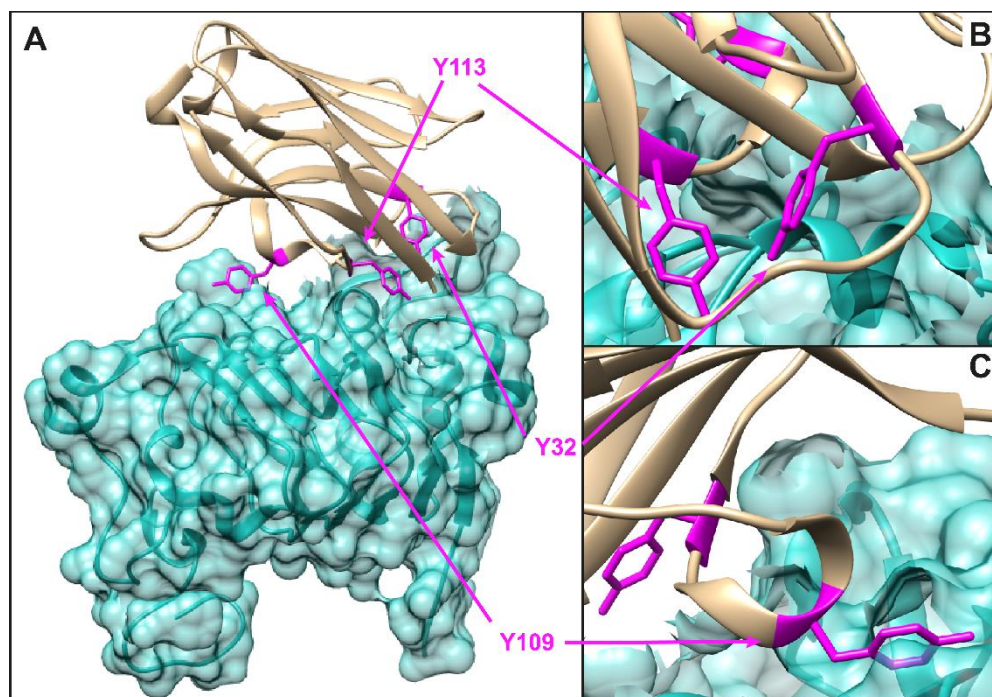


Figure 4.3: Crystal structure complex of 7D12-EGFR showing VHH 7D12 bound to domain III of sEGFR (sEGFRd3). A) VHH 7D12 in complex with sEGFRd3, 7D12 coloured cream with highlighted tyrosine

mutants (Y32, Y109, and Y113) in magenta and domain III of EGFR coloured cyan. B) View of interface region between VHH 7D12 and sEGFRd3 with focus placed on protruding side chains of Y32 and Y113. C) Alternative view of interface region between VHH 7D12 and sEGFRd3 highlighting the parallel orientation of Y109 has to EGFR surface. These structures were generated using UCSF Chimera software.

Similar methodology as the cloning strategy for lysine TAG mutations was used to replace the tyrosine residues. As discussed earlier, visualisation software was used to select three tyrosine residues out of the possible seven, and three gBlocks were designed with Gibson overhangs (Appendix Table A.3; GB020-22). The gBlock for Y32TAG was inserted after digesting pSANG10-7D12 with XbaI and Sall. The gBlocks for Y109TAG and Y113TAG were inserted after digesting pSANG10-7D12 with Sall and HindIII. After cloning, sequences were verified using Sanger sequencing and this resulted in the construction of three new plasmids (pSANG10-7D12-Y32TAG/Y109TAG/Y113TAG).

Amber mutants of another antibody fragment, VHH 2Rs15d, were also constructed. The results from chapter 3 showed successful cloning and expression of the anti-HER2 VHH 2Rs15d from the expression vector pSANG10-VHH-2Rs15d. To identify potential tyrosine residues for development of photoactive 2Rs15d, molecular dynamics simulations were performed by Dr Saher Shaikh to simulate pcY incorporation into various tyrosine positions and to predict effects of their binding to HER2. Simulation methods are described in detail in Bridge *et al.*, 2019. The tyrosine residue in position 37 was chosen as an ideal candidate for photocaging due to the predicted inhibition it would cause to HER2 binding. To replace tyrosine at position 37 with photocaged tyrosine, site-directed mutagenesis was performed. Detailed methodology on site-directed mutagenesis is listed in methods (2.1.8.9) and mutagenic primers (Appendix Table A.2; D119 and D120) were designed and ordered from IDT. After cloning, sequences were verified using Sanger sequencing and this resulted in the plasmid pSANG10-VHH-2Rs15d-Y37TAG.

4.2.2 Construction of suppressor plasmids

For incorporation of ncAA in response to an amber stop codon, a suppressor plasmid containing orthogonal aminoacyl- tRNA synthetase (aaRS)/ tRNA pairs is required. The first suppressor plasmid made during this study was for the incorporation of photocaged lysine. Photocaged lysine aaRS was PCR amplified from plasmid AG73_PCKRS_PyltRNA using Q5 High-Fidelity DNA Polymerase (NEB) according to the manufacturers recommendations. The PCR primers (Appendix Table A.2; D029, D030) were designed to generate Gibson overhangs corresponding to plasmid pCDF_PyIRS/PyltRNA_{CUA}. Plasmid pCDF_PyIRS/PyltRNA_{CUA} was then digested with NdeI, and PstI-HF restriction enzymes, and PCR product was ligated using Gibson assembly. The resulting plasmid pCDF_PcKRS/PyltRNA_{CUA} was transformed into DH10B cells and plated on kanamycin agar plates for overnight growth (37°C, 16 hours). Plasmid DNA was extracted from a single colony, and the correct insert was verified by Sanger sequencing.

Next, we designed a suppressor plasmid for incorporation of photocaged tyrosine in response to an amber stop codon. Based on previous work on incorporation of pcY (Deiters *et al.*, 2006) we designed synthetic geneblocks with five mutations in *MjTyrRS*, viz, Tyr₃₂ → Gly₃₂, Leu₆₅ → Gly₆₅, Phe₁₀₈ → Glu₁₀₈, Asp₁₅₈ → Ser₁₅₈ and Leu₁₆₂ → Glu₁₆₂. This gblock has appropriate overhangs for insertion into the pULTRA plasmid using Gibson assembly (Appendix Table A.3; GB024). The plasmid pULTRA_CNF was digested with NotI restriction enzyme, and *MjTyrRS* was separated from pULTRA backbone before the *MjPCY-RS* gBlock was inserted. The resulting plasmid pULTRA-PCY was transformed into DH10B cells and plated on kanamycin agar plates for overnight growth (37°C, 16 hours). Plasmid DNA was extracted from a single colony, and correct insert was verified by Sanger sequencing.

Before attempting to incorporate photocaged amino acids into the structure of VHH 7D12, it was essential to investigate the most efficient suppressor systems (*MjTyrRS* or *Mm/MbPyIRS*). This was achieved by an extensive comparison between commonly

used suppressor plasmids and is discussed in the next section of this chapter. To test PylRS/tRNA pair efficiency in the pULTRA plasmid, the aaRS/tRNA genes were cloned from pCDF_PylRS/PyItRNA_{CUA} plasmid into pULTRA_CNF. To replace the aaRS/tRNA pair, a two-step cloning strategy was designed first to replace the *Mj*TyrRS with *Mb*PylRS, followed by the replacement of *Mj*tRNA with *Mb*tRNA. Primers (Appendix Table A.2; D055, D056) were designed to amplify the *Mb*PylRS from pCDF_PylRS/PyItRNA_{CUA} and add Gibson overhangs for Gibson ligation into digested pULTRA backbone. The plasmid pULTRA_CNF was digested with NotI to remove *Mj*TyrRS, digested product was separated by size on 1% agarose gel, and pULTRA backbone was extracted from the gel. Gibson assembly was used to insert the PylRS PCR product into pULTRA resulting in the plasmid pULTRA-PylRS. After sequence verification pULTRA-PylRS was digested with PstI and XhoI to remove *Mj*tRNA, backbone was gel extracted, and the PyItRNA gBlock (Appendix Table A.3; GB031) was inserted by Gibson assembly. The final plasmid pULTRA-PylRS-PyItRNA showed successful replacement of the *Mj*TyrRS/tRNA pair with the *Mb*PylRS/tRNA pair.

4.2.3 Comparison of suppressor plasmids

As discussed earlier, there are two commonly used orthogonal aminoacyl-tRNA (aaRS)/tRNA pairs for genetically encoding non-colonial amino acids (ncAA) into proteins in *E. coli*. The *Methanosarcina mazei* (*Mm*) pyrrolysyl-tRNA synthetase pair (*Mm*PylRS/*Mm*tRNA_{CUA}) and the homologous *Methanosarcina barkeri* (*Mb*) pair (*Mb*PylRS/*Mb*tRNA_{CUA}) have been extensively developed for incorporation of many types of ncAA. The alternative derived from *Methanocaldococcus janaschii* (*Mj*) TyrRS/tRNA_{CUA} pair has been primarily used in the incorporation of aromatic ncAA related to phenylalanine. Over the past decade, there have been many iterations of highly efficient suppressor plasmids that have emerged within the literature, which has overall been significant for the development of this field. However, as there has been no comparative review it is difficult to compare the efficiencies of these suppressor plasmids. In this section we screen four frequently used suppressor

plasmids (pCDF_3xPylRS/PyltRNA, pSUP_MjCNFRS/6xMjtRNA, pEvolv_2xMjCNFRS/MjtRNA and pULTRA_MjCNFRS/MjtRNA) to determine which of these plasmids is most efficient for incorporating certain ncAAs into VHH 7D12. The results from this study would determine which suppressor plasmids would be used later for incorporation of photocaged amino acids into VHH 7D12. The first comparison was between plasmids containing *Mm* or *Mb* PylRS/tRNA pairs and *Mj* TyrRS/tRNA pairs. The plasmid pCDF_PylRS/PyltRNA was used for incorporation of N6-(tert-butoxycarbonyl)-L-lysine (BocK) in VHH 7D12, as this ncAA is a substrate for incorporation with PylRS. Plasmids containing MjTyrRS; pSUP_MjCNFRS/MjtRNA, pEvolv_MjCNFRS/MjtRNA and pULTRA_MjCNFRS/MjtRNA were used for incorporation of *p*-azido-phenylalanine (AzF). To investigate the efficiency of site-specific incorporation of ncAA we co-transformed these suppressor plasmids with pSANG10-7D12-Y32TAG in BL21 (DE3) pLysS cells. These transformed cells were used in a small-scale expression (10 mL) and the media was supplemented with either 4mM AzF or 8mM BocK (all samples induced with IPTG). ncAA were dissolved in NaOH and were added to positive samples. After addition of ncAA to the growth media, the same amount of HCl was added and the pH of the media was adjusted to 7. Extracted proteins were analyzed by Western blot, as shown in Figure 4.4. The *Mj*TyrRS plasmids used in this study show the evolutionary steps Peter Schultz group made on their suppressor plasmids, starting with pSUP (Ryu & Schultz, 2006) being refined to pEvolv (Guo *et al.*, 2009) and finally resulting in pULTRA (Chatterjee *et al.*, 2013). The pCDF PylRS/tRNA plasmid (Sachdeva *et al.*, 2014) designed later by the Chin group uses the PylRS system for incorporation of ncAA in response to both amber stop codon and quadruplet codons in *E. coli*.

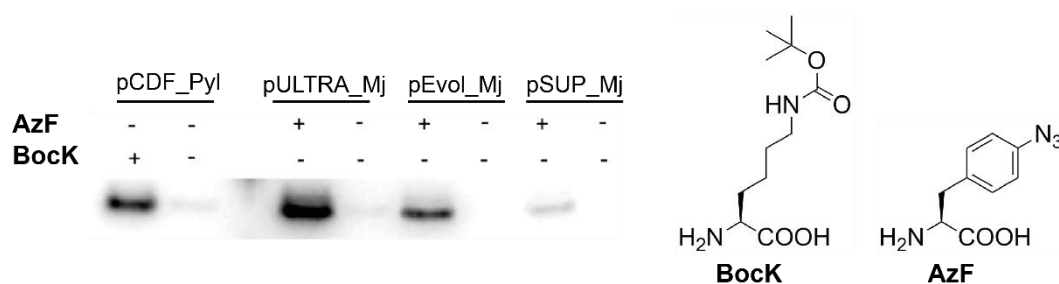


Figure 4.4: Screening of amber suppression efficiency of pCDF_3xMbPylRS/MbPyltRNA_{CUA}, pSUP_MjCNFRS/6xMjtRNA_{CUA}, pEvolv_2xMjCNFRS/MjtRNA_{CUA} and pULTRA_MjCNFRS/MjtRNA_{CUA}

plasmids. Comparison of band intensities of his-tagged VHH 7D12-Y32 (loaded by normalised culture OD₆₀₀) with Western blot shows pULTRA suppressor plasmid is most efficient at incorporation of 4-Azido-L-phenylalanine (AzF) using *Mj*RS/*Mj*tRNA pair and slight reduction of expression is shown in the incorporation of N6-(tert-butoxycarbonyl)-L-lysine (Bock) with *Mb*PyIRS/*Mb*PyItRNA pair in 7D12.

The Western blot results showed expression of his-tagged recombinant proteins relied on the addition of ncAA in the media. Furthermore, the suppressor plasmids containing *Mj* CNFRS/ *Mj*tRNA_{CUA} pair allowed incorporation of AzF at position 32 in 7D12 at varying levels. The highest to lowest efficiency for incorporation of AzF was pULTRA, pEvolv and then pSUP, which follows the time frame of published literature.

As higher expression was observed using the *Mj* system of pULTRA, we next wanted to investigate if transferring the PyIRS/tRNA pair CDS from pCDF to pULTRA would further increase the efficiency of site-specific incorporation of Bock or N6-[(2-propynyloxy)carbonyl]-L-lysine (CAK) and to also test incorporation of pcY using the mutated plasmid pULTRA_PCY. Bock and CAK have been shown as two excellent substrates for PyIRS incorporation. The three suppressor plasmids (pULTRA_CNF, pULTRA_PCY and pULTRA_Pyl) were separately transformed into BL21 (DE3) pLysS containing pSANG10-7D12-Y32TAG. To compare wt7D12 expression with incorporation efficiency of the suppressor plasmids we co-transformed pULTRA_CNF and pSANG10-7D12(wt). The media was supplemented with either 8mM Bock/CAK or 4mM pcY/AzF. Proteins were expressed in 100 mL cultures and purified with Ni-NTA before concentration with Vivaspin 500 (MWCO 3K). Samples were then resolved on SDS-PAGE, as shown in Figure 4.5.

High levels of ncAA incorporation were seen with pULTRA_CNF and pULTRA_PCY. There was a slight reduction in the expression of 7D12-Y32 AzF with pULTRA_CNF compared to wt7D12 levels. However, incorporation and expression of 7D12-Y32pcY was similar to wt7D12. Unfortunately, expression levels of pULTRA_Pyl were not comparable to the other pULTRA plasmids. Both CAK and Bock had a decrease in incorporation of 7D12-Y32. To compare pCDF efficiency to pULTRA_Pyl, we designed a similar experiment for incorporating CAK and Bock.

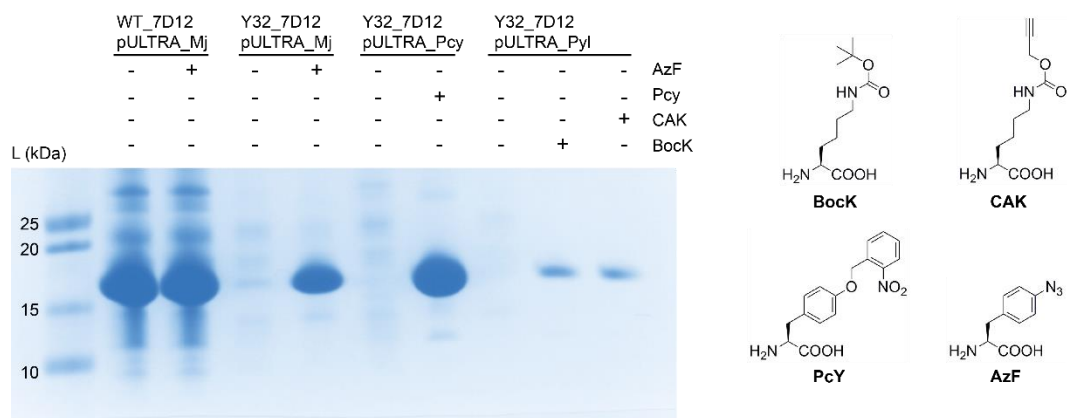


Figure 4.5: Screening of several versions of pULTRA suppressor plasmid with the genetic site-specific incorporation of various ncAA in VHH 7D12-Y32TAG. The observed band intensities in the Coomassie stained gel (loaded by normalised culture OD₆₀₀) demonstrated a slight reduction in expression of 7D12 with the incorporation of 4-Azido-L-phenylalanine (AzF) with pULTRA-CNF suppressor plasmid compared to wild-type 7D12 expression. The incorporation of *o*-nitrobenzyl-*O*-tyrosine (pcY) in 7D12 with pULTRA-PCY was shown have similar expression to wild-type 7D12, while incorporation efficiency of pULTRA-Pyl showed significant reduction in expression compared to wild-type when encoding N6-(tert-butoxycarbonyl)-L-lysine (BocK) and N6-[(2-propynyloxy)carbonyl]-L-lysine (CAK).

The two suppressor plasmids (pCDF-Pyl and pULTRA_Pyl) were transformed into BL21 (DE3) pLysS containing pSANG10-7D12-Y32TAG. A single colony was used to inoculate a 5 mL starter culture which was incubated overnight (2xTY, Kanamycin, Spectinomycin, 4% glucose; 37°C, 16 hours, 200 rpm). The next day, the starter culture was used to subculture 100 mL fresh 2xTY-GKS to an OD₆₀₀ of 0.1 and grown until OD₆₀₀ of 0.4-0.6. Once the desired OD₆₀₀ was reached, either 8mM BocK or CAK was added to the culture along with IPTG (1 mM) to all samples to induce expression of 7D12-Y32TAG and grown overnight (30°C, 160 rpm). After harvesting cells as described in 2.1.9 the periplasmic fraction was filtering through a 0.2-µm filter unit and dialysed overnight (Slide-A-Lyzer dialysis cassette, 12-30 mL, 3500 MWCO) against 1X PBS. His-tagged recombinant proteins expressed in the periplasm were purified using Ni-NTA gravity-flow columns as described in 2.1.10 before concentration with Vivaspin 500 (MWCO 3K). Purified his-tagged proteins were resolved by size using SDS-PAGE and stained with Coomassie InstantBlue (Sigma-Aldrich) for analysis (Figure 4.6).

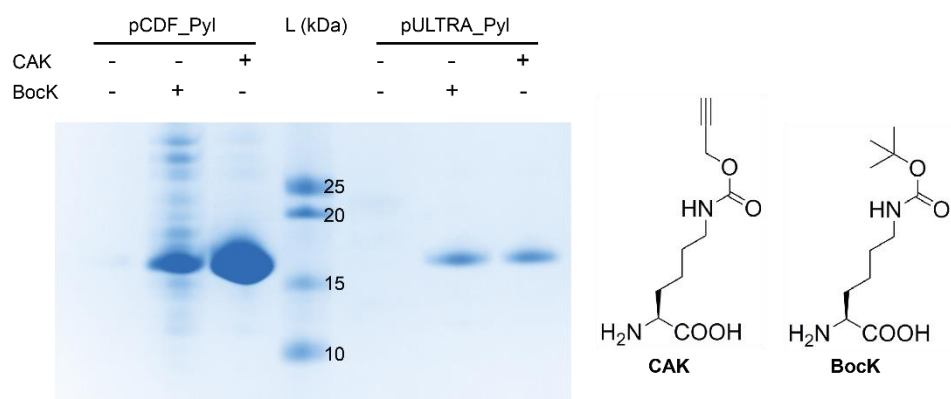


Figure 4.6: Suppressor plasmid efficiency comparison between PylRS/tRNA pair in pULTRA and pCDF vectors. The observed band intensities in the Coomassie stained gel (loaded by normalised culture OD₆₀₀) demonstrated higher genetic incorporation efficiency of N6-(tert-butoxycarbonyl)-L-lysine (BocK) and N6-[(2-propynyloxy)carbonyl]-L-lysine (CAK) in 7D12-Y32 with pCDF suppressor plasmid compared to pULTRA suppressor plasmid.

Both plasmids containing PylRS/tRNA pairs (pCDF and pULTRA) showed expression of 7D12-Y32TAG containing nCAA only with the addition of nCAA to the growth media. Higher expression of 7D12-Y32TAG with pCDF-PylRS/tRNA was observed when using CAK compared to BocK, signifying that the nCAA CAK is a more suited substrate for PylRS incorporation. However, when comparing pCDF-Pyl efficiency to pULTRA-Pyl a significant decrease is observed in the production of 7D12-Y32TAG. These results are likely due to differences in promoters and the number of copies of PylRS present on pCDF-Pyl and pULTRA-Pyl. A single copy of PylRS and tRNA are present on pULTRA-Pyl, and expression of PyltRNA on pULTRA vector is controlled by *proK* promoter and terminator while the PylRS is under the inducible *tac* promoter. Compared to the optimised expression of pCDF-Pyl vector that contains 3 copies of PylRS that are under control of the weak *glnS'* constitutive promoter while the single copy of PyltRNA was under the inducible expression of the relatively strong *lpp* promoter. The substantial decrease in nCAA encoding efficiency between pCDF-Pyl and pULTRA-Pyl is possibly caused by insufficient optimization of pULTRA plasmid for the ideal level of aaRS/tRNA pairs within the host organism.

4.2.4 Expression of VHH 7D12 containing site-specifically incorporated photocaged tyrosine

To investigate the expression of light activated antibody fragments by site-specific incorporation of photocaged amino acids, both the amber mutant expression vector and suppressor plasmid were co-transformed into *E. coli* for periplasmic expression. We initially planned to incorporate photocaged lysine (pK) into 7D12, which would be encoded using the plasmid pCDF_PcKRS/PyltRNA_{CUA}. While plasmid construction was being carried out, the PylRS/tRNA incorporation efficiency was tested with the site-specific encoding of Bock in the five amber codon locations (Lysine-TAG mutations). To test incorporation efficiency at these mutants using pCDF-Pyl, BL21 (DE3) pLysS *E. coli* cells were transformed with pSANG10-7D12 (WT and K-TAG mutants) and pCDF_PylRS/PyltRNA_{CUA}, and grown in presence of kanamycin and spectinomycin. In addition, we also tested incorporation of AzF using pULTRA vector in one of these amber mutants, K76TAG. Using similar methods as above, pULTRA_MjRS/tRNA_{CUA} was co-transformed with pSANG10-7D12-K76TAG. A single colony of the transformed cells was selected and inoculated in started culture which were used to subculture 10 mL 2xTY-GKS (4% glucose, kanamycin, spectomycin). Periplasmic expression and extraction was carried out as described in methods (2.1.9) followed by Ni-NTA purification (2.1.10) and protein concentration (2.1.11). The resulting protein extract was resolved on precast stain free Mini-PROTEAN TGX gel (Figure 4.8.A) followed by transfer to PVDF membrane and detection of his-tagged proteins by Western blot (Figure 4.8.B).

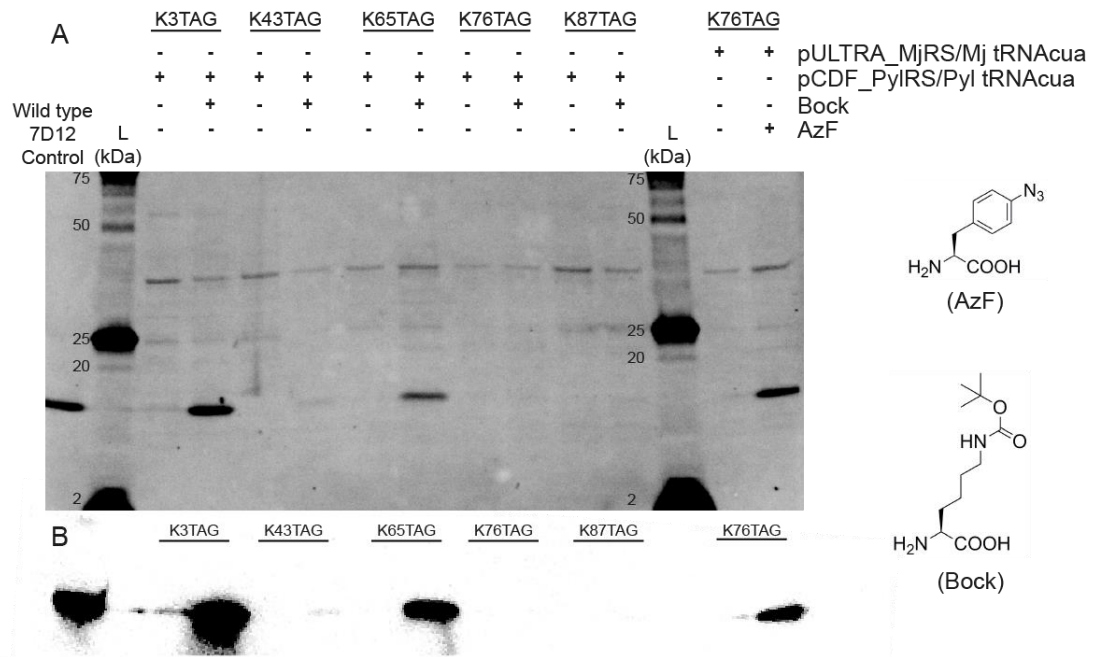


Figure 4. 7: Expression of 7D12 with genetic site-specific incorporation of two nCAA in response to five lysine amber mutants. (A) Observed band intensities on stain free TGX gel (loaded by normalised culture OD₆₀₀) demonstrated efficient incorporation of N6-(tert-butoxycarbonyl)-L-lysine (Bock) in response to amber mutants at position K3 and K65 with pCDF-PylRS/tRNA suppressor plasmid. Band corresponding to 7D12 detected in response to amber mutant at position K76 with the addition of 4-Azido-L-phenylalanine (AzF) and pULTRA-MjRS/tRNA. (B) Following transfer of proteins on TGX gel to PVDF membrane, Western blot detection of his-tagged proteins resulted in similar identification of 7D12.

Likewise to previous expressions of recombinant proteins encoded with nCAA, the successful expression of full-length protein relied on the addition of nCAA in the culture. The encoding of Bock into K3TAG resulted in similar levels of expressed recombinant protein to wild type VHH 7D12, while a slight reduction of expressed protein was observed with Bock incorporation at position 65. However, little to no expression of VHH 7D12 was detected for K43TAG, K65TAG and K87TAG indicating unsuccessful incorporation of Bock in these positions. Interesting, the incorporation of AzF in position 76 with pULTRA-CNF plasmid resulted in expression similar to wild type which could, in theory, be signifying that the suppressor plasmid pULTRA has increased suitability in the genetic encoding of nCAA. Due to difficulties in the synthesis of photocaged lysine, and to not delay experimental results, we next

planned to proceed with the investigation of genetically encoding a photocaged tyrosine. Photocaged tyrosine was successfully synthesised by Dr Amit Sachdeva during this time.

A similar approach was used to site-specifically incorporate photocage tyrosine in VHH 7D12. First, pSANG10-7D12 (WT and Y-TAG mutants) were co-transformed into BL21 (DE3) pLysS *E. coli* cells with pULTRA_PCY. A single colony of cells containing these plasmids (due to resistance to kanamycin and spectinomycin) was used to inoculate a starter culture, which was then used to subculture 100ml 2xTY-GKS. To induce expression 1 mM final concentration of IPTG was added to all samples and 4 mM final concentration of pcY dissolved in NaOH was added to positive samples. After addition of pcY, the same amount of HCl was added and the pH was adjusted to 7. The total protein extract was then purified using Ni-NTA and concentrated using Vivaspin columns (3K MWCO). The resulting protein was resolved by size on SDS-PAGE and high levels of expressed protein can be seen, shown in Figure 4.8.

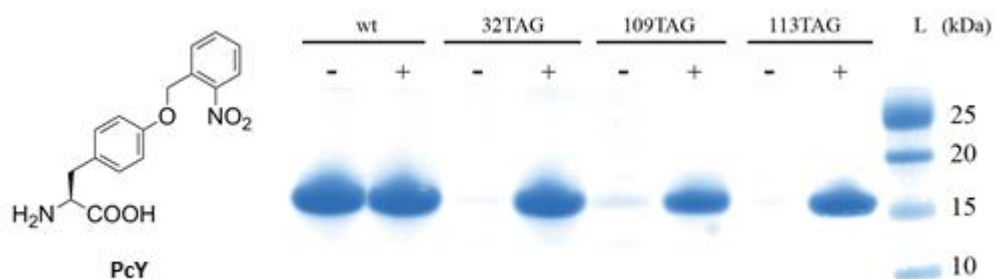


Figure 4.8: Genetic site-specific incorporation of pcY in VHH 7D12. The expression of three amber mutants of 7D12 (7D12-Y32TAG, 7D12-Y109TAG and 7D12-Y113TAG) only occurs in the presence of *o*-nitrobenzyl-*O*-tyrosine (pcY). Comparison of band intensities for amber mutants with wt7D12 shows efficient incorporation of pcY.

The yield of wt7D12, 7D12-Y32pcY, 7D12-Y109pcY and 7D12-Y113pcY were 10.1, 5.3, 3.2, 1.7 mg per litre of culture, respectively. The protein expression was performed in the presence and absence of pcY, for amber mutants of 7D12, full length 7D12 was only expressed when the media was supplemented with pcY. The variability of amber

codon suppression and subsequent differences in expressed yield of 7D12 with site-specific encoding of pcY are a result of multiple factors such as codon context effects in which surrounding nucleotides of an amber codon in a specific location can affect suppression efficiency. Although only a slight variation in the levels of expressed protein was observed for these three amber mutants, these factors can significantly reduce the expression of recombinant proteins and will be discussed in detail later in this chapter. The small difference in molecular weight with the addition of the photocaged group cannot be resolved on SDS-PAGE, therefore we further confirmed that pcY had been incorporated using Electrospray Ionization Mass Spectrometry (ESI-MS), shown in Figure 4.9.

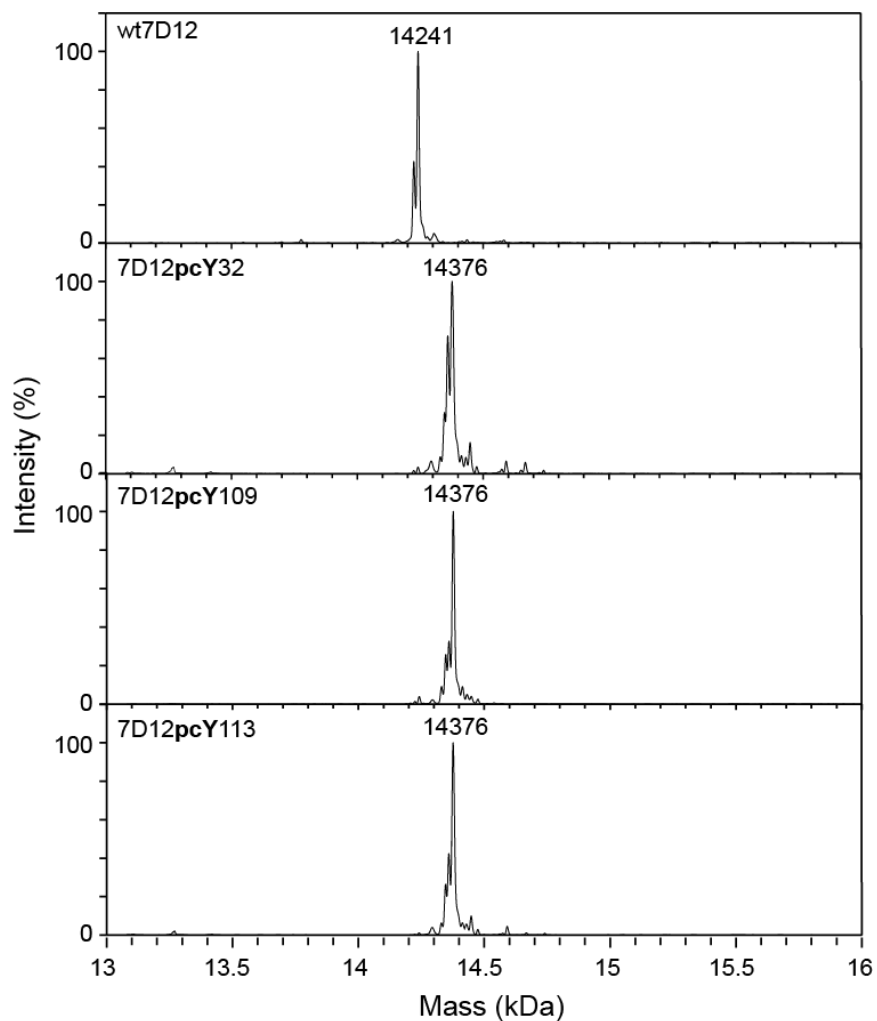


Figure 4.9: Electrospray Ionization Mass Spectrometry (ESI-MS) measurements of expressed 7D12 and three amber mutants (Y32, Y109, and Y113). Wild type VHH 7D12 resulted in a measured mass of

14241 Da and corresponded to ExPASy ProtParam calculated mass. The three amber mutants with site-specific incorporation of pcY in positions Y32, Y109 and Y113 resulted in an increased mass of 14376 Da which relates to the additional mass of photocaged group.

The calculated mass for wt7D12 was predicted using the ProtParam tool (ExPASy) and the addition of pcY was calculated to give the predicted mass of 7D12-Y32pcY, 7D12-Y109pcY and 7D12-Y113pcY. The shift in mass from 14241 Da to 14376 Da shows the successful addition of photocaged tyrosine at three positions within VHH 7D12. To investigate if the photo-caged group can be removed upon irradiation with 365 nm light, we designed mass spectrometry based experiments. 7D12 samples containing site-specifically incorporated pcY were exposed to 4 minutes of 365nm light using a UV transilluminator. To load the sample, 50 μ L of caged 7D12 was pipetted onto an autoclaved glass coverslip before being irradiated for 4 minutes. The resulting de-caged sample was collected and analysed by ESI-MS (Figure 4.10).

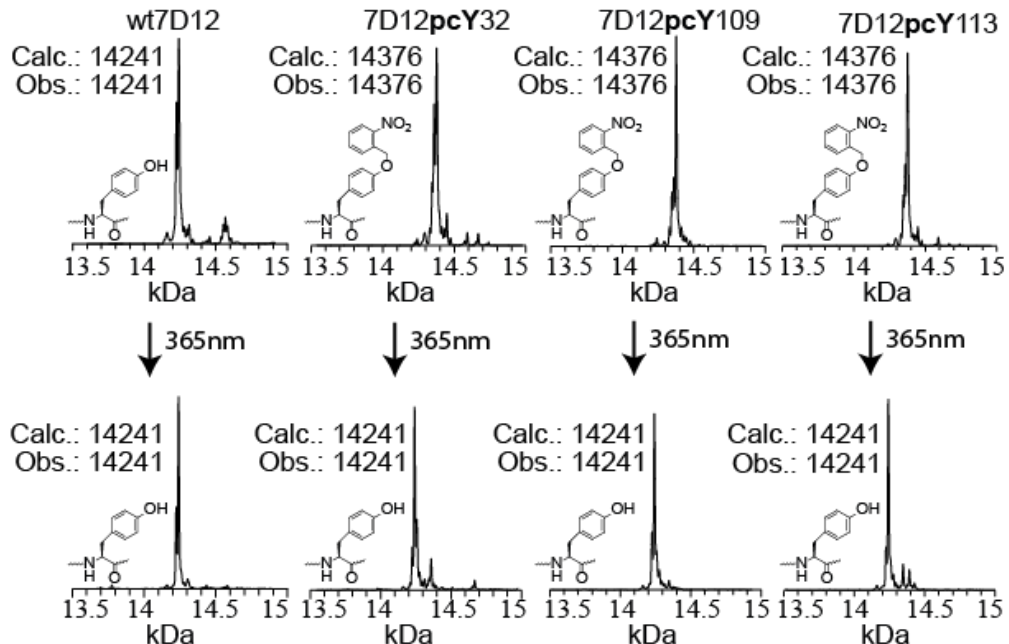


Figure 4.10: Electrospray Ionization Mass Spectrometry (ESI-MS) measurements of expressed 7D12 and three amber mutants (Y32, Y109, and Y113) before and after irradiation with light (365 nm, 4 minutes). First row represents before irradiation, observed mass of wild-type VHH 7D12 is 14241 Da while three mutants with pcY incorporation have increased mass of 14376 Da. After irradiation, the second row demonstrates de-caging of pcY mutants and decreased mass to wild-type level.

The ESI-MS results from before de-caging shows a mass of 14241 Da for 7D12 and an increased mass of 14376 Da for 7D12-Y32pcY, 7D12-Y109pcY and 7D12-Y113pcY. After 4 minutes of 365 nm irradiation all four samples show the mass of 14241 Da, consistent with conversion to wild type VHH 7D12. This demonstrates the successful de-caging of genetically encoded pcY and the de-protection of tyrosine residue resulting in the ncAA reverting back to a native tyrosine.

4.2.5 Expression and optimisation of VHH 2Rs15d with photocaged ncAA

After optimizing pcY incorporation into VHH 7D12, we next wanted to investigate the genetic encoding of pcY into other antibody fragments. The results from chapter 3 showed the successful cloning and expression of the anti-HER2 VHH 2Rs15d from the expression vector pSANG10-VHH-2Rs15d. To identify potential tyrosine residues for amber codon mutation, modelling software was developed by Dr Saher Shaikh to simulate pcY incorporation into various tyrosine positions and to predict effects on binding affinities to HER2. The tyrosine residue in position 37 was chosen as a good candidate for photocaging due to the predicted inhibition it would cause to HER2 binding. Following the construction of the plasmid pSANG10-2Rs15d-Y37TAG, it was co-transformed into BL21(DE3)pLysS with pULTRA-PCY. To compare expression between wild type VHH 2Rs15d and VHH 2Rs15d with site-specific encoded pcY, the plasmid pSANG10-VHH-2Rs15d was co-transformed into BL21(DE3)pLysS with pULTRA-PCY. As a control pSANG10-7D12(wt) and pSANG10-7D12-Y32TAG were co-transformed BL21(DE3)pLysS with pULTRA-PCY for comparison between 7D12 and 2Rs15d antibody fragment expression. A single colony of cells conferring kanamycin and spectinomycin resistance was used to inoculate a starter culture which was then used to subculture 10ml 2xTY-GKS. To induce expression, 1 mM final concentration of IPTG was added to all samples and 4mM final concentration of pcY dissolved in NaOH was added to positive samples. After addition of pcY, the same amount of HCl was added and the pH was adjusted to 7. Extracted periplasmic proteins were directly loaded onto an SDS-PAGE for separation by size before being transferred to

nitrocellulose membrane for Western blotting. Detection of his-tagged proteins was achieved with primary antibody incubation targeted to His-tag followed by secondary antibody incubation which contained an HRP conjugate for chemiluminescence. The developing reagent SuperSignal chemiluminescence substrate (Thermo Scientific) was added to the membrane and chemiluminescence was imaged on a GelDoc XR+ system (Figure 4.11).

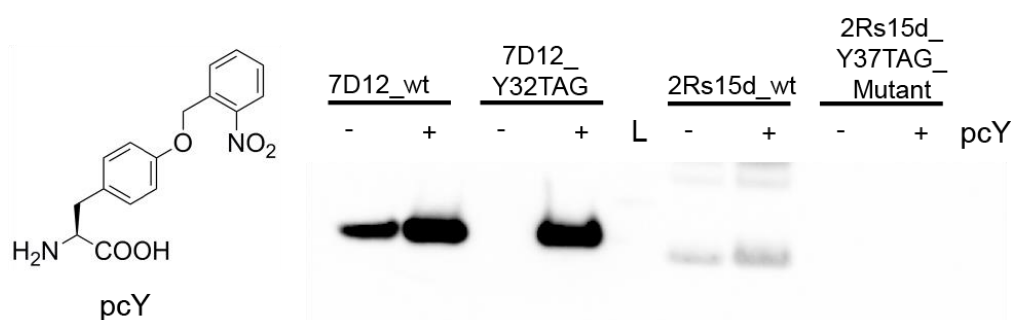


Figure 4.11: Western blot detection of his-tagged proteins from the expression of pSANG10-7D12 (And Y32TAG mutant) compared to pSANG10-VHH-2Rs15d (And Y37TAG mutant). All samples were induced with IPTG and positive and negative samples defined by addition of pcY. Intense band of pSANG10-7D12 and Y32 amber mutant indicate high levels of expression of VHH 7D12. Similar expression of 2Rs15d is not observed from the expression of pSANG10-VHH-2Rs15d and Y37 mutant (loaded by normalised culture OD₆₀₀).

Similar to previous results, the expression of VHH 7D12 with/without pcY from the expression plasmid pSANG10 showed a high yield of his-tagged recombinant proteins. The expected results from wild type VHH 7D12 in the absence and presence of pcY should have yielded similar levels of recombinant protein as both samples were induced with IPTG. However, the observed results indicate a decrease in expression from the sample without pcY. This is likely due to experimental error, additionally, with consideration of previous expression studies (that wt7D12 yield is similar to that of 7D12-Y32pcY) it is logical to assume that the band corresponding to wild type VHH 7D12 (with pcY) is the correct level of expression. In contrast to VHH 7D12 expression, a significant decrease in yield is shown in the expression of VHH 2Rs15d. The efficiency of ncAA incorporation in response to an amber codon can be

highly variable, and several factors affecting the efficiency of amber suppression are largely unknown (Schwark *et al.*, 2018). Two factors that are thought to affect the variability of amber codon suppression: 1) reduced expression due to the competition between amber suppression and endogenous release factors (RF1), and 2) codon context effects (Brar, 2016). A substantial amount of research has been focused on the generation of GRO systems to reduce or remove competing RF1, these systems are discussed in the first chapter so will not be reviewed in this section. However, the codon context, the effect of neighbouring codons to the amber suppression efficiency are largely unexplored. In a recent study (Schwark *et al.*, 2018), an investigation into the effects of the nucleotide identity of the 3'-side of the amber codon (+4 position, the first three being the amber codon) showed that improved amber incorporation was achieved when the location was occupied with a purine nucleotide (specifically, highest efficiency was achieved with +4 adenine) and decreased efficiency was demonstrated with a pyrimidine nucleotide (+4 cytosine exhibited lowest efficiency). The mechanisms behind this are currently unclear; however, one hypothesis is that the potential preference of +4 position purine is a result of base stacking stability between suppressor tRNA–mRNA interactions.

To investigate the specific reading context of the suppressed codon in VHH 2Rs15d-Y37TAG, and whether pcY incorporation efficiency could be improved, a mutagenesis study was designed to mutate the codon downstream (R38) of Y37TAG. As the direct mutation of the +4 position from a cytosine to an adenine would change the amino acid incorporated from an arginine to a serine, we decided to conserve the Arg residue at position 38 and mutate it to synonymous variations. There are six codons that code for arginine (CGC, AGA, CGA, CGG, AGG, and CGT) with various levels of usage in *E. coli* organism. Mutagenic primers (Table 4.3) were designed for a site-directed mutagenesis experiment resulting in 6 amber codon plasmids with alternative downstream codons.

Table 4.3: Synonymous codon mutations made to downstream arginine codon (R38).

Codon	<i>E. coli</i> usage*	Mutagenic primers**	Plasmid
CGC (Original)	36%	N/A	pSANG10-VHH-2Rs15d (Y37TAG)
AGA	7%	D164, D165	pSANG10-VHH-2Rs15d (R38AGA)
CGA	7%	D200, D204	pSANG10-VHH-2Rs15d (R38CGA)
CGG	11%	D216, D217	pSANG10-VHH-2Rs15d (R38CGG)
AGG	4%	D214, D215	pSANG10-VHH-2Rs15d (R38AGG)
CGT	36%	D218, D219	pSANG10-VHH-2Rs15d (R38CGT)

* % use of codon in *E. coli* compared to its synonymous variations.

** Appendix Table A.2 for full sequences

For expression of VHH 2Rs15d with the site-specific genetic encoding of pcY, a similar 10 mL expression was performed as above. Seven expression plasmids (wt2Rs15d and six variations of Y37TAG) were co-transformed with pULTRA-PCY. Protein expression was performed both in absence and presence of pcY, while all samples had IPTG. Extracted his-tagged recombinant proteins were detected by Western blot (Figure 4.12).

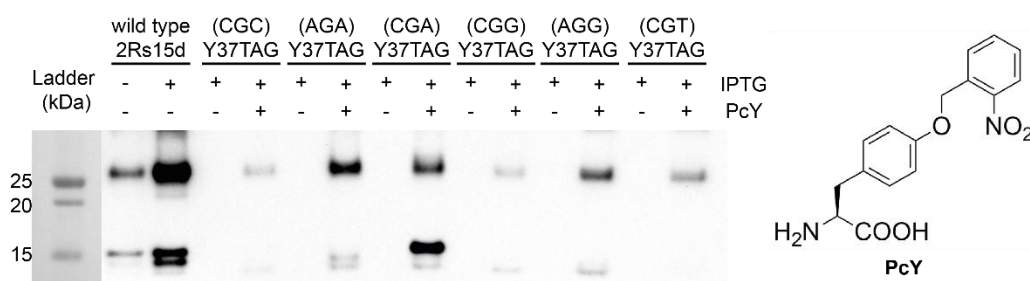


Figure 4.12: Screening of pSANG10-VHH-2Rs15d amber codon context at position Y37 with the incorporation of pcY. Six synonymous codon mutations (at position R38) resulted in various levels of expressed 2Rs15d (loaded by normalised culture OD₆₀₀) in the presence of pcY.

Similarly to results discussed in chapter 3, the likely presence of a dimeric molecular species of 2Rs15d is observed with the successful expression of 2Rs15d. Further similarities are seen with the reduced expression of Y37TAG (CGC; original downstream codon) which are in agreement with previous results (figure 4.11). Interestingly, the effect of downstream codon mutations on incorporation of pcY at position 37 in Rs15d shows drastically varying levels of expression. The original hypothesis that the +4 position nucleotide mutation from purine to pyrimidine (C to A) has shown minor improvements in incorporation efficiency of pcY, both AGA and AGG mutations demonstrate slightly higher expression than original CGC arginine codon. However, the highest difference in incorporation efficiency can be seen with the mutation of the arginine codon to CGA (similar expression to wild type 2Rs15d), which suggests that the +4 nucleotide position of the amber codon at this location is not directly linked to incorporation efficiency. Higher incorporation efficiency of pcY is observed with the mutation of CGC arginine codon to less frequently used synonymous codons. The expression of AGA, CGA and AGG mutants resulted in the three highest yields of recombinant protein of the six codons tested and each of these three codons have an *E. coli* usage of less than 7%, while in contrast, the reduced expression of CGC and CGT mutants have a codon usage of 36% in *E. coli*. However, not enough data is available to conclusively determine the variation in expression levels observed with the synonymous mutations of the downstream codon. For a clearer understanding of the processes behind this mechanism, multiple tyrosine amber mutant locations would need to be investigated, along with testing these expression systems in GRO containing RF1 knockout as a method of reducing endogenous amber codon competing systems.

CHAPTER 5

Assessment of antibody-antigen binding on the surface of live cancer cells

5.1 Introduction

The last two chapters have demonstrated the optimisation and characterisation of an expression vector pSANG10 and the screening of several suppressor plasmids leading to the development of a suppressor plasmid pULTRA-PCY for insertion of the non-canonical amino acid (ncAA), *o*-nitrobenzyl-*O*-tyrosine (photocaged tyrosine or pcY) in response to an amber nonsense codon. The expression vector pSANG10 was utilised to express high yields of heavy chain only antibody fragments (VHH 7D12; Schmit *et al.*, 2014) that had previously been developed to target epidermal growth factor receptor (EGFR).

Mutations affecting EGFR overexpression or activity have been linked to many cancers including, lung, colon, head, and neck and have resulted in becoming a widespread therapeutic drug target in oncology. Mutations, amplification or misregulations of EGFR have been shown to lead to constant receptor activation and uncontrolled cell division which results in unregulated growth and tumour formation. Several EGFR inhibitors have been developed and clinically approved for the direct treatment of EGFR positive cancers. However, common adverse effects (found in more than 90% of patients) can result in a papulopustular rash that spreads across the face and torso (Liu *et al.*, 2013). Similar outcomes are seen with the use of anti-EGFR monoclonal antibodies, and necessitate the improvement of current immunotherapeutics to reduce non-specific targeting.

As discussed in the previous chapter, the development of a highly efficient system for genetic site-specific incorporation of pcY in 7D12 was accomplished. Three mutants of 7D12, viz. 7D12-32pcY, 7D12-109pcY and 7D12-113pcY, which have pcY at positions 32, 109 and 113 in 7D12, were successfully expressed in *E. coli*. ESI-MS confirmed the increased mass of expressed mutant 7D12 bearing pcY compared to wild type 7D12, indicating successful incorporation of pcY. Upon exposure to 365 nm irradiation the ESI-MS confirms mass loss corresponding to the *o*-nitrobenzyl moiety, with pcY reverting back to its native analog (tyrosine).

It was hypothesised that the addition of a photocaged moiety in the antigen binding site of 7D12 would result in an inactive form of the antibody fragment which could be restored to the active antibody upon irradiation with 365 nm light. As such the ability to facilitate photo-control over antibody-antigen binding would enable spatiotemporal control over the immunotherapeutic treatment and could reduce the commonly reported adverse effects of EGFR targeting antibodies.

In this chapter, a brief discussion of commonly used assays to measure protein-protein interactions will be presented. Subsequently, in the results and discussion an on-cell assay is described, developed as part of this thesis work, to assess the binding of 7D12 to EGFR on the surface of live cancer cells. Finally, experimental results on measurement of light-mediated binding between photocaged mutants of 7D12 and EGFR will be presented.

5.1.1 Techniques to measure binding affinity and kinetics of antibody-antigen interactions

5.1.1.1 Enzyme-linked immunosorbent assay

The enzyme-linked immunosorbent assay (ELISA) was simultaneously described by two research teams in 1971 (Engvall & Perlmann, 1971; Van Weemen & Schuurs, 1971). However, the method was primarily pioneered by Engvall and Perlmann, when they employed this technique to determine the level of IgG in rabbit serum. Since then, ELISA has become a method routinely used in research and diagnostic laboratories around the world for the detection and quantification of substances such as peptides, proteins, antibodies and hormones (Aydin, 2015). ELISA is typically performed by immobilising an antigen of interest to a stationary phase (such as microplate surface) for either direct detection by primary antibody or indirectly by a secondary antibody that recognises the primary (Figure 5.1). Separation between bound and non-bound material can be achieved by washing during the assay which removes non-specifically bound materials and enables detection of specific analytes.

To measure bound primary or secondary antibody, typically the antibody is linked to a fluorophore or an enzyme for detection. The most commonly used enzymes in ELISA are horseradish peroxidase (HRP) and alkaline phosphatase (AP). A broad range of substrates can be used to develop enzyme marker signal and often the selection of the substrate is dependent on the experimental design or instruments available for signal detection. Another popular ELISA format is the sandwich assay, developed in 1977 (Kato *et al.*, 1977). In this format the analyte is bound (or sandwiched) between two primary antibodies (the capture and detection antibody). The ELISA sandwich method has been reported to be 2-5 times more sensitive than other ELISA formats (Aydin, 2015). Outside of the direct, indirect, and sandwich ELISA formats (Figure 5.1), several other ELISA strategies have been developed, such as competitive ELISA, and in-cell ELISA. However, as this section is only a general overview of ELISA technique these formats will not be discussed.

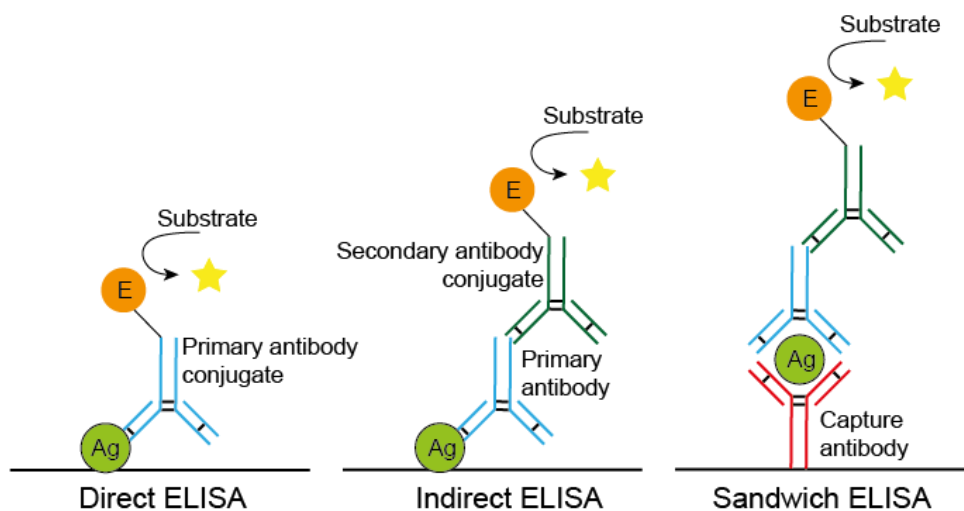


Figure 5.1: Schematic representation of common ELISA formats. For direct and indirect ELISA, the antigen of interest (Ag) is immobilised onto a solid surface for either direct detection using enzyme marker (E) linked primary antibody or indirectly detected with first the primary antibody which is then targeted by secondary antibody linked to an enzyme. For the sandwich ELISA technique, capture antibody is immobilised onto the solid surface that targets antigen of interest, which is then detected with relevant primary and secondary antibodies.

Over the last several decades the rising popularity of ELISA can in part be credited to the simplicity and speed of the method while having the ability to design experiments

that can rapidly handle a large number of samples in parallel, and while this method is a popular choice for the evaluation of various diagnostic targets it can have certain limitations. As detection is accomplished by assessing the measurable product produced from a substrate after incubation, the evaluated interactions are not monitored in real-time. Furthermore, weak interactions between antigen-antibody can occasionally be overlooked as detection of low affinity antibodies can be removed by the incubation and wash steps.

5.1.1.2 Surface plasmon resonance (SPR)

Another technique that has been gaining popularity since its inception 30 years ago is surface plasmon resonance (SPR) based affinity measurements. The use of SPR has been widely embraced for the characterisation of antibody-antigen interactions. Due to the ability of SPR to monitor biomolecular interactions in real time, it is considered the “gold” standard for monitoring a diverse range of protein-protein interactions (Olaru *et al.*, 2015). In contrast to ELISA, SPR based techniques allow for the visualisation of binding events in real time without the requirement of ligand or analyte labelling. The label free and real-time monitoring attributes of SPR facilitate accurate kinetic measurements and rapid analysis while reducing possible complications associated with ELISA.

SPR-based instruments use an optical method to monitor molecular interactions on a removable sensor chip. In order to detect molecular interactions, a ligand is immobilised onto the surface of the sensor chip and its binding partner (the analyte) is injected in aqueous solution over the sensor chip. Running buffers and sample buffers are delivered to the chip under continuous flow *via* a microfluidic system. A typical SPR biosensor chip is designed on a glass chip coated with a thin layer of chemically inert metal (usually gold) with an additional adhesive layer which acts as an anchor for the attachment of the immobilisation matrix (Figure 5.2.A). Ligands or

target molecules can be attached to the immobilisation matrix by either chemical coupling or capture coupling.

The SPR optical phenomenon describes changes in monitored refractive index *via* quantum mechanical principles. Although the underlying physical principals of SPR are complex and detailed theoretical understanding of SPR is not required for a working knowledge of the technique, a brief overview is presented here. When a beam of light is directed through a high refractive index medium, such as a prism, to the surface of gold-coated chip that is in contact with a low refractive index medium, such as a physiological buffer, some light is reflected from the interface (Figure 5.2.B). Depending on the angle at which the light strikes the interface, the light rays can exit the prism by refraction or can be totally internally reflected back through the prism for detection by a photodiode array detector. Furthermore, when the interface (glass chip) is coated with an inert metal film (usually gold) the reflection is not total as photons are absorbed by the gold layer and reduction in light intensity occurs in the reflected light. This reduction in light can be measured as a shift when mass changes occur above the gold chip surface. Specifically, the change of mass causes changes to the local refractive index, and as the reflected light profile is sensitive to changes in refractive index, the specific reflection angle shifts which is detected by photodiode array.

As the analyte binds to the immobilised ligand, the refractive index close to the surface changes in proportion to the mass of material bound. As biomolecular interactions are measured in real-time, the resulting change in refractive index is displayed as a sensorgram, plotted as binding response (resonance units; RUs) on the y-axis against time on the x-axis (Figure 5.3.C).

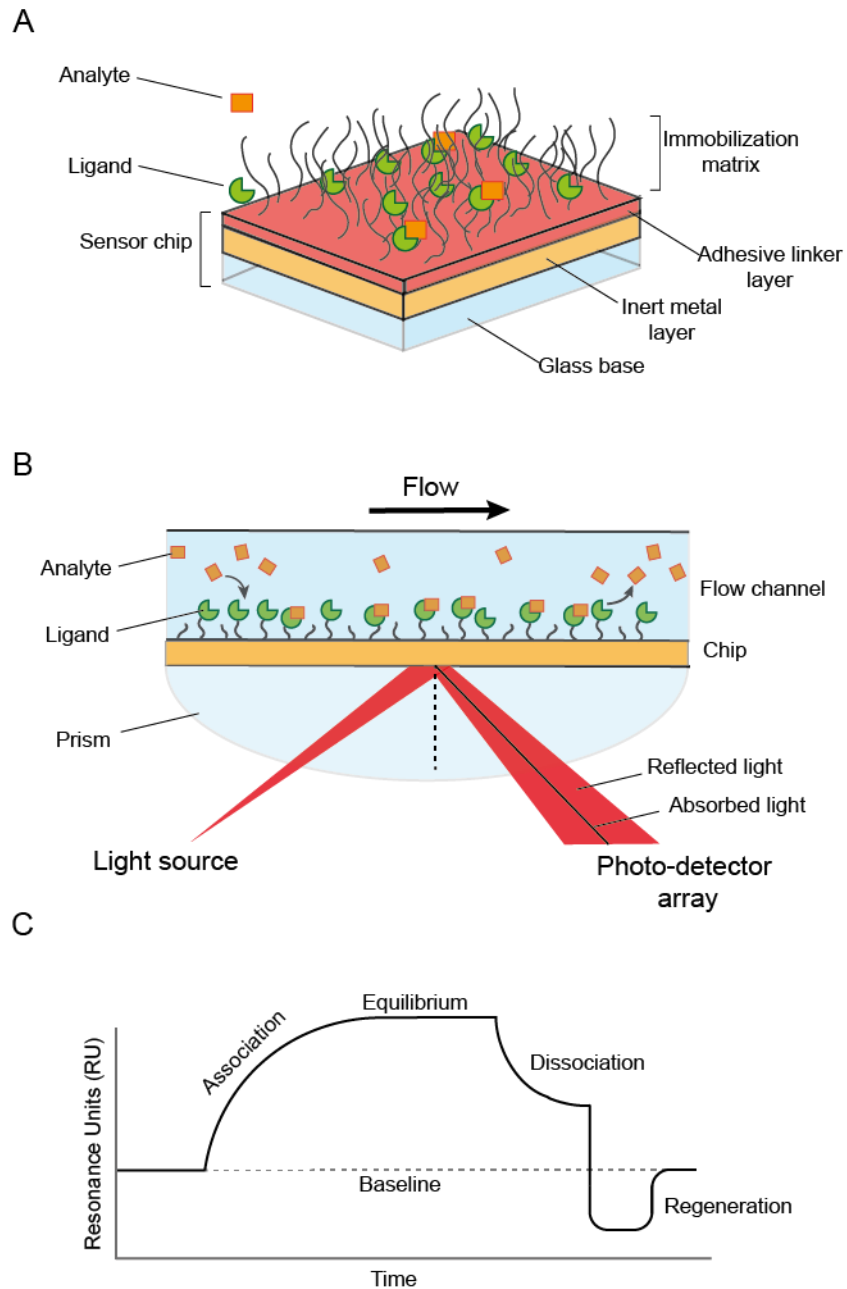


Figure 5.2: Schematic representation of key features in surface plasmon resonance based affinity measurements. (A) Characteristic layout of SPR sensor chip, a chemically inert metal (typically gold) is layered over a glass base. Adhesive layer anchors immobilisation matrix to inert metal film. (B) Cross-section of flow cell to demonstrate the real-time event of analyte delivery to immobilised ligand *via* microfluidic system. As analyte interacts and binds to ligand, the increased mass applied to sensor chip effects local refractive index which is measured by photodetector array. (C) Example sensorgram of measured change in refractive index by photodiode array in real time.

5.1.1.3 Isothermal titration calorimetry

Isothermal titration calorimetry (ITC) is a technique that can be used to determine the thermodynamic parameters of heat change during complex formation at constant temperature. The instrument is sensitive enough to characterise biomolecular interactions by detecting heat absorbed or released during a binding event (the change in binding enthalpy) to generate a complete thermodynamic profile relating to the parameters of the mechanism involved in binding to a biomolecule, this includes enthalpy changes, binding affinity/association constant and stoichiometry (Freyer & Lewis, 2008). As changes in heat or enthalpy occur in almost all chemical and biochemical interactions, the method can be used for a wide range of application such as antibody-antigen (Yamashita *et al.*, 2019), ligand-protein (Bronowska, 2011), nucleic acid-protein (Kutnowski *et al.*, 2019) small molecule/drug-protein (Marzabadi *et al.*, 1996) interactions.

Commonly used techniques such as ELISA or SPR, as mentioned above, often require the modification of the targeted biomolecule (with enzyme or affinity tags). These manipulations can perturb biological functionality of the targeted biomolecule which can cause detrimental effects on measured affinity interactions. Another characteristic related to these methods is the prerequisite of physically attaching the target molecule to a surface before characterising biomolecular interactions. This stipulation can result in unfavourable orientation or positioning of the target molecule on the solid phase prompting difficult to access active sites and causing a decrease in measured biomolecular interactions (Doyle, 1997). In comparison, ITC can characterise binding interactions with unmodified forms of the biomolecule in solution and is not affected by the drawbacks mentioned above.

The ITC instrument consists of two cells (sample cell and reference cell) that are designed with efficient thermal conducting material and surrounded by an adiabatic jacket to regulate consistent temperatures. To measure heat change during biomolecular interactions at constant temperature the instrument is based on a cell feedback system where the measured differential heat effects of the reference cell

(typically filled with buffer or water) are detected and directs a feedback circuit to regulate temperature of the sample cell (containing macromolecule) in order to maintain isothermal conditions between the two cells. As the ligand is titrated into the sample cell by long-needled syringe in precisely known aliquots, the measured heat fluctuation (either increase or decrease depending on the nature of the reaction) of the sample cell results in an increase or decrease in power to maintain equal temperature to the reference cell. Exothermic reactions cause the feedback power to decrease to maintain reference cell temperature, while endothermic reactions lead to an increase in feedback power. Power output observations for temperature control of the sample cell during injections are plotted against time (min) which results in a series of peaks of heat flow. As the effect of heat change (and consequently, power output) corresponds to ligand and macromolecule interactions, the analysis of recorded heat flow over time can be used to calculate thermodynamic parameters of the interacting partners under study (Perozzo & Scapozza, 2004).

ITC has been shown as a robust method for measuring molecular interactions and has several advantages compared to related affinity measurement techniques. The label-free characteristic of ITC enables measurements of binding interactions with unmodified native forms of the target molecule under study. This characteristic avoids possible immobilisation complications (physical attachment to solid surface can decrease performance metrics) as the experiment is performed in solution. Furthermore, by measuring interactions in solution, a wide range of biologically relevant conditions (pH, salt, temperature) can be tested. However, several design considerations need to be taken into account before experimentation. Both interacting components of the experiment require thorough purification to remove any contaminating enzymatic activity as measuring changes in heat or enthalpy of noncovalent interactions could apply to contaminants and could affect results of investigated event. Furthermore, large amounts of highly purified interacting biomolecules are required for the sample cell and titration, which can lead to time consuming expression and purification experiments and additional associated costs. However, this drawback has reduced considerably with the development of NanoITC

system (TA instruments) which reports higher sensitivity with low sample concentration (Nevola & Giralt, 2015).

5.1.2 Experimental drawbacks of current techniques to measure antibody-antigen interactions

ELISA, SPR, and ITC are commonly used techniques for the investigation into protein-protein interactions, and have several useful qualities as well as certain limitations. Depending on the therapeutic or diagnostic setting, the individual techniques can be utilised as powerful tools to gain a wealth of knowledge. However, three constraining aspects of the discussed techniques compelled investigations into the development of a novel binding assay for the analysis of 7D12 and EGFR interactions:

1. The requirement of sophisticated instrumentation to perform and/or analyse the experiment. The ELISA technique is less affected by this potential challenge as the only essential instrument required is a microplate reader for acquisition of the enzyme produced signal. Although microplate washers and microplate incubator shakers are useful instruments for reducing experimental run time and facilitating reproducibility between experiments, cost effective alternatives are available. As microplate readers are a standard instrument found within biological laboratories around the world and a broad range of substrates are available for the development of a variety of enzyme markers, the associated instrumental expenses are relatively low. However, ITC systems (such as NanoITC; TA instruments) and SPR based instruments such as BIAcore (GE Lifesciences) have high initial expenses of the instrument accompanied with maintenance costs and comprehensive technological working knowledge.
2. The large amounts of purified ligand required for extensive investigations into protein-protein interactions. In terms of an experimental setup to investigate

affinity interactions between the binding partners 7D12 and EGFR, the receptor (EGFR) would require attachment to microplate for ELISA experiments, immobilisation on a sensor chip for SPR based analysis or highly purified concentrations of sEGFR for ITC methods. Multiple methods have been developed for the recombinant expression and purification of EGFR, and typically expression is reported in mammalian expression cell lines such as Chinese hamster ovary (CHO) cell lines (Cadena & Gill, 1993; Makabe *et al.*, 2008) and Human embryonic kidney (HEK) cell lines (Wang *et al.*, 2018). Additionally, extensive reviews into optimisation of CHO and HEK cell production of recombinant proteins have been published (Kim *et al.*, 2012b; Thomas & Smart, 2005). Furthermore, several studies have reported the recombinant expression of soluble EGFR (sEGFR) domains from baculovirus-infected Sf9 cells (Ferguson *et al.*, 2000; Li *et al.*, 2005). However, the development and optimisation of EGFR expression systems is often time-consuming and labour intensive. Alternatively, purified EGFR is available from various commercial suppliers, and numerous studies have used this route to acquire purified EGFR (Hong *et al.*, 2010; Dubois *et al.*, 2008; Prado *et al.*, 2010). The options of optimising an EGFR expression system or purchasing large quantities of EGFR from commercial suppliers were not ideal choices during the preliminary stages of investigations into binding interactions of light activation of VHH 7D12 and contributed to the decision to develop a cell-based assay to measure antibody-antigen interactions.

3. ELISA, SPR, and ITC, measure binding interactions in non-native environments using purified proteins. Although this parameter reduces variability and can improve repeatability between experiments due to finer control over experimental design, it does not give insight into non-specific interaction in a cellular environment in the presence of other cell surface antigens and can reduce the applicability of the measured biomolecule.

5.2 Results & discussion

5.2.1 Development of on-cell assay to measure the interaction of an antibody to cell surface antigen

To investigate interactions between 7D12 and EGFR, we designed an assay that would report on binding in a cellular environment in the presence of other cell surface antigens. Similar cell based methods have been designed for the quantitative detection of cell surface molecules, such as radio immunobinding assay (RIA), cell-enzyme-linked immunosorbent assay (cELISA; Lourenço, & Roque-Barreira, 2010), live-cell ELISA (Jiang *et al.*, 2014), and on-cell Western (Abadier *et al.*, 2015). Similarities of the designed cell based assay can be made in relation to in-direct cell-ELISA where a primary detection antibody is chosen for specific interaction with a cell surface protein and is identified by a secondary antibody linked to an enzyme marker for the production of a detectable signal (Lourenço, & Roque-Barreira, 2010). However, in these protocols the addition of the binding partner is often carried out at 4°C for 1 hour in ELISA buffer (PBS containing 1% bovine serum albumin) to minimize the endocytosis of cell surface molecules. Although these binding conditions may result in a higher concentration of bound biomolecules on the cell surface and consequently higher detectable signal, they are not performed under physiologically relevant conditions, which in certain aspects can reduce the efficacy of the experiment. For the cell based assay designed during this thesis, cells overexpressing the targeted cell surface receptor were grown in a 96-well plate before treatment of binding partner (containing a His-tag) in physiologically relevant conditions (37°C, complete medium). After incubation of binding partner and multiple washes to remove non-specific interactions, cells were fixed with the addition of formaldehyde solution. Bound biomolecules were detected by primary antibody (Anti-His tag) which was identified by secondary antibody linked to HRP for signal development (Figure 5.3).

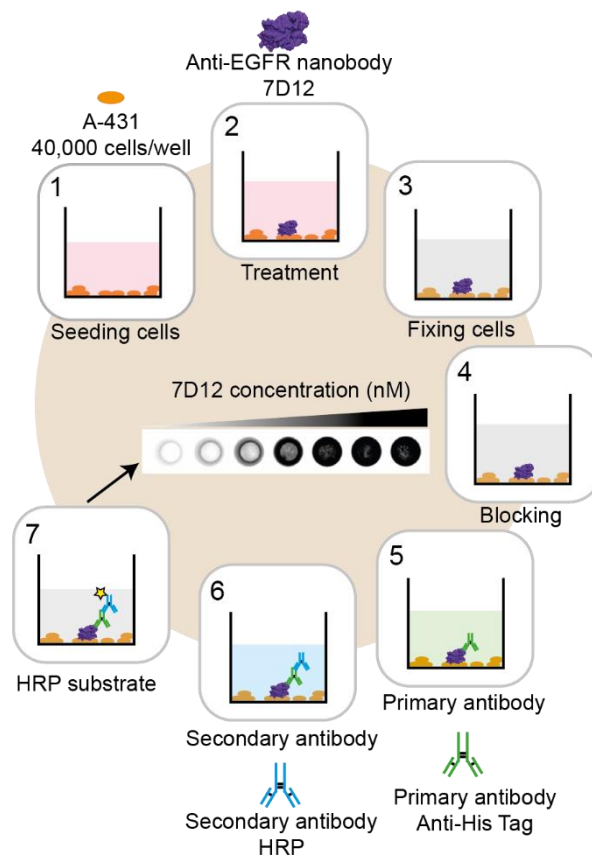


Figure 5.3: On-cell assay for measurement of binding between antibody fragment to cell surface antigen. (1) 40,000 cells were seeded into each well of a 96-well plate. (2) Addition of His-tagged VHH in fresh complete medium is incubated for 10 minutes. (3) The antibody solution was replaced with 3.7% formaldehyde solution for fixing the cells. (4) Non-specific interactions of cell surface antigens blocked with blocking solution. (5) Incubation with primary antibody specific for histidine tag. (6) Incubation with HRP-linked secondary antibody that targets primary antibody. (7) The substrate for HRP was added, and the cells were imaged for chemiluminescence by GelDoc XR+ system.

The design of this cell-based assay placed a high priority on developing a readily accessible and economical method while retaining precision and reliability. Designing a technique in which the live cells provided the antigens needed for the assay, removed the requirement of obtaining purified antigen.

5.2.2 Optimisation of on-cell ELISA

5.2.2.1 Preliminary investigation of VHH 7D12 binding interactions with A431 carcinoma cell line

The initial investigations of binding interactions of 7D12-EGFR by on-cell assay used human epidermal carcinoma cells A431 (Sigma-Aldrich), which express high levels of cell surface EGFR. Using standard tissue culture procedures (2.1.4) these cells were counted and diluted to 200 cells/ μL , then 200 μL of this solution was seeded into a white 96-well plate (40,000 cells/well) and grown in complete medium overnight to 80-90% confluence (16-20 hours, 37°C, 5% CO_2). After desired confluence was observed, complete medium was replaced with serum-free medium to remove any detached cells and incubated (4 hours, 37°C, 5% CO_2) to serum starve the cells. Dilutions of 7D12 and pcY mutants were separately prepared in a clear 96-well plate in complete medium and transferred in duplicates to the white 96-well plate containing cells *via* a multichannel pipette. The plate was incubated for 10 minutes (37°C, 5% CO_2), then medium was removed, and non-specific binding removed by washing with serum free medium (200 μL to each well). To fix cells, 150 μL of 3.7% formaldehyde solution was added to each well and incubated at room temperature for 20 minutes. Formaldehyde solution was removed, and cells were washed 5 times (200 μL , 15 minutes, gentle rocking) with PBST (1x PBS with 0.1% Tween-20). Cell surface antigens that might bind non-specifically to primary antibody were blocked by incubating with 10% milk-PBST (100 μL /well) for 1 hour at room temperature with gentle rocking. The blocking buffer was removed, and 50 μL of primary anti-6X-HIS tag antibody solution was added and incubated at room temperature for 1 hour with gentle rocking. The primary antibody solution contained mouse anti-6x-His tag antibody (Thermo Fisher Scientific) at 1:500 dilution and 1% milk in PBST. Another five washes were performed with PBST to remove residual primary antibody, and 50 μL of secondary antibody solution was added to each well and incubated at room temperature for 1 hour. The secondary antibody solution contained HRP-linked antibody (Anti-mouse, IgG, HPR-linked) at a dilution of 1:1000 in 1% milk and PBST.

Secondary antibody was removed, and cells in each well were washed five times with PBST (200 μ L, 15 minutes, gentle rocking). Finally, 200 μ L of SuperSignal chemiluminescent substrate (Thermo Scientific) was added and incubated for 10 minutes at room temperature before plate imaging using BIORAD GelDoc XR+ (figure 5.4).

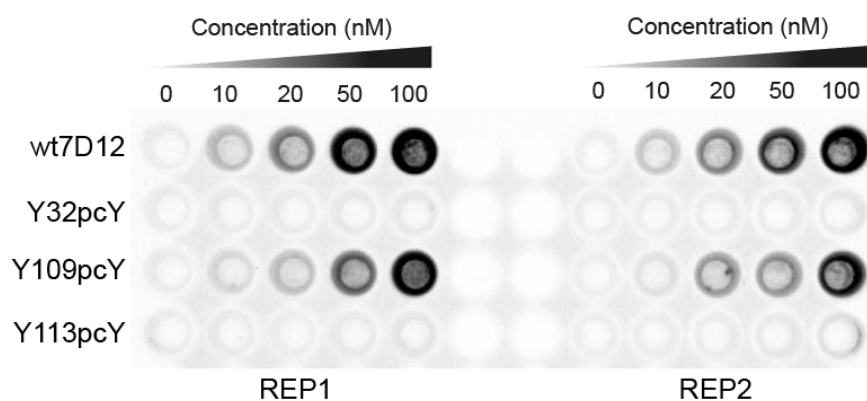


Figure 5.4: Cell-based assay experiments to assess the interaction of wt7D12 and three pcY mutants to EGFR on the surface of A431 cells. Chemiluminescence signal detected with wt7D12 and Y109pcY indicate affinity to EGFR while background signal from Y32pcY and Y113pcY demonstrate binding inhibition due to addition of pcY. Representative image from three experiments in duplicates.

Using the BIORAD GelDoc XR+ system to detect chemiluminescence signal produced by HRP linked secondary antibody resulted in an increase of observed signal in relation to increasing concentration of wt7D12 (0-100 nM). The initial results from the cell-based assay demonstrated inhibition of binding affinity between EGFR and 7D12 when positions Y32 and Y113 are replaced with photocaged tyrosine. However, pcY incorporation into position Y109 of 7D12 resulted in similar detected signal to wt7D12.

Note that the tyrosine residues at positions 32, 109 and 113 were selected after careful analysis of the crystal structure of 7D12-EGFR domain III complex (PDB; 4KRL). These residues were in close proximity to the binding interface and it was theorised that photocaging these positions would have inhibitory effect on 7D12-EGFR binding. However, it was also observed that while the tyrosine at position 109 was within

close proximity of the binding interface, the orientation of the amino acid was parallel to the EGFR surface and pointing away from the binding interface, and hence its significance in 7D12-EGFR binding were uncertain. The results in Figure 5.4 indicate that the incorporation of pcY into position Y109 does not interfere with binding interactions of 7D12-EGFR.

5.2.2.2 Adjusting on-cell assay to reduce background signal

Although clearly defined chemiluminescence signals were detected in Figure 5.4, the required exposure time to detect chemiluminescence signal using GelDoc XR+ system was relatively high (>60 seconds). In Western blot experiments, high exposure times can help in the generation of a clear band. However, high exposure can cause an increase in background signal (Mahmood, & Yang, 2012).

To minimise background signal in future cell-based assays, several amendments were made to the protocol, such as reducing the number and incubation time for specific washing steps. The washing steps after cell fixation and primary antibody incubation were reduced from 5 washes for 15 minutes each to 3 washes for 5 minutes each. Wash steps after secondary antibody were carried out the same number of times (5 washes) but wash times were reduced to 5 minutes. These small changes in the protocol resulted in higher signal detection and a reduction of exposure time (<5 seconds) while not compromising the detected signal from the well where 7D12 is absent (data not shown). Further experimentation to evaluate optimum dilutions of primary and secondary antibodies resulted in no changes to the protocol (primary antibody; 1:500, secondary antibody; 1:1000), but illustrated the effect of varying either detection antibody can have on produced chemiluminescence signal (Appendix Figure A.2).

5.2.2.3 Investigations into cell line serum starvation

As previously discussed, one of the aims of developing this cell based binding assay was to replicate (to an extent) physiologically relevant conditions to gain a more complete biological understanding of 7D12 binding to EGFR. The on-cell assay designed so far differed to similar binding assays that use isolated antigens to test binding interactions (ELISA, SPR, and ITC), and a different approach was taken to binding assays that are cell based (cELISA, live-cell ELISA, and on-cell Western) in which antibody-antigen incubation steps are often performed at 4°C in binding buffers. The methods used so far have required serum starvation of A431 cells before testing 7D12-EGFR interactions; in this section, we investigated the implications of removing the serum starvation step from the protocol.

Serum starvation is a frequently used technique in molecular biology and is often considered as a routine method to be applied to cells before experimentation. However, the inconsistencies in the literature in defining standardised terminology, and methodology have resulted in ambiguous descriptions of the correct procedure to follow (Pirkmajer & Chibalin, 2011). Commonly, serum starvation is used as a method to synchronise proliferating cells (to enter G₀/G₁ phase from cell cycle) to promote homogeneity (Cooper, 2003) or as a method to completely remove serum as an experimental precaution, as serum is a poorly defined complex that could have undesirable interference with experimental results (Mannello & Tonti, 2007). It has also been used to study metabolic cellular stress responses (Levin *et al.*, 2009) and apoptosis (Hasan *et al.*, 1999) however serum starvation duration and serum concentration need to be determined for each cell line as starvation can elicit complex and unpredictable cellular responses which could subsequently interfere with experimental results and conclusions (Eichelbaum *et al.*, 2012; Grada *et al.*, 2017).

To address this important issue, an on-cell assay was performed with and without serum. The experimental design was similar to the methods described above. Human epidermal carcinoma cells A431 were seeded into a white 96-well plate (40,000

cells/well) and grown in complete medium overnight to 80-90% confluence (16-20 hours, 37°C, 5% CO₂). When 80-90% confluence was observed, complete medium was replaced with either fresh complete medium or serum free medium and cells were incubated for 4 hours (37°C, 5% CO₂). After incubation, a range of concentrations of wt7D12 (5, 10, 20, 50, 100, 200 nM) were diluted in either complete medium or serum free medium on a separate plate before being transferred to cells and incubated for 10 minutes (37°C, 5% CO₂). Following the 7D12 treatment step, the standard protocol was adopted, and chemiluminescence was imaged by GelDoc XR+ system and quantified by CLARIOstar plate reader (Figure 5.5).

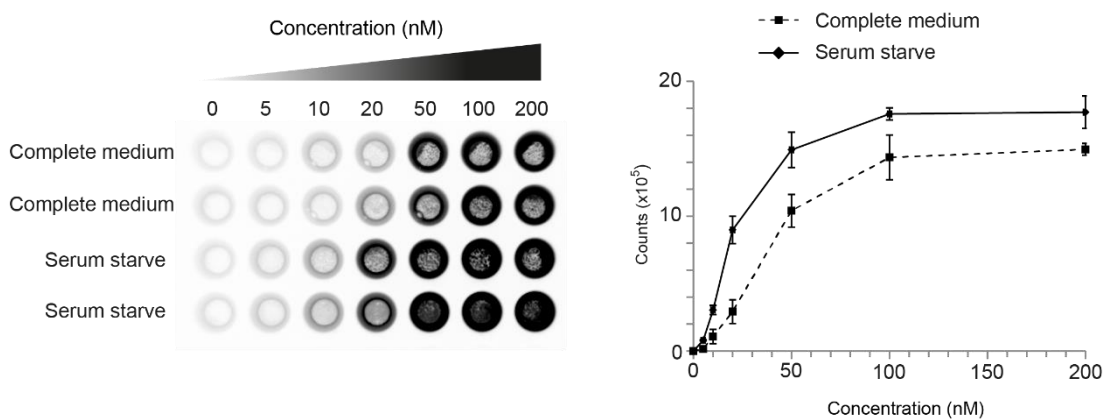


Figure 5.5: On-cell assay assessing wt7D12 affinity to EGFR on A431 cells treated with and without serum starvation. Higher chemiluminescence signal from serum starved cells demonstrates increased affinity of wt7D12 to EGFR when cells are pre-treated with serum starvation. Representative image from three experiments in duplicates

The on-cell assay resulted in higher overall chemiluminescence signal detected from serum starved A431 cells incubated with wt7D12. Interestingly, differences of detected signal between starved and non-starved at higher concentrations of wt7D12 (100 and 200 nM) resulted in a 15-20% decrease in signal in the latter, while lower concentration of wt7D12 (5, 10, 20, 50 nM) demonstrated a decrease of up to 50%. The reasons for the apparent higher binding affinity of wt7D12 to serum starved cells remain unclear. However, a hypothesis to explain this occurrence is that the fetal bovine serum used in complete medium contains epidermal growth factor (EGF)

or other unknown analytes that may compete with 7D12 for binding to EGFR. Another possibility is that the process of serum starvation on A431 cells causes metabolic stress on the cells as they attempt to adjust to changing conditions (Levin *et al.*, 2009) by inducing signal transduction pathways which could influence cell surface EGFR activity. Although a small decrease in binding affinity was observed with non-starved A431 cells, we performed further experimentation using serum as this was physiologically relevant.

The results from this section of the thesis were used to finalise the on-cell assay methodology listed in the methods chapter (2.1.16). All further on-cell assay discussed in this chapter follow the finalised protocol unless specified.

5.2.4 Evaluation of the on-cell assay efficacy with control experiments

5.2.4.1 Negative EGFR cell line control

From the initial experimental results and following optimisation of the on-cell assay, the measured antibody-antigen interactions indicate positive correlation between 7D12 binding affinities to EGFR on the surface of A431 cells. However, as the assay has not tested 7D12 binding affinity to alternative control cell lines, it is unknown if the produced chemiluminescence signal is caused by non-specific binding of 7D12 to the surface of A431 cells.

To confirm 7D12 specificity to EGFR, an EGFR-negative human breast adenocarcinoma cell line (MDA-MB-231) was selected for further analysis. MDA-MB-231 cell line is triple-negative breast cancer cell line (Chavez *et al.*, 2010) that lacks the three commonly identified molecular markers that are used for the classification of breast cancer tumours (expression of estrogen receptor and progesterone receptor, and amplification of HER2). In a study reviewing seventeen commonly used breast cancer cell lines (Subik *et al.*, 2010); MDA-MB-231 cell line demonstrated basal levels of EGFR which makes it an ideal candidate for 7D12 binding comparison studies

with EGFR overexpressing cell line A431. It was hypothesised that in the event that 7D12 is specific to EGFR interactions, a significant increase in on-cell assay chemiluminescence signal would be observed with A431 cells compared to MDA-MB-231. However, as the basal level of EGFR is present on MDA-MB-231 cell surface, it was expected that detection of minor signal would occur.

To measure and compare 7D12 binding affinities to A431 and MDA-MB-231, the cell lines were seeded into a white 96-well plate (40,000 cells/well) and grown in complete medium overnight to 80-90% confluence. Once 80-90% confluence was observed, the on-cell assay experimental procedures were followed (Methods 2.1.16). The wt7D12 cell surface interactions were measured by chemiluminescence signal on CLARIOstar (BMG labtech) plate reader and imaged by GelDoc XR+ system (Figure 5.6).

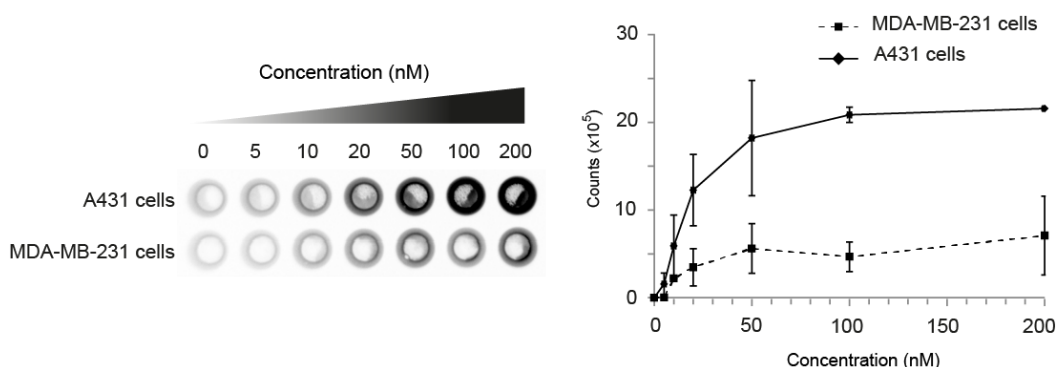


Figure 5.6: Experimental control of on-cell assay determining specificity of wt7D12 to EGFR on positive cell line (A431) and negative cell line (MDA-MB-231). Significant increase in chemiluminescence signal detected on EGFR positive cell line indicates that VHH 7D12 has higher affinity to A431 cells. Representative image from three experiments in triplicates.

The observed chemiluminescence signal produced from the detection of wt7D12 demonstrated a clear difference between the two carcinoma cell lines. Similar to previous investigations of wt7D12 binding interactions to A431, the signal observed increased sharply until saturation at approximately 100 nM. On comparison with wt7D12 binding to MDA-MB-231, a significantly lower chemiluminescence signal

(approximately 70-80% lower than for A431 cells) was observed. These results are consistent with the proposed hypothesis that a significant decrease would be observed between A431 and MDA-MB-231; however, due to basal levels of EGFR present on MDA-MB-231 cell surface, minor chemiluminescence signal would be detected. These findings indicate that wt7D12 is specific to EGFR on the cell surface of A431 and that the produced chemiluminescence signal is a direct response to 7D12 interactions with EGFR.

5.2.4.2 Negative VHH control

The previous section described investigations into the specificity of 7D12 binding interactions with EGFR by comparing measurements of bound 7D12 to two carcinoma cell lines; A431 that overexpresses EGFR and MDA-MB-231 that has basal levels of EGFR. We next wanted to explore binding interactions of a non-specific his-tagged VHH antibody fragment to A431 cell surface, to evaluate if the observed signal of VHH 7D12 to A431 is due to specific interactions between the VHH and EGFR and is not as a consequence of some other property of the surface of A431 cells. The negative VHH antibody fragment used in this binding assay was briefly discussed in chapter 3, the anti-RR6 (azo-dye reactive red), VHH-R2 (PDB: 1QD0) was selected due to its frequent use in the literature as a negative control (Van Der Meel *et al.*, 2012). The VHH R2 is generated against the hapten azo-dye Reactive Red (RR6) small molecule (Spinelli *et al.*, 2000) and has no reported affinity to EGFR. In the event that VHH R2 does not interact with A431 cell surface proteins, only a background signal would be expected.

As discussed in chapter 3, the negative control VHH-R2 was expressed and purified using the same methodology as wt7D12. An on-cell assay experiment was designed to analyse 7D12 and R2 binding affinities to EGFR positive cell line A431. On-cell assay protocol listed in methods (2.1.16) was followed where A431 cells were seeded and grown in a 96-well plate for the analysis of a range of concentrations of 7D12 and R2.

Cell surface interactions were measured by chemiluminescence signal on CLARIOstar plate reader and imaged by GelDoc XR+ system (Figure 5.7).

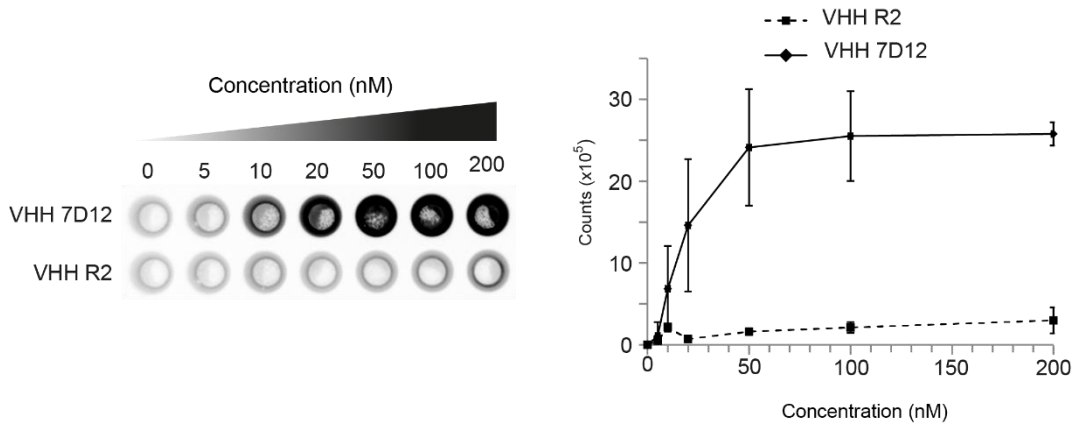


Figure 5.7: Experimental control of on-cell assay determining specificity of his-tagged heavy chain only antibody fragments to A431 cell surface. The assay demonstrates background interaction of negative VHH R2 compared to VHH 7D12. Representative image from three experiments in triplicates.

The observed results in Figure 5.7 supports the suggested hypothesis that the chemiluminescence signal is due to the specific targeted binding of 7D12 to EGFR on A431 cells, and not due to non-specific binding of a heavy-chain only antibody fragments to EGFR or the surface of A431 cells. Figure 5.7 shows that the chemiluminescence signal for wt7D12 increases until saturation at 100-200 nM, which is in close agreement with previous on-cell assays. However, the negative VHH-R2 has near background level of signal, indicating minimal binding to EGFR or A431 cell surface.

5.2.5 Restoring EGFR binding affinity to photocaged VHH 7D12

The preliminary results shown in Figure 5.4 demonstrated successful inhibition of 7D12 binding to EGFR (on A431 cell surface) with the addition of genetically incorporated pcY in two positions (Y32TAG and Y113TAG). In contrast, the site-

specific encoding of pcY in position Y109TAG appeared to have only minor effects on binding inhibition and possible reasons relating to this observation were discussed earlier in this chapter. To investigate the light promoted restoration of binding affinity of 7D12 mutants containing pcY, an on-cell assay was designed to measure interactions of wt7D12 and the three amber mutants containing pcY (Y32, Y109, and Y113) to A431 cell surface EGFR under physiologically relevant conditions, before and after decaging. Similar methods were used in de-caging VHH 7D12 (wt and pcY mutants) with 365 nm light, as described in chapter 4 (2.1.15). Photocaged and de-caged samples were then applied to an on-cell assay to identify if binding has been restored for photocaged samples upon exposure to light (Figure 5.8).

The observed chemiluminescence signal in Figure 5.8 demonstrated inhibition and the subsequent photo-activation of 7D12 with the site-specific incorporation of pcY at positions Y32 and Y113. Similar to the preliminary data (Figure 5.4), before irradiation with 365 nm light, wt7D12 and Y109pcY exhibited similar binding affinities to EGFR. However, when photocaged tyrosine is substituted into position Y32 or Y113, the binding to EGFR is blocked. It is observed that pcY at position Y32 shows significant inhibition of EGFR binding up to 500 nM, which is restored to near wildtype levels when de-caged by irradiation with 365 nm light. It is also shown that pcY at position Y113 is slightly less effective at inhibiting binding to EGFR compared to position Y32. However, the chemiluminescence signal is significantly lower than wildtype and signal is restored to near wild-type levels upon irradiation with 365 nm light. This experiment demonstrates an elegant and robust method of photocontrol over an antibody fragment with a single amino acid site replacement to a photocaged analogue. Further research invested into computational methods to model 7D12-EGFR interaction would assist in selecting key residues for mutational studies, expediting the discovery of such photoactive antibody fragments.

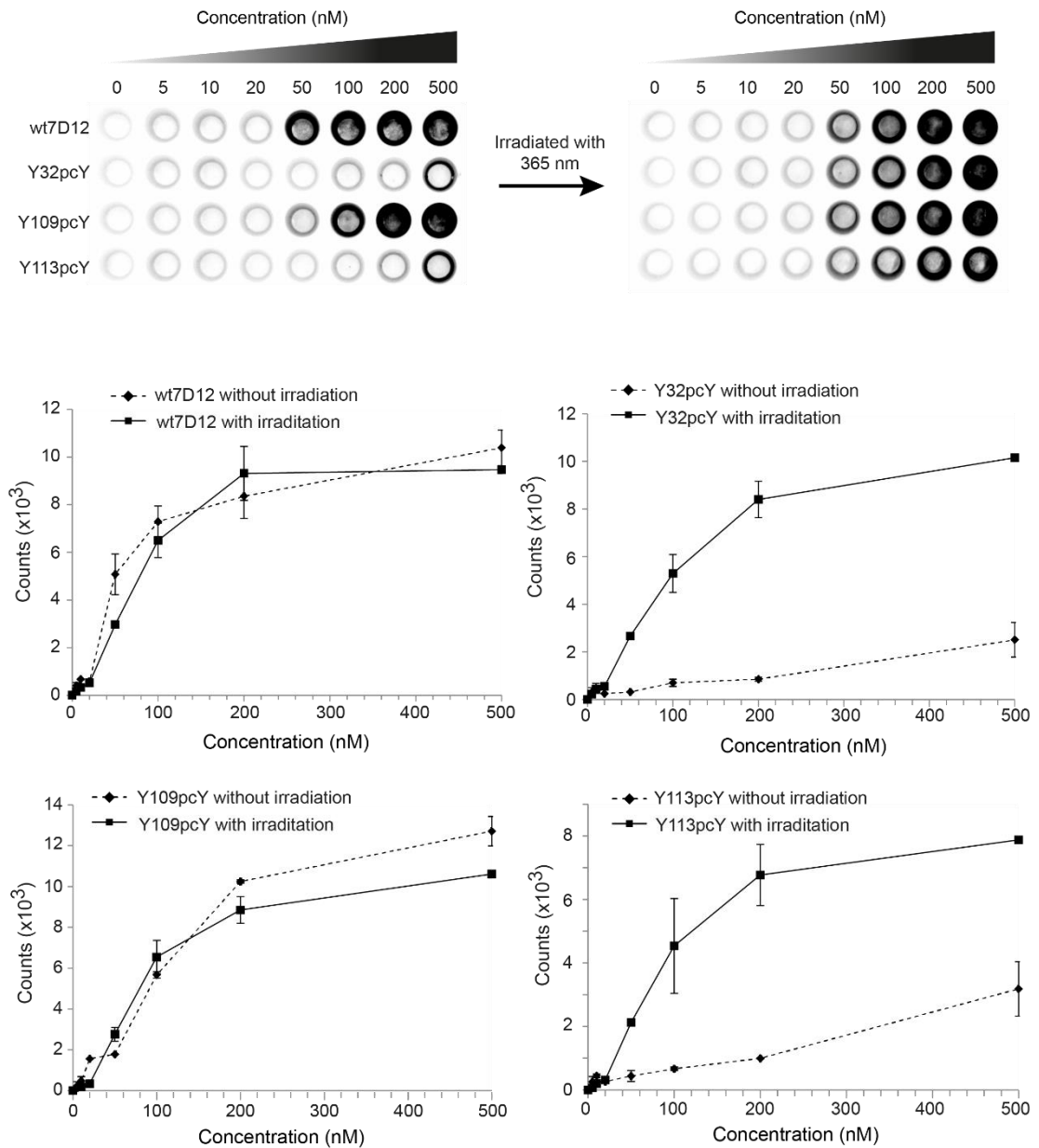


Figure 5.8: On-cell assay binding experiments to assess the interaction of EGFR with wt7D12 and amber mutants containing site-specifically incorporated pcY. On-cell assays performed on the surface of A431 cells demonstrates that the presence of pcY at positions 32 and 113 in 7D12 inhibits its binding to EGFR. However, Y109pcY mutant shows binding affinity similar to wt7D12. The binding of Y32pcY and Y113pcY mutants are restored upon irradiation with 365 nm light. Representative image from three experiments in duplicates.

5.2.6 Determining binding affinity of VHH 7D12 to EGFR using on-cell assay

To determine the parameters involved in binding affinity/association of 7D12 to EGFR and subsequent photocaging and photo-deprotection effects on inhibited 7D12, an on-cell Western was designed.

A similar experimental design was used as previously described (5.2.5) an increased number of data points. Nine concentrations (between 0.5 – 500 nM) were chosen to give a concentration range over 4 orders of magnitude and experiments were performed in triplicates (full GelDoc XR+ data provided in Appendix Figure A.2). The measured chemiluminescence intensity was quantified using CLARIOstar plate reader and plotted against log(concentration) of 7D12. The data trend was fitted to sigmoidal nonlinear curve using graphpad data analysis and graphing software resulting in the generated graphs (Figure 5.9) and calculated K_D values (Table 5.1).

The fitted sigmoidal nonlinear curves of the quantified chemiluminescence intensity of wt7D12 (with and without irradiation) showed an increase in signal from 5 to 100 nM concentration of VHH followed by saturation of chemiluminescence signal at higher concentrations. For 7D12 with the addition of pcY in positions Y32 and Y113 (Y32pcY and Y113pcY), near background chemiluminescence signal was observed up to 500 nM when samples were not irradiated, demonstrating the inhibition of 7D12-EGFR interactions due to the presence of pcY at these two positions. The binding of Y32pcY and Y113pcY was recovered to almost wt7D12 levels upon sample irradiation with 365 nm light indicating light-mediated control over antibody-antigen interactions. Slight reduction in chemiluminescence intensity and saturation of Y109pcY without irradiation was observed when compared to the irradiated version, which could indicate minor binding interference with the addition of pcY in position Y109.

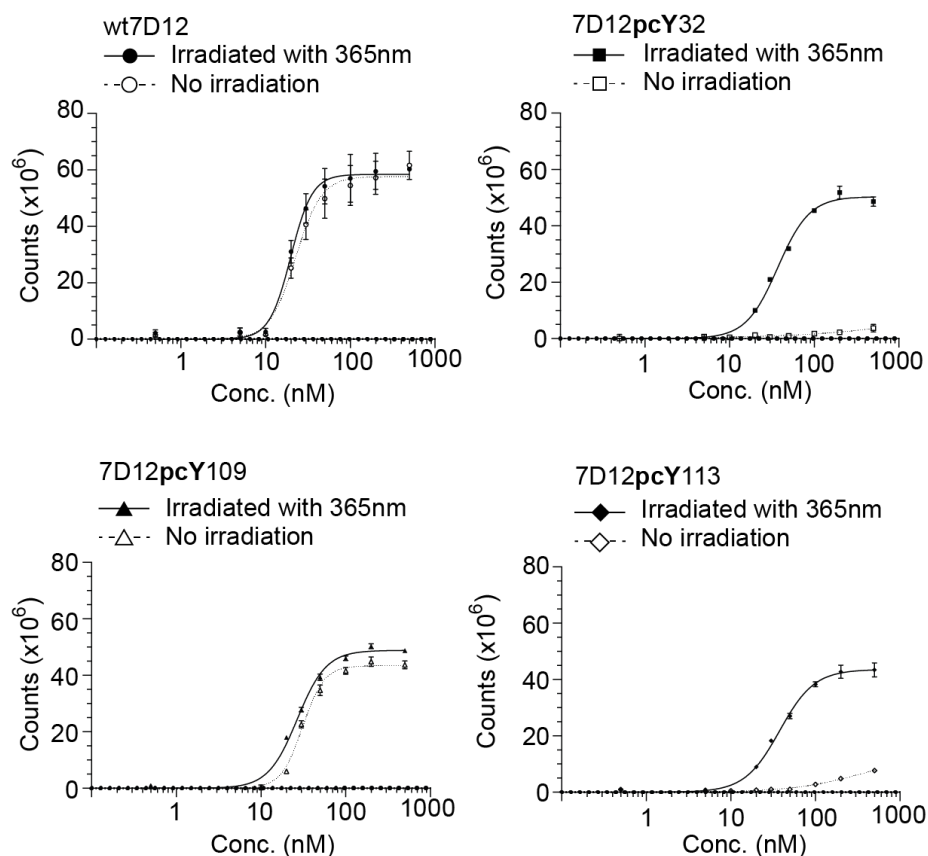


Figure 5.9: On-cell assay analysis to determine the binding kinetics of 7D12 (wt and pcY mutants) to EGFR in the presence and absence of 365 nm light. Chemiluminescence intensities obtained from cell based binding experiments for wt7D12, Y32pcY, Y109pcY and Y113pcY, before and after irradiation with 365 nm light, were quantified using CLARIOstar plate reader and plotted against log(concentration) of 7D12. Fitted trend line was plotted as sigmoidal nonlinear equation using graphpad data analysis and graphing software.

Table 5.1: Parameters obtained after fitting the data to the sigmoidal nonlinear equation using graphpad.

Sample	I_{max}	K_D (nM)	R^2
wt7D12 with irradiation (+)	$5.8 (\pm 0.28) \times 10^7$	$20 (\pm 1.8)$	0.98
wt7D12 without irradiation (-)	$5.8 (\pm 0.33) \times 10^7$	$23 (\pm 2.6)$	0.97
Y32pcY with irradiation (+)	$5.0 (\pm 0.17) \times 10^7$	$37 (\pm 2.6)$	0.99

Y32pcY without irradiation (-)	N/A	N/A	N/A
Y109pcY with irradiation (+)	4.9 (± 0.14) $\times 10^7$	27 (± 1.6)	0.99
Y109pcY without irradiation (-)	4.3 (± 0.12) $\times 10^7$	31 (± 1.5)	0.99
Y113pcY with irradiation (+)	4.4 (± 0.14) $\times 10^7$	38 (± 2.6)	0.99
Y113pcY without irradiation (-)	N/A	N/A	N/A

The curve fitting parameters generated by graphpad as a result of plotting the quantified chemiluminescence intensity against log(concentration) of 7D12 are listed in Table 5.1. The estimated binding affinity of 7D12 to EGFR on the surface of A431 cells was reported by the equilibrium dissociation constant (K_D), which can be used to evaluate the strengths of biomolecular interactions. The curve fitting parameters resulted in an estimated wt7D12 (before irradiation) K_D of 22 nM (± 2.4). Comparable 7D12 affinity measurements calculated with different techniques have been described in the literature. SPR analysis of 7D12 interactions with sEGFRd3 resulted in a reported K_D of 47 nM (± 3.6 ; Schmitz *et al.*, 2013) and in another study, ^{125}I -labelled 7D12 affinity to live A431 cells had a reported K_D value of 25.7 nM (Roovers *et al.*, 2011).

The slightly reduced affinity of Y109pcY before irradiation (compared to wt7D12) demonstrated in Figure 5.9 is consistent with affinity values reported in Table 5.1. The reduced K_D of 30.7 nM (± 2.3) indicates weaker interactions with EGFR likely due to the presence of pcY. Upon irradiation improved affinity is reported with a K_D value of 23.9 nM (± 4.6). For Y32pcY and Y113pcY before irradiation, near background levels of chemiluminescence were detected up to 500 nM due to pcY mediated binding inhibition to EGFR, which subsequently prevented affinity estimations. However, upon irradiation with 365 nm light and the restoration of binding, Y32pcY and Y113pcY reported K_D measurements of 29.4 nM (± 8.1) and 27.3 nM (± 10.6) respectively.

This chapter has illustrated extensive optimisation of the on-cell assay with investigations into effects of serum starvation, confirming validity of experimental design with control studies on negative cell lines and heavy-chain only antibody fragments, and small refinements to the protocol (reduced washing steps and investigated detection antibody dilutions) to reduce background signal. These experiments have contributed to the development of a robust, inexpensive and straightforward new tool that offers a highly sensitive alternative to other commonly used assays for the qualitative and quantitative data analysis of biomolecule interactions with cell surface antigens.

CHAPTER 6

Light dependent real-time delivery of
fluorophores to the surface of live cells

6.1 Introduction

With the initial development and optimisation of efficient periplasmic expression platforms, to the comprehensive characterisation of suppressor plasmids for efficient site-specific encoding of photocaged ncAAs into recombinant proteins, to the subsequent establishment of *in vitro* methods to investigate biomolecular interactions, this thesis has demonstrated the generation of heavy chain only antibody fragments (VHH) that depend on light-mediated activation to bind to a cell surface antigen.

The previous chapter described the development of an *in vitro* live-cell assay to evaluate mediated antibody-antigen binding. Using this assay, we demonstrated light-dependent activation of VHH 7D12 to EGFR when *o*-nitrobenzyl-*O*-tyrosine (photocaged tyrosine or pcY) was incorporated at either Y32 or Y113 position in 7D12. Numerous control experiments were performed to scrutinise the assay validity, leading to the development of a robust, economical and straightforward technique that offers highly sensitive analysis of antibody-antigen interactions.

An intrinsic characteristic of a VHH antibody fragment is the ability for enhanced tissue permeability compared to other antibody formats due to the comparatively low molecular mass (12-15 kDa). However, these therapeutic molecules and other fragmented antibody formats suffer in their ability to elicit an immune response and the subsequent triggering of antibody dependent cellular cytotoxicity (ADCC) due to the lack of an Fc region, which can be seen as a potential drawback to the therapeutic value of these antibody formats. To circumvent the problem of reduced cell cytotoxicity of such antibody formats, researchers have developed methods to increase the cytotoxicity of the antibodies with the additional linkage of cytotoxic drugs. Antibodies and antibody fragments linked to cytotoxic drugs are called antibody-drug conjugates (ADC).

A key mechanism essential to several cancer immunotherapeutics (especially ADCs) is the process of receptor mediated internalisation of the therapeutic antibody and

delivery of a cytotoxic drug to the intracellular target in the case of ADCs. Although the developed *in vitro* cell based assay in this thesis could be utilised as a powerful tool for revealing antibody-antigen interactions, minimal insight is gained on the dynamic biological processes as a result of 7D12 binding to surface EGFR. To capture such dynamic biological processes, receptor-mediated antibody internalisation, and to investigate delivery of 7D12 bound molecules to the intracellular environment of carcinoma cell lines, we designed live-cell microscopy experiments.

6.1.1 Receptor-mediated internalisation

Cellular internalisation of external material plays an essential role in a cell's ability to communicate with its environment. Small molecules like ions and organic molecules can pass through the plasma membrane (PM) by passive diffusion, dedicated channels, or ion pumps. The control over the movement of larger biomolecules in and out of the cell requires the alternative biological processes of endocytosis (internalisation to intracellular environment), and exocytosis (release to extracellular environment). Several variations of endocytosis exist, including phagocytosis, macropinocytosis, clathrin-mediated endocytosis (CME), clathrin-independent endocytosis (CIE), and caveolin-mediated endocytosis (Doherty & McMahon, 2009). These important processes have unique functions and have been shown to be critical cellular functions, such as the regulation of cell membrane homeostasis, migration, nutrient uptake, and signal transduction (Scita & Di Fiore, 2010; Sigismund *et al.*, 2012). Due to the internalisation characteristic of endocytosis, receptor related endocytic properties have become a key determinant in the selection of antigens for targeting by ADCs. Of the numerous pathways for endocytic entry of proteins and lipids at the plasma membrane, CME has been the most extensively studied and is becoming increasingly understood. This vesicular transport event describes the endocytosis and recycling of receptors *via* the formation of clathrin-coated pits (David *et al.*, 1996) followed by a subsequent scission to form clathrin-coated vesicles (Sorkin, 2004). CME vesicles undergo fusion with early endosomal sorting

compartments (Schmid, 1997) where the endosome is either directed to recycling compartments or matures to a late endosome which fuse to the lysosome (Thottacherry *et al.*, 2019).

Although simplified in certain aspects, the aim of this overview is to provide a basic description of clathrin-mediated endocytosis, which is involved in the internalisation of activated EGFR (Lemmon & Schlessinger, 2010). The ErbB family of receptors are receptor tyrosine kinases (RTKs) and include HER1 (EGFR, or ErbB1), HER2 (ErbB2), HER3 (ErbB3), and HER4 (ErbB4). The activation of ErbB RTKs by growth factor ligands results in various downstream signalling cascades, the downregulation of the receptor and subsequent intracellular receptor and ligand degradation (Sorkin & Goh, 2009). In fact, it is the misregulation of downstream signalling transduction which can cause uncontrolled cellular division and tumour proliferation in carcinoma cells overexpressing EGFR. Upon binding to EGF, EGFR forms activated clusters due to conformational changes and is subsequently internalised by both the CME and CIE endocytic pathways. However, at low physiological concentrations of EGF, CME is considered the main internalisation pathway (Sorkin & Goh, 2009; Wiley, 1988). The CME vesicular transport event of EGFR endocytosis from the plasma membrane describes the internalisation of EGFR clusters *via* the formation and scission of clathrin-coated pits to clathrin-coated vesicles which fuse with early endosomes and sorting compartments. Receptors are then either recycled back to the plasma membrane or directed for degradation in the lysosome (Figure 6.1). Visualisation of 7D12-EGFR endocytosis using live-cell microscopy experiments can in principle provide vital information about 7D12 mediated delivery of small molecules to cancer cells. (Figure 6.1).

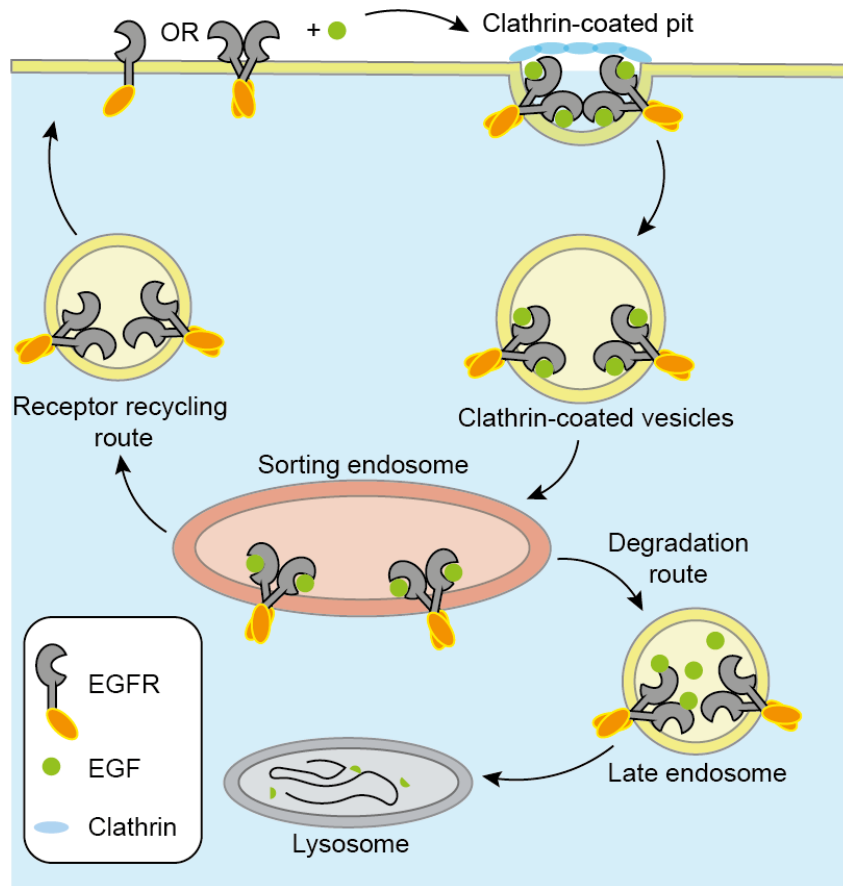


Figure 6.1: Diagram overview of activated EGFR clathrin-mediated endocytosis. EGFR can function on the plasma membrane as monomer or pre-dimer, and upon binding to EGF, the receptors form clusters in budding invagination pits of the plasma membrane. This results in a clathrin-coated pit which is cleaved from the plasma membrane forming clathrin-coated vesicle. After uncoating clathrin, the vesicle fuses to a sorting endosome where it is directed to the lysosome for degradation, receptor recycling or other pathways.

6.1.2 Live-cell microscopy design considerations

Live-cell imaging has become an integral part of modern biological and medical sciences and provides researchers with a wide range of tools to investigate dynamic processes occurring at the molecular, cellular or whole organism level in living systems. Development of live-cell imaging techniques has transformed the way biologists study cellular dynamics, proteins, and a plethora of biological processes and molecular interactions. Observation and measurements of dynamic changes at

the cellular level in a live cell setting can provide greater insight into biological interactions when compared to snapshots of fixed cells at a particular time point. The use of live or fixed cells in imaging require numerous experimental considerations and processing procedures, and have both advantages and disadvantages depending on the experiment.

Methods containing fixation procedures often suffer from the fact that the fixation processes alter the structure of the surface molecules that might be targets of investigation (Schnell *et al.*, 2012) and cellular conformation may be changed. Furthermore, as the cells are preserved at a particular time point, less functional information of dynamic processes is attained. Despite several disadvantages, cellular fixation is often required because of limitations imposed by imaging experiment and apparatus. Furthermore, benefits such as greater preservation and stability of cellular structures, and minimisation of cellular movement and sample degradation can be preferential factors contributing to experimental design.

Compared to fixed cell imaging, capturing meaningful and physiological relevant microscopy data across space and time of live-cell imaging experiment is often challenging because of compromises between image quality and maintaining cell health. This compromise results in a fine balance between minimising phototoxicity and photobleaching (while maintaining a useful signal-to-noise ratio), and providing suitable environmental conditions for cell replication and viability. While the generation of images that are both biologically relevant and aesthetically pleasing are often regarded as a high priority in experimental design, the process of imaging the biological samples should not compromise cellular health. Several factors that contribute to the maintenance of cellular health (such as physiological temperature control, pH, humidity, osmolality, and media composition) should be actively observed, maintained and/or optimised as required by the experiment (Cole, 2014).

6.1.3 Fluorescent tools for live-cell imaging

The use of fluorescent tools to aid in the visualisation, probing, tracking, and quantifying of cellular processes has become well-established. Typically, a small molecule fluorophore or fluorescent protein (FP) is linked to the biomolecule of interest for imaging purpose. The genetic encoding of FPs allows for the generation of fluorescent labels within the cell using transgenic approaches, or alternatively the FP can be fused to recombinant proteins ensuring a 1:1 ratio of expressed protein to fluorophore. Although extensive optimisation in optical and biochemical properties of FP have resulted in a diverse range of available fluorescent proteins, they are large (typically around 25 kDa) compared to organic fluorophores (~1 kDa) and can perturb stability, function and localisation of labelled protein. Alternatively, the generation of small molecule fluorescent dyes by organic synthesis has resulted in numerous organic dyes that span the visible wavelength range. During this chapter, several small molecule fluorophores (Table 6.1) were chemically conjugated to VHH 7D12 and its photocaged mutants to investigate their binding and internalisation.

Table 6.1: List of small molecule fluorophores used in this study.

Fluorophore	Abs (nm)	Em (nm)	Characteristics
Protonex Green 500	443	502	pH-sensitive fluorescence. Non-fluorescent at physiological pH, increasing fluorescence as pH decreases.
BODIPY-FL	505	513	pH-insensitive fluorescence. Narrow spectral bandwidth.
pHrodo Green	505	525	pH-sensitive fluorescence. Non-fluorescent at physiological pH, increasing fluorescence as pH decreases.
BODIPY-TMR-X	542	574	pH-insensitive fluorescence.
Alexa Fluor 555	556	575	pH-insensitivity fluorescence between pH 4 to 10.

			Brightest fluorescence output compared to spectrally similar dyes.
pHrodo Red	560	585	pH-sensitive fluorescence. Non-fluorescent at physiological pH, increasing fluorescence as pH decreases.
Protonex Red 600	575	597	pH-sensitive fluorescence. Non-fluorescent at physiological pH, increasing fluorescence as pH decreases.
Atto 647N	647	661	pH-insensitivity fluorescence between pH 2 to 11.

These fluorescent dyes often demonstrate enhanced optical properties compared to fluorescent proteins with improved brightness, photostability and narrower wavelength bandwidths (Toseland, 2013). However, as methods to link these reactive dyes typically involve attachment to biomolecule *via* specific functional groups, such as amine, thiol, azide, tetrazine functional groups, problems can emerge with the loss of site-specific control and the number of fluorophores conjugated to the biomolecule resulting in heterogeneous mixtures containing a range of dye to protein ratios (Lu & Zenobi, 1999). For example, the widely used amine reactive fluorophores for the modification of biomolecules typically target lysine residues in the protein. However, lysine residues frequently play an important role in protein structure, such as formation of salt bridges with a negatively charged aspartate or glutamate residues to increase protein stability (Barnes, 2007). Furthermore, lysine residues are commonly located in protein active/binding sites. These contributing factors can affect function and stability of labelled proteins.

6.2 Results & discussion

6.2.1 Optimisation of live-cell microscopy experimental procedures

Initial investigations were performed using a plate-based endpoint assay, in which live cells were incubated with the labelled antibody fragment 7D12 and amber mutants for set time points before imaging. These experiments enabled high-throughput analysis of several conditions and facilitated the experimental troubleshooting required before real-time observations of 7D12-EGFR interactions.

One of the mostly versatile and commonly used techniques for labelling proteins is to use chemical groups that react with primary amines (-NH₂). These amines exist in the side-chain of lysine amino acid residues and at the terminus of the protein. To confer fluorescence to VHH 7D12, labelling reactions were carried out using N-hydroxysuccinimide ester (NHS ester) containing synthetic fluorescent dye that can react with primary amines in 7D12 under slightly basic conditions (pH 8) to form stable amide bonds. Typically, a labelling reaction would consist of 37.5 µL solution of antibody fragments (100 µM), 51 µL of water, 1.5 µL of 10 mM dye in DMF and 10 µL of 1M NaHCO₃ (pH 8). The reaction mixture was incubated at 25°C for 1 h with shaking (600rpm). To remove excess fluorophore, the labelled samples were applied to Zebra desalting columns (MWCO 7000 Da). To ensure that all the unbound fluorophores was removed, desalting was performed three times for each sample.

The initial plate-based microscopy experimental design involved seeding 300,000 A431 cells in a 24-well plate that were grown until 80% confluence (16-18 hours, 37°C, 5% CO₂). Once desired confluence was reached, cells were washed three times with imaging medium and 297 µL of fresh imaging medium was added to each well. 3 µL stocks of 100x labelled VHH 7D12 were added to each well making the total volume 300 µL, then 24-well plate was incubated for 10 minutes (37°C, 5% CO₂) and washed with fresh imaging medium before acquiring data. Cells were imaged on a Zeiss Axiovert 200M microscope at 37°C using Zeiss AxioVision software. Brightfield and fluorescence images were captured using a 10x objective lens and a Zeiss AxioCam MRm CCD camera. Preliminary microscopy analysis was performed at 10x

magnification (results not shown) with 200nM concentration of 7D12(wt), Y32pcY, Y109pcY and Y113pcY labelled with BODIPY-FL. The GFP filter set (Zeiss cube #13 dichroic, Ex = 472 ± 15 nm, Dichroic = 495 nm (Zeiss), Em = 520 ± 17.5 nm) was used to excite and collect BODIPY-FL fluorescence. The collected fluorescence signal from these experiments was achieved from 2000ms of exposure, which can be considered relatively high depending on imaging frequency and total time period of the experiment. In the case of the designed plate-based experiment, high exposure time could result in false-positive signal detection from autofluorescence and have a negative influence on cellular health. The acquired fluorescent images using 10x objective were processed by Fiji (ImageJ) and demonstrated poor signal-to-noise ratio of VHH 7D12 (and three photocaged mutants) to A431 cell surface EGFR. Difficulties in differentiating well defined cells in acquired microscopy data resulted in the decision to increase the objective lens magnification.

Similar methodology was applied in the design of further plate-based microscopy experiments to test a higher magnification objective lens (20x). Initial investigations (results not shown) demonstrated similar results to preliminary data, where minimal fluorescence signal was detected. As the objective lens both illuminates the sample and collects photons emitted from fluorescence to generate the microscopy image, increasing the objective lens magnification decreases image intensity as smaller pixels generally collect fewer photons (Waters, 2009). To compensate for intensity loss, higher exposure times (20 seconds) were required to capture BODIPY-FL fluorescence. Although the resulting microscopy images (Figure 6.2) demonstrated higher detectable fluorescence, an increase in autofluorescence was likewise observed.

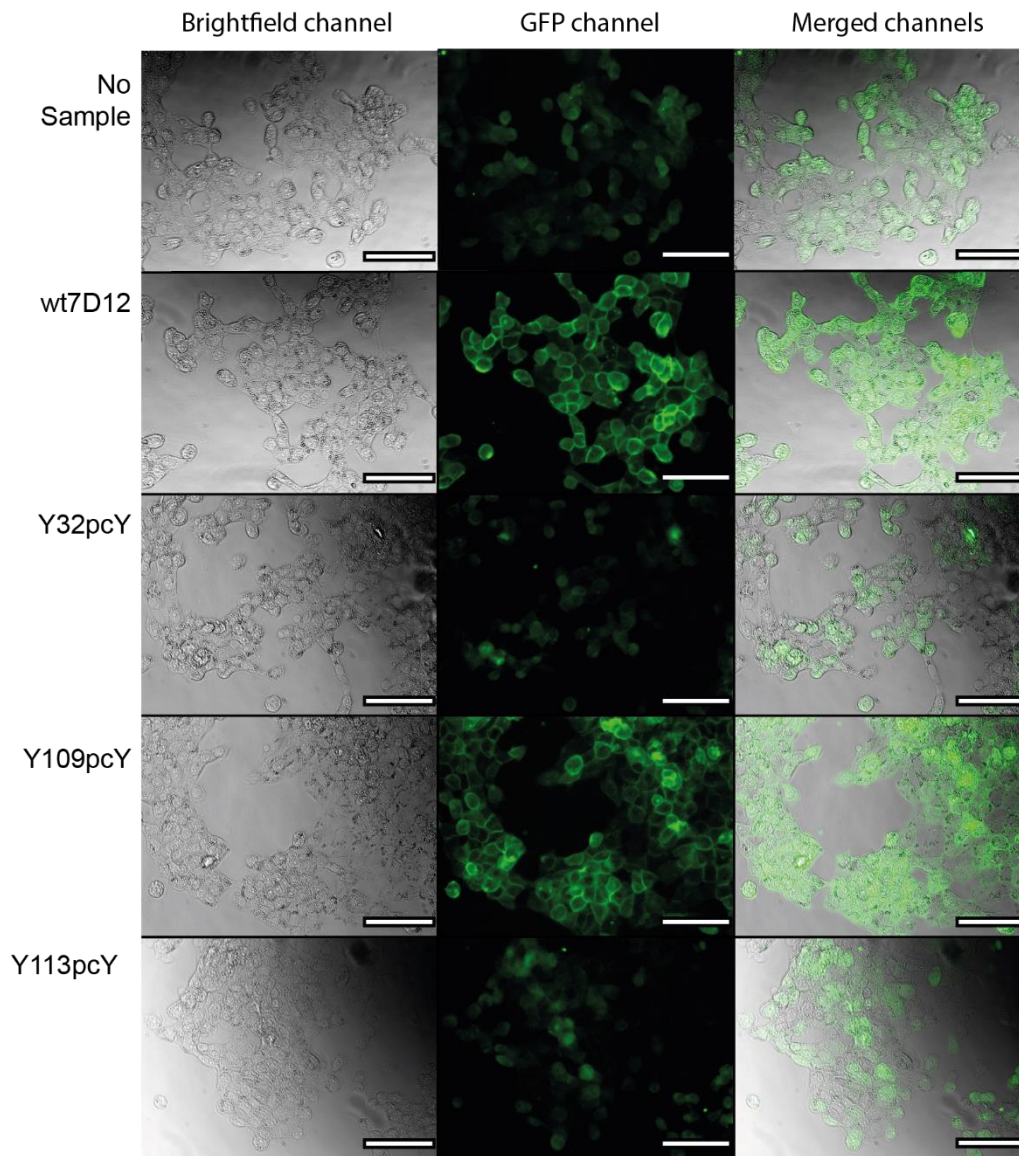


Figure 6.2: Assessment of interaction between wt7D12, 7D12-32pcY, 7D12-109pcY and 7D12-113pcY with EGFR on the surface of A431 cells using fluorescence widefield microscopy. 100nM BODIPY-FL labelled 7D12 and its pcY mutants (Y32pcY, Y109pcY, and Y113pcY) were incubated with A431 cells for 10 minutes, subsequently the solution was removed and the plates were washed with imaging media before acquiring images with Zeiss Axiovert 200M microscope (20X) on brightfield channel and GFP channel (20000ms exposure). Images were processed in Fiji (ImageJ), scale bar = 100 microns.

The extended exposure time resulted in the detection of fluorescence from A431 cells in the absence of VHH, and caged 7D12 (Y32pcY, and Y113pcY). Fluorescence imaging of A431 cells in the absence of BODIPY-FL labelled VHH should result in no detectable signal. Furthermore, in previous analysis of binding interactions of caged

7D12 (Y32pcY and Y113pcY) to EGFR using on-cell assay resulted in antibody-antigen affinity inhibition which should have corresponded to reduced or no signal detected in this experiment. Although certain experimental design considerations could have caused increased background fluorescence signal of caged 7D12 (Such as insufficient washing before imaging, or inadequate purification after BODIPY-FL labelling), as similar signal was detected from absence of VHH, it was hypothesised that the observed signal was due to high exposure times causing autofluorescence. Despite high background fluorescence detected for caged 7D12 samples, a significant difference in fluorescence was observed between wt7D12 and autofluorescence from caged samples. In the presence of wt7D12 labelled with BODIPY-FL, highly saturated fluorescence was observed surrounding A431 cells which could indicate 7D12-EGFR cell surface interactions. This observation is further demonstrated with caged 7D12 Y109pcY, which is in agreement with previous work that showed binding was not inhibited with the site-specific addition of pcY at position Y109. For 7D12 Y32pcY and 7D12 Y113pcY, a fluorescence signal similar to samples without any fluorophore was consistent with on-cell experiments discussed in the previous chapter.

In an attempt to reduce exposure time, four different fluorescent dyes were tested (Results not shown). NHS-esters of these dyes (BODIPY-FL, BODIPY-TMR-X, Atto 647N, Alexa 555) were covalently attached to wt7D12 as described above, and purified using Zebra Spin columns (MWCO 7000 Da). BODIPY-FL and BODIPY-TMR-X resulted in highest detected fluorescence of the four tested dyes. The fluorescence signal detected from wt7D12 BODIPY-FL resulted in the highest signal with the lowest exposure time, and was therefore selected for further optimisation. To confirm that the fluorescent signal was due to 7D12-EGFR interactions, the binding of BODIPY-FL labelled 7D12 to an EGFR-negative cell line was investigated.

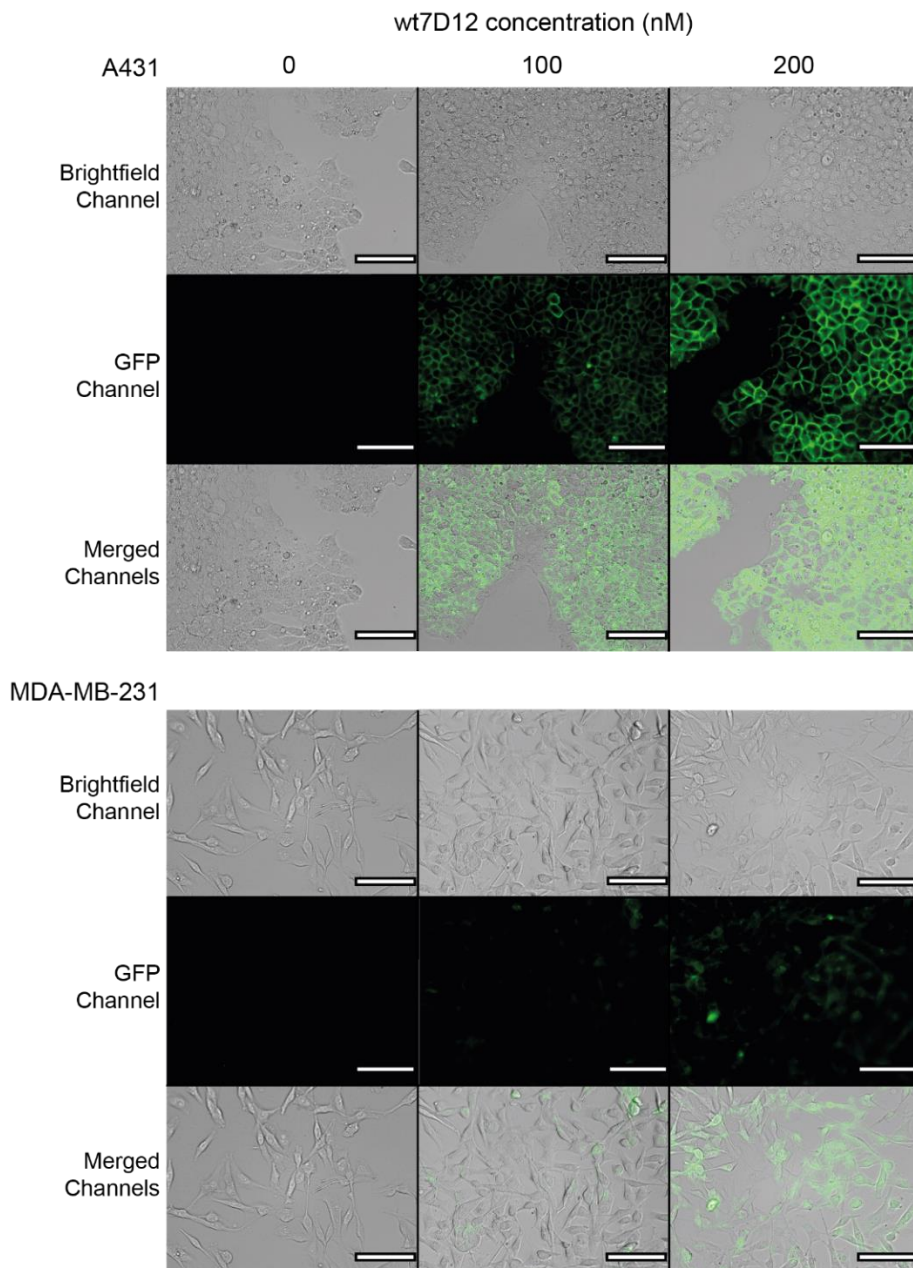


Figure 6.3: Assessment of interaction between wt7D12 with EGFR on the surface of A431 and MDA-MB-231 cells using fluorescence widefield microscopy. 100nM BODIPY-FL labelled 7D12 were incubated with A431 and MDA-MB-231 cells for 10 minutes, subsequently the solution was removed and the plates were washed with imaging media before acquiring images with Zeiss Axiovert 200M microscope (20X) on brightfield channel and GFP channel (15000ms exposure). Images were processed in Fiji (ImageJ), scale bar = 100 microns.

The results in Figure 6.3 show that at 100nM and 200nM concentration of BODIPY-FL labelled wt7D12, significant fluorescence signal was detected on A431 cells, while a much reduced signal was observed with MDA-MB-231. These results are consistent

with our hypothesis that we are visualising specific interaction between 7D12 and EGFR, using BODIPY-FL labelled 7D12. The results are also in agreement with on-cell experiments described in chapter 5 (5.2.4.1). The minor fluorescent signal detected on MDA-MB-231 is likely due to basal level of EGFR on the surface of MDA-MB-231. These microscopy images also demonstrate no autofluorescence in the absence of labelled 7D12, which is likely due to reduced exposure time of 15 sec compared to 20 sec as in figure 6.2. However, 15 sec exposure is still long and can have detrimental effect on cell health. In an attempt to optimise exposure time, 200nM wt7D12-BODIPY-FL, Y32pcY-BODIPY-FL, Y109pcY-BODIPY-FL and Y113pcY-BODIPY-FL were incubated with A431 cells for 10 minutes before washing with imaging medium. Fluorescence images were acquired with 20 seconds and 5 seconds exposure (Figure 6.4).

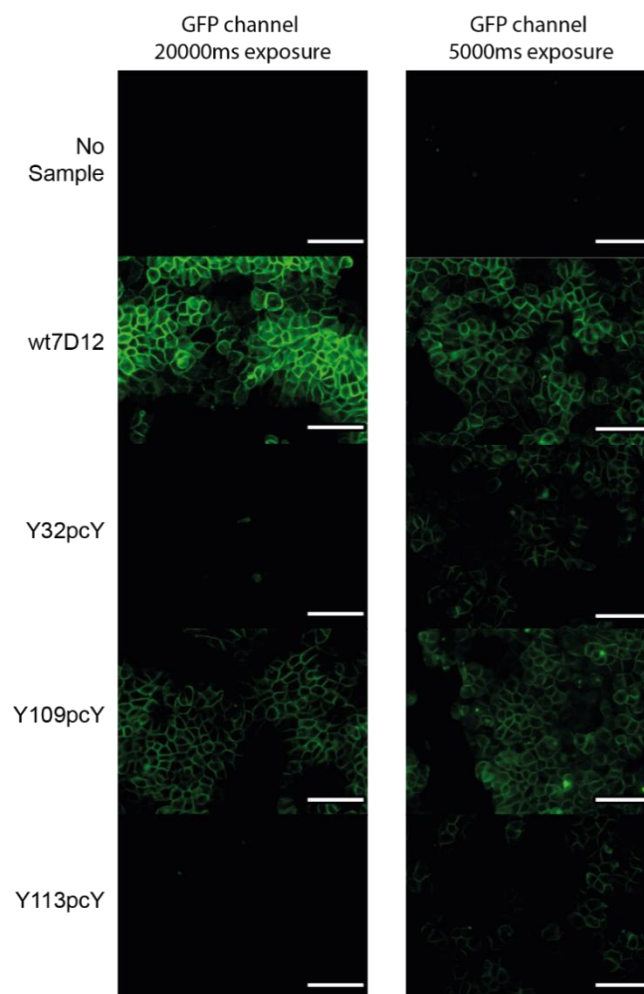


Figure 6.4: Microscopy investigation into reduction of exposure time. Images of BODIPY-FL labelled 7D12 (200nM) binding interactions to A431 cell surface EGFR. Images were acquired with Zeiss

Axiovert 200M widefield microscope (20X) on and GFP channel (20 seconds or 5 seconds exposure). Images were processed in Fiji (ImageJ), scale bar = 100 microns, Brightness/contrast (B/C) = 1700/3000 and 600/1500 for 20s and 5s exposure, respectively.

At 20 second exposure, no fluorescence was detected in the absence of labelled VHH indicating reduced background signal. Only minor fluorescence was detected from two caged samples (Y32pcY-BODIPY-FL and Y113pcY-BODIPY-FL) indicating that with the addition of pcY in either positions (Y32 or Y113) within 7D12 inhibit their interaction with EGFR. Compared to the background fluorescence from caged samples (and absence of VHH), wt7D12-BODIPY-FL and Y109pcY-BODIPY-FL both had significant fluorescence indicating binding to EGFR which is in agreement with previous on-cell assay experiments. It is interesting to note that there is quite a stark difference in fluorescence between wt7D12 and 7D12-109pcY at 20 sec exposure but much less difference at 5 sec exposure. This might be due to non-linear change in fluorescence intensity with exposure time.

The Zeiss Axiovert 200M microscope used in these experiments captures analogue images with a CCD camera which converts (*via* 12-bit analog-to-digital (A/D) converter) to a digital image containing 4096 grey values (2×10^{12}). By adjusting the displayed range of grey values at defined thresholds (minimum and maximum) the brightness and contrast of the image is directly affected. Although the radiant intensity (magnitude or quantity of light detected) of the sample is not affected, by changing the minimum and maximum thresholds to 600/1500 of images attained from 5000ms exposure, the overall brightness is increased. However, this decreases the image resolution and quality of the digital image which is determined by total number of pixels and range of brightness values. The decrease image resolution (of images acquired at 5000ms exposure) shows a significant difference of quality when compared to images acquired with 20000ms (thresholds set to 1700/3000). However, longer exposure times cause additional complications and require a balance between image quality and cell viability. Although the aim of reducing exposure was achieved, by shorting the range of grey values this has accentuated

background signal that can be seen in no sample, Y32pcY-BODIPY-FL and Y113pcY-BODIPY-FL with 5 seconds exposure.

6.2.2 Real-time live-cell imaging with pH-sensitive dyes

Use of BODIPY-FL fluorophore for visualising binding of 7D12 to EGFR on the surface of A431 cells required several washing steps that can potentially interfere with experimental observations. To circumvent this challenge and to visualise the process of endocytosis of 7D12, the use of pH sensitive dyes as a method of generating fluorescence was investigated. These dyes are designed to be non-fluorescent outside the cell at physiological pH and their fluorescence increases at lower pH of the endosome upon endocytosis. Previous studies have investigated the receptor-mediated internalization of antibodies (Hazin *et al.*, 2015; Casalini *et al.*, 1993). However, these studies often labelled antibodies with radioisotopes or pH-insensitive fluorescent molecules. To detect internalized antibodies by fluorescence or radioactivity the cell membrane is often washed with low pH buffer or ice cold PBS and fixed with formaldehyde. These methods are end-point assays as cell fixation causes irreversible damage to the cells. Similarly, there were studies examining internalization of antibodies labelled with pH sensitive dyes (Göstring *et al.*, 2010; Berguig *et al.*, 2012). Although these studies gave an impressive snapshot of endosomes and lysosomes at specific time periods, they did not show the real-time process of receptor-mediated antibody internalization.

The same labelling methodology as above was applied to label wt7D12 with pHrodo Red and Protonex Red 600. A431 cells were grown on glass coverslips (18 mm) by seeding 400,000 cells per well in a 6-well Ultra-Low Attachment plate (Corning, 3471). After growing for 18-20 hours (37°C, 5% CO₂) the coverslip was mounted in a Ludin chamber (Life imaging services) for imaging with 40x (1.3 NA) Plan-Neofluar, oil-immersion objective lens. The cells were washed 3 times with pre-warmed imaging medium, and 198 µL of fresh imaging medium was added to the chamber

and loaded on the Zeiss Axiovert 200M microscope. Initial checks on cell health and autofluorescence was done by imaging cells with before treatment, then 2 μL of 100x labelled VHH 7D12 was added to the chamber imaging medium to make the final concentration 200 nM. With the addition of labelled 7D12 the time-lapse was initiated, the time-lapse was programmed to capture on brightfield and red filter set (TexRed, Zeiss cube #43HE, Ex = 572 ± 14 nm, Dichroic = 593 nm) every 1 minute for a total of 15 minutes. Exposure time of the TexRed channel was set to 80ms for 7D12-Protonex Red 600 and 1000ms for 7D12-pHrodo Red. Conjugation of pH-sensitive dyes to 7D12 prompted significant reduction in exposure while retaining high levels of fluorescence (Figure 6.5).

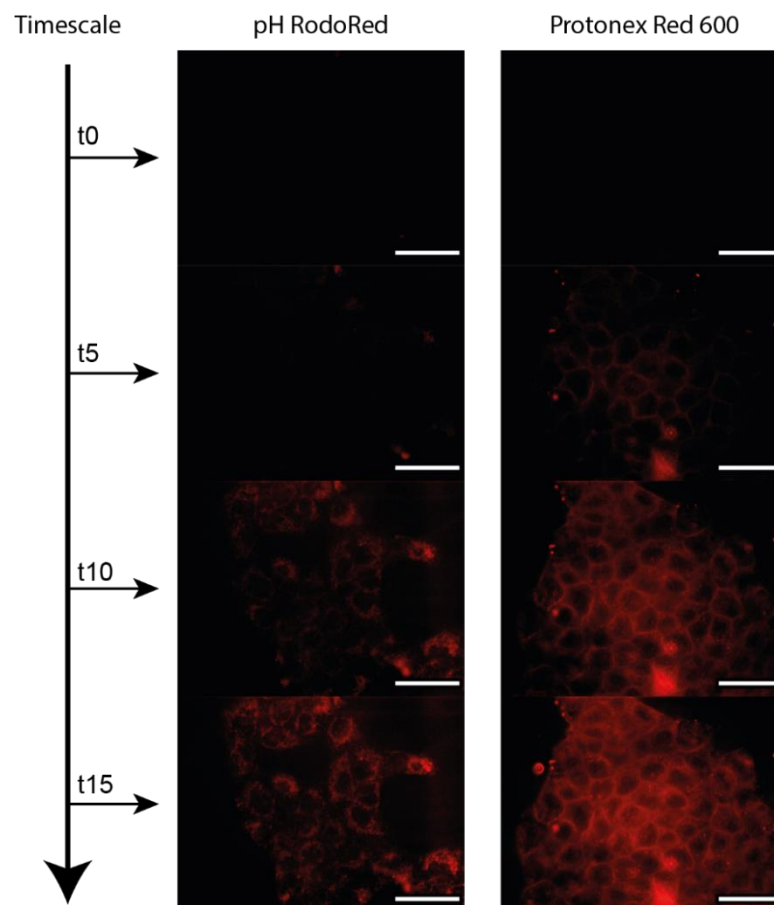


Figure 6.5: Exploring the use of pH-sensitive dyes. Microscopy images of pHrodo Red and Protonex Red 600 labelled wt7D12 (200nM) binding interactions to A431 cell surface EGFR. Images were acquired with Zeiss Axiovert 200M widefield microscope (40X) on TexRed channel (pHrodo Red = 1000 ms exposure, Protonex Red 600 = 80 ms exposure). Images were processed in Fiji (ImageJ), scale bar = 50 microns, Brightness/contrast (B/C) = 2000/2600 and 850/1150 for Protonex Red 600 and pHrodo Red respectively.

Although initial results were encouraging, further controls were required to fully validate the experiment. Due to considerable reduction required in exposure time for fluorescent imaging of 7D12 labelled with Protonex Red 600, further analysis was necessary to determine if fluorescence was attributed to decreased pH from EGFR mediated endocytosis, or as a result of other factors. A similar time-lapse experiment was designed with A431 cells to measure fluorescence of wt7D12 Protonex Red 600 and 7D12-Y32pcY Protonex Red 600 (with and without irradiation at 365nm). To de-cage labelled 7D12-Y32pcY, the DAPI microscope filter set (blue filter set, Zeiss cube #49, Ex = 365 nm, Em = 445/450 nm) was used to irradiate VHH sample and cells for 30 seconds. The resulting fluorescence in Figure 6.6 shows comparable signal between wt7D12, caged 7D12-Y32pcY, and de-caged 7D12-Y32pcY.

The expected fluorescence from caged 7D12-Y32pcY should have resulted in decreased detected signal due to inhibited binding to EGFR due to photocaged tyrosine in 7D12. Therefore, it was speculated that the fluorescence signal observed from caged VHH 7D12 was not caused by the EGFR mediated internalization and subsequent pH decrease. An alternative explanation for the observed fluorescence is as a result of inefficient purification of free fluorescent dye molecules from the labelling reaction. With the addition of free dye molecules in the medium, non-specific internalisation and subsequent fluorescence could occur, a process in which small particles are internalized from the cell surface (Alberts et al, 2013). To investigate this hypothesised non-specific small molecule internalisation, internalisation of Protonex Red 600 labelled wt7D12 and 7D12 Y32pcY was analysed on EGFR-negative, MDA-MB-231 cells. A431 and MDA-MB-231 cells were grown on 18mm coverslips as described above, and were treated with 100 nM of Protonex Red 600 labelled 7D12 Y32pcY. As a control, A431 cells were also treated with Protonex Red 600 labelled wt7D12. Time-lapse images were captured every 1 minute for a total of 15 minutes.

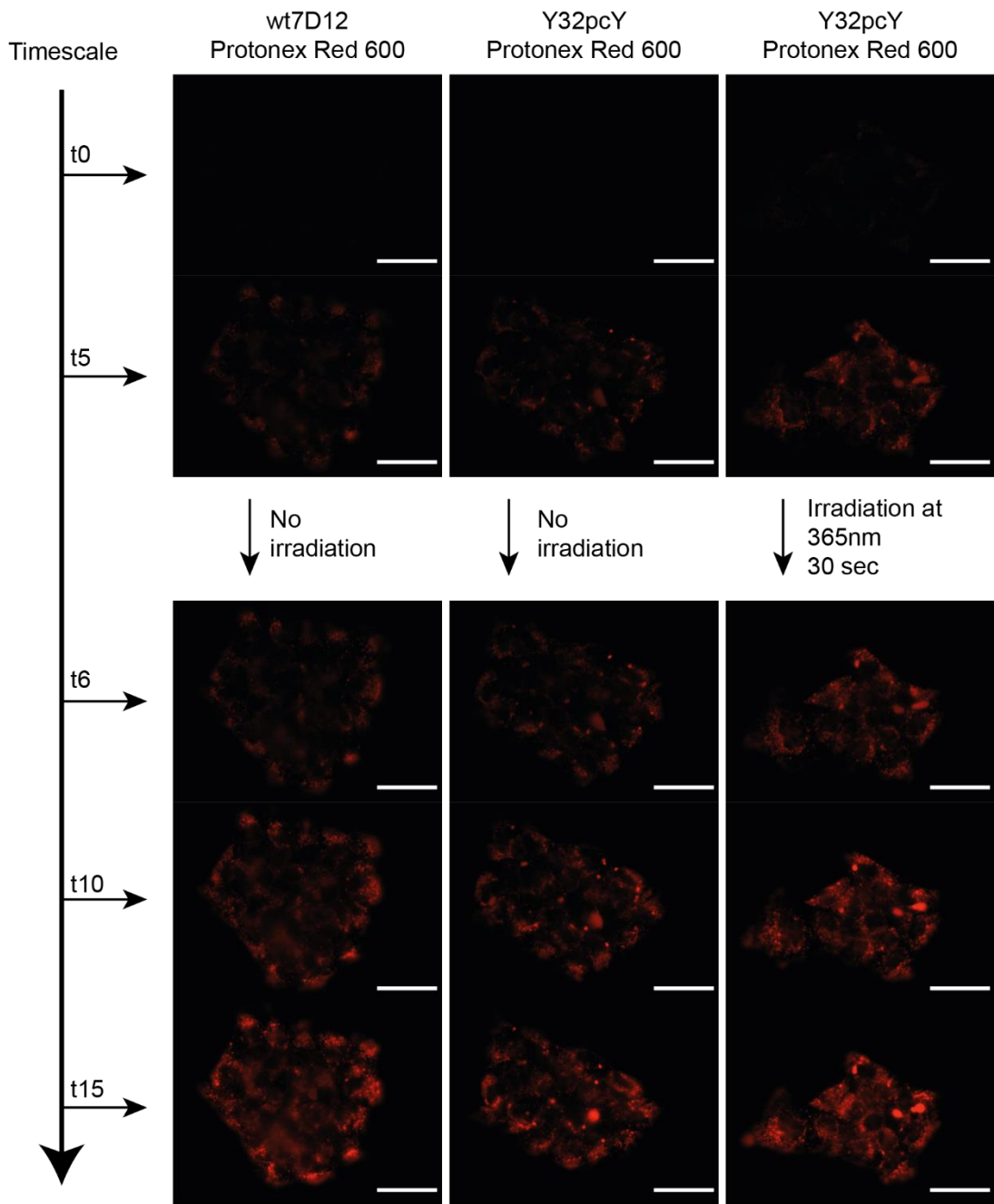


Figure 6.6: Evaluating the efficacy of Protonex Red 600 labelled 7D12 (wild type and Y32pcY) to A431 cells. Microscopy images were acquired with Zeiss Axiovert 200M widefield microscope (40X) on TexRed channel (25 ms exposure). Images were processed in Fiji (ImageJ), scale bar = 50 microns, Brightness/contrast (B/C) = 100/1500.

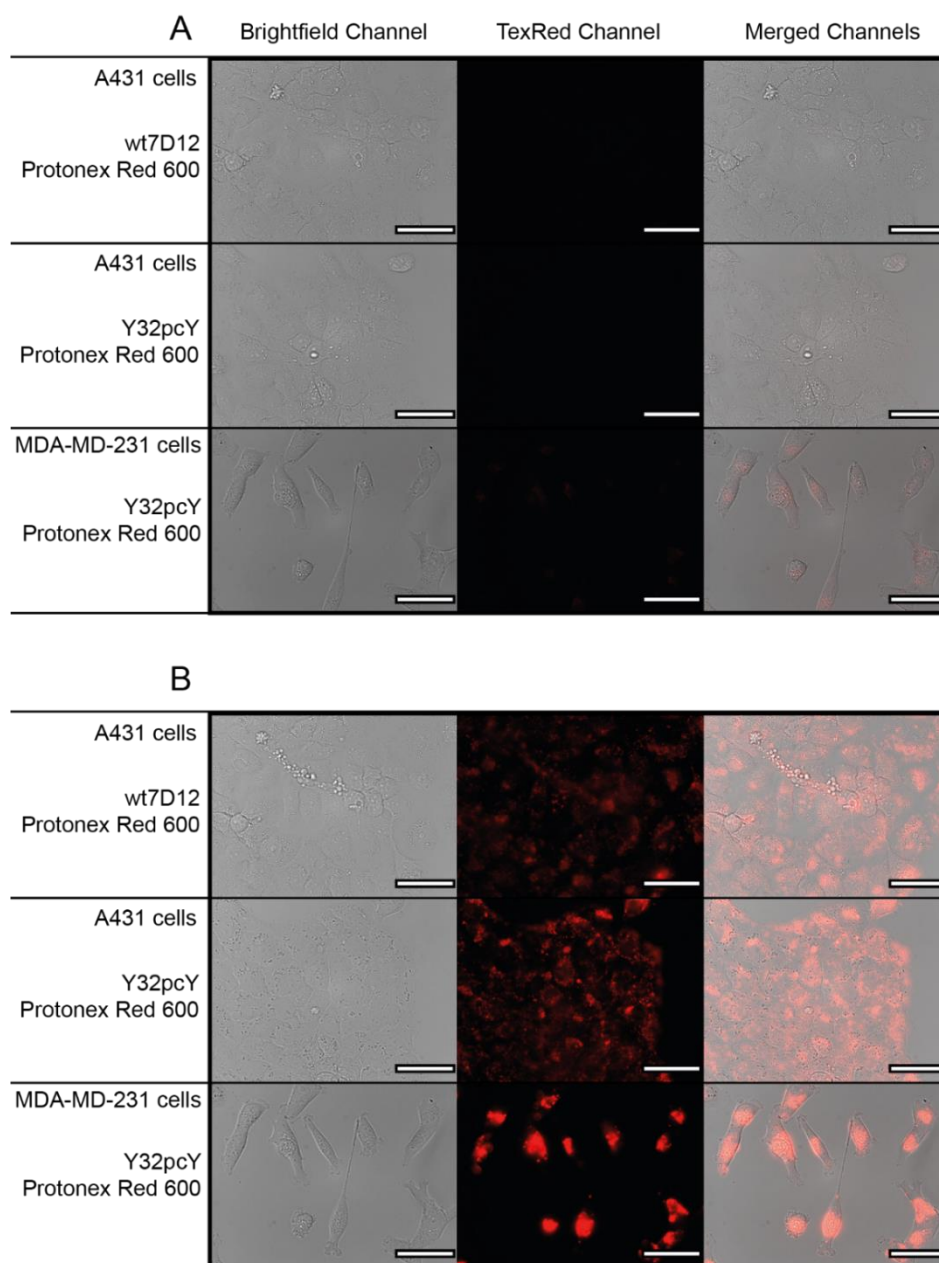


Figure 6.7: Evaluating the efficacy of Protonex Red 600 labelled 7D12 (wild type and Y32pcY) to A431 and MDA-MB-231 cells. Microscopy images were acquired with Zeiss Axiovert 200M widefield microscope (40X) on TexRed channel (50 ms exposure) and brightfield channel. Images were processed in Fiji (ImageJ), scale bar = 50 microns, Brightness/contrast (B/C) = 300/2000. A) Images acquired following 100 nM sample treatment at t=0. B) Images acquired after 15 minutes incubation with treatment showed similar fluorescence signal.

Figure 6.7 shows that after 15 minutes Protonex Red 600 labelled 7D12-Y32pcY have significant and comparable fluorescence on A431 and MDA-MB-231 cells to the control wt7D12 fluorescence on A431 cells. This indicates that the fluorescence signal

observed is likely caused by insufficient removal of excess dye in the labelling reaction. To address this challenge, more rigorous purification protocol was adopted. It was observed that Protonex Red 600 dye did not dissolve completely during the labelling reaction. Thus, after labelling, the excess undissolved dye was removed by centrifugation at 16000 rcf. Subsequently, the labelled protein was passed through desalting columns several times. With the additional purification steps in place, three dyes, pHrodo Red, pHrodo Green and Protonex Red 600, were investigated for visualising endocytosis of wt7D12. These dyes were conjugated to wt7D12 *via* NHS ester reaction to primary amines in the protein. In addition, 7D12-32pcY was labelled with pHrodo Red, as this dye had shown some promise (data not shown).

A431 cells were seeded into a 6-well ultra-low attachment plate containing 18mm glass cover slip as described above. A final concentration of 500 nM of labelled wt7D12 and 7D12-Y32pcY was used in a 15 minute real-time live cell imaging experiment and resulting fluorescence was captured and analysed (Figure 6.8). Despite increasing the concentration of labelled VHH to 500nM, with the additional purification procedures performed the observed fluorescence over a 15 minute period remained low. Note that an overall decrease in fluorescence is observed compared to previous experiments in Figure 6.7, which is consistent with the hypothesis that fluorescence observed in Figure 6.7 is due to residual free dye in the labelled sample. pHrodo red labelled 7D12 sample shows minor increase in fluorescence signal after 15 minutes, whereas 7D12 labelled with other dyes show no change in fluorescence after 15 minutes (Figure 6.8). The relatively small increase in fluorescence over the cellular pH range in question from pH sensitive dyes have been reported as a potential limitation to their applicability (Liao-Chan 2015). Due to these difficulties with pH sensitive dyes, alternative methods for visualisation of 7D12-EGFR interaction on live cells were pursued.

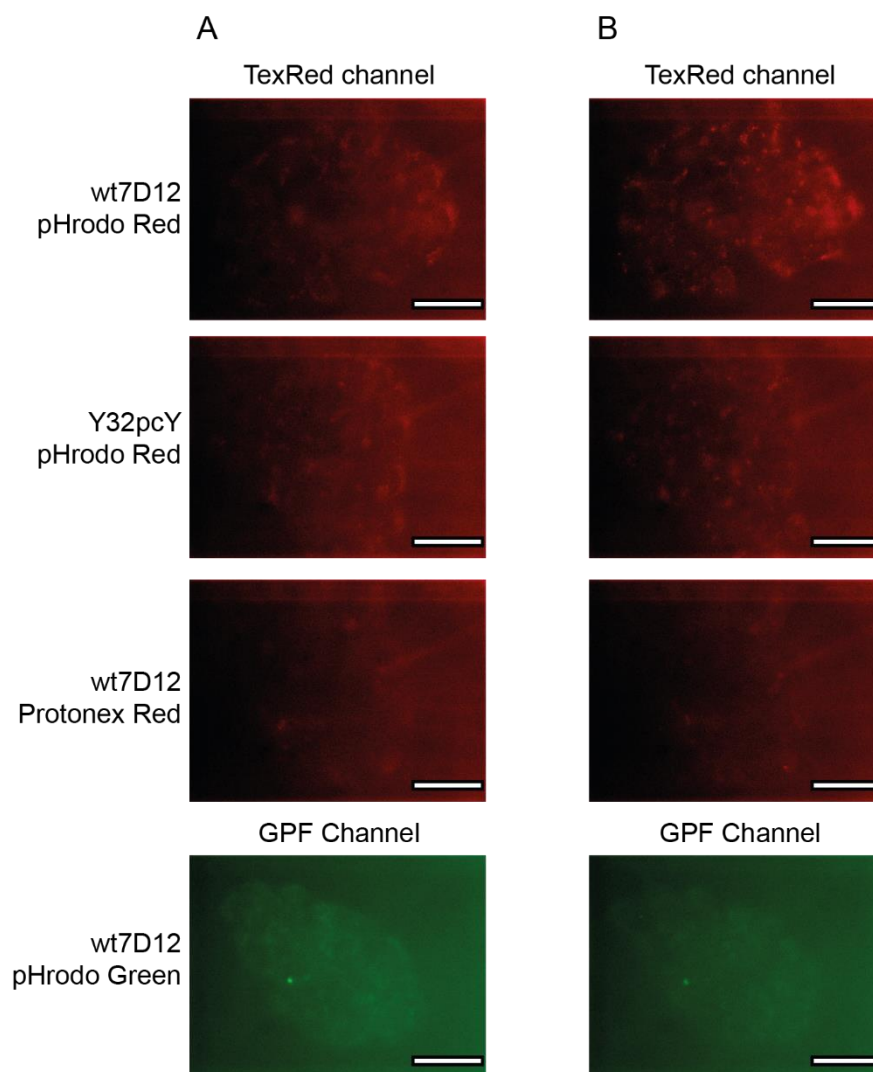


Figure 6.8: Detected fluorescence signal from pHrodo Red, Protonex Red and pHrodo Green labelled 7D12 (wild type and Y32pcY) with additional purification steps. Images acquired with Zeiss Axiovert 200M widefield microscope (40X) on TexRed channel (500 ms exposure) and GFP channel (750 ms exposure). Images were processed in Fiji (ImageJ), scale bar = 50 microns, Brightness/contrast (B/C) = 1350/1500 (Red channel) and 750/1000 (Green channel). A) The immediate acquisition of fluorescence images after treatment of 500nM 7D12 (wild type and Y32pcY) to A431 cells. B) Fluorescent images acquired after 15 minutes time-lapse.

6.2.3 Dynamic real-time live-cell imaging

With minor radiant intensity increase over the time-lapse period with the use of pH-sensitive fluorophores, an alternative experimental design was required for visualisation of VHH 7D12 interactions with EGFR. Due to the real-time conditions of

the experimental design, the use of pH insensitive fluorophores would likely impose experimental challenges as washing procedures to remove non-specific fluorescence were not implemented in the methodology. The previous real-time imaging strategy relied on the increase in fluorescent intensity when the VHH was internalised, and that unbound non-internalised labelled VHH would produce no fluorescence at physiological pH of the medium. If these experiments had worked, the real-time live-cell imaging would not require washing of unbound VHH, and immediate time-lapse capture of receptor mediated internalisation would have been possible. However, if this experimental strategy was applied to pH-insensitive fluorophores, the expected results would be high background signal from unbound VHH that would fluoresce at physiological pH.

An alternative method was adopted to remove the static nature of the experiment to allow use of non-pH sensitive dyes that have improved quantum yields. This was achieved by incorporating a peristaltic pump into the delivery system and by applying a constant flow of fresh medium over cells with an additional option of switching the flow to medium supplemented with the VHH. This setup allowed the design of a dynamic microscopy experiment which inherently removes non-specific fluorescence signal. The schematic shown in Figure 6.9 shows the details of the system including inputs and total running volume required.

For the first dynamic time-lapse microscopy experiment, wt7D12 and 7D12-Y32pcY were labelled with BODIPY-FL as discussed earlier. A 6-well ultra-low attachment plate containing 18mm glass coverslip was seeded with 400,000 A431 cells per well and grown until 80% confluence (37°C, 5% CO₂). Glass coverslip with attached A431 cells was mounted into the Ludin microscopy chamber and washed three times with pre-warmed imaging medium. The peristaltic pump was connected to the microscope chamber, and fresh medium flowed over cells for 5 minutes. Once chamber volume had equalised, the time-lapse was started. The Zeiss Axiovert microscopy software was programmed to capture brightfield images and images using the GFP channel every 30 seconds for 43 minutes.

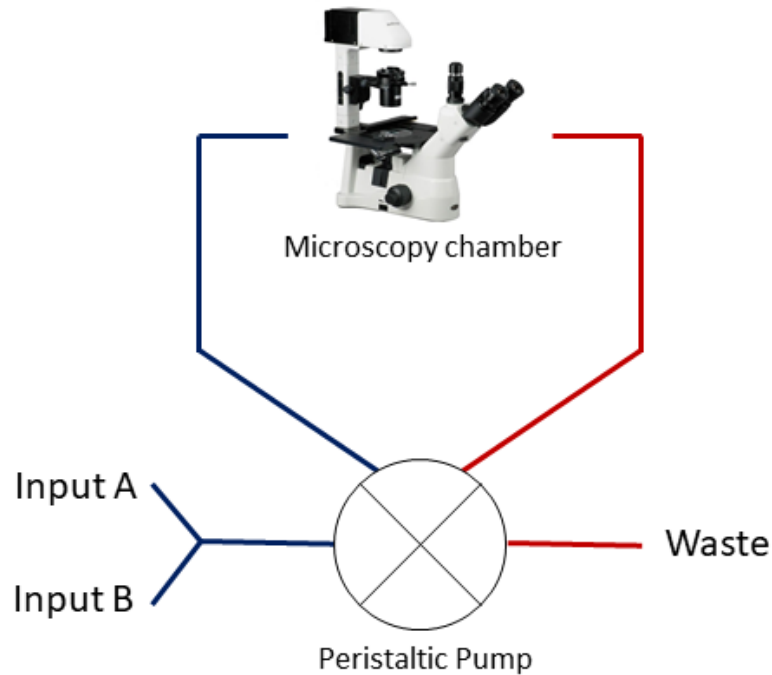


Figure 6.9: Diagram of dynamic microscopy setup for time-lapse experiments of live-cells with constant flow. Switchable line from input A/B to Ludin microscopy chamber required 1 mL total running volume, and 200 μL to fill chamber.

For first 5 minutes of the time-lapse, fresh pre-warmed medium (input A, Figure 6.9) was passed over the cells at a rate of 400 $\mu\text{L}/\text{min}$. Next, the input was switch to input B (Figure 6.9) and medium supplemented with 200 nM 7D12-Y32pcY BODIPY-FL was circulated over the cells. After 5 minutes of treatment, the system was switched back to imaging medium for 10 minutes. A snapshot image from the GFP channel at 2.5 minutes after the flow of labelled 7D12-32pcY was stopped show near background fluorescence signal (Figure 6.10A), consistent with inhibition of binding due to pcY at position 32 in 7D12. Next, 7D12-Y32pcY BODIPY-FL was de-caged with the DAPI channel (irradiated with 365 nm light) on the microscope, the same procedure as above for circulating 7D12-Y32pcY BODIPY-FL was used, however after 2 minutes of treatment the DAPI channel was turned on for 1 minute to de-cage 7D12-Y32pcY. Following the de-caging step, 10 minutes of imaging medium was flowed over the

cells. Contrary to expectation, the snapshot image from the GFP channel at 2.5 minutes after the flow of decaged 7D12-Y32pcY was stopped, showed near background fluorescence signal (Figure 6.10B). It was hypothesised that this might be due to inefficient decaging of 7D12-Y32pcY on the microscope as caged 7D12 was passed over the cells for a total of 5 minutes, with only 1 minute of decaging with DAPI channel. Finally, control treatment with wt7D12 was performed, and wt7D12-BODIPY-FL was passed over cells for 5 minutes. Here, as expected, the image from GFP channel 2.5 minutes after the flow of wt7D12 was stopped shows clear fluorescence signal (Figure 6.10C).

Due to the use of non-pH sensitive dyes, highly saturated non-specific fluorescence was observed for each sample as they were initially passed over the cells. The initial saturation of non-specific fluorescence was removed by fresh complete medium, and remaining 7D12 interactions with A431 cells were observed (Figure 6.10 A, B, C). Full time-lapse video can be viewed in Appendix A.4.1.

To further investigate if de-caging of 7D12-Y32pcY on the microscope was presenting a problem for these experiments, de-caging 7D12-pcY off the microscope was performed. Previous methods used in chapter 4 (2.1.15) were used to decage 7D12-Y32pcY; this sample was then labelled with BODIPY-FL and applied in a similar dynamic experiment. Pre-warmed medium was circulated over cells for 5 minutes, and 200nM wt7D12 BODIPY-FL was passed over the cells for 5 minutes. As expected, significant fluorescence signal was observed 3 minutes after stopping the flow of wt7D12 BODIPY-FL (Figure 6.11A). Then 10 minutes of medium was passed over cells which was followed by 5 minutes of treatment with 200 nM de-caged 7D12-Y32pcY-BODIPY-FL. Here, significant fluorescence signal was observed even after 3 minutes of stopping the flow of decaged 7D12-32pcY-BODIPY-FL (Figure 6.11B). For this experiment, brightfield and fluorescence images were acquired over 35 min time-lapse period with images captured every 30 seconds (Figure 6.11). Full time-lapse video can be viewed in Appendix A.4.2.

A significant fluorescence difference is demonstrated between the two methods of de-caging (*via* microscope DAPI channel and UV transilluminator) shown in Figure

6.10 and Figure 6.11 signifying that the use of the microscope DAPI channel (for one minute) as a method of de-caging is inefficient and further optimisation is required for successful de-caging by the microscope.

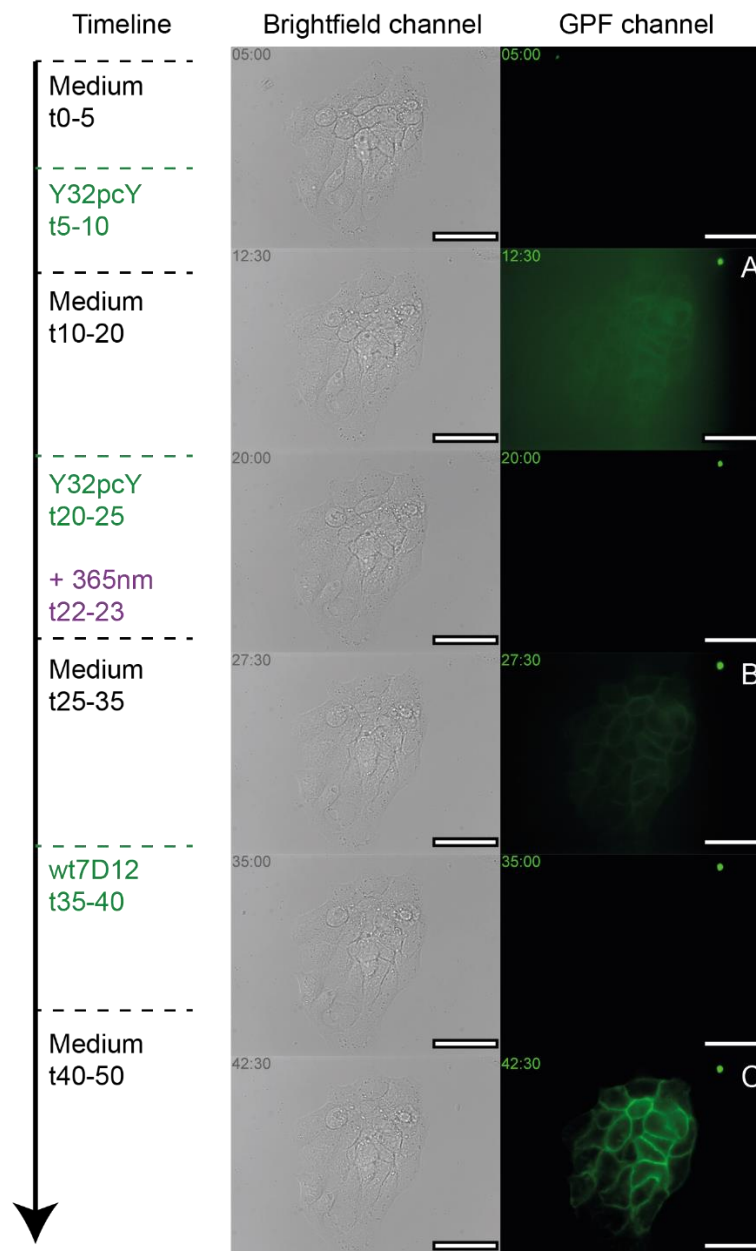


Figure 6.10: Dynamic microscopy experiment investigating de-caging of Y32pcY-BODIPY-FL with microscope DAPI channel and measuring subsequent binding to A431 cell surface. Images acquired with Zeiss Axiovert 200M widefield microscope (40X) with time-lapse capturing GFP channel (500 ms exposure) and brightfield channel images at 1 minute intervals. De-caging of Y32pcY occurred at t=22 with DAPI channel exposure for 1 minute. Images were processed in Fiji (ImageJ), scale bar = 50 microns, B/C = 600/1100. A) Caged Y32pcY-BODIPY-FL (200 nM) injected over cells for 5 minutes (at a

rate of 400 $\mu\text{L}/\text{minute}$) resulted in minimal binding to A431 cell surface. B) Caged Y32pcY-BODIPY-FL (200 nM) injected over A431 cells with additional irradiation for 365 nm light for 1 minute to de-cage. Minor binding to A431 cell surface is observed. C) Positive control sample (wt7D12-BODIPY-FL, 200 nM) injected over A431 cells to demonstrate wild type binding and subsequent fluorescence signal detected. Full time-lapse video available in Appendix A.4.1.

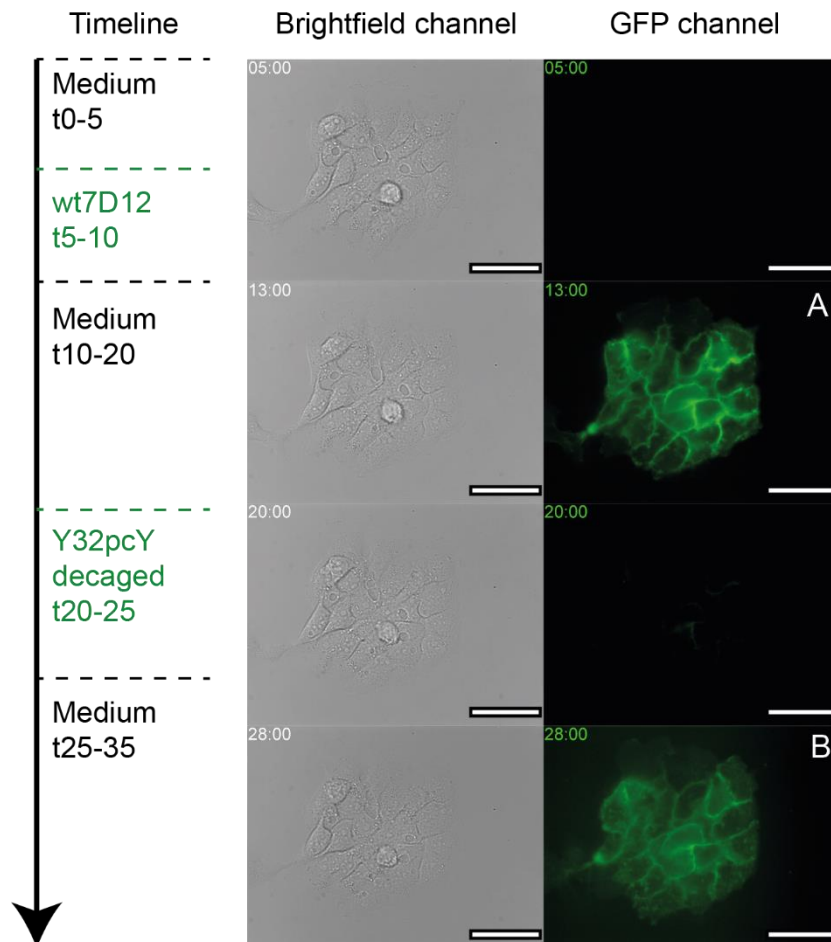


Figure 6.11: Dynamic microscopy experiment investigating de-caged Y32pcY-BODIPY-FL (de-caged *via* UV transilluminator) and measurements of binding to A431 cell surface. Images acquired with Zeiss Axiovert 200M widefield microscope (40X) with time-lapse capturing GFP channel (500 ms exposure) and brightfield channel images at 1 minute intervals. Images were processed in Fiji (ImageJ), scale bar = 50 microns, B/C = 600/1100. A) Positive control sample (wt7D12-BODIPY-FL, 200 nM) injected over A431 cells to demonstrate wild type binding and subsequent fluorescence signal detected. B) De-caged Y32pcY-BODIPY-FL (200 nM) injected over A431 cells resulted in similar fluorescence signal as wild type levels. Full time-lapse video available in Appendix A.4.2.

While it has been shown that an increase in fluorescence is observed when de-caging 7D12-Y32pcY-BODIPY-FL before microscopy experiments, one of the aims of the dynamic microscopy experiment is to simulate the physiological conditions of drug delivery to a targeted receptor. Future application of such photoactive antibodies would require that: 1) such antibodies could be decaged in the presence of cells; 2) can bind to the receptors within the timeframe of decaging; and 3) if the presence of photocaging group influences the folding of the antibody, the antibody should be able to revert back to its native folded state after being decaged and bind to its receptor antigen, when unbound antibody is constantly getting removed by flowing blood in the body. Therefore, it was important to further explore the possibility of decaging on the microscope in this dynamic experiment.

It was hypothesised that the negative result in Figure 6.10 was due to problems with the experimental design, such as low concentration of decaged antibody (caged antibody was irradiated for only 1 minute of the total 5 minutes flow time) and slower clearance of non-specifically bound antibody. This prompted changes to the experimental design: 1) The flow rate was increased from 400 $\mu\text{L}/\text{min}$ to 1000 $\mu\text{L}/\text{min}$. This would allow for additional delivery of sample (antibody) to the cells per unit time, allowing for easier detection by increased fluorescence. In addition, faster flow rate would help faster clearance of the non-specifically bound antibody, thus allowing detection of specifically bound antibody earlier. In the new experimental setup, the antibody (caged or decaged) was passed for 2 minutes compared to 5 minutes in earlier experiments. The decaging was still be performed for 1 minute, thus increasing the fraction of decaged antibody compared to earlier experiment in Figure 6.10; 2) Instead of labelling 7D12 with BODIPY-FL, BODIPY-TMR-X was used. The latter is excited using longer wavelength, thus reducing potential phototoxicity due to imaging. Furthermore, as earlier static experiments in Figure 6.2 demonstrated autofluorescence when imaging with the GFP channel, the use of BODIPY-TMR-X, which is excited by red light and can potentially reduce the background signal; and 3) The concentration of labelled antibody was increased to 500 nM instead of 200 nM used in previous experiments.

Figure 6.12 shows the resulting fluorescence detected from three sample injections (wt7D12, caged 7D12-Y32pcY and de-caged 7D12-Y32pcY) over A431 cells during a 41 minutes time period.

First, pre-warmed medium was circulated over cells for 5 minutes, and background fluorescence was checked (Figure 6.12 A). Then, 2 mL of 500 nM caged 7D12-Y32pcY BODIPY-TMR-X was passed over the cells at a rate of 1000 $\mu\text{L}/\text{min}$ (t: 5-7). The initial high fluorescence of caged 7D12-Y32pcY BODIPY-TMR-X flowing over the cells is observed in Figure 6.12 D, however subsequent snapshot images (Figure 6.12 E, F) show near background fluorescence signal, consistent with inhibition of binding due to pcY at position 32 in 7D12. Imaging medium was passed over the cells for 10 minutes (t: 7-17), and background fluorescence was checked (Figure 6.12 B). Then, 2 mL of 500nM 7D12-Y32pcY BODIPY-TMR-X was passed over the cells (t: 17-19) with 1 minute irradiation (DAPI channel, t: 19-20) using 365 nm light to de-cage sample. Three snapshot images with the TexRed channel (Figure 6.12 G, H, I) show the fluorescence of decaged Y32pcY BODIPY-TMR-X over a 1.5 minute period. With the addition of 1 minute irradiation at 365nm to decage 7D12-Y32pcY a significant increase in fluorescence is observed (Figure 6.12 G) with longer retention time (Figure 6.12 H, I) of 7D12 on A431 cells. Imaging medium was then passed over the cells for 10 minutes (t: 19-29), and background fluorescence was checked (Figure 6.12 C). Finally, as a control, 2 mL of 500nM wt7D12 BODIPY-TMR-X was passed over the cells (t: 29-31). As expected, significant fluorescence signal was observed (Figure 6.12 J, K, L). Full time-lapse video can be viewed in Appendix A.4.3.

The difference of fluorescence between wt7D12 and de-caged 7D12 has been attributed to the de-caging constraints of the experiment, where total sample injection time is 2 minutes, and de-caging process occurs for 1 minute. No signal was detected before 7D12 treatments (figure 6.12.A, B, and C) suggesting minimal signal contamination between sample injections.

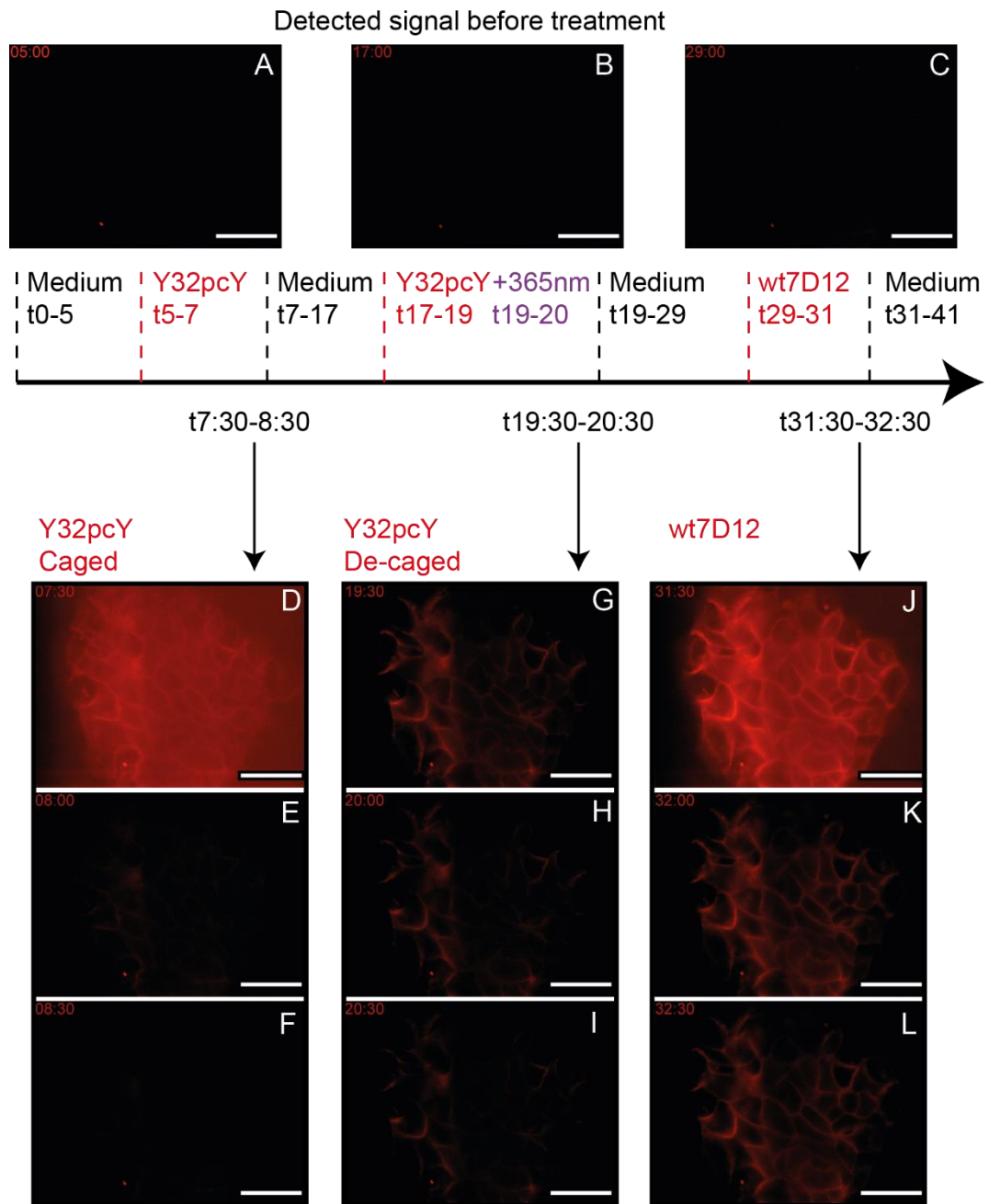


Figure 6.12: Dynamic microscopy experiment investigating Y32pcY-BODIPY-TMR-X binding to A431 cells in the presence and absence of 365 nm irradiation (*via* DAPI exposure for 1 minute), with subsequent positive control fluorescence of wt7D12-BODIPY-TMR-X binding to A431. Images were acquired with Zeiss Axiovert 200M widefield microscope (40X) set up to capture time-lapse images of TexRed channel (500 ms exposure) and brightfield channel at 30 second intervals. Flow rate = 1 mL/min, B/C = 1150/1500, scale bar = 50 microns. A, B, and C show fluorescence signal before treatment of labelled 7D12. D, E, and F show caged Y32pcY-BODIPY-TMR-X (500nM) over a 1.5 minute period to demonstrate initial fluorescent intensity and retention time. G, H, and I show caged Y32pcY-BODIPY-TMR-X with additional de-caging by DAPI exposure of 365 nm light (1 minute) and resulting fluorescence intensity. J, K, and L show fluorescence intensity of positive control wt7D12-BODIPY-TMR-X (500nM).

6.2.4 Assessing the binding influence caused by fluorophore on labelled VHH 7D12

During the microscopy experiments in this chapter, the labelling of VHH 7D12 with multiple different fluorophores has been achieved by reacting primary amines contained within the VHH with NHS esters reactive groups of a fluorophore to form stable amide bonds. Typically, this results in the fluorescence dye being labelled to the side chain of lysine. However, as lysine residues are frequently located in protein active/binding sites, the subsequent labelling of these residues can negatively contribute to the properties of the labelled proteins and specifically, the antigen binding affinity of labelled antibodies.

To measure and compare BODIPY-TMR-X labelled and unlabelled 7D12 binding affinities to A431 cells, an on-cell assay was used as described in the methods chapter (2.1.16). The wt7D12 cell surface interactions were measured by chemiluminescence signal on CLARIOstar (BMG labtech) plate reader and imaged by GelDoc XR+ system (Figure 6.13).

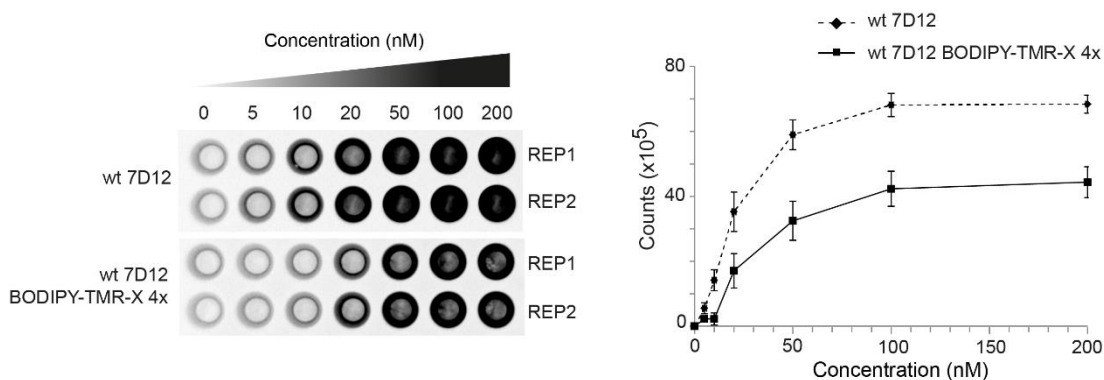


Figure 6.13: Comparison of binding of labelled and unlabelled wt7D12 to EGFR assessed using on-cell assay on the surface of A431 cells shows a reduction in binding by approximate 1.5-fold at saturation due to the presence of BODIPY-TMR-X label. Representative image from three experiments with two replicates.

Conjugation of wt7D12 with BODIPY-TMR-X was achieved using labelling methods described in chapter 2 (2.1.17). Figure 6.13 demonstrates an approximate 1.5-fold decrease in affinity of VHH 7D12 due to presence of BODIPY-TMR-X. This was

calculated by comparing the saturation chemiluminescence signal of unlabelled and labelled 7D12 (100-200 nM). Despite this reduction in binding due to presence of BODIPY-TMR-X dye, significant binding of BODIPY-TMR-X labelled 7D12 is observed, further validating our microscopy experiments.

Several conjugation strategies such as the chemoselective targeting of deprotonated thiolate nucleophile of cysteine residues or the methods used in this chapter with the targeting of amine reactive lysine residues have been used to modify biomolecules with synthetic moieties for investigating into several fundamental research areas. However, these targets can often be limited by the importance of the targeted residue (cysteine residues are often required for correct protein folding, and lysine residues are often located in active/binding sites of proteins) and the number of residues targeted (multiple targeted sites in a protein and cause heterogeneous labelled protein product). An alternative labelling strategy which could be highly relevant to this thesis is the site-specific encoding nCAA containing bioorthogonal handles for specific labelling of proteins. With the precise site-selective encoding an nCAA with a unique moiety that is biocompatible and chemically selective with labelling reactions, a technique that allows control over location and number of reacting sites can be utilised as a conjugation strategy to avoid the potential limiting effects of alternative methods listed above. Research done by the Schultz group (Wang *et al.*, 2003) showed the *in vivo* incorporation of a keto nCAA (*p*-acetyl-L-phenylalanine) into proteins within *E. coli* for subsequent *in vitro* selective modification with a small molecule fluorophore. Applying this strategy for the labelling of VHH 7D12 with a fluorophore could improve the resulting binding affinities that had been reduced *via* amine targeted conjugation as shown in Figure 6.13, however to introduce two moieties (photocontrol and bioorthogonal conjugation) to VHH 7D12 would require the *in vivo* incorporation of two distinct nCAA into the recombinant protein in *E. coli* which would require further optimisation of current expression and suppression systems.

6.2.5 Evaluating the effect of 365 nm light on cell viability

One potential concern of the current experimental design is the apparent toxicity of 365 nm irradiation to live cells when de-caging 7D12. UVB (280–315 nm) and UVC (100–280 nm) irradiation of live cells have been well documented as a direct cause of DNA damage and is widely used as a method of sterilisation. However, low doses of UVA (315–400 nm) have generally been accepted as biocompatible and used in biological settings for a wide range of biochemical applications and have been shown as non-toxic to live-cells. Several studies have shown that large fluxes of UVA light exposure on live-cells can cause the formation of free radicals and cause severe membrane damage (Guvendiren & Burdick, 2012; Klotz *et al.*, 1999; Vile *et al.*, 1995). However, studies employing low dose UVA exposure to live cells typically establish cell health *via* live/dead cell viability assays and microscopy after treatment to demonstrate non-toxic effects of irradiation at 365 nm (Jang *et al.*, 2019; Bryant *et al.*, 2000).

To evaluate the cytotoxic effects of 365 nm exposure to live-cells in similar conditions as the experiments above, two cell viability assays were designed. To measure live/dead cells after exposure to 365 nm light, a resazurin-based assay (AlamarBlue, Sigma-Aldrich) was used. Resazurin exhibits a blue colour and low fluorescence in metabolically inactive cells but is converted to a highly fluorescent product (resorufin) upon metabolism by viable cells. Full methodology is described in 2.1.20. Briefly, A431 cells were seeded (200,000 cells/mL) into ultra-low attachment 6-well plate containing 18 mm coverslip and incubated overnight (37°C, 5% CO₂). For irradiation with 365 nm light, glass coverslip was transferred to either a microscopy chamber for 1 minute DAPI exposure *via* Zeiss Axiovert 200M microscope or placed on UV transilluminator (GelDocMega; BioSystematica) for 4 minutes with 365 nm exposure. After exposure to 365 nm light, coverslips were transferred to a 6-well plate containing fresh complete medium for 48 hour incubation (37°C, 5% CO₂). To measure cell viability with AlamarBlue, A431 cells were detached from coverslip with trypsin, centrifuged (300 g, 5 minutes), resuspended in 500 µl of complete medium

and 200 μL /well of this solution was added in a well of 96-well plate. alamarBlue was added to the cells in a 1:10 dilution for 2 h at 37 °C and fluorescence was then measured on a Flexstation 3 plate reader (Ex= 570 nm, Em= 600 nm). Resulting fluorescence was analysed in figure 6.14.

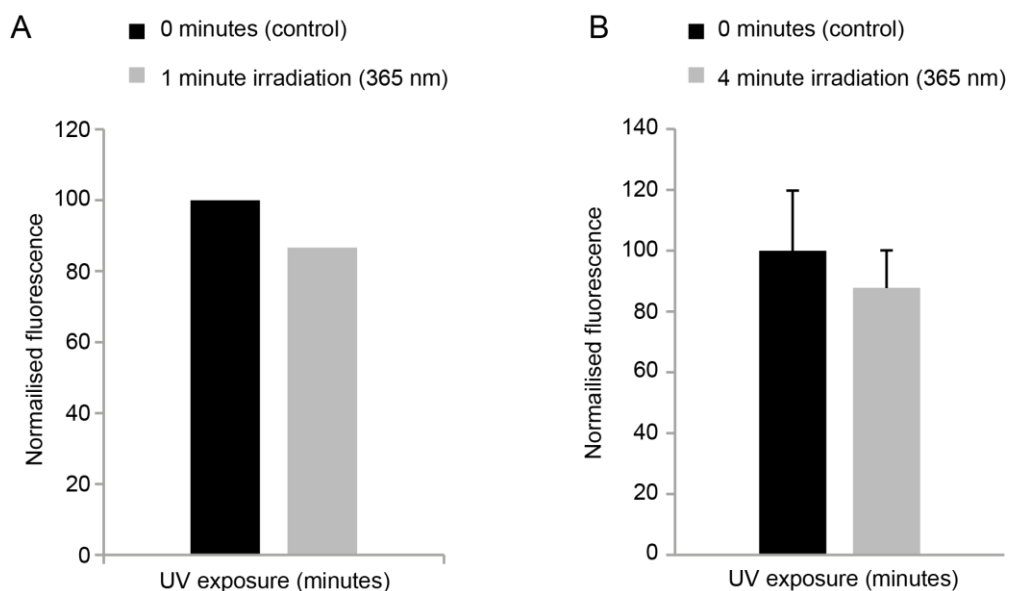


Figure 6.14: Cell viability assay of irradiated A431 cells demonstrated minor decreases in cell growth after 48 hour incubation. A) 365 nm irradiation of cells achieved with microscope DAPI channel for 1 minute. B) 365 nm irradiation of cells achieved *via* UV transilluminator for 4 minutes.

Positive control (0 minutes irradiation) was normalised to 100% and compared to the irradiated sample. Typically, to perform an alamarBlue live/dead cell viability assay the investigated cells would be seeded into a 96-well plate, followed by treatment, replacement of medium and addition of alamarBlue for direct measurements of fluorescence. However, a modified version of this procedure was used to replicate irradiation conditions for on-cell experiments (described in 2.1.15) and the microscopy experiments described earlier in this chapter (Section 6.2.3). In these experiments, the 365 nm light exposure was performed on cells attached to 18 mm coverslip. The procedure followed introduced variability into the experiment as the detachment from the coverslip, resuspending and transferring to 96-well plate can potentially cause loss of cells and cellular disruption. As a result, significant error bars are observed in Figure 6.14, and more replicates of these experiments could not be

performed due to time constraints. Although the results in figure 6.14 indicate a possible reduction in cell viability with 365 nm treatment, observations made under the microscopy indicated similar cellular growth (results not shown) between non-irradiated and irradiated samples.

CHAPTER 7

Discussion and future work

7.1 Introduction

The ability to genetically encode an expanding set of new chemical and physical properties (*via* noncanonical amino acids or ncAAs) into recombinant proteins have allowed researchers to probe and manipulate the structure and function of macromolecules to increase our understanding of complex molecular processes within biological systems. These emerging strategies have diverse applications in probing, imaging, and controlling protein function and has allowed for the unprecedented precision in the engineering of novel therapeutics.

The site-specific incorporation of designer amino acids into antibodies could allow for the development of novel therapeutics. In this thesis, a photo-caged ncAA was genetically encoded into a heavy chain antibody fragment to allow control over antibody-antigen binding by light. The primary strategy used for generating biologically active light responsive antibodies involved the site-specific incorporation of photocaged ncAA with the suppression of a canonical stop codon (TAG) with mutually orthogonal aaRS/tRNA pairs. This modification of the protein of interest allowed for the incorporation of a light responsive protective group making the molecule inactive until exposed to light. This strategy not only enable photo-control over antibody-antigen binding but achieved this with a molecular weight difference of less than 1% from the original molecule. To the best of my knowledge, the site-specific incorporation of a photocaged ncAA into a therapeutically relevant antibody fragment to gain control over bioactivity has not been achieved before.

The overall aims of this thesis were to explore spatial and temporal control over antigen-antibody binding, which could allow for interesting applications in investigations of antibody-dependent biological processes in cell culture, tissues, and animals. To achieve this a few key areas were explored which are highlighted below:

- I. Developing expression systems for recombinant expression of antibody fragments in *E. coli*.

- II. Investigating and improving the incorporation efficiency of nCAA into recombinant antibody fragments.
- III. Development of a novel, robust assay to measure antibody affinity to cell surface antigens.
- IV. Direct visualisation of light-mediated binding of antibody to cell surface antigen using live-cell microscopy.

The collective data from experiments performed during this thesis should help further our understanding of the spatial and temporal control over antigen-antibody binding by light and highlight its importance as a potential therapeutic molecule. The novelty and importance of the work done during this thesis is emphasised with the patent application on photoactive antibodies and an article just accepted for publication in *Angewandte Chemie* (DOI: 10.1002/anie.201908655).

7.2 Discussion

7.2.1 Importance of immunotherapeutics to oncology

Antibody therapeutic technology has become and remained the most dominant biological therapeutic platform in the pharmaceutical market (Urquhart, 2018). Significant advancements in antibody treatment strategies have allowed for the development in the selective targeting of numerous diseases, including autoimmune disorders, cancers, infections, and cardiovascular diseases. In the last few decades, several clinically approved cancer immunotherapies (naked whole mAb and fragment mAb formats) have made it to the pharmaceutical market, with hundreds more currently in clinical trial. Nevertheless, the single targeting approach of naked whole antibody therapies have suffered in poor tissue penetration due to the relatively

large molecular weight (140-160 kDa), limiting their transport through physiological barriers. A typical full-length antibody format consists of four peptide chains (two light and two heavy chains) that are bound together with a combination of disulfide bonds and interchain non-covalent interactions. A conventional antibody contains two paratopes (specific to a particular epitope of an antigen) and an Fc region which is responsible for engaging the body's immune response and can target bound antigens for destruction. By selectively including or removing components of the antigen-binding variable region and the Fc region, researchers have radically improved efficacy of antibodies with the design and development of smaller antibody formats such as Fabs, scFv's and VHH. These antibody fragments have reported enhanced tissue penetration due to a combination of the small size and high affinity binding capacity when compared to whole mAb formats.

The research in this thesis has focused on the expression and characterisation of antibodies that target a select few of ErbB family of proteins. In humans, the ErbB family contains four receptor tyrosine kinases that include EGFR (ErbB-1), HER2 (ErbB-2), HER3 (ErbB-3), and HER4 (ErbB-4). The overexpression and excessive signalling of these receptors have been associated with the progression of several human cancers and have received widespread interest as a potential immunotherapeutic target in oncology. Mutations, amplification or misregulations of ErbB receptors have been shown to lead to constant receptor activation and uncontrolled cell division which results in unregulated growth and tumour formation. However, as the native function of the ErbB receptors found on healthy cells are responsible for signal transduction pathways that are involved in regulating cellular proliferation, differentiation, and survival (Riese & Stern, 1998), the targeting of these receptors can lead to severe side effects through non-specific targeting. For example, the toxicity profile for several EGFR inhibitors that have been developed and clinically approved for the direct treatment of EGFR positive cancers have commonly reported adverse effects (found in more than 90% of patients) which result in a rash that primarily spreads across the face, head, and torso (Liu *et al.*, 2013; Herbst, 2004). These findings result in similar outcomes with the use of anti-

EGFR monoclonal antibodies and necessitate the improvement of current immunotherapeutics to reduce off-target cytotoxicity.

7.2.2 Spatial and temporal control over antibody-antigen binding with light

In chapter 3, the periplasmic expression of VHH fragments were demonstrated for the targeting of EGFR (7D12) and HER2 (2Rs15d). In the subsequent chapters (5 and 6), the characterisation of 7D12 binding to EGFR was achieved with the development of an on-cell assay and dynamic live-cell microscopy on the surface of A431 epidermoid carcinoma cell line. To gain spatial and temporal control over antibody-antigen binding of 7D12, the non-canonical amino acid (ncAA) *o*-nitrobenzyl-*O*-tyrosine (photocaged tyrosine or pcY) was genetically encoded in response to amber nonsense codon at three positions in 7D12 (Y32TAG, Y109TAG, and Y113TAG). The three tyrosine mutations were based on crystal structure analysis of 7D12:sEGFRdIII complex. This resulted in mutants of 7D12 that bind to EGFR upon irradiation with 365 nm light (Figure 7.1).

As the results demonstrate, light dependent binding control over 7D12 can be achieved with the site-specific incorporation of pcY in positions 32 and 113. With the ability to spatially and temporally control binding of 7D12 to EGFR, this methodology could allow for interesting applications in anti-cancer therapeutics owing to reduced off-target binding and subsequent reduction in undesirable side effects often reported in similar anti-EGFR inhibition treatments.

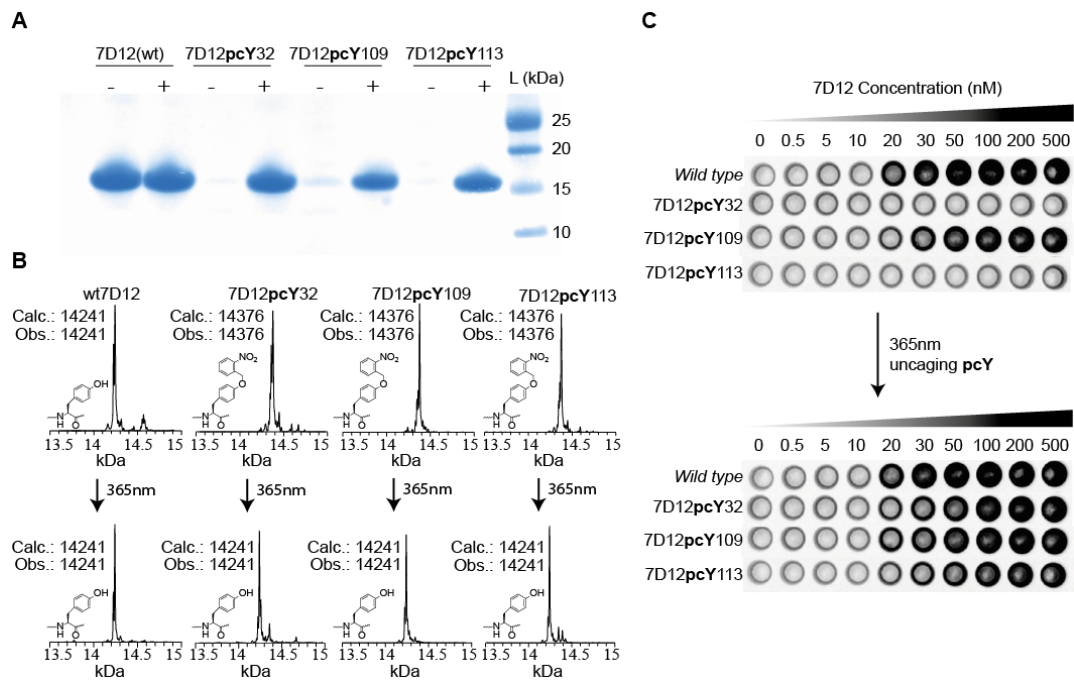


Figure 7.1: The site-specific genetic incorporation of pcY and subsequent photo-control over antibody-antigen binding. A) The expression of three amber mutants of 7D12 (7D12-Y32TAG, 7D12-Y109TAG and 7D12-Y113TAG) only occurs in the presence of *o*-nitrobenzyl-*O*-tyrosine (pcY). Comparison of band intensities for amber mutants with wt7D12 shows efficient incorporation of pcY. B) Electrospray ionization Mass Spectrometry (ESI-MS) measurements of expressed 7D12 and three amber mutants (Y32, Y109, and Y113) before and after irradiation with light (365 nm, 4 minutes). First row represents before irradiation, observed mass of wild-type VHH 7D12 is 14241 Da while three mutants with pcY incorporation have increased mass of 14376 Da. After irradiation, the second row demonstrates decaging of pcY mutants and decreased mass to wild-type level. C) on-cell assay binding experiments to assess the interaction of EGFR with wt7D12 and amber mutants containing site-specifically incorporated pcY. On-cell assays performed on the surface of A431 cells demonstrates that the presence of pcY at positions 32 and 113 in 7D12 inhibits binding to EGFR. However, site-specific encoding of pcY at position 109 results in similar binding affinity to wt7D12. The binding of Y32pcY and Y113pcY mutants are restored upon irradiation with 365 nm light.

The use of light as an activation mechanism has gained considerable attention due to the ability for localised non-invasive altering of chemical and physical properties of photodynamic molecules in a range of applications, including in the presence of live cells. Low-intensity long-wavelength UV light is an easily accessible and commonly used energy source for activation of light responsive biomolecule and has been used during this thesis for the photo de-caging of pcY. Two potential challenges

have been associated with the use of such energy sources; shallow tissue penetration that can limit the therapeutic viability of photoactivatable treatments, and the risk related to cellular damage *via* UV irradiation. As discussed in chapter 1, numerous methods are available to increase the tissue penetration and therapeutic range of 365 nm light. Methods such as upconverting nanoparticles, two-photon absorption, and biocompatible LEDs that can emit UV radiations are all promising tools that can be used in combination with the photoactive therapeutics described in this thesis.

UV light can be divided into three categories; UVA (315-400 nm), UVB (280–315 nm), and UVC (100–280 nm). The cytotoxic effects of UVB and UVC occurs *via* direct DNA damage, while UVA in some instances (dependant on environmental and intensity factors) may induce indirect DNA damage *via* the production of free radicals. However, typical exposure conditions for cell-based photoactivation experiments using low-intensity long-wavelength UV light (365 nm, Photon flux = 5-20 mW/cm², t = 2-20 minutes) is generally accepted as biocompatible (Bryant *et al.*, 2000; Jang *et al.*, 2019). Cell viability assays reported in chapter 6 demonstrated 365 nm light is not toxic to A431 cells in two settings; 4 minutes irradiation by UV transilluminator and 1 minute by microscope DAPI channel.

With the combination of existing methods to increase tissue penetration range, this thesis has shown a novel method to precisely target EGFR expressing cells with light by conferring photoactivity to a current immunotherapeutic.

7.2.3 Light induced delivery of toxic payload to EGFR positive cancers

The demonstrated control over antibody-antigen binding by light with photocaged 7D12 could reduce the negative consequences of non-specific targeting of healthy cells. However, a limitation to the described treatment is the lack of cytotoxicity to the cancer cell, which is required to eradicate solid tumours. Both *in vivo* and *in vitro* studies have shown that naked antibody fragment formats have reduced cytotoxic

activity and reduced stimulation of immune system response due to the omission of the Fc domain.

Further improvements to these immunotherapies can be found in the combination of antibodies against different targets (bispecific antibodies) or with the addition of alternative therapeutic motifs (cytotoxic drugs or drug carriers). In chapter 6, an investigation into 7D12 receptor mediated endocytosis was performed to evaluate the efficacy of further 7D12 drug conjugation experiments as many cytotoxic compounds require an intracellular localization for their activity. Further work is required for the visualisation of 7D12 endocytosis using pH-sensitive dyes. However, the development of the dynamic live-cell microscopy procedure allowed for the visualisation of 7D12 binding to A431 cell surface EGFR and demonstrated decaging of 7D12-Y32pcY with the microscope in physiological relevant conditions of drug delivery to a targeted receptor.

7.3 Future work

7.3.1 Applying photo-control strategies to alternative antibody fragments

Several examples of expressed VHH have been demonstrated by *in vivo* periplasmic expression in bacterial hosts. Current efforts towards the expression of Fab fragments were also illustrated but required further optimisation before successful production. Preliminary investigations of facilitating photo-control over 2Rs15d (anti-HER2, VHH) has resulted in the apparent site-specific incorporation of pcY in position 37, and investigations into the effect of codon context on genetic incorporation of pcY resulted in interesting outcomes of the site-specific incorporation efficiency of pcY. However, further research is required in the analysis and characterisation by on-cell assay and microscopy to determine the inhibitory effects of pcY in 2Rs15d.

Another interesting research direction for the work done in this thesis would be to apply photo-control strategies to full-length mAbs that have had clinical success, such as Cetuximab (anti-EGFR), and Trastuzumab (anti-HER2). This would require the

development of mammalian expression systems to generate therapeutically active mAbs, and investigations into efficient suppressor plasmids that could be used in mammalian cells. Research done by Chin and colleagues have demonstrated the successful site-specific incorporation of *o*-nitrobenzyl-*O*-tyrosine (photocaged tyrosine) into recombinant proteins using PylRS/tRNA_{CUA} pair in mammalian cells (Arbely *et al.*, 2012). This research could be implemented into expression systems for the generation of photocaged mAbs.

7.3.2 Improving binding affinity using phage display

The research demonstrated in this thesis is the consolidation of work performed at the University of East Anglia. During this period of work, a three month scholarship was awarded to collaborate with Professor Umetsu at Tohoku University in Japan. During these three months, the research was focused on investigating improvements of 7D12 binding affinity with phage display (results not shown). Phage display is a powerful *in vitro* screening technique that can be used for the rapid identification and isolation of high specific (to a molecular target) peptides and proteins from a diverse library. To investigate improving 7D12 specificity to EGFR saturation mutagenesis was used with synthetic oligonucleotide primers to randomise residues in 7D12 CDR1 as NNK (N=A, C, T, or G, K=T or G). Although preliminary data indicated the identification of a mutant 7D12 with improved binding affinity to EGFR, due to time constraints it was not possible to complete full characterisation and analysis. Future work could include further analysis on potential 7D12 with improved binding affinity to EGFR and would require additional characterisation with the use of the on-cell assay developed in this thesis. Recently, an efficient phage display system has been used to incorporate ncAAs into proteins displayed on phage (Oller-Salvia & Chin, 2019), and could have interesting applications in the development of improved therapeutic molecules.

References

- Abadier, M., Haghayegh Jahromi, N., Cardoso Alves, L., Boscacci, R., Vestweber, D., Barnum, S., Deutsch, U., Engelhardt, B. and Lyck, R., 2015. Cell surface levels of endothelial ICAM-1 influence the transcellular or paracellular T-cell diapedesis across the blood–brain barrier. *European journal of immunology*, 45(4), pp.1043-1058.
- Adams, G.P., Schier, R., McCall, A.M., Simmons, H.H., Horak, E.M., Alpaugh, R.K., Marks, J.D. and Weiner, L.M., 2001. High affinity restricts the localization and tumor penetration of single-chain fv antibody molecules. *Cancer research*, 61(12), pp.4750-4755.
- Agasti, S.S., Chompoosor, A., You, C.C., Ghosh, P., Kim, C.K. and Rotello, V.M., 2009. Photoregulated release of caged anticancer drugs from gold nanoparticles. *Journal of the American Chemical Society*, 131(16), pp.5728-5729.
- Ai, H.W., Shen, W., Sagi, A., Chen, P.R. and Schultz, P.G., 2011. Probing Protein–Protein Interactions with a Genetically Encoded Photo-crosslinking Amino Acid. *Chembiochem*, 12(12), pp.1854-1857.
- Ai, X., Mu, J. and Xing, B., 2016. Recent advances of light-mediated theranostics. *Theranostics*, 6(13), pp.2439.
- Alberts, B., Bray, D., Hopkin, K., Johnson, A.D., Lewis, J., Raff, M., Roberts, K. and Walter, P., 2013. *Essential cell biology*. Garland Science. pp.516.
- Michael Dcona, M. and Matthew, C.T., 2015. Near infrared light mediated release of doxorubicin using upconversion nanoparticles. *Chemical Communications*, 51(40), pp.8477-8479.
- Amiri-Kordestani, L., Blumenthal, G.M., Xu, Q.C., Zhang, L., Tang, S.W., Ha, L., Weinberg, W.C., Chi, B., Candau-Chacon, R., Hughes, P. and Russell, A.M., 2014. FDA approval: adotrastuzumab emtansine for the treatment of patients with HER2-positive metastatic breast cancer. *Clinical Cancer Research*, 20(17), pp.4436-4441.
- Anderson, J.C., Wu, N., Santoro, S.W., Lakshman, V., King, D.S. and Schultz, P.G., 2004. An expanded genetic code with a functional quadruplet codon. *Proceedings of the National Academy of Sciences*, 101(20), pp.7566-7571.
- Appelbaum, F.R. and Bernstein, I.D., 2017. Gemtuzumab ozogamicin for acute myeloid leukemia. *Blood, The Journal of the American Society of Hematology*, 130(22), pp.2373-2376.
- Arbely, E., Torres-Kolbus, J., Deiters, A. and Chin, J.W., 2012. Photocontrol of tyrosine phosphorylation in mammalian cells via genetic encoding of photocaged tyrosine. *Journal of the American Chemical Society*, 134(29), pp.11912-11915.

- Axup, J.Y., Bajjuri, K.M., Ritland, M., Hutchins, B.M., Kim, C.H., Kazane, S.A., Halder, R., Forsyth, J.S., Santidrian, A.F., Stafin, K. and Lu, Y., 2012. Synthesis of site-specific antibody-drug conjugates using unnatural amino acids. *Proceedings of the National Academy of Sciences*, 109(40), pp.16101-16106.
- Aydin, S., 2015. A short history, principles, and types of ELISA, and our laboratory experience with peptide/protein analyses using ELISA. *Peptides*, 72, pp.4-15.
- Baeuerle, P.A. and Reinhardt, C., 2009. Bispecific T-cell engaging antibodies for cancer therapy. *Cancer research*, 69(12), pp.4941-4944.
- Baker, R.T., 1996. Protein expression using ubiquitin fusion and cleavage. *Current opinion in biotechnology*, 7(5), pp.541-546.
- Balzer, S., Kucharova, V., Megerle, J., Lale, R., Brautaset, T. and Valla, S., 2013. A comparative analysis of the properties of regulated promoter systems commonly used for recombinant gene expression in Escherichia coli. *Microbial cell factories*, 12(1), pp.26.
- Baneyx, F., 1999. Recombinant protein expression in Escherichia coli. *Current opinion in biotechnology*, 10(5), pp.411-421.
- Bartrop, J.A. and Schofield, P., 1962. Photosensitive protecting groups. *Tetrahedron Letters*, 3(16), pp.697-699.
- Barnes, M.R. ed., 2007. *Bioinformatics for geneticists: a bioinformatics primer for the analysis of genetic data*. John Wiley & Sons. pp.328.
- Barton, D.H.R., Chow, Y.L., Cox, A. and Kirby, G.W., 1962. Photosensitive protection of functional groups. *Tetrahedron Letters*, 3(23), pp.1055-1057.
- Baselga, J., 2001. The EGFR as a target for anticancer therapy—focus on cetuximab. *European journal of cancer*, 37, pp.16-22.
- Baselga, J. and Arteaga, C.L., 2005. Critical update and emerging trends in epidermal growth factor receptor targeting in cancer. *Journal of Clinical Oncology*, 23(11), pp.2445-2459.
- Bentley, W.E., Mirjalili, N., Andersen, D.C., Davis, R.H. and Kompala, D.S., 1990. Plasmid-encoded protein: the principal factor in the “metabolic burden” associated with recombinant bacteria. *Biotechnology and bioengineering*, 35(7), pp.668-681.
- Berguig, G.Y., Convertine, A.J., Shi, J., Palanca-Wessels, M.C., Duvall, C.L., Pun, S.H., Press, O.W. and Stayton, P.S., 2012. Intracellular delivery and trafficking dynamics of a

- lymphoma-targeting antibody–polymer conjugate. *Molecular pharmaceuticals*, 9(12), pp.3506-3514.
- Betts, M.J. and Russell, R.B., 2003. Amino acid properties and consequences of substitutions. *Bioinformatics for geneticists*, 317, pp.289.
- Birch, J.R. and Racher, A.J., 2006. Antibody production. *Advanced drug delivery reviews*, 58(5-6), pp.671-685.
- Blight, S.K., Larue, R.C., Mahapatra, A., Longstaff, D.G., Chang, E., Zhao, G., Kang, P.T., Green-Church, K.B., Chan, M.K. and Krzycki, J.A., 2004. Direct charging of tRNA CUA with pyrrolysine in vitro and in vivo. *Nature*, 431(7006), pp.333-335.
- Bolivar, F., Rodriguez, R.L., Greene, P.J., Betlach, M.C., Heyneker, H.L., Boyer, H.W., Crosa, J.H. and Falkow, S., 1977. Construction and characterization of new cloning vehicle. II. A multipurpose cloning system. *Gene*, 2(2), pp.95-113.
- Bose, M., Groff, D., Xie, J., Brustad, E. and Schultz, P.G., 2006. The Incorporation of a Photoisomerizable Amino Acid into Proteins in *E. coli*. *Journal of the American Chemical Society*, 128(2), pp.388-389.
- Boss, M.A., Kenten, J.H., Wood, C.R. and Emtage, J.S., 1984. Assembly of functional antibodies from immunoglobulin heavy and light chains synthesised in *E. coli*. *Nucleic acids research*, 12(9), pp.3791-3806.
- Brar, G.A., 2016. Beyond the triplet code: context cues transform translation. *Cell*, 167(7), pp.1681-1692.
- Bridge, T., Shaikh, S.A., Thomas, P., Botta, J., McCormick, P.J. and Sachdeva, A., 2019. Site-Specific Encoding of Photoactivity in Antibodies Enables Light-Mediated Antibody–Antigen Binding on Live Cells. *Angewandte Chemie*, 131(50), pp.18154-18161.
- Brieke, C., Rohrbach, F., Gottschalk, A., Mayer, G. and Heckel, A., 2012. Light-controlled tools. *Angewandte Chemie International Edition*, 51(34), pp.8446-8476.
- Bronowska, A.K., 2011. Thermodynamics of ligand-protein interactions: implications for molecular design. In *Thermodynamics-Interaction Studies-Solids, Liquids and Gases*. IntechOpen.
- Brosius, J., Erfle, M. and Storella, J., 1985. Spacing of the -10 and -35 regions in the tac promoter. Effect on its in vivo activity. *Journal of biological chemistry*, 260(6), pp.3539-3541.

- Brouns, S.J., Jore, M.M., Lundgren, M., Westra, E.R., Slijkhuis, R.J., Snijders, A.P., Dickman, M.J., Makarova, K.S., Koonin, E.V. and Van Der Oost, J., 2008. Small CRISPR RNAs guide antiviral defense in prokaryotes. *Science*, 321(5891), pp.960-964.
- Bryant, S.J., Nuttelman, C.R. and Anseth, K.S., 2000. Cytocompatibility of UV and visible light photoinitiating systems on cultured NIH/3T3 fibroblasts in vitro. *Journal of Biomaterials Science, Polymer Edition*, 11(5), pp.439-457.
- Bucher, M.H., Evdokimov, A.G. and Waugh, D.S., 2002. Differential effects of short affinity tags on the crystallization of *Pyrococcus furiosus* maltodextrin-binding protein. *Acta Crystallographica Section D: Biological Crystallography*, 58(3), pp.392-397.
- Cadena, D.L. and Gill, G.N., 1993. Expression and purification of the epidermal growth factor receptor extracellular domain utilizing a polycistronic expression system. *Protein expression and purification*, 4(3), pp.177-186.
- Carrio, M.M. and Villaverde, A., 2002. Construction and deconstruction of bacterial inclusion bodies. *Journal of biotechnology*, 96(1), pp.3-12.
- Cary, S.P., Lee, J., Wagenknecht, R. and Silverman, G.J., 2000. Characterization of superantigen-induced clonal deletion with a novel clan III-restricted avian monoclonal antibody: exploiting evolutionary distance to create antibodies specific for a conserved VH region surface. *The Journal of Immunology*, 164(9), pp.4730-4741.
- Casalini, P., Caldera, M., Canevari, S., Menard, S., Mezzanzanica, D., Tosi, E., Gadina, M. and Colnaghi, M.I., 1993. A critical comparison of three internalization assays applied to the evaluation of a given mAb as a toxin-carrier candidate. *Cancer Immunology, Immunotherapy*, 37(1), pp.54-60.
- Cellitti, S.E., Jones, D.H., Lagpacan, L., Hao, X., Zhang, Q., Hu, H., Brittain, S.M., Brinker, A., Caldwell, J., Bursulaya, B. and Spraggon, G., 2008. In vivo incorporation of unnatural amino acids to probe structure, dynamics, and ligand binding in a large protein by nuclear magnetic resonance spectroscopy. *Journal of the American Chemical Society*, 130(29), pp.9268-9281.
- Chang, A.C. and Cohen, S.N., 1978. Construction and characterization of amplifiable multicopy DNA cloning vehicles derived from the P15A cryptic miniplasmid. *Journal of bacteriology*, 134(3), pp.1141-1156.
- Charlton, K.A., 2004. Expression and isolation of recombinant antibody fragments in *E. coli*. In *Antibody Engineering* (pp. 245-254). Humana Press.

- Chatterjee, A., Sun, S.B., Furman, J.L., Xiao, H. and Schultz, P.G., 2013. A versatile platform for single-and multiple-unnatural amino acid mutagenesis in *Escherichia coli*. *Biochemistry*, 52(10), pp.1828-1837.
- Chatterjee, A., Xiao, H. and Schultz, P.G., 2012. Evolution of multiple, mutually orthogonal prolyl-tRNA synthetase/tRNA pairs for unnatural amino acid mutagenesis in *Escherichia coli*. *Proceedings of the National Academy of Sciences*, 109(37), pp.14841-14846.
- Chaulk, S.G. and MacMillan, A.M., 2007. Synthesis of oligo-RNAs with photocaged adenosine 2'-hydroxyls. *Nature protocols*, 2(5), pp.1052.
- Chavez, K.J., Garimella, S.V. and Lipkowitz, S., 2010. Triple negative breast cancer cell lines: one tool in the search for better treatment of triple negative breast cancer. *Breast disease*, 32(1-2), pp.35.
- Chen, P.R., Groff, D., Guo, J., Ou, W., Cellitti, S., Geierstanger, B.H. and Schultz, P.G., 2009. A facile system for encoding unnatural amino acids in mammalian cells. *Angewandte Chemie International Edition*, 48(22), pp.4052-4055.
- Chiang, Y.L., Sheng-Dong, R., Brow, M.A. and Larrick, J.W., 1989. Direct cDNA cloning of the rearranged immunoglobulin variable region. *Biotechniques*, 7(4), pp.360-366.
- Chin, J.W., 2014. Expanding and reprogramming the genetic code of cells and animals. *Annual review of biochemistry*, 83, pp.379-408.
- Chin, J.W., Martin, A.B., King, D.S., Wang, L. and Schultz, P.G., 2002a. Addition of a photocrosslinking amino acid to the genetic code of *Escherichia coli*. *Proceedings of the National Academy of Sciences*, 99(17), pp.11020-11024.
- Chin, J.W., Santoro, S.W., Martin, A.B., King, D.S., Wang, L. and Schultz, P.G., 2002b. Addition of p-Azido-l-phenylalanine to the Genetic Code of *Escherichia coli*. *Journal of the American Chemical Society*, 124(31), pp.9026-9027.
- Cochlovius, B., Kipriyanov, S.M., Stassar, M.J., Schuhmacher, J., Benner, A., Moldenhauer, G. and Little, M., 2000. Cure of Burkitt's lymphoma in severe combined immunodeficiency mice by T cells, tetravalent CD3× CD19 tandem diabody, and CD28 costimulation. *Cancer research*, 60(16), pp.4336-4341.
- Cole, R., 2014. Live-cell imaging: The cell's perspective. *Cell adhesion & migration*, 8(5), pp.452-459.
- Conrath, K.E., Lauwereys, M., Wyns, L. and Muyldermans, S., 2001. Camel single-domain antibodies as modular building units in bispecific and bivalent antibody constructs. *Journal of Biological Chemistry*, 276(10), pp.7346-7350.
- Cooper, S., 2003. Reappraisal of serum starvation, the restriction point, G0, and G1 phase arrest points. *The FASEB journal*, 17(3), pp.333-340.

- Corisdeo, S. and Wang, B., 2004. Functional expression and display of an antibody Fab fragment in *Escherichia coli*: study of vector designs and culture conditions. *Protein expression and purification*, 34(2), pp.270-279.
- Cortez-Retamozo, V., Lauwereys, M., Hassanzadeh Gh, G., Gobert, M., Conrath, K., Muyldermans, S., De Baetselier, P. and Revets, H., 2002. Efficient tumor targeting by single-domain antibody fragments of camels. *International journal of cancer*, 98(3), pp.456-462.
- Cunningham, D., Humblet, Y., Siena, S., Khayat, D., Bleiberg, H., Santoro, A., Bets, D., Mueser, M., Harstrick, A., Verslype, C. and Chau, I., 2004. Cetuximab monotherapy and cetuximab plus irinotecan in irinotecan-refractory metastatic colorectal cancer. *New England journal of medicine*, 351(4), pp.337-345.
- Currie, G.P., Lee, D.K. and Lipworth, B.J., 2006. Long-Acting β 2-Agonists in Asthma. *Drug safety*, 29(8), pp.647-656.
- David, C., McPherson, P.S., Mundigl, O. and De Camilli, P., 1996. A role of amphiphysin in synaptic vesicle endocytosis suggested by its binding to dynamin in nerve terminals. *Proceedings of the National Academy of Sciences*, 93(1), pp.331-335.
- De Boer, H.A., Comstock, L.J. and Vasser, M., 1983. The tac promoter: a functional hybrid derived from the trp and lac promoters. *Proceedings of the National Academy of Sciences*, 80(1), pp.21-25.
- de Claro, R.A., McGinn, K., Kwitkowski, V., Bullock, J., Khandelwal, A., Habtemariam, B., Ouyang, Y., Saber, H., Lee, K., Koti, K. and Rothmann, M., 2012. US Food and Drug Administration approval summary: brentuximab vedotin for the treatment of relapsed Hodgkin lymphoma or relapsed systemic anaplastic large-cell lymphoma. *Clinical Cancer Research*, 18(21), pp.5845-5849.
- De Genst, E., Silence, K., Decanniere, K., Conrath, K., Loris, R., Kinne, J., Muyldermans, S. and Wyns, L., 2006. Molecular basis for the preferential cleft recognition by dromedary heavy-chain antibodies. *Proceedings of the National Academy of Sciences*, 103(12), pp.4586-4591.
- De Marco, A., Vigh, L., Diamant, S. and Goloubinoff, P., 2005. Native folding of aggregation-prone recombinant proteins in *Escherichia coli* by osmolytes, plasmid-or benzyl alcohol-overexpressed molecular chaperones. *Cell stress & chaperones*, 10(4), pp.329.
- Deeks, E.D., 2019. Polatuzumab vedotin: first global approval. *Drugs*, 79(13), pp.1467-1475.
- Deiters, A., Cropp, T.A., Mukherji, M., Chin, J.W., Anderson, J.C. and Schultz, P.G., 2003. Adding amino acids with novel reactivity to the genetic code of *Saccharomyces cerevisiae*. *Journal of the American Chemical Society*, 125(39), pp.11782-11783.

- Deiters, A., Groff, D., Ryu, Y., Xie, J. and Schultz, P.G., 2006. A genetically encoded photocaged tyrosine. *Angewandte Chemie International Edition*, 45(17), pp.2728-2731.
- Del Solar, G. and Espinosa, M., 2000. Plasmid copy number control: an ever-growing story. *Molecular microbiology*, 37(3), pp.492-500.
- Del Solar, G., Giraldo, R., Ruiz-Echevarría, M.J., Espinosa, M. and Díaz-Orejas, R., 1998. Replication and control of circular bacterial plasmids. *Microbiol. Mol. Biol. Rev.*, 62(2), pp.434-464.
- Dennis, M.S., Zhang, M., Meng, Y.G., Kadkhodayan, M., Kirchhofer, D., Combs, D. and Damico, L.A., 2002. Albumin binding as a general strategy for improving the pharmacokinetics of proteins. *Journal of Biological Chemistry*, 277(38), pp.35035-35043.
- Deuschle, U., Pepperkok, R., Wang, F.B., Giordano, T.J., McAllister, W.T., Ansorge, W. and Bujard, H., 1989. Regulated expression of foreign genes in mammalian cells under the control of coliphage T3 RNA polymerase and lac repressor. *Proceedings of the National Academy of Sciences*, 86(14), pp.5400-5404.
- Dhimolea, E. and Reichert, J.M., 2012, January. World bispecific antibody summit, September 27–28, 2011, Boston, MA. In *MABs* (Vol. 4, No. 1, pp. 4-13). Taylor & Francis.
- D'Huyvetter, M., De Vos, J., Xavier, C., Pruszynski, M., Sterckx, Y.G., Massa, S., Raes, G., Caveliers, V., Zalutsky, M.R., Lahoutte, T. and Devoogdt, N., 2017. 131I-labeled anti-HER2 camelid sdAb as a theranostic tool in cancer treatment. *Clinical Cancer Research*, 23(21), pp.6616-6628.
- Doherty, G.J. and McMahon, H.T., 2009. Mechanisms of endocytosis. *Annual review of biochemistry*, 78, pp.857-902.
- Donaldson, J.M., Kari, C., Fragoso, R.C., Rodeck, U. and Williams, J.C., 2009. Design and development of masked therapeutic antibodies to limit off-target effects: application to anti-EGFR antibodies. *Cancer biology & therapy*, 8(22), pp.2147-2152.
- Doyle, M.L., 1997. Characterization of binding interactions by isothermal titration calorimetry. *Current Opinion in Biotechnology*, 8(1), pp.31-35.
- Dubendorf, J.W. and Studier, F.W., 1991. Controlling basal expression in an inducible T7 expression system by blocking the target T7 promoter with lac repressor. *Journal of molecular biology*, 219(1), pp.45-59.

- Dubois, M., Fenaille, F., Clement, G., Lechmann, M., Tabet, J.C., Ezan, E. and Becher, F., 2008. Immunopurification and mass spectrometric quantification of the active form of a chimeric therapeutic antibody in human serum. *Analytical chemistry*, 80(5), pp.1737-1745.
- Dumas, A., Lercher, L., Spicer, C.D. and Davis, B.G., 2015. Designing logical codon reassignment—Expanding the chemistry in biology. *Chemical science*, 6(1), pp.50-69.
- Edwards, H. and Schimmel, P.A.U.L., 1990. A bacterial amber suppressor in *Saccharomyces cerevisiae* is selectively recognized by a bacterial aminoacyl-tRNA synthetase. *Molecular and cellular biology*, 10(4), pp.1633-1641.
- Eichelbaum, K., Winter, M., Diaz, M.B., Herzig, S. and Krijgsveld, J., 2012. Selective enrichment of newly synthesized proteins for quantitative secretome analysis. *Nature biotechnology*, 30(10), p.984.
- Engels, J. and Schlaeger, E.J., 1977. Synthesis, structure, and reactivity of adenosine cyclic 3', 5'-phosphate-benzyltriesters. *Journal of medicinal chemistry*, 20(7), pp.907-911.
- Engvall, E. and Perlmann, P., 1971. Enzyme-linked immunosorbent assay (ELISA). *Protides of the biological fluids*, pp.553-556.
- Fahmi, N.E., Dedkova, L., Wang, B., Golovine, S. and Hecht, S.M., 2007. Site-specific incorporation of glycosylated serine and tyrosine derivatives into proteins. *Journal of the American Chemical Society*, 129(12), pp.3586-3597.
- Fekner, T., Li, X., Lee, M.M. and Chan, M.K., 2009. A pyrrolysine analogue for protein click chemistry. *Angewandte Chemie International Edition*, 48(9), pp.1633-1635.
- Ferguson, K.M., Darling, P.J., Mohan, M.J., Macatee, T.L. and Lemmon, M.A., 2000. Extracellular domains drive homo-but not hetero-dimerization of erbB receptors. *The EMBO journal*, 19(17), pp.4632-4643.
- Fleige, E., Quadir, M.A. and Haag, R., 2012. Stimuli-responsive polymeric nanocarriers for the controlled transport of active compounds: concepts and applications. *Advanced drug delivery reviews*, 64(9), pp.866-884.
- Fredens, J., Wang, K., de la Torre, D., Funke, L.F., Robertson, W.E., Christova, Y., Chia, T., Schmied, W.H., Dunkelmann, D.L., Beránek, V. and Uttamapinant, C., 2019. Total synthesis of *Escherichia coli* with a recoded genome. *Nature*, 569(7757), pp.514-518.
- Freinkman, E., Chng, S.S. and Kahne, D., 2011. The complex that inserts lipopolysaccharide into the bacterial outer membrane forms a two-protein plug-and-barrel. *Proceedings of the National Academy of Sciences*, 108(6), pp.2486-2491.

- Freyer, M.W. and Lewis, E.A., 2008. Isothermal titration calorimetry: experimental design, data analysis, and probing macromolecule/ligand binding and kinetic interactions. *Methods in cell biology*, 84, pp.79-113.
- Georgiou, G. and Segatori, L., 2005. Preparative expression of secreted proteins in bacteria: status report and future prospects. *Current opinion in biotechnology*, 16(5), pp.538-545.
- Ghrayeb, J., Kimura, H., Takahara, M., Hsiung, H., Masui, Y. and Inouye, M., 1984. Secretion cloning vectors in Escherichia coli. *The EMBO journal*, 3(10), pp.2437-2442.
- Gibson, D.G., Young, L., Chuang, R.Y., Venter, J.C., Hutchison, C.A. and Smith, H.O., 2009. Enzymatic assembly of DNA molecules up to several hundred kilobases. *Nature methods*, 6(5), pp.343-345.
- Giordano, T.J., Deuschle, U., Bujard, H. and McAllister, W.T., 1989. Regulation of coliphage T3 and T7 RNA polymerases by the lac repressor-operator system. *Gene*, 84(2), pp.209-219.
- Göstring, L., Chew, M.T., Orlova, A., Höidén-Guthenberg, I., Wennborg, A., Carlsson, J. and Frejd, F.Y., 2010. Quantification of internalization of EGFR-binding Affibody molecules: Methodological aspects. *International journal of oncology*, 36(4), pp.757-763.
- Grada, A., Otero-Vinas, M., Prieto-Castrillo, F., Obagi, Z. and Falanga, V., 2017. Research techniques made simple: analysis of collective cell migration using the wound healing assay. *Journal of Investigative Dermatology*, 137(2), pp.e11-e16.
- Gratz, S.J., Cummings, A.M., Nguyen, J.N., Hamm, D.C., Donohue, L.K., Harrison, M.M., Wildonger, J. and O'Connor-Giles, K.M., 2013. Genome engineering of Drosophila with the CRISPR RNA-guided Cas9 nuclease. *Genetics*, 194(4), pp.1029-1035.
- Groff, D., Thielges, M.C., Cellitti, S., Schultz, P.G. and Romesberg, F.E., 2009. Efforts toward the direct experimental characterization of enzyme microenvironments: tyrosine100 in dihydrofolate reductase. *Angewandte Chemie International Edition*, 48(19), pp.3478-3481.
- Gross, L.A., Baird, G.S., Hoffman, R.C., Baldridge, K.K. and Tsien, R.Y., 2000. The structure of the chromophore within DsRed, a red fluorescent protein from coral. *Proceedings of the National Academy of Sciences*, 97(22), pp.11990-11995.
- Guo, J., Melançon III, C.E., Lee, H.S., Groff, D. and Schultz, P.G., 2009. Evolution of amber suppressor tRNAs for efficient bacterial production of proteins containing nonnatural amino acids. *Angewandte Chemie International Edition*, 48(48), pp.9148-9151.

- Gustafsson, C., Govindarajan, S. and Minshull, J., 2004. Codon bias and heterologous protein expression. *Trends in biotechnology*, 22(7), pp.346-353.
- Guvendiren, M. and Burdick, J.A., 2012. Stiffening hydrogels to probe short-and long-term cellular responses to dynamic mechanics. *Nature communications*, 3(1), pp.1-9.
- Hakim, R. and Benhar, I., 2009, May. "Inclonals" IgGs and IgG-enzyme fusion proteins produced in an E. coli expression-refolding system. In *MABs* (Vol. 1, No. 3, pp. 281-287). Taylor & Francis.
- Hamann, P.R., Hinman, L.M., Hollander, I., Beyer, C.F., Lindh, D., Holcomb, R., Hallett, W., Tsou, H.R., Upeslakis, J., Shochat, D. and Mountain, A., 2002. Gemtuzumab ozogamicin, a potent and selective anti-CD33 antibody– calicheamicin conjugate for treatment of acute myeloid leukemia. *Bioconjugate chemistry*, 13(1), pp.47-58.
- Hamers-Casterman, C.T.S.G., Atarhouch, T., Muyldermans, S., Robinson, G., Hammers, C., Songa, E.B., Bendahman, N. and Hammers, R., 1993. Naturally occurring antibodies devoid of light chains. *Nature*, 363(6428), pp.446-448.
- Hao, B., Gong, W., Ferguson, T.K., James, C.M., Krzycki, J.A. and Chan, M.K., 2002. A new UAG-encoded residue in the structure of a methanogen methyltransferase. *Science*, 296(5572), pp.1462-1466.
- Harding, J. and Burtness, B., 2005. An epidermal growth factor receptor chimeric human-murine monoclonal antibody. *Drugs Today (Barc)*, 41, pp.107-127.
- Hasan, N.M., Adams, G.E. and Joiner, M.C., 1999. Effect of serum starvation on expression and phosphorylation of PKC- α and p53 in V79 cells: Implications for cell death. *International journal of cancer*, 80(3), pp.400-405.
- Hassaine, G., Deluz, C., Grasso, L., Wyss, R., Tol, M.B., Hovius, R., Graff, A., Stahlberg, H., Tomizaki, T., Desmyter, A. and Moreau, C., 2014. X-ray structure of the mouse serotonin 5-HT₃ receptor. *Nature*, 512(7514), pp.276-281.
- Hazin, J., Moldenhauer, G., Altevogt, P. and Brady, N.R., 2015. A novel method for measuring cellular antibody uptake using imaging flow cytometry reveals distinct uptake rates for two different monoclonal antibodies targeting L1. *Journal of immunological methods*, 423, pp.70-77.
- Hemphill, J., Borchardt, E.K., Brown, K., Asokan, A. and Deiters, A., 2015. Optical control of CRISPR/Cas9 gene editing. *Journal of the American Chemical Society*, 137(17), pp.5642-5645.
- Herbst, R.S., 2004. Review of epidermal growth factor receptor biology. *International Journal of Radiation Oncology* Biology* Physics*, 59(2), pp.S21-S26.

- Hershberg, R., Bejerano, G., Santos-Zavaleta, A. and Margalit, H., 2000. *PromEC*, Available at: <http://margalit.huji.ac.il/promec/index.html> [Accessed: 18th July 2019].
- Hochuli, E., Bannwarth, W., Döbeli, H., Gentz, R. and Stüber, D., 1988. Genetic approach to facilitate purification of recombinant proteins with a novel metal chelate adsorbent. *Bio/technology*, 6(11), pp.1321-1325.
- Holliger, P., Prospero, T. and Winter, G., 1993. "Diabodies": small bivalent and bispecific antibody fragments. *Proceedings of the National Academy of Sciences*, 90(14), pp.6444-6448.
- Holmes, D., 2011. Buy buy bispecific antibodies. *Nat Rev Drug Discov*, (10), pp. 798–800.
- Hong, K.W., Kim, C.G., Lee, S.H., Chang, K.H., Shin, Y.W., Ryoo, K.H., Kim, S.H. and Kim, Y.S., 2010. A novel anti-EGFR monoclonal antibody inhibiting tumor cell growth by recognizing different epitopes from cetuximab. *Journal of biotechnology*, 145(1), pp.84-91.
- Hori, A., Sasada, R., Matsutani, E., Naito, K., Sakura, Y., Fujita, T. and Kozai, Y., 1991. Suppression of solid tumor growth by immunoneutralizing monoclonal antibody against human basic fibroblast growth factor. *Cancer Research*, 51(22), pp.6180-6184.
- Hsu, P.D., Scott, D.A., Weinstein, J.A., Ran, F.A., Konermann, S., Agarwala, V., Li, Y., Fine, E.J., Wu, X., Shalem, O. and Cradick, T.J., 2013. DNA targeting specificity of RNA-guided Cas9 nucleases. *Nature biotechnology*, 31(9), pp.827.
- Hughes, R.A. and Ellington, A.D., 2010. Rational design of an orthogonal tryptophanyl nonsense suppressor tRNA. *Nucleic acids research*, 38(19), pp.6813-6830.
- Jäger, M., Schoberth, A., Ruf, P., Hess, J. and Lindhofer, H., 2009. The trifunctional antibody ertumaxomab destroys tumor cells that express low levels of human epidermal growth factor receptor 2. *Cancer research*, 69(10), pp.4270-4276.
- Jang, Y., Kim, T.I., Kim, H., Choi, Y. and Kim, Y., 2019. Photoactivatable BODIPY Platform: Light-Triggered Anticancer Drug Release and Fluorescence Monitoring. *ACS Applied Bio Materials*, 2(6), pp.2567-2572.
- Jiang, W., Cossey, S., Rosenberg, J.N., Oyler, G.A., Olson, B.J. and Weeks, D.P., 2014. A rapid live-cell ELISA for characterizing antibodies against cell surface antigens of *Chlamydomonas reinhardtii* and its use in isolating algae from natural environments with related cell wall components. *BMC plant biology*, 14(1), pp.244.
- Johnson, D.B., Xu, J., Shen, Z., Takimoto, J.K., Schultz, M.D., Schmitz, R.J., Xiang, Z., Ecker, J.R., Briggs, S.P. and Wang, L., 2011. RF1 knockout allows ribosomal incorporation of unnatural amino acids at multiple sites. *Nature chemical biology*, 7(11), pp.779-786.

- Johnson, I., 2010. Chapter 1—Fluorophores and Their Amine-Reactive Derivatives. 1.5 Fluorescein, Oregon Green and Rhodamine Green Dyes. *The Molecular Probes® Handbook*, (Part VI).
- Joiner, C.M., Breen, M.E., Clayton, J. and Mapp, A.K., 2017. A bifunctional amino acid enables both covalent chemical capture and isolation of in vivo protein–protein interactions. *ChemBioChem*, 18(2), pp.181-184.
- Jones, P.T., Dear, P.H., Foote, J., Neuberger, M.S. and Winter, G., 1986. Replacing the complementarity-determining regions in a human antibody with those from a mouse. *Nature*, 321(6069), pp.522.
- Kaplan, J.H., Forbush III, B. and Hoffman, J.F., 1978. Rapid photolytic release of adenosine 5'-triphosphate from a protected analog: utilization by the sodium: potassium pump of human red blood cell ghosts. *Biochemistry*, 17(10), pp.1929-1935.
- Kapp, K., 2010. *Signal Peptide Database*. [online] Signalpeptide.de. Available at: <http://www.signalpeptide.de/> [Accessed 17 Jul. 2019].
- Karimi, M., Ghasemi, A., Zangabad, P.S., Rahighi, R., Basri, S.M.M., Mirshekari, H., Amiri, M., Pishabad, Z.S., Aslani, A., Bozorgomid, M. and Ghosh, D., 2016. Smart micro/nanoparticles in stimulus-responsive drug/gene delivery systems. *Chemical Society Reviews*, 45(5), pp.1457-1501.
- Kato, K., Hamaguchi, Y., Okawa, S., Ishikawa, E., Kobayashi, K. and Katunuma, N., 1977. Use of rabbit antibody IgG bound onto plain and aminoalkylsilyl glass surface for the enzyme-linked sandwich immunoassay. *The Journal of Biochemistry*, 82(1), pp.261-266.
- Kim, C.H., Axup, J.Y., Dubrovskaya, A., Kazane, S.A., Hutchins, B.A., Wold, E.D., Smider, V.V. and Schultz, P.G., 2012a. Synthesis of bispecific antibodies using genetically encoded unnatural amino acids. *Journal of the American Chemical Society*, 134(24), pp.9918-9921.
- Kim, J.Y., Kim, Y.G. and Lee, G.M., 2012b. CHO cells in biotechnology for production of recombinant proteins: current state and further potential. *Applied microbiology and biotechnology*, 93(3), pp.917-930.
- Klotz, L.O., Pellieux, C., Briviba, K., Pierlot, C., Aubry, J.M. and Sies, H., 1999. Mitogen-activated protein kinase (p38-, JNK-, ERK-) activation pattern induced by extracellular and intracellular singlet oxygen and UVA. *European journal of biochemistry*, 260(3), pp.917-922.
- Köhler, G. and Milstein, C., 1975. Continuous cultures of fused cells secreting antibody of predefined specificity. *nature*, 256(5517), pp.495-497.

- Korpimäki, T., Kurittu, J. and Karp, M., 2003. Surprisingly fast disappearance of β -lactam selection pressure in cultivation as detected with novel biosensing approaches. *Journal of microbiological methods*, 53(1), pp.37-42.
- Kozak, M., 1983. Comparison of initiation of protein synthesis in procaryotes, eucaryotes, and organelles. *Microbiological reviews*, 47(1), pp.1.
- Krauss, G. and Schönbrunner, N., 2003. *Biochemistry of signal transduction and regulation* (Vol. 3, pp. 1-87). Weinheim: Wiley-VCh.
- Kularatne, S.A., Deshmukh, V., Ma, J., Tardif, V., Lim, R.K., Pugh, H.M., Sun, Y., Manibusan, A., Sellers, A.J., Barnett, R.S. and Srinagesh, S., 2014. A CXCR4-Targeted Site-Specific Antibody–Drug Conjugate. *Angewandte Chemie International Edition*, 53(44), pp.11863-11867.
- Kunkel, T.A., 1985. Rapid and efficient site-specific mutagenesis without phenotypic selection. *Proceedings of the National Academy of Sciences*, 82(2), pp.488-492.
- Kutnowski, N., Shmulevich, F., Davidov, G., Shahar, A., Bar-Zvi, D., Eichler, J., Zarivach, R. and Shaanan, B., 2019. Specificity of protein–DNA interactions in hypersaline environment: structural studies on complexes of Halobacterium salinarum oxidative stress-dependent protein hs RosR. *Nucleic acids research*, 47(16), pp.8860-8873.
- Lajoie, M.J., Kosuri, S., Mosberg, J.A., Gregg, C.J., Zhang, D. and Church, G.M., 2013b. Probing the limits of genetic recoding in essential genes. *Science*, 342(6156), pp.361-363.
- Lajoie, M.J., Rovner, A.J., Goodman, D.B., Aerni, H.R., Haimovich, A.D., Kuznetsov, G., Mercer, J.A., Wang, H.H., Carr, P.A., Mosberg, J.A. and Rohland, N., 2013a. Genomically recoded organisms expand biological functions. *science*, 342(6156), pp.357-360.
- Lamb, Y.N., 2017. Inotuzumab ozogamicin: first global approval. *Drugs*, 77(14), pp.1603-1610.
- Lauwereys, M., Ghahroudi, M.A., Desmyter, A., Kinne, J., Hölzer, W., De Genst, E., Wyns, L. and Muyldermans, S., 1998. Potent enzyme inhibitors derived from dromedary heavy-chain antibodies. *The EMBO journal*, 17(13), pp.3512-3520.
- Lee, H.S., Dimla, R.D. and Schultz, P.G., 2009. Protein–DNA photo-crosslinking with a genetically encoded benzophenone-containing amino acid. *Bioorganic & medicinal chemistry letters*, 19(17), pp.5222-5224.
- Lefranc, M.P., Giudicelli, V., Ginestoux, C., Jabado-Michaloud, J., Folch, G., Bellahcene, F., Wu, Y., Gemrot, E., Brochet, X., Lane, J. and Regnier, L., 2009. IMGT®, the international ImMunoGeneTics information system®. *Nucleic acids research*, 37(suppl_1), pp.D1006-D1012.

- Lei, S.P., Lin, H.C., Wang, S.S., Callaway, J. and Wilcox, G., 1987. Characterization of the *Erwinia carotovora pelB* gene and its product pectate lyase. *Journal of bacteriology*, *169*(9), pp.4379-4383.
- Lemmon, M.A. and Schlessinger, J., 2010. Cell signaling by receptor tyrosine kinases. *Cell*, *141*(7), pp.1117-1134.
- Lessard, J.C., 2013. Molecular cloning. In *Methods in Enzymology* (Vol. 529, pp. 85-98). Academic Press.
- Levin, V.A., Panchabhai, S.C., Shen, L., Kornblau, S.M., Qiu, Y. and Baggerly, K.A., 2010. Different changes in protein and phosphoprotein levels result from serum starvation of high-grade glioma and adenocarcinoma cell lines. *Journal of proteome research*, *9*(1), pp.179-191.
- Li, J., Yu, J., Zhao, J., Wang, J., Zheng, S., Lin, S., Chen, L., Yang, M., Jia, S., Zhang, X. and Chen, P.R., 2014. Palladium-triggered deprotection chemistry for protein activation in living cells. *Nature chemistry*, *6*(4), pp.352.
- Li, S., Schmitz, K.R., Jeffrey, P.D., Wiltzius, J.J., Kussie, P. and Ferguson, K.M., 2005. Structural basis for inhibition of the epidermal growth factor receptor by cetuximab. *Cancer cell*, *7*(4), pp.301-311.
- Liao-Chan, S., Daine-Matsuoka, B., Heald, N., Wong, T., Lin, T., Cai, A.G., Lai, M., D'Alessio, J.A. and Theunissen, J.W., 2015. Quantitative assessment of antibody internalization with novel monoclonal antibodies against Alexa fluorophores. *PLoS One*, *10*(4).
- Lin, S., He, D., Long, T., Zhang, S., Meng, R. and Chen, P.R., 2014. Genetically encoded cleavable protein photo-cross-linker. *Journal of the American Chemical Society*, *136*(34), pp.11860-11863.
- Lin-Chao, S. and Bremer, H., 1986. Effect of the bacterial growth rate on replication control of plasmid pBR322 in *Escherichia coli*. *Molecular and General Genetics MGG*, *203*(1), pp.143-149.
- Lisser, S. and Margalit, H., 1993. Compilation of *E. coli* mRNA promoter sequences. *Nucleic acids research*, *21*(7), pp.1507-1516.
- Liu, C.C. and Schultz, P.G., 2010. Adding new chemistries to the genetic code. *Annual review of biochemistry*, *79*, pp.413-444.
- Liu, D.R. and Schultz, P.G., 1999. Progress toward the evolution of an organism with an expanded genetic code. *Proceedings of the National Academy of Sciences*, *96*(9), pp.4780-4785.

- Liu, H.B., Wu, Y., Lv, T.F., Yao, Y.W., Xiao, Y.Y., Yuan, D.M. and Song, Y., 2013. Skin rash could predict the response to EGFR tyrosine kinase inhibitor and the prognosis for patients with non-small cell lung cancer: a systematic review and meta-analysis. *PLoS one*, 8(1).
- Lobstein, J., Emrich, C.A., Jeans, C., Faulkner, M., Riggs, P. and Berkmen, M., 2012. SHuffle, a novel Escherichia coli protein expression strain capable of correctly folding disulfide bonded proteins in its cytoplasm. *Microbial cell factories*, 11(1), pp.753.
- Lourenço, E.V. and Roque-Barreira, M.C., 2010. Immunoenzymatic quantitative analysis of antigens expressed on the cell surface (cell-ELISA). In *Immunocytochemical Methods and Protocols* (pp. 301-309). Humana Press.
- Lu, J. and Zenobi, R., 1999. Matrix-assisted laser desorption/ionization time-of-flight mass spectrometry for identifying the composition of labeled proteins. *Analytical biochemistry*, 269(2), pp.312-316.
- Luo, X., Fu, G., Wang, R.E., Zhu, X., Zambaldo, C., Liu, R., Liu, T., Lyu, X., Du, J., Xuan, W. and Yao, A., 2017. Genetically encoding phosphotyrosine and its nonhydrolyzable analog in bacteria. *Nature chemical biology*, 13(8), pp.845.
- Lv, X., Yu, Y., Zhou, M., Hu, C., Gao, F., Li, J., Liu, X., Deng, K., Zheng, P., Gong, W. and Xia, A., 2015. Ultrafast photoinduced electron transfer in green fluorescent protein bearing a genetically encoded electron acceptor. *Journal of the American Chemical Society*, 137(23), pp.7270-7273.
- Mahmood, T. and Yang, P.C., 2012. Western blot: technique, theory, and trouble shooting. *North American journal of medical sciences*, 4(9), pp.429.
- Majmudar, C.Y., Lee, L.W., Lancia, J.K., Nwokoye, A., Wang, Q., Wands, A.M., Wang, L. and Mapp, A.K., 2009. Impact of nonnatural amino acid mutagenesis on the in vivo function and binding modes of a transcriptional activator. *Journal of the American Chemical Society*, 131(40), pp.14240-14242.
- Makabe, K., Nakanishi, T., Tsumoto, K., Tanaka, Y., Kondo, H., Umetsu, M., Sone, Y., Asano, R. and Kumagai, I., 2008. Thermodynamic consequences of mutations in vernier zone residues of a humanized anti-human epidermal growth factor receptor murine antibody, 528. *Journal of Biological Chemistry*, 283(2), pp.1156-1166.
- Mali, P., Yang, L., Esvelt, K.M., Aach, J., Guell, M., DiCarlo, J.E., Norville, J.E. and Church, G.M., 2013. RNA-guided human genome engineering via Cas9. *Science*, 339(6121), pp.823-826.

- Mannello, F. and Tonti, G.A., 2007. Concise review: no breakthroughs for human mesenchymal and embryonic stem cell culture: conditioned medium, feeder layer, or feeder-free; medium with fetal calf serum, human serum, or enriched plasma; serum-free, serum replacement nonconditioned medium, or ad hoc formula? All that glitters is not gold!. *Stem cells*, 25(7), pp.1603-1609.
- Marzabadi, M.R., Gruys, K.J., Pansegrau, P.D., Walker, M.C., Yuen, H.K. and Sikorski, J.A., 1996. An EPSP synthase inhibitor joining shikimate 3-phosphate with glyphosate: synthesis and ligand binding studies. *Biochemistry*, 35(13), pp.4199-4210.
- Mentel, M., Laketa, V., Subramanian, D., Gillandt, H. and Schultz, C., 2011. Photoactivatable and cell-membrane-permeable phosphatidylinositol 3, 4, 5-trisphosphate. *Angewandte Chemie International Edition*, 50(16), pp.3811-3814.
- Mergulhão, F.J.M., Summers, D.K. and Monteiro, G.A., 2005. Recombinant protein secretion in Escherichia coli. *Biotechnology advances*, 23(3), pp.177-202.
- Minnihan, E.C., Young, D.D., Schultz, P.G. and Stubbe, J., 2011. Incorporation of fluorotyrosines into ribonucleotide reductase using an evolved, polyspecific aminoacyl-tRNA synthetase. *Journal of the American Chemical Society*, 133(40), pp.15942-15945.
- Minton, N.P., 1984. Improved plasmid vectors for the isolation of translational lac gene fusions. *Gene*, 31(1-3), pp.269-273.
- Moore, P.A., Zhang, W., Rainey, G.J., Burke, S., Li, H., Huang, L., Gorlatov, S., Veri, M.C., Aggarwal, S., Yang, Y. and Shah, K., 2011. Application of dual affinity retargeting molecules to achieve optimal redirected T-cell killing of B-cell lymphoma. *Blood, The Journal of the American Society of Hematology*, 117(17), pp.4542-4551.
- Morrison, S.L., Johnson, M.J., Herzenberg, L.A. and Oi, V.T., 1984. Chimeric human antibody molecules: mouse antigen-binding domains with human constant region domains. *Proceedings of the National Academy of Sciences*, 81(21), pp.6851-6855.
- Murakami, H., Hohsaka, T., Ashizuka, Y., Hashimoto, K. and Sisido, M., 2000. Site-directed incorporation of fluorescent nonnatural amino acids into streptavidin for highly sensitive detection of biotin. *Biomacromolecules*, 1(1), pp.118-125.
- Nakamura, K. and Inouye, M., 1979. DNA sequence of the gene for the outer membrane lipoprotein of E. coli: an extremely AT-rich promoter. *Cell*, 18(4), pp.1109-1117.
- Nakamura, Y., Gojobori, T. and Ikemura, T., 2000. Codon usage tabulated from international DNA sequence databases: status for the year 2000. *Nucleic acids research*, 28(1), pp.292-292.

- Nath, N., Godat, B., Zimprich, C., Dwight, S.J., Corona, C., McDougall, M. and Urh, M., 2016. Homogeneous plate based antibody internalization assay using pH sensor fluorescent dye. *Journal of immunological methods*, 431, pp.11-21.
- Neumann, H., Hazen, J.L., Weinstein, J., Mehl, R.A. and Chin, J.W., 2008a. Genetically encoding protein oxidative damage. *Journal of the American Chemical Society*, 130(12), pp.4028-4033.
- Neumann, H., Peak-Chew, S.Y. and Chin, J.W., 2008b. Genetically encoding N ϵ -acetyllysine in recombinant proteins. *Nature chemical biology*, 4(4), pp.232-234.
- Neumann, H., Wang, K., Davis, L., Garcia-Alai, M. and Chin, J.W., 2010. Encoding multiple unnatural amino acids via evolution of a quadruplet-decoding ribosome. *Nature*, 464(7287), pp.441-444.
- Nevola, L. and Giralt, E., 2015. Modulating protein–protein interactions: the potential of peptides. *Chemical Communications*, 51(16), pp.3302-3315.
- Nguyen, A., Hoang, V., Laquer, V. and Kelly, K.M., 2009a. Angiogenesis in cutaneous disease: part I. *Journal of the American Academy of Dermatology*, 61(6), pp.921-942.
- Nguyen, D.P., Lusic, H., Neumann, H., Kapadnis, P.B., Deiters, A. and Chin, J.W., 2009b. Genetic encoding and labeling of aliphatic azides and alkynes in recombinant proteins via a pyrrolysyl-tRNA synthetase/tRNACUA pair and click chemistry. *Journal of the American Chemical Society*, 131(25), pp.8720-8721.
- Nguyen, D.P., Mahesh, M., Elsässer, S.J., Hancock, S.M., Uttamapinant, C. and Chin, J.W., 2014. Genetic encoding of photocaged cysteine allows photoactivation of TEV protease in live mammalian cells. *Journal of the American Chemical Society*, 136(6), pp.2240-2243.
- Nguyen, V., Su, C., Muyldermans, S. and van der Loo, W., 2002. Heavy-chain antibodies in Camelidae; a case of evolutionary innovation. *Immunogenetics*, 54(1), pp.39-47.
- Nilsson, J., Ståhl, S., Lundeberg, J., Uhlén, M. and Nygren, P.Å., 1997. Affinity fusion strategies for detection, purification, and immobilization of recombinant proteins. *Protein expression and purification*, 11(1), pp.1-16.
- O'Donoghue, P., Prat, L., Heinemann, I.U., Ling, J., Odoi, K., Liu, W.R. and Söll, D., 2012. Near-cognate suppression of amber, opal and quadruplet codons competes with aminoacyl-tRNAPyl for genetic code expansion. *FEBS letters*, 586(21), pp.3931-3937.
- Oehler, S., Eismann, E.R., Krämer, H. and Müller-Hill, B., 1990. The three operators of the lac operon cooperate in repression. *The EMBO journal*, 9(4), pp.973-979.

- Oka, T., Sakamoto, S., Miyoshi, K.L., Fuwa, T., Yoda, K., Yamasaki, M., Tamura, G. and Miyake, T., 1985. Synthesis and secretion of human epidermal growth factor by *Escherichia coli*. *Proceedings of the National Academy of Sciences*, 82(21), pp.7212-7216.
- Olaru, A., Bala, C., Jaffrezic-Renault, N. and Aboul-Enein, H.Y., 2015. Surface plasmon resonance (SPR) biosensors in pharmaceutical analysis. *Critical reviews in analytical chemistry*, 45(2), pp.97-105.
- Oliveira, S., Van Dongen, G.A., Walsum, M.S.V., Roovers, R.C., Stam, J.C., Mali, W., Van Diest, P.J. and van Bergen en Henegouwen, P.M., 2012. Rapid visualization of human tumor xenografts through optical imaging with a near-infrared fluorescent anti-epidermal growth factor receptor nanobody. *Molecular imaging*, 11(1), pp.7290-2011.
- Oller-Salvia, B. and Chin, J.W., 2019. Efficient Phage Display with Multiple Distinct Non-Canonical Amino Acids Using Orthogonal Ribosome-Mediated Genetic Code Expansion. *Angewandte Chemie*, 131(32), pp.10960-10964.
- Oller-Salvia, B., Kym, G. and Chin, J.W., 2018. Rapid and Efficient Generation of Stable Antibody-Drug Conjugates via an Encoded Cyclopropene and an Inverse-Electron-Demand Diels-Alder Reaction. *Angewandte Chemie International Edition*, 57(11), pp.2831-2834.
- Olsen, J.V., Blagoev, B., Gnadt, F., Macek, B., Kumar, C., Mortensen, P. and Mann, M., 2006. Global, in vivo, and site-specific phosphorylation dynamics in signaling networks. *Cell*, 127(3), pp.635-648.
- Ormö, M., Cubitt, A.B., Kallio, K., Gross, L.A., Tsien, R.Y. and Remington, S.J., 1996. Crystal structure of the *Aequorea victoria* green fluorescent protein. *Science*, 273(5280), pp.1392-1395.
- Ostrov, N., Landon, M., Guell, M., Kuznetsov, G., Teramoto, J., Cervantes, N., Zhou, M., Singh, K., Napolitano, M.G., Moosburner, M. and Shrock, E., 2016. Design, synthesis, and testing toward a 57-codon genome. *Science*, 353(6301), pp.819-822.
- Park, H.S., Hohn, M.J., Umehara, T., Guo, L.T., Osborne, E.M., Benner, J., Noren, C.J., Rinehart, J. and Söll, D., 2011. Expanding the genetic code of *Escherichia coli* with phosphoserine. *Science*, 333(6046), pp.1151-1154.
- Pastrnak, M., Magliery, T.J. and Schultz, P.G., 2000. A new orthogonal suppressor tRNA/aminoacyl-tRNA synthetase pair for evolving an organism with an expanded genetic code. *Helvetica Chimica Acta*, 83(9), pp.2277-2286.

- Pearson, A.D., Mills, J.H., Song, Y., Nasertorabi, F., Han, G.W., Baker, D., Stevens, R.C. and Schultz, P.G., 2015. Trapping a transition state in a computationally designed protein bottle. *Science*, 347(6224), pp.863-867.
- Perozzo, R., Folkers, G. and Scapozza, L., 2004. Thermodynamics of protein–ligand interactions: history, presence, and future aspects. *Journal of Receptors and Signal Transduction*, 24(1-2), pp.1-52.
- Peters, F.B., Brock, A., Wang, J. and Schultz, P.G., 2009. Photocleavage of the polypeptide backbone by 2-nitrophenylalanine. *Chemistry & biology*, 16(2), pp.148-152.
- Philipson, K.D., Gallivan, J.P., Brandt, G.S., Dougherty, D.A. and Lester, H.A., 2001. Incorporation of caged cysteine and caged tyrosine into a transmembrane segment of the nicotinic ACh receptor. *American Journal of Physiology-Cell Physiology*, 281(1), pp.C195-C206.
- Pirkmajer, S. and Chibalin, A.V., 2011. Serum starvation: caveat emptor. *American Journal of Physiology-Cell Physiology*, 301(2), pp.C272-C279.
- Plotkin, J.B. and Kudla, G., 2011. Synonymous but not the same: the causes and consequences of codon bias. *Nature Reviews Genetics*, 12(1), pp.32-42.
- Plumbridge, J. and Söll, D., 1987. The effect of dam methylation on the expression of glnS in *E. coli*. *Biochimie*, 69(5), pp.539-541.
- Polycarpo, C.R., Herring, S., Bérubé, A., Wood, J.L., Söll, D. and Ambrogelly, A., 2006. Pyrrolysine analogues as substrates for pyrrolysyl-tRNA synthetase. *FEBS letters*, 580(28-29), pp.6695-6700.
- Pothoulakis, G. and Ellis, T., 2015. Using Spinach aptamer to correlate mRNA and protein levels in *Escherichia coli*. In *Methods in enzymology* (Vol. 550, pp. 173-185). Academic Press.
- Prado, S.M.D., Cedrún, J.L.L., Rey, R.L., Villaamil, V.M., García, A.Á., Ayerbes, M.V. and Aparicio, L.A., 2010. Evaluation of COX-2, EGFR, and p53 as biomarkers of non-dysplastic oral leukoplakias. *Experimental and molecular pathology*, 89(2), pp.197-203.
- Przepiorka, D., Ko, C.W., Deisseroth, A., Yancey, C.L., Candau-Chacon, R., Chiu, H.J., Gehrke, B.J., Gomez-Broughton, C., Kane, R.C., Kirshner, S. and Mehrotra, N., 2015. FDA approval: blinatumomab. *Clinical Cancer Research*, 21(18), pp.4035-4039.
- Rackham, O. and Chin, J.W., 2005. A network of orthogonal ribosome· mRNA pairs. *Nature chemical biology*, 1(3), pp.159-166.

- Raran-Kurussi, S. and Waugh, D.S., 2012. The ability to enhance the solubility of its fusion partners is an intrinsic property of maltose-binding protein but their folding is either spontaneous or chaperone-mediated. *PLoS one*, 7(11).
- Riese, D.J. and Stern, D.F., 1998. Specificity within the EGF family/ErbB receptor family signaling network. *Bioessays*, 20(1), pp.41-48.
- Roberts, M.C., 1996. Tetracycline resistance determinants: mechanisms of action, regulation of expression, genetic mobility, and distribution. *FEMS microbiology reviews*, 19(1), pp.1-24.
- Roberts, M.C., 2005. Update on acquired tetracycline resistance genes. *FEMS microbiology letters*, 245(2), pp.195-203.
- Rogerson, D.T., Sachdeva, A., Wang, K., Haq, T., Kazlauskaitė, A., Hancock, S.M., Huguenin-Dezot, N., Muqit, M.M., Fry, A.M., Bayliss, R. and Chin, J.W., 2015. Efficient genetic encoding of phosphoserine and its nonhydrolyzable analog. *Nature chemical biology*, 11(7), pp.496.
- Roovers, R.C., Vosjan, M.J., Laeremans, T., el Khoulati, R., de Bruin, R.C., Ferguson, K.M., Verkleij, A.J., van Dongen, G.A. and van Bergen en Henegouwen, P.M., 2011. A biparatopic anti-EGFR nanobody efficiently inhibits solid tumour growth. *International journal of cancer*, 129(8), pp.2013-2024.
- Rosano, G.L. and Ceccarelli, E.A., 2014. Recombinant protein expression in Escherichia coli: advances and challenges. *Frontiers in microbiology*, 5, pp.172.
- Rouet, R., Lowe, D., Dudgeon, K., Roome, B., Schofield, P., Langley, D., Andrews, J., Whitfeld, P., Jermutus, L. and Christ, D., 2012. Expression of high-affinity human antibody fragments in bacteria. *nature protocols*, 7(2), pp.364.
- Ryu, Y. and Schultz, P.G., 2006. Efficient incorporation of unnatural amino acids into proteins in Escherichia coli. *Nature methods*, 3(4), pp.263-265.
- Sachdeva, A., Wang, K., Elliott, T. and Chin, J.W., 2014. Concerted, rapid, quantitative, and site-specific dual labeling of proteins. *Journal of the American Chemical Society*, 136(22), pp.7785-7788.
- Santoro, S.W., Wang, L., Herberich, B., King, D.S. and Schultz, P.G., 2002. An efficient system for the evolution of aminoacyl-tRNA synthetase specificity. *Nature biotechnology*, 20(10), pp.1044-1048.
- Schmid, S.L., 1997. Clathrin-coated vesicle formation and protein sorting: an integrated process. *Annual review of biochemistry*, 66(1), pp.511-548.

- Schmitz, K.R., Bagchi, A., Roovers, R.C., en Henegouwen, P.M.V.B. and Ferguson, K.M., 2013. Structural evaluation of EGFR inhibition mechanisms for nanobodies/VHH domains. *Structure*, 21(7), pp.1214-1224.
- Schnell, U., Dijk, F., Sjollem, K.A. and Giepmans, B.N., 2012. Immunolabeling artifacts and the need for live-cell imaging. *Nature methods*, 9(2), pp.152.
- Schultz, K.C., Supekova, L., Ryu, Y., Xie, J., Perera, R. and Schultz, P.G., 2006. A genetically encoded infrared probe. *Journal of the American Chemical Society*, 128(43), pp.13984-13985.
- Schwark, D.G., Schmitt, M.A. and Fisk, J.D., 2018. Dissecting the contribution of release factor interactions to amber stop codon reassignment efficiencies of the *Methanocaldococcus jannaschii* orthogonal pair. *Genes*, 9(11), pp.546.
- Scita, G. and Di Fiore, P.P., 2010. The endocytic matrix. *Nature*, 463(7280), pp.464-473.
- Shaw, W.V., 1983. Chloramphenicol acetyltransferase: enzymology and molecular biology. *Critical Reviews in Biochemistry*, 14(1), pp.1-46.
- Sheehan, J.C. and Wilson, R.M., 1964. Photolysis of desyl compounds. A new photolytic cyclization. *Journal of the American Chemical Society*, 86(23), pp.5277-5281.
- Shine, J. and Dalgarno, L., 1974. The 3'-terminal sequence of Escherichia coli 16S ribosomal RNA: complementarity to nonsense triplets and ribosome binding sites. *Proceedings of the National Academy of Sciences*, 71(4), pp.1342-1346.
- Siegele, D.A. and Hu, J.C., 1997. Gene expression from plasmids containing the araBAD promoter at subsaturating inducer concentrations represents mixed populations. *Proceedings of the National Academy of Sciences*, 94(15), pp.8168-8172.
- Sievers, E.L. and Senter, P.D., 2013. Antibody-drug conjugates in cancer therapy. *Annual review of medicine*, 64, pp.15-29.
- Sigismund, S., Confalonieri, S., Ciliberto, A., Polo, S., Scita, G. and Di Fiore, P.P., 2012. Endocytosis and signaling: cell logistics shape the eukaryotic cell plan. *Physiological reviews*, 92(1), pp.273-366.
- Simmons, L.C., Reilly, D., Klimowski, L., Raju, T.S., Meng, G., Sims, P., Hong, K., Shields, R.L., Damico, L.A., Rancatore, P. and Yansura, D.G., 2002. Expression of full-length immunoglobulins in Escherichia coli: rapid and efficient production of aglycosylated antibodies. *Journal of immunological methods*, 263(1-2), pp.133-147.
- Sinha, D.K., Neveu, P., Gagey, N., Aujard, I., Benbrahim-Bouzidi, C., Le Saux, T., Rampon, C., Gauron, C., Goetz, B., Dubruille, S. and Baaden, M., 2010. Photocontrol of Protein

- Activity in Cultured Cells and Zebrafish with One-and Two-Photon Illumination. *ChemBioChem*, 11(5), pp.653-663.
- Smith, D.B. and Johnson, K.S., 1988. Single-step purification of polypeptides expressed in *Escherichia coli* as fusions with glutathione S-transferase. *Gene*, 67(1), pp.31-40.
- Smolskaya, S. and Andreev, Y.A., 2019. Site-specific incorporation of unnatural amino acids into *Escherichia coli* recombinant protein: methodology development and recent achievement. *Biomolecules*, 9(7), pp.255.
- Snyder, L. and Champness, W., 2013. The bacterial chromosome: DNA structure, replication, and segregation. *Molecular genetics of bacteria*.
- Som, T. and Tomizawa, J.I., 1982. Origin of replication of *Escherichia coli* plasmid RSF 1030. *Molecular and General Genetics MGG*, 187(3), pp.375-383.
- Soma, A. and Himeno, H., 1998. Cross-species aminoacylation of tRNA with a long variable arm between *Escherichia coli* and *Saccharomyces cerevisiae*. *Nucleic acids research*, 26(19), pp.4374-4381.
- Sorkin, A., 2004. Cargo recognition during clathrin-mediated endocytosis: a team effort. *Current opinion in cell biology*, 16(4), pp.392-399.
- Sorkin, A. and Goh, L.K., 2009. Endocytosis and intracellular trafficking of ErbBs. *Experimental cell research*, 315(4), pp.683-696.
- Spiess, C., Zhai, Q. and Carter, P.J., 2015. Alternative molecular formats and therapeutic applications for bispecific antibodies. *Molecular immunology*, 67(2), pp.95-106.
- Spinelli, S., Frenken, L.G., Hermans, P., Verrips, T., Brown, K., Tegoni, M. and Cambillau, C., 2000. Camelid heavy-chain variable domains provide efficient combining sites to haptens. *Biochemistry*, 39(6), pp.1217-1222.
- Srinivasan, G., James, C.M. and Krzycki, J.A., 2002. Pyrrolysine encoded by UAG in Archaea: charging of a UAG-decoding specialized tRNA. *Science*, 296(5572), pp.1459-1462.
- Steer, B.A. and Schimmel, P., 1999. Major anticodon-binding region missing from an archaeobacterial tRNA synthetase. *Journal of Biological Chemistry*, 274(50), pp.35601-35606.
- Studier, F.W., 1991. Use of bacteriophage T7 lysozyme to improve an inducible T7 expression system. *Journal of molecular biology*, 219(1), pp.37-44.
- Subik, K., Lee, J.F., Baxter, L., Strzepak, T., Costello, D., Crowley, P., Xing, L., Hung, M.C., Bonfiglio, T., Hicks, D.G. and Tang, P., 2010. The expression patterns of ER, PR, HER2,

- CK5/6, EGFR, Ki-67 and AR by immunohistochemical analysis in breast cancer cell lines. *Breast cancer: basic and clinical research*, 4, p.117822341000400004.
- Summerer, D., Chen, S., Wu, N., Deiters, A., Chin, J.W. and Schultz, P.G., 2006. A genetically encoded fluorescent amino acid. *Proceedings of the National Academy of Sciences*, 103(26), pp.9785-9789.
- Sutcliffe, J.G., 1978. Nucleotide sequence of the ampicillin resistance gene of *Escherichia coli* plasmid pBR322. *Proceedings of the National Academy of Sciences*, 75(8), pp.3737-3741.
- Szynol, A., De Soet, J.J., Sieben-van Tuyl, E., Bos, J.W. and Frenken, L.G., 2004. Bactericidal effects of a fusion protein of llama heavy-chain antibodies coupled to glucose oxidase on oral bacteria. *Antimicrobial agents and chemotherapy*, 48(9), pp.3390-3395.
- Tabor, S. and Richardson, C.C., 1985. A bacteriophage T7 RNA polymerase/promoter system for controlled exclusive expression of specific genes. *Proceedings of the National Academy of Sciences*, 82(4), pp.1074-1078.
- Thomas, P. and Smart, T.G., 2005. HEK293 cell line: a vehicle for the expression of recombinant proteins. *Journal of pharmacological and toxicological methods*, 51(3), pp.187-200.
- Thottacherry, J.J., Sathe, M., Prabhakara, C. and Mayor, S., 2019. Spoiled for Choice: Diverse Endocytic Pathways Function at the Cell Surface. *Annual review of cell and developmental biology*, 35, pp.55-84.
- Tippmann, E.M., Liu, W., Summerer, D., Mack, A.V. and Schultz, P.G., 2007. A genetically encoded diazirine photocrosslinker in *Escherichia coli*. *ChemBioChem*, 8(18), pp.2210-2214.
- Toseland, C.P., 2013. Fluorescent labeling and modification of proteins. *Journal of chemical biology*, 6(3), pp.85-95.
- Umezawa, H., 1979. Studies on aminoglycoside antibiotics: enzymic mechanism of resistance and genetics. *The Japanese journal of antibiotics*, 32, pp.S1-14.
- Urquhart, L., 2018 Top drugs and companies by sales in 2017. *Nat Rev Drug Discov* 17, pp.232.
- Uy, R. and Wold, F., 1977. Posttranslational covalent modification of proteins. *Science*, 198(4320), pp.890-896.
- Van Der Meel, R., Oliveira, S., Altintas, I., Haselberg, R., Van Der Veecken, J., Roovers, R.C., en Henegouwen, P.M.V.B., Storm, G., Hennink, W.E., Schiffelers, R.M. and Kok, R.J.,

2012. Tumor-targeted Nanobullets: Anti-EGFR nanobody-liposomes loaded with anti-IGF-1R kinase inhibitor for cancer treatment. *Journal of controlled release*, 159(2), pp.281-289.
- Van der Vaart, J.M., Pant, N., Wolvers, D., Bezemer, S., Hermans, P.W., Bellamy, K., Sarker, S.A., Van der Logt, C.P.E., Svensson, L., Verrips, C.T. and Hammarstrom, L., 2006. Reduction in morbidity of rotavirus induced diarrhoea in mice by yeast produced monovalent llama-derived antibody fragments. *Vaccine*, 24(19), pp.4130-4137.
- Van, M.K. and Pauwels, E.K., 1988. Human immunological response to mouse monoclonal antibodies in the treatment or diagnosis of malignant diseases. *Nuclear medicine communications*, 9(11), pp.919-930.
- Van Weemen, B.K. and Schuurs, A.H.W.M., 1971. Immunoassay using antigen—enzyme conjugates. *FEBS letters*, 15(3), pp.232-236.
- Vera, A., González-Montalbán, N., Arís, A. and Villaverde, A., 2007. The conformational quality of insoluble recombinant proteins is enhanced at low growth temperatures. *Biotechnology and bioengineering*, 96(6), pp.1101-1106.
- Vile, G.F., Tanew-Iliitschew, A. and Tyrrell, R.M., 1995. Activation of NF- κ B in human skin fibroblasts by the oxidative stress generated by UVA radiation. *Photochemistry and photobiology*, 62(3), pp.463-468.
- Vlastaridis, P., Papakyriakou, A., Chaliotis, A., Stratikos, E., Oliver, S.G. and Amoutzias, G.D., 2017. The pivotal role of protein phosphorylation in the control of yeast central metabolism. *G3: Genes, Genomes, Genetics*, 7(4), pp.1239-1249.
- Vogel, C.L., Cobleigh, M.A., Tripathy, D., Gutheil, J.C., Harris, L.N., Fehrenbacher, L., Slamon, D.J., Murphy, M., Novotny, W.F., Burchmore, M. and Shak, S., 2002. Efficacy and safety of trastuzumab as a single agent in first-line treatment of HER2-overexpressing metastatic breast cancer. *Journal of Clinical Oncology*, 20(3), pp.719-726.
- Wan, W., Huang, Y., Wang, Z., Russell, W.K., Pai, P.J., Russell, D.H. and Liu, W.R., 2010. A facile system for genetic incorporation of two different noncanonical amino acids into one protein in *Escherichia coli*. *Angewandte Chemie International Edition*, 49(18), pp.3211-3214.
- Wang, J., Xie, J. and Schultz, P.G., 2006. A genetically encoded fluorescent amino acid. *Journal of the American Chemical Society*, 128(27), pp.8738-8739.
- Wang, K., Neumann, H., Peak-Chew, S.Y. and Chin, J.W., 2007. Evolved orthogonal ribosomes enhance the efficiency of synthetic genetic code expansion. *Nature biotechnology*, 25(7), pp.770-777.

- Wang, K., Sachdeva, A., Cox, D.J., Wilf, N.M., Lang, K., Wallace, S., Mehl, R.A. and Chin, J.W., 2014. Optimized orthogonal translation of unnatural amino acids enables spontaneous protein double-labelling and FRET. *Nature chemistry*, 6(5), pp.393.
- Wang, L., Brock, A., Herberich, B. and Schultz, P.G., 2001. Expanding the genetic code of *Escherichia coli*. *Science*, 292(5516), pp.498-500.
- Wang, L., Magliery, T.J., Liu, D.R. and Schultz, P.G., 2000. A new functional suppressor tRNA/aminoacyl-tRNA synthetase pair for the in vivo incorporation of unnatural amino acids into proteins. *Journal of the American Chemical Society*, 122(20), pp.5010-5011.
- Wang, L., Yan, J., Yan, J., Xu, H., Zhang, D., Wang, X. and Sheng, J., 2018. Expression and purification of the human epidermal growth factor receptor extracellular domain. *Protein expression and purification*, 144, pp.33-38.
- Wang, L., Zhang, Z., Brock, A. and Schultz, P.G., 2003. Addition of the keto functional group to the genetic code of *Escherichia coli*. *Proceedings of the National Academy of Sciences*, 100(1), pp.56-61.
- Wang, X., Feng, M., Xiao, L., Tong, A. and Xiang, Y., 2016. Postsynthetic modification of DNA phosphodiester backbone for photocaged dnzyme. *ACS chemical biology*, 11(2), pp.444-451.
- Wanner, B.L., Kodaira, R. and Neidhardt, F.C., 1978. Regulation of lac operon expression: reappraisal of the theory of catabolite repression. *Journal of bacteriology*, 136(3), pp.947-954.
- Warther, D., Gug, S., Specht, A., Bolze, F., Nicoud, J.F., Mouro, A. and Goeldner, M., 2010. Two-photon uncaging: New prospects in neuroscience and cellular biology. *Bioorganic & medicinal chemistry*, 18(22), pp.7753-7758.
- Waters, J.C., 2009. Accuracy and precision in quantitative fluorescence microscopy. *J Cell Biol*, 185(7), pp.1135-1148.
- Wiley, H.S., 1988. Anomalous binding of epidermal growth factor to A431 cells is due to the effect of high receptor densities and a saturable endocytic system. *The Journal of cell biology*, 107(2), pp.801-810.
- Wu, C., Ying, H., Grinnell, C., Bryant, S., Miller, R., Clabbers, A., Bose, S., McCarthy, D., Zhu, R.R., Santora, L. and Davis-Taber, R., 2007. Simultaneous targeting of multiple disease mediators by a dual-variable-domain immunoglobulin. *Nature biotechnology*, 25(11), pp.1290-1297.
- Yamashita, T., Mizohata, E., Nagatoishi, S., Watanabe, T., Nakakido, M., Iwanari, H., Mochizuki, Y., Nakayama, T., Kado, Y., Yokota, Y. and Matsumura, H., 2019. Affinity

- Improvement of a Cancer-Targeted Antibody through Alanine-Induced Adjustment of Antigen-Antibody Interface. *Structure*, 27(3), pp.519-527.
- Yanagisawa, T., Ishii, R., Fukunaga, R., Kobayashi, T., Sakamoto, K. and Yokoyama, S., 2008. Multistep engineering of pyrrolysyl-tRNA synthetase to genetically encode N ϵ -(o-azidobenzoyloxycarbonyl) lysine for site-specific protein modification. *Chemistry & biology*, 15(11), pp.1187-1197.
- Young, T.S., Ahmad, I., Yin, J.A. and Schultz, P.G., 2010. An enhanced system for unnatural amino acid mutagenesis in E. coli. *Journal of molecular biology*, 395(2), pp.361-374.
- Zhang, M.S., Brunner, S.F., Huguenin-Dezot, N., Liang, A.D., Schmied, W.H., Rogerson, D.T. and Chin, J.W., 2017. Biosynthesis and genetic encoding of phosphothreonine through parallel selection and deep sequencing. *Nature methods*, 14(7), p.729.
- Zhao, J., Gover, T.D., Muralidharan, S., Auston, D.A., Weinreich, D. and Kao, J.P., 2006. Caged vanilloid ligands for activation of TRPV1 receptors by 1-and 2-photon excitation. *Biochemistry*, 45(15), pp.4915-4926.
- Zhang, Z., Schwartz, S., Wagner, L. and Miller, W., 2000. A greedy algorithm for aligning DNA sequences. *Journal of Computational biology*, 7(1-2), pp.203-214.
- Zhou, Q., Stefano, J.E., Manning, C., Kyazike, J., Chen, B., Gianolio, D.A., Park, A., Busch, M., Bird, J., Zheng, X. and Simonds-Mannes, H., 2014. Site-specific antibody–drug conjugation through glycoengineering. *Bioconjugate chemistry*, 25(3), pp.510-520.
- Zorn, J.A. and Wells, J.A., 2010. Turning enzymes ON with small molecules. *Nature chemical biology*, 6(3), p.179.

Appendix

A.1 Recipes

A.1.1 *Luria-Bertani (LB) Broth*

10 g Tryptone

10 g NaCl

5 g Yeast extract

Or 25 g Pre-blended LB broth Miller (Formedium)

Adjust to 1 L with Mili-Q H₂O

Sterilise by autoclaving on media cycle

A.1.2 *Super Optimal Broth (SOB)*

5 g Yeast Extract

20 g Tryptone

0.584 g NaCl

0.186 g KCl

2.4 g MgSO₄

Adjust to 1 L with Mili-Q H₂O

Sterilise by autoclaving on media cycle

A.1.3 *Luria-Bertani (LB) Agar*

10 g Tryptone

10 g NaCl

5 g Yeast extract

15 g Agar

Or 40g Pre-blended LB Agar Miller (Formedium)

Adjust to 1 L with Mili-Q H₂O

Sterilise by autoclaving on media cycle

A.1.4 2XTY

16 g Tryptone

5 g NaCl

10 g Yeast extract

Adjust to 1 L with Mili-Q H₂O

Sterilise by autoclaving on media cycle

A.1.5 Antibiotics

Table A.1 Antibiotic stock solutions.

Antibiotic	Stock concentration	Working concentration
Ampicillin	100 mg/mL	100 µg/mL
Chloramphenicol*	25 mg/mL	25 µg/mL
Kanamycin	50 mg/mL	50 µg/mL
Tetracycline	10 mg/mL	10 µg/mL
Spectinomycin	100 mg/mL	100 µg/mL

* Dissolve in EtOH, no filtration

Dissolve in Mili-Q H₂O and sterilise by 0.22 µm syringe filter

A.1.6 1% Agarose-TAE gel

1 g Agarose powder

100 mL TAE (1X)

10 μ L 10,000X SYBR safe (Fisher Scientific)

A.1.7 Transformation buffer 1

7.4 g KCl

30 mL 1M CH₃CO₂K

1.5 g CaCl₂ · 2H₂O

150 g Glycerol

Adjust to 950 mL with Mili-Q H₂O and adjust pH to 6.4 with 0.2M acetic acid

Sterilise by autoclaving on media cycle

50 mL 1M Cl₂Mn · 4H₂O , filter sterilised

A.1.8 Transformation buffer 2

0.74 g KCl

11g CaCl₂ · 2H₂O

150 g Glycerol

Adjust to 980 mL with Mili-Q H₂O

Sterilise by autoclaving on media cycle

20ml 0.5M MOPS buffer, filter sterilised

A.1.9 1X Phosphate-buffered saline (PBS)

9.93g Pre-blended Phosphate buffered saline (Formedium)

Adjust to 1 L with Mili-Q H₂O

Sterilise by autoclaving on media cycle

A.1.10 Periplasmic buffer 1

200 g Sucrose

Adjust to 700 mL with Mili-Q H₂O and dissolve sucrose

100 mL 1M Tris-HCL

Adjust pH to 8 and adjust to 998 mL with Mili-Q H₂O

2 mL 0.5M EDTA

Sterilise by 0.22 µm vacuum filter

A.1.11 Periplasmic buffer 2

5 mL 1M MgCl₂

Adjust to 1 L with Mili-Q H₂O

Sterilise by 0.22 µm vacuum filter

A.1.12 Ni-NTA Wash buffer

17.5 g NaCl

1.36g Imidazole

Adjust to 950 mL with Mili-Q H₂O

50 mL 1M Tris-HCL

Adjust pH to 8

Sterilise by 0.22 µm vacuum filter

A.1.13 Ni-NTA Elution buffer

17.5 g NaCl

13.6g Imidazole

Adjust to 950 mL with Mili-Q H₂O

50 mL 1M Tris-HCL

Adjust pH to 8

Sterilise by 0.22 µm vacuum filter

A.1.14 1X Phosphate-buffered saline-Tween 0.1% (PBST)

1L 1X Phosphate-buffered saline (PBS)

1 mL Tween 20 (Sigma-Aldrich)

A.1.15 Western blot blocking buffer

10 mL PBST

1 g Milk powder

A.1.16 Western blot primary antibody (1:1000)

1 mL Western blot blocking buffer

9 mL PBST

10 μ L primary antibody

A.1.17 Western blot secondary antibody (1:3000)

1 mL Western blot blocking buffer

9 mL PBST

3.3 μ L secondary antibody

A.1.18 Imaging medium

7.24 g NaCl

0.384 g KCl

0.303 g CaCl₂ · 2H₂O

0.209 g MgCl₂ · 6H₂O

0.161 g Na₃PO₄

0.087 g NaHCO₃

6.20 g HEPES

Adjust to 980 mL with Mili-Q H₂O

Adjust pH to 7.3

2 g Glucose

0.1 g myo-Inositol

20 mL BME Amino acids (Sigma)

0.290 g Glutamine

Sterilise by 0.22 µm vacuum filter

A.1.19 Complete medium

To 500 mL DMEM (containing L-glutamine, 4.5 g/L D-Glucose, 110 mg/L Sodium pyruvate)

50 mL sterile-filtered foetal bovine serum (FBS)

5.5 mL (100X) Penicillin-Streptomycin

A.2 Primers

Table A.2: Primers used throughout this study.

Code	Name	Sequence
D029	wtPylRS Forward	TACGCTTTGAGGAATCCCATATGATGGATAAAAAACCG CT
D030	wtPylRS Reverse	TTTAGCGTTTGAAACTGCAGTTACAGGTTTCGTGCTAAT GC
D055	AS61_pULTRA_PylR S_f	CAATTTACAAAGGAGGTGCGGCCGCATGATGGATAAA AAACCGCTGGATGT
D056	AS61_pULTRA_PylR S_r	GAGACCGTTTAAACGCGGCCGCTTATTACAGGTTTCGTG CTAATGCCGTTATA
D119	2Rs15d_Y37TAG_F	CTTGTGGGATGGGCTGGTAGCGCCAGTCACCGGGACGC
D120	2Rs15d_Y37TAG_R	GCGTCCCGGTGACTGGCGCTACCAGCCCATCCCACAAG
D143	HC_pSANG- FAB225-AraTT_F	CCGAGGTGCAGCTGCTCGAGCAGGTGCAGTTGAAGCAG TCAGGTCC
D144	HC_pSANG- FAB225-AraTT_R	TGGCCGGCCTGGCCACTAGTGGTTTTGTACAGCTTTT GGGTTCAACTT
D145	LC_pSANG-FAB225- AraTT_F	GTGGCCAGGCGGCCGAGCTCGACATTCTTCTGACACA ATCTCCGGTG

D146	LC_pSANG-FAB225-AraTT_R	TCCTAATTAATTATCTAGAATCAGCATTGCGCCGCGATTAAAGCT
D164	RS15d SM CGC-AGA F	CTTGTGGGATGGGCTGGTAGAGACAGTCACCGGGACGCGAGCG
D165	RS15d SM CGC-AGA R	CGCTCGCGTCCCGGTGACTGTCTCTACCAGCCCATCCCACAAG
D200	RS15d SM CGC-CGA F	CTTGTGGGATGGGCTGGTAGCGACAGTCACCGGGACGCGAGCG
D204	RS15d SM CGC-CGA R	CGCTCGCGTCCCGGTGACTGTCTCTACCAGCCCATCCCACAAG
D214	Rs15d CGC-AGG F	TGGGATGGGCTGGTAGAGGCAGTCACCGGGACG
D215	Rs15d CGC-AGG R	CGTCCCGGTGACTGCCTCTACCAGCCCATCCCA
D216	Rs15d CGC-CGG F	GGATGGGCTGGTAGCGGCAGTCACCGGGA
D217	Rs15d CGC-CGG R	TCCCGGTGACTGCCGCTACCAGCCCATCC
D218	Rs15d CGC-CGT F	GGGATGGGCTGGTAGCGTCAGTCACCGGGAC
D219	Rs15d CGC-CGT R	GTCCCGGTGACTGACGCTACCAGCCCATCCC
D177	pAraTT_Seq_F	TGGACAAGAAAGTTGAGCCC
D178	pAraTT_Seq_R	TAGCGAAACCAGCCAGTGCC
D181	pAraTT_Seq_F2	ATGTAGGCGGTGCTACAGAG
D182	pAraTT_Seq_R2	GCTCATCAGATGGCGGGAAG
D183	pAraTT_Seq_R3	GTTTAAACGCCGATTGAGGCC
D184	pAraTT_Seq_R4	CGATCAACTCTATTTCTCGC
D185	pAraTT_Seq_F3	CGCAGTCTCCAGGCACCCTG
D186	pAraTT_Seq_F4	GCATCGTAAAGAACATTTTG

A.3 gBlock list

Table A.3: gBlocks used throughout this study.

Name and sequence
7D12_pSANG10_NdeI_HindIII (GB002) TTAACTTTAAGAAGGAGATATACATATGAAATCGCTGATTACTCCGATTGCTGCCGGATT ACTGTTGGCGTTTTTCCAATACTCGTTGGCGCAGGTAATAATAGAAGAATCTGGGGGTGG GTCCGTTTCAGACGGGTGGAAGTCTGCGCTTGACATGTGCCGCGTCTGGGCGCACATCACG CTCATATGGAATGGGCTGGTTCCGTCAAGCTCCTGGCAAGGAGCGTGAGTTCGTATCCGG TATCTCATGGCGCGGTGACTCAACCGGATATGCTGACTCAGTAAAGGGGCGTTTCACCAT CTCTCGTGATAATGCGAAGAATACTGTCGACTTACAAATGAACTCACTTAAACCAGAGGA TACCGCTATTTACTACTGCGCTGCTGCGGCAGGGTCTGCATGGTACGGTACACTGTACGA GTACGACTACTGGGGGCAGGGCACCCAGGTCACGGTTTCTTCTCACCACCATCACCACCA CTGATAAAAGCTTTAATAAGTCGAGCACC
7D12_pRSF_D11-G9 (GB003) TATGGTGACTTAACTCGTCTGGATCCAGACCTGGTACCAGCGCCCAATACGCAAACCGCC TCTCCCCGCGCGTTGGCCGATTCATTAATGCAGCTGGCACGACAGGTTTTCCCGACTGGAA AGCGGGCAGTGAGCGCAACGCAATTAATGTGAGTTAGCTCACTCATTAGGCACCCCAGGC TTTACACTTTATGCTTCCGGCTCGTATGTTGTGTGGAATTGTGAGCGGCTCGAGACAATT TTCATATCCCTCCGCAAATGAAATCCCTTATTACTCCAATCGCGGCGGGGTTATTGCTTG CTTTTAGTCAATATAGCCTGGCACAGGTGAAGCTGGAGGAATCTGGAGGTGGAAGTGTCC AAACAGGGGGCTCGCTTTCGTCTTACCTGTGCGGCATCAGGCCGCACAAGTCGTAGTTACG GAATGGGCTGGTTTCGCCAGGCCCCCGGTAAGGAACGTGAGTTTGTATCAGGTATTTTCGT GGCGCGGTGACTCCACAGGATATGCTGACAGCGTAAAAGGGCGCTTTACAATCAGCCGCG ACAATGCTAAGAATACAGTGACCTTCAAATGAACTCGTTAAAGCCTGAAGACACCCGCA TTTACTATTGCGCCGCTGCGGCAGGGTCGGCTTGGTATGGCACGTTGTATGAGTACGACT ACTGGGGACAGGGTACACAGGTCACGGTATCCTCACACCACCATCATCACTAAGACC TTAAGTCTCATAAGCTTAATTAGCTGACCTACTAGTCGGCCGTACGGGCCCTTTTCG
MpSANG10-7D12 K3TAG (GB004) ATTGTGAGCGGATAACAATTCCTCTAGAAATAATTTTGTTTAACTTTAAGAAGGAGAT ATACATATGAAATCGCTGATTACTCCGATTGCTGCCGGATTACTGTTGGCGTTTTTCCCAA TACTCGTTGGCGCAGGTATAGTTAGAAGAATCTGGGGGTGGGTCCGTTTCAGACGGGTGGA AGTCTGCGCTTGACATGTGCCGCGTCTGGGCGCACATCACGCTCATATGGAATGGGCTGG TTCCGTCAAGCTCCTGGCAAGGAGCGTGAGTTTCGTATCCGGTATCTCATGGCGCGGTGAC TCAACCGGATATGCTGACTCAGTAAAGGGGCGTTTCACCATCTCTCGTGATAATGCGAAG AATACTGTGCACTTACAAATGAACTCACTTAAACCA

MpSANG10-7D12 K43TAG (GB005)

ATTGTGAGCGGATAACAATTCCCCTCTAGAAATAATTTTGTTTAACTTTAAGAAGGAGAT
ATACATATGAAATCGCTGATTACTCCGATTGCTGCCGGATTACTGTTGGCGTTTTCCCAA
TACTCGTTGGCGCAGGTAAAATTAGAAGAATCTGGGGGTGGGTCCGTTTCAGACGGGTGGA
AGTCTGCGCTTGACATGTGCCGCTCTGGGCGCACATCACGCTCATATGGAATGGGCTGG
TTCCGTCAAGCTCCTGGCTAGGAGCGTGAGTTCGTATCCGGTATCTCATGGCGCGGTGAC
TCAACCGGATATGCTGACTCAGTAAAGGGCGTTTTACCATCTCTCGTGATAATGCGAAG
AATACTGTGCGACTTACAAATGAACTCACTTAAACCA

MpSANG10-7D12 K65TAG (GB006)

ATTGTGAGCGGATAACAATTCCCCTCTAGAAATAATTTTGTTTAACTTTAAGAAGGAGAT
ATACATATGAAATCGCTGATTACTCCGATTGCTGCCGGATTACTGTTGGCGTTTTCCCAA
TACTCGTTGGCGCAGGTAAAATTAGAAGAATCTGGGGGTGGGTCCGTTTCAGACGGGTGGA
AGTCTGCGCTTGACATGTGCCGCTCTGGGCGCACATCACGCTCATATGGAATGGGCTGG
TTCCGTCAAGCTCCTGGCAAGGAGCGTGAGTTCGTATCCGGTATCTCATGGCGCGGTGAC
TCAACCGGATATGCTGACTCAGTATAGGGGCGTTTTACCATCTCTCGTGATAATGCGAAG
AATACTGTGCGACTTACAAATGAACTCACTTAAACCA

MpSANG10-7D12 K76TAG (GB007)

ATTGTGAGCGGATAACAATTCCCCTCTAGAAATAATTTTGTTTAACTTTAAGAAGGAGAT
ATACATATGAAATCGCTGATTACTCCGATTGCTGCCGGATTACTGTTGGCGTTTTCCCAA
TACTCGTTGGCGCAGGTAAAATTAGAAGAATCTGGGGGTGGGTCCGTTTCAGACGGGTGGA
AGTCTGCGCTTGACATGTGCCGCTCTGGGCGCACATCACGCTCATATGGAATGGGCTGG
TTCCGTCAAGCTCCTGGCAAGGAGCGTGAGTTCGTATCCGGTATCTCATGGCGCGGTGAC
TCAACCGGATATGCTGACTCAGTAAAGGGGCGTTTTACCATCTCTCGTGATAATGCGTAG
AATACTGTGCGACTTACAAATGAACTCACTTAAACCA

MpSANG10-7D12 K87TAG (GB008)

TCTCGTGATAATGCGAAGAATACTGTGCGACTTACAAATGAACTCACTTTAGCCAGAGGAT
ACCGCTATTTACTACTGCGCTGCTGCGGCAGGGTCTGCATGGTACGGTACACTGTACGAG
TACGACTACTGGGGCAGGGCACCCAGGTCACGGTTTTCTTCTCACCACCATCACCACCAC
TGATAAAAGCTTTAATAAGTCGAGCACCACCA

FabC225_pSANG_HindIII_2 (GB015)

AACTTCCGGCGGAAGTGCAGCACTGGGATGTTTAGTTAAGGATTACTTTCCCGAACCCGT
TACTGTCAGTTGGAACAGCGGAGCCCTTACTTCAGGTGTTACACTTTCCCTGCTGTATT
GCAAAGCTCGGGATTGTACTCTCTGAGTTCTGTGCTTACGGTTCCTCCTCGTCCTTAGG
CACCCAGACCTACATTTGCAATGTGAACCATAAGCCCTCAAACACTAAGGTTGATAAAAA

AGTTGAACCCAAAAGCTGTGACAAAACCCACCATCATCACCATCACTGATAAGGTACCTA
GAAATAATTTTGTTTAACTTTAAGAAGGAGATATACATATGAAGCAGTCCACAATCGCCT
TAGCGTTGTTGCCTTTGTTGTTACCCCTGTAACCAAGGCAGACATTCTTCTGACACAAT
CTCCGGTGATTCTTTCCGTATCTCCCGGCGAACGTGTATCTTTCTCCTGTGCGCGGAGCC
AGTCAATTGGGACGAATATCCACTGGTATCAGCAACGCACCAATGGATCTCCACGTCTTC
TTATTAATACGCGTCAGAAAGCATCAGCGGCATTCCCAGTCGTTTTTCTGGCAGCGGCA
GCGGTACAGACTTTACTTTGAGTATCAACAGCGTGGAGTCGGAAGACATTGCAGACTACT
ACTGTCAACAAAACAACAATTGGCCACTACATTCGGAGCAGGGACTAAGCTGGAATTGA
AGCGCACGGTGCCTGCCCAAGTGTTTTTATTTTTCTCCGAGTGATGAACAATTGAAAT
CTGGGACTGCGTCGGTCGTCTGCTTACTTAACAATTTTTATCCGCGCGAAGCCAAAGTAC
AATGAAAAGTCGATAATGCGTTACAATCAGGCAATAGTCAGGAGTCCGTCACGGAACAGG
ACAGTAAAGATAGCACGTACAGCCTGTCGAGCACCTTACTTTATCGAAGGCGGACTACG
AAAAACATAAGGTCTACGCCTGCGAAGTGACTCACCAGGGGCTGAGCTCGCCCGTTACCA
AGAGCTTTAATCGCGCGAATGCTGATAAAGCTTTAATAAGTCGAGCACCACCACCAC

FabC225_pSANG_XbaI_1 (GB016)

GAATTGTGAGCGGATAACAATTTCCCTCTAGAAATAATTTTGTTTAACTTTAAGAAGGAG
ATATACATATGAAAAAGACAGCAATCGCTATCGCAGTCGCACTTGCTGGCTTCGCAACCG
TAGCGCAGGCTCAGGTGCAGTTGAAGCAGTCAGGTCCGGGTTTGGTCCAGCCGTCCAAA
GTTTGTCCATTACGTGCACAGTGTCCGGCTTCAGCTTGACCAACTACGGGGTACACTGGG
TACGTCAATCACCAGGTAAGGGGCTTGAATGGCTTGGTGTATCTGGTCAGGAGGAAACA
CGGACTACAACACCCCTTTCACCTCCCGTTTTGTCGATTAATAAAGATAACAGTAAGTCTC
AAGTATTTTTCAAATGAACTCGTTACAGTCAAACGATACTGCGATCTACTATTGCGCCC
GTGCCCTTACCTACTACGATTACGAATTTGCTTACTGGGGCAGGGTACGTTAGTTACCG
TCTCAGCAGCATCGACGAAAGGGCCTAGCGTTTTCCCTTTAGCGCCTTCCCTCGAAGTCAA
CTTCCGGCGGAAGTGCAGCACTG

7D12_Y32TAG_XbaI_SalI (GB020)

AATTGTGAGCGGATAACAATTTCCCTCTAGAAATAATTTTGTTTAACTTTAAGAAGGAGA
TATACATATGAAATCGCTGATTACTCCGATTGCTGCCGGATTACTGTTGGCGTTTTCCCA
ATACTCGTTGGCGCAGGTAATAATAGAAGAATCTGGGGGTGGTCCGTTTACAGCGGGTGG
AAGTCTGCGCTTGACATGTGCCGCTCTGGGCGCACATCACGCTCATAGGGAATGGGCTG
GTTCCGTCAAGCTCCTGGCAAGGAGCGTGAGTTCGTATCCGGTATCTCATGGCGCGGTGA
CTCAACCGGATATGCTGACTCAGTAAAGGGGCGTTTTACCATCTCTCGTGATAATGCGAA
GAATACTGTCGACTTACAAATGAACTCACTTAAACCAG

7D12_Y109TAG_SalI_HindIII (GB021)

GTGATAATGCGAAGAATACTGTGACTTACAAAATGAACTCACTTAAACCAGAGGATACCG
CTATTTACTACTGCGCTGCTGCGGCAGGGTCTGCATGGTACGGTACACTGTAGGAGTACG
ACTACTGGGGGCAGGGCACCCAGGTCACGGTTTTCTTCTCACCACCATCACCACCCTGAT
AAAAGCTTTAATAAGTCGAGCACCACCA

7D12_Y113TAG_Sall_HindIII (GB022)

GTGATAATGCGAAGAATACTGTGACTTACAAATGAACTCACTTAAACCAGAGGATACCG
CTATTTACTACTGCGCTGCTGCGGCAGGGTCTGCATGGTACGGTACACTGTACGAGTACG
ACTAGTGGGGGCAGGGCAGCCAGGTCACGGTTTCTTCTCACCACCATCACCACCACTGAT
AAAAGCTTTAATAAGTCGAGCACCACCA

pULTRA_PCY_NotI (GB024)

CGGATAACAATTTACAAAGGAGGTGCGGCCGCATGGATGAATTTGAAATGATCAAACGC
AATACGTCTGAAATCATCAGTGAAGAAGAATTGCGTGAAGTATTAATAAAGGACGAGAAG
AGCGCGGGCATTGGTTTTGAGCCCTCGGGCAAGATTCATCTTGACACTATCTGCAAATT
AAAAAGATGATCGACCTTCAAACGCAGGCTTTGACATCATCATTGGGCTGGCAGACTTA
CATGCATACCTTAACCAGAAAGGTGAATTGGACGAGATTCGTAAGATTGGAGATTACAAC
AAAAAGTTTTTTGAGGCTATGGGATTGAAGGCAAAGTATGTTACGGATCCGAAGAACAG
TTAGATAAAGACTATACGTTGAATGTGTACCGCCTTGCTCTGAAGACCACGTTGAAACGT
GCGCGTCGTTCAATGGAATTGATCGCCCGGAAGATGAGAACCCGAAAGTGGCCGAAGT
ATTTACCCTATCATGCAAGTAAACAGTATTCATTATGAAGGGGTGGACGTCGCAGTAGGC
GGGATGGAACAGCGTAAGATCCACATGCTTGCGCGTGAGTTGCTGCCAAAAAAGTCGTC
TGCATTCATAATCCCCTGCTTACCGGCTTAGATGGTGAAGGGAAGATGAGCTCAAGCAAA
GGAACTTCATCGCGGTGGACGACAGTCCAGAAGAAATTCGCGCAAAGATTAAGAAAGCC
TACTGTCCTGCTGGTGTGCTCGAGGGCAATCCTATCATGGAGATCGCGAAAATACTTCTTG
GAGTATCCATTGACCATTAACGCCCTGAGAAAATTCGGTGGGGATCTTACAGTGAACAGT
TACGAAGAAGTGAATCGTTATTCAAGAACAAGAGCTTCACCCGATGGATTTGAAGAAC
GCCGTTGCCGAAGAAGTATCAAATTCCTTGAACCGATTTCGAAGCGTCTTTAATAAGCG
GCCGCTTTAAACGGTCTCCAGCTTGGCTG

pULTRA_PyltRNA_PstI_XhoI (GB031)

CATCCCATAATCCTTGTTAGCCTGCAGGTAATTCGCTTCGCAACATGTGAGCACCGGT
TTATTGACTACCGGAAGCAGTGTGACCGTGTGCTTCTCAAATGCCTGAGGCCAGTTTGCT
CAGGCTCTCCCCGTGGAGGTAATAATTGACGATATGATCAGTGCACGGCTAACTAAGCGG
CCTGCTGACTTTCTCGCCGATCAAAGGCATTTTGCTATTAAGGGATTGACGAGGGCGTA
TCTGCGCAGTAAGATGCGCCCCGATTGGaAACCTGATCATGTAGATCGAATGGActCTA
aaTCCGTTTCCAGCCGGGTTAGATTCCCAGGGTTTCCGCCAAATTCGAAAAGCCTGCTCAAC
GAGCAGGCTTTTTTGCATGCTCGAGCAGCTCAGGGTCGAATTTGCCA

VHH_R2_pSANG_NdeI_HindIII (GB032)

TGAGCGGATAACAATCCCCTCTAGAAATAATTTGTTTAACTTTAAGAAGGAGATATAC
ATATGAAATCGCTGATTACTCCGATTGCTGCCGGATTACTGTTGGCGTTTTTCCCAATACT
CGTTGGCGCAAGTGCAGTTGCAAGAAAGTGGAGGTGGGCTGGTACAAGCGGGAGGGTCCCT
TGCGTTTGTGCTGCGCGGCCTCTGGACGTGCGGCAAGCGGACACGGCCATTACGGCATGG
GCTGGTTCGCTCAAGTGCCAGGCAAGGAGCGTGAGTTCGTGGCAGCCATTTCGTTGGTCCG
GCAAGGAACTTGGTACAAAGATTCAGTAAAAGGTCGTTTCACTATTAGCCGTGACAACG
CAAAAACCACAGTGTACCTTCAAATGAACAGTTTGAAGGGCAGGATACGGCTGTTTACT
ACTGCGCTGCTCGCCCGGTACGTGTCGCAGATATTTGCTGCCTGTAGGGTTTGATTACT

GGGGTCAGGGCACCCAAGTAACGGTGTCTGAGTCATCACCACCATCATCATTTAAAAGCTTT
AATAAGTCGAGCACCA

2Rs15d_pSANG_NdeI_HindIII (GB033)

TTAACTTTAAGAAGGAGATATACATATGAAATCGCTGATTACTCCGATTGCTGCCGGATT
ACTGTTGGCGTTTTCCCAATACTCGTTGGCGCAAGTCCAGTTACAGGAATCAGGCGGCGG
AATGTGCAGGCTGGAGGGTCTTTAAAGCTGACGTGTGCAGCATCGGGTTACATTTTCAAC
TCTTGTGGGATGGGCTGGTATCGCCAGTCACCGGGACGCGAGCGCGAACTTGTTAGCCGC
ATCTCTGGTGATGGTGACACCTGGCATAAAGAAAGCGTCAAAGGCCGTTTTACTATCTCG
CAAGATAATGTCAAGAAGACACTGTATCTGCAGATGAACTCGTTAAAGCCAGAGGATACT
GCGGTTTATTTTTGTGCGGTGTGCTATAATCTGGAACTTACTGGGGTCAAGGGACGCAA
GTAACAGTCTCGTCTCACCACCATCACCACCCTGATAAAAAGCTTTAATAAGTCGAGCAC

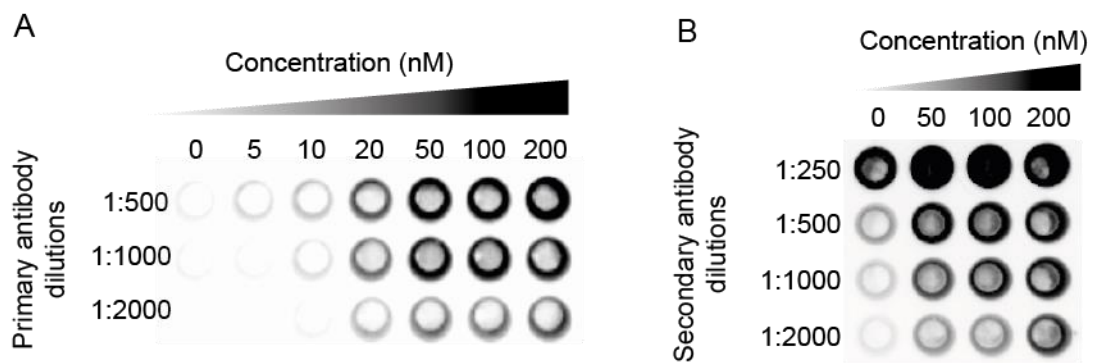


Figure A.1: On-cell assay evaluating optimum dilutions of primary and secondary antibody for detection of wt7D12 binding interactions to EGFR.

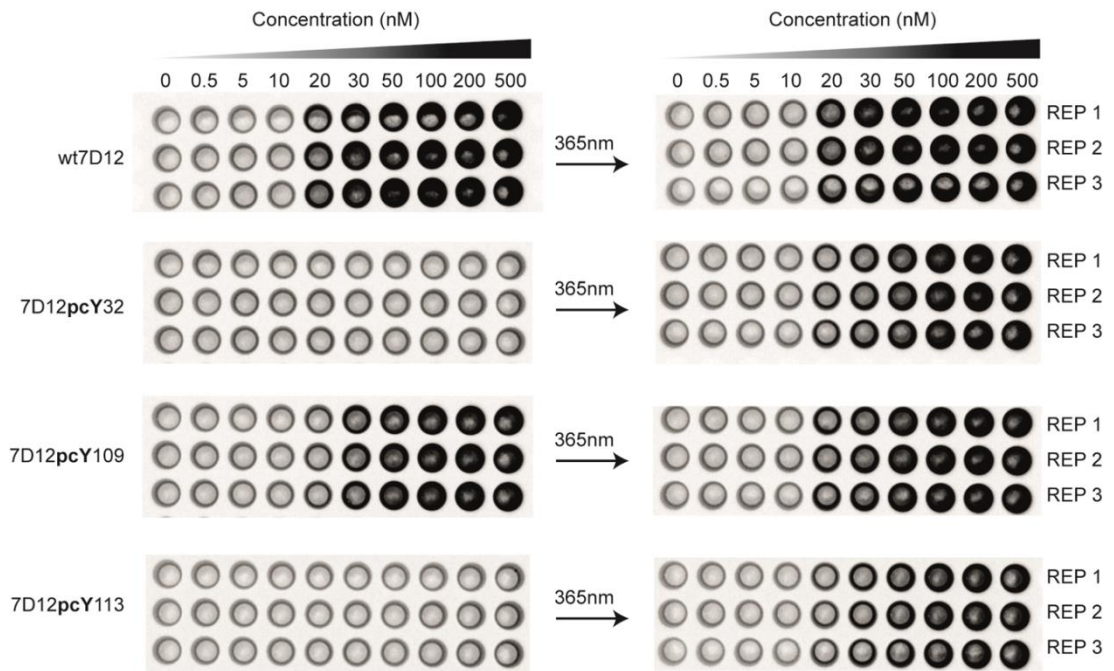


Figure A.2: On-cell assay to determine the binding kinetics of 7D12 (wt and pcY mutants) to EGFR in the presence and absence of 365 nm light. On-cell assays performed on the surface of A431 cells demonstrates that the presence of pcY at positions 32 and 113 in 7D12 inhibits its binding to EGFR. However, 7D12pcY109 mutant shows binding affinity similar to wt7D12. The binding to 7D12pcY32 and 7D12pcY113 mutants is restored upon irradiation with 365 nm light. These experiments were performed in triplicates, REP1, REP2 and REP3, to ensure reproducibility of data.

A.4 Microscopy videos

A.4.1 BODIPY-FL de-caging on the microscope

Filename: A431 BODIPY FL wt7D12 and Y32 -+ de-caged on

A.4.2 BODIPY-FL de-caging off the microscope

Filename: A431 BODIPY FL wt7D12 and Y32 de-caged off

A.4.3 BODIPY-TMR-X dynamic microscopy of light-dependent binding to A431 cell surface

Filename: A431 BODIPY TMRX wt7D12 and Y32 -+